Topographic differential analysis and function of age-related protein expression in the retinal pigment epithelium of *Callithrix jacchus*

Inaugural-Dissertation

zur

Erlangung des Doktorgrades

Dr. rer. nat.

der Fakultät für Biologie

an der

Universität Duisburg-Essen

vorgelegt von

Karina Hadrian

aus Hamm

Oktober 2019

DOI: 10.17185/duepublico/71782
URN: urn:nbn:de:hbz:465-20220720-110703-6

Die der vorliegenden Arbeit zugrunde liegenden Experimente wurden in der Klinik für Augenheilkunde, Universitätsklinikum Essen durchgeführt.

1. Gutachter: PD Dr. Michael Böhm
2. Gutachter: Prof. Dr. Gero Hilken

Vorsitzende des Prüfungsausschusses: Prof. Dr. Perihan Nalbant

Tag der mündlichen Prüfung: 01.04.2020

"Happiness can be found, even in the darkest of times,

if one only remembers to turn on the light!"

Albus Dumbledore

In the context of this doctoral work, the following articles were published:

K. Hadrian, H. Melkonyan, S. Schlatt, J. Wistuba, S. Wasmuth, A. Heiligenhaus, S. Thanos, M.R.R. Böhm (2019)

"Age-related distribution and potential role of SNCB in topographically different retinal areas of the common marmoset *Callithrix jacchus*, including the macula"

Experimental Eye Research, May 23;185:107676

S. König, K. Hadrian, S. Schlatt, J. Wistuba, S. Thanos, M.R.R. Böhm (2018)

"Topographic protein profiling of the age-related proteome in the retinal pigment epithelium of *Callithrix jacchus* with respect to macular degeneration"

Journal of Proteomics, Jan 16;191:1-15

Table of content

List of abbreviations

4-HNE	4-Hydroxynonenal
7AAD	7-Amino-Actinomycin
8-HGN	8-Hydroxyguanosine
AMD	Age-related macular degeneration
APS	Ammonium persulfate
Aq. Dest	Aqua destillata
BASP1	Brain abundant membrane attached signal protein 1
BMEC	Brain microvascular endothelial cells
BRB	Blood-retina-barrier
BSA	Bovine serum albumin
C:N	Cytoplasm-Nucleus
C. jacchus	*Callithrix jacchus*
cDNA	Complementary DNA
CNV	Central nervous system
CNV	Choroidal neovascularization
COL4A2	Collagen Typ IV, α2
C_T	Cycle Threshold
CTSB	Cathepsin B
DCF	2′,7′-dichlorofluorescein
DEPC	Diethyl dicarbonate
DJ1	Parkinson disease 7/DJ1
DMEM	Dulbecco's modified Eagle's medium
DMSO	Dimethyl sulfoxide
DNA	Deoxyribonucleic acid
dNTP	Deoxyribonucleoside triphosphates
DTT	Dithiothreitol
EA	Enrichment analysis
EDTA	Ethylenediaminetetraacetic acid
EMT	Epithelial-mesenchymal transition
FACS	Fluorescence-activated cell sorting
FCS	Fetal Calve Serum
FDA	U.S. Food and Drug Administration

FDR	False Discovery Rate
FMOD	Fibromodulin
FRET	Förster resonance energy transfer
FSC-H	Forward scatter height
FU	Fluorescence unit
gaAMD	AMD with geographic atrophy
GAPDH	glycerinaldehyde-3-phosphate-Dehydrogenase
GCL	Retinal ganglion cell layer
GCLC	Glutamate-cysteine ligase catalytic subunit
GCLM	Glutamate-cysteine ligase regulatory subunit
GLUT	Glutamate transporters
GOI	Gene of interest
GSEA	Gene Set Enrichment Analysis
H_2DCFDA	Dichlordihydrofluorescein-diacetat
HBSS	Hanks' Balanced Salt Solution
HCl	Hydrochloric acid
HEPES	4-(2-hydroxyethyl)-1-piperazineethanesulfonic acid
HMOX1	Heme oxygenase (decycling) 1
HRP	Horseradish peroxidase
HSP	Heat-shock protein
HUVEC	Human Umbilical Vein Endothelial Cells
IL	Interleukin
INL	Inner nuclear layer
IPL	Inner plexiform layer
JAK	Janus Kinase
LUM	Lumican
MDM2	Mouse double minute 2 homolog
$MgCl_2$	Magnesium chloride
MTT	3-(4,5-Dimethylthiazol-2-yl)-2,5-Diphenyltetrazolium Bromide
NaCl	Sodium chloride
nAMD	Neovascular AMD
NaN_3	Sodium acide
NES	Normalized Enrichment Score
NFL	Nerve fiber layer

NGS	Next Generation Sequencing
NID1	Nidogen 1
NOX4	Nicotinamide adenine dinucleotide phosphate oxidase 4
NRP1	Neuropilin 1
ONL	Outer nuclear layer
OPL	Outer plexiform layer
OS	Outer segment
P/S	Penicillin/Streptomycin
*p*19ARF	ARF tumor suppressor
PBS	Phosphate Buffered Saline
PC	Principal components
PCA	Principle component analysis
PCR	Polymerase chain reaction
PDGF	Platelet-derived growth factor
PE	Phycoerythrin
PEDF	Pigment epithelium-derived growth factor
PFA	Paraformaldehyde
PGF	Placental growth factor
PLD2	Phospholipase D2
POI	Protein of interest
POS	Photoreceptor outer segments
ppRPE	Primary porcine RPE
PRDX	Peroxiredoxin
PVDF	Polyvinylidene fluoride
qRT-PCR	Quantitative Real-Time-PCR
rCTSB	Recombinant Cathepsin B
RIN	RNA integrity number
RNA	Ribonucleic acid
ROS	Reactive oxygen species
RPE	Retinal pigment epithelium
RPKM	Reads per kilobase million
rSNCB	Recombinant β-Synuclein
RT	Reverse transcriptase
S. scrofa	*Sus scrofa domesticus*

SA β-gal	Senescence-associated β-galactosidase
SDS	Sodium dodecyl sulfate
SDS-PAGE	SDS-polyacrylamide gel electrophoresis
SNCA	α-Synuclein
SNCB	β-Synuclein
SOD	Superoxide dismutase
SSC-A	Side scatter area
SSC-H	Side scatter height
STAT	Signal transducer and activator of transcription
STAT3	Signal Transducers and Activators of Transcription 3
STC1	Stanniocalcin 1
TBP	TATA-binding protein
TBS	Tris-buffered saline
TBST	Tris-buffered saline with tween
TE	Tris-EDTA buffer
TEMED	Tetramethylethylenediamine
tert-BHP	*Tert*-butylhydroperoxide
TGFβ	Transforming growth factor β
THBS1	Thrombospondin 1
TNFα	Tumor necrosis factor α
Tris	Tris base
TSchG	Tierschutzgesetz (German Animal Protection Law)
TUNEL	Terminal deoxynucleotidyl transferase dUTP nick end labeling
VEGF	Vascular endothelial growth factor
VEGFB	Vascular endothelial growth factor B
VEGFR	Vascular endothelial growth factor receptor
w/o	Without
X-Gmean	Geometric mean
XBP1	X-box binding protein 1
ZO	Zonulae occludents

List of figures

List of tables

Summary

The work presented here addresses the topographic differential analysis and function of the age-related protein expression in the retinal pigment epithelium (RPE) of *Callithrix jacchus* (*C. jacchus*). The modern medicine is responsible for an increased life span, with an increase of approximately three years in every generation with no evidence of an impending limit. The healthy, physiological cellular aging process is often accompanied by age-related dysfunctions which can lead to pathologies and affects many organs, including the eye. The conversion from the physiological aging process into a severe pathology is not fully understood.

During the aging process of the eye, morphological as well as molecular changes in the retina as well as in the RPE can be observed. On a morphological basis, alterations occur in the intracellular granules in the RPE, including a decrease of unoccupied space in the cytoplasm of RPE cells, a lipofuscin redistribution by degranulation and enlargement and thickening of the RPE cell area. Additionally, the efficiency of some of the RPE functions, due to increased oxidative stress, are affected. Oxidative stress refers to a progressive cellular damage caused by reactive oxygen species (ROS) leading to protein misfolding and functional disbalance during cellular senescence. RPE cells digest photoreceptor outer segments, that are endocytosed and fused with lysosomes to be degraded. In aged RPE cells, lysosomal degradation is impaired resulting in accumulation of lipofuscin and protein damage, however the proteasomal and autophagy protein clearance systems are not working as effectively as in young RPE cells. The misfolded proteins are moved via exocytosis outside of the RPE cells. This material might be involved in drusen formation together with chronic inflammation and inflammatory cells. Drusen are a typical clinical sign of age-related macular degeneration.

To understand the cellular mechanism of retinal aging, several analyses of the proteome of the retina in aging tissue were performed in the common marmoset *C. jacchus* and Sprague-Dawley rats to identify proteins for which the expression profiles are altered with maturation and aging.

In the presented work, the whole transcriptome and the comparative analysis with the whole proteome of the RPE in aging *C. jacchus* was studied. Topological aspects regarding macular and peripheral parts of the RPE were considered to study age-related alterations. The analysis of the transcriptome revealed nearly 1500 genes whose expression significantly differed between macula and periphery in aged tissue,

whereas only 114 genes were found to show such differences in neonatal tissue. Nearly 3000 genes are expressed significantly different in the neonatal macula versus the senile macula. These results are comparable with the proteomic data. Out of those data, the expression of several genes and proteins, including Nidogen 1, Thrombospondin 1 and Cathepsin B (CTSB), was analyzed and confirmed in further studies.

Additionally, the presented work deals with the functional characterization of selected proteins, which were found in the transcriptomal analysis and previous studies regarding the aging retina in. One of these proteins is β-synuclein (SNCB). As an antagonist of α-synuclein, its role in the neuronal system is partially investigated, but the role of SNCB in the aging RPE remains still unclear. Distinct age-related alterations of the topological and intracellular distribution of SNCB have been observed in the macula compared to periphery in the RPE of *C. jacchus*. In the macula, SNCB is mainly present in the cell membrane, whereas in the periphery it is mainly present in the cytoplasm and nucleus. For a functional characterization, ARPE-19 cells were incubated with recombinant SNCB. Decreased apoptosis rates, as well as an activation of the *p*53-pathway, promote senescence-related processes. Increased HMOX1 and NOX4 levels indicate an elevated oxidative stress and inflammatory response. The different distribution of SNCB in the primate RPE and alterations of cellular functions in SNCB-exposed cells promote its role in the aging RPE. The observation of an endorsed inflammatory response may indicate stress-related properties of SNCB.

During the transcriptome analysis, CTSB was detected as a gene upregulated in aged tissue of *C. jacchus*. As it is involved in many functions correlating with the cellular aging process, it gained further research interest in this study. Comparable to SNCB, the function of CTSB is well investigated, but its role in the aging RPE is unknown.

ARPE-19 cells exposed to recombinant CTSB show decreased cell viability and disrupted staining patterns of ZO-1 and Occludin, indicating a decreased integrity of intercellular tight junctions of RPE cells. Furthermore, a dose-depended alteration of the *p*53/MDM2 signaling cascade has been demonstrated. An elevated vascular endothelial growth factor expression indicates pro-angiogenic properties of recombinant CTSB-exposed RPE cells. ARPE-19 cells exposed to recombinant CTSB revealed alterations of relevant cellular conditions, like viability, intercellular tight junctions, and pro-angiogenic factors. Lastly, CTSB was introduced in a premature senescence model, to study the influence of CTSB on the RPE *in-vitro*. First, the

premature senescence model was established in ARPE-19 cells using *tert*-butylhydroperoxide (*tert*-BHP).

The activity of β-galactosidase as well as oxidation of nucleic acids and lipids increased, indicating early senescence of ARPE-19 cells. The viability of the cells showed little change, while proliferation, the level of ROS and phagocytosis rate are significantly affected. While *tert*-BHP reduced proliferation, it increased intracellular ROS level and phagocytosis rate. The phagocytosis rate is also significantly increased by the additive exposure to *tert*-BHP and CTSB compared to the untreated control, whereas the apoptosis, proliferation and ROS production were not altered by CTSB. The study shows that in the model used early cellular senescence can be induced *in-vitro*. Furthermore, CTSB seems to selectively influence the functional behavior of senescent ARPE-19 cells.

Summarized, this study gives a closer insight in the molecular aging process of the aging RPE in *C. jacchus* on gene as well as on protein level. By the number of genes whose expression differed significantly, one can conclude, that the macula is aging differently than the periphery, indicating that the functions of the single proteins involved in the aging process may differ between macula and periphery. Moreover, the functions of these proteins was mostly unclear. This study however gives an insight into the function of SNCB and CTSB in the (aging) RPE.

Zusammenfassung

Die vorliegende Arbeit befasst sich mit der topografischen Differentialanalyse und der Funktion der altersbedingten Proteinexpression im retinalen Pigmentepithel (RPE) von *Callithrix jacchus* (*C. jacchus*). Die moderne Medizin ist verantwortlich für eine höhere Lebenserwartung, welche in jeder Generation um ungefähr drei Jahre zunimmt, ohne Anzeichen einer bevorstehenden Limitierung. Der gesunde, physiologische zelluläre Alterungsprozess geht häufig mit altersbedingten Funktionsstörungen einher, welche zu Pathologien führen, die viele Organe, einschließlich des Auges, betreffen. Der Übergang vom physiologischen Alterungsprozess in eine Pathologie ist nicht vollständig verstanden.

Während des Alterungsprozesses des Auges können sowohl morphologische als auch molekularbiologische Veränderungen in der Retina sowie im RPE beobachtet werden. Morphologisch gesehen treten Veränderungen im intrazellulären Granulat des RPEs auf, einschließlich einer Abnahme des freien Raums im Zytoplasma von RPE-Zellen, einer Lipofuszin-Umverteilung durch Degranulation und Vergrößerung sowie Verdickung der RPE-Zellen. Darüber hinaus wird die Effizienz einiger RPE-Funktionen aufgrund von erhöhtem oxidativem Stress beeinträchtigt. Oxidativer Stress führt zu einer fortschreitende Zellschädigung, die durch reaktive Sauerstoffspezies (ROS) verursacht wird und zu Proteinfehlfaltung und Funktionsstörungen während der Zellalterung führt. RPE-Zellen verdauen Photorezeptoraußensegmente, welche endozytiert und mit abzubauenden Lysosomen fusioniert werden. In gealterten RPE-Zellen wird der lysosomale Abbau beeinträchtigt, was zu einer Anhäufung von Lipofuszin und falsch gefalteten Proteinen führt. Die Proteom- und Autophagie-Protein-Clearance-Systeme funktionieren jedoch nicht so effektiv wie in jungen RPE-Zellen. Die fehlgefalteten Proteine werden durch Exozytose aus den RPE-Zellen transportiert. Dieses Material kann zusammen mit chronischen Entzündungen und Entzündungszellen an der Bildung von Drusen beteiligt sein. Drusen sind ein typisches klinisches Zeichen einer altersbedingten Makuladegeneration.

Um den zellulären Mechanismus der Alterung der Retina zu verstehen, wurden mehrere Analysen des Proteoms der Netzhaut in alterndem Gewebe des Weißbüschelaffe *C. jacchus* und Sprague-Dawley-Ratten durchgeführt, um Proteine zu identifizieren, welche während des Alterungsprozesses signifikant unterschiedlich exprimiert werden.

In der vorliegenden Arbeit wurde das gesamte Transkriptom alternden RPEs von *C. jacchus* untersucht und ein Vergleich mit Daten aus Proteomanalysen durchgeführt. Topologische Aspekte in Bezug auf Makula und Peripherie des RPEs wurden hierbei berücksichtigt. Die Analyse des Transkriptoms ergab fast 1500 Gene, die in gealtertem RPE zwischen Makula und Peripherie signifikant unterschiedlich exprimiert werden, während in neugeborenem Gewebe nur 114 solcher Gene gefunden wurden. Nahezu 3.000 Gene sind in der neugeborenen Makula im Vergleich zur senilen Makula signifikant unterschiedlich exprimiert. Diese Ergebnisse sind mit den Daten aus der Proteom-Studie vergleichbar. Auf Grundlage diesen Daten wurde die Expression mehrerer Gene und Proteine, einschließlich Nidogen 1, Thrombospondin 1 und Cathepsin B (CTSB), analysiert und in weiteren Studien bestätigt.

Darüber hinaus befasst sich die vorgestellte Arbeit mit der funktionellen Charakterisierung ausgewählter Proteine, die in früheren Studien zur alternden Retina sowie in der Transkriptomanalyse gefunden wurden. Eines dieser Proteine ist β-Synuclein (SNCB). Als Antagonist von α-Synuclein wurde seine Rolle im neuronalen System teilweise untersucht, die Rolle der SNCB beim alternden RPE ist jedoch unklar. Im RPE von *C. jacchus* wurden deutliche altersbedingte und topografische Veränderungen der intrazellulären Verteilung von SNCB in der Makula und Peripherie gefunden. In der Makula wird SNCB hauptsächlich in der Zellmembran, in der Peripherie hauptsächlich im Zytoplasma und im Zellkern exprimiert.

Zur funktionellen Charakterisierung wurden ARPE-19-Zellen mit rekombinantem SNCB inkubiert. Eine verringerte Apoptoserate sowie eine Aktivierung des *p*53-Signalwegs in ARPE-19 Zellen fördern zelluläre Seneszenz. Erhöhte HMOX1- und NOX4-Spiegel deuten auf erhöhten oxidativen Stress und eine Entzündungsreaktion in ARPE-19-Zellen hin. Die unterschiedliche Verteilung von SNCB im Primaten-RPE und Veränderungen der Zellfunktionen in SNCB-exponierten Zellen zeigen dessen Rolle im alternden RPE. Die Beobachtung einer inflammatorischen Reaktion kann auf stressbedingte Eigenschaften der SNCB hinweisen.

Während der Transkriptomanalyse wurde eine erhöhte Expression von CTSB in Gewebe von senilen *C. jacchus* nachgewiesen. Da CTSB an einigen im Alterungsprozess relevanten Funktionen beteiligt ist, wurde seine Funktion in dieser Studie weitergehen untersucht. Verglichen mit SNCB ist die Funktion dieses Proteins gut untersucht, die Rolle von CTSB bei der Alterung von RPE ist jedoch nicht bekannt.

ARPE-19-Zellen, die rekombinantem CTSB ausgesetzt waren, zeigten eine verminderte Lebensfähigkeit und eine veränderte Expression von ZO-1 und Occludin, was auf eine Abnahme der Integrität von Tight Junctions der RPE-Zellen hindeutet. Darüber hinaus wurde eine Veränderung des *p*53-Signalweges gezeigt. Eine erhöhte Expression des vaskulären endothelialen Wachstumsfaktors zeigt die proangiogenen Eigenschaften von rekombinanten CTSB-exponierten RPE-Zellen. ARPE-19-Zellen, die rekombinanten CTSB ausgesetzt waren, zeigten Veränderungen von zellulärem Verhalten in der Lebensfähigkeit, Tight Junctions und proangiogenen Faktoren. Um den Einfluss von CTSB auf die RPE *in-vitro* zu untersuchen, wurde zunächst ein Modell der vorzeitigen Seneszenz eingeführt. Zunächst wurde dafür das Modell in ARPE-19-Zellen unter Verwendung von *tert*-Butylhydroperoxid (*tert*-BHP) etabliert.

Die Aktivität von β-Galaktosidase sowie die Oxidation von Nukleinsäuren und Lipiden nahmen zu, was auf eine frühe Seneszenz von ARPE-19-Zellen hinweist. Die Lebensfähigkeit der Zellen zeigte nur geringe Veränderungen, während die Proliferation, der Gehalt an ROS und die Phagozytoserate signifikant beeinflusst wurden. Während *tert*-BHP die Proliferation reduziert, erhöht es den intrazellulären ROS-Spiegel und die Phagozytoserate. Die Phagozytoserate wird auch durch die additive Exposition von *tert*-BHP und CTSB im Vergleich zur unbehandelten Kontrolle signifikant erhöht, wohingegen Apoptose, Proliferation und ROS-Produktion durch CTSB nicht verändert werden. Die Studie zeigt, dass in dem verwendeten Modell eine frühe zelluläre Seneszenz *in-vitro* induziert werden kann. Darüber hinaus scheint CTSB das Funktionsverhalten von seneszenten ARPE-19-Zellen selektiv zu beeinflussen.

Zusammenfassend gibt diese Studie einen genaueren Einblick in den molekularen Alterungsprozess des alternden RPE im *C. jacchus* sowohl auf Gen- als auch auf Proteinebene. Anhand der Anzahl signifikant unterschiedlich exprimierter Gene kann darauf geschlossen werden, dass die Makula anders altert als die Peripherie, was darauf hinweist, dass die Funktionen der einzelnen am Alterungsprozess beteiligten Proteine zwischen Makula und Peripherie unterschiedlich sein können. Darüber hinaus ist die Funktion der meisten dieser Proteine unklar. Diese Studie gibt einen Einblick in die Funktion von SNCB und CTSB im (alternden) RPE.

1 Introduction

1.1 The anatomy of the human eye

The human eye is one of the most complex organs in the human body. In addition to fat and connective tissue, the eye is embedded in the bony orbit consists essentially of the eyeball (with attached muscles) and optic nerve (*Nervus opticus*) as well as the complex blood and lymph vessels. A schematic diagram of the eye is shown in Figure 1. The subdivision of the posterior part is described in section 1.1.1.

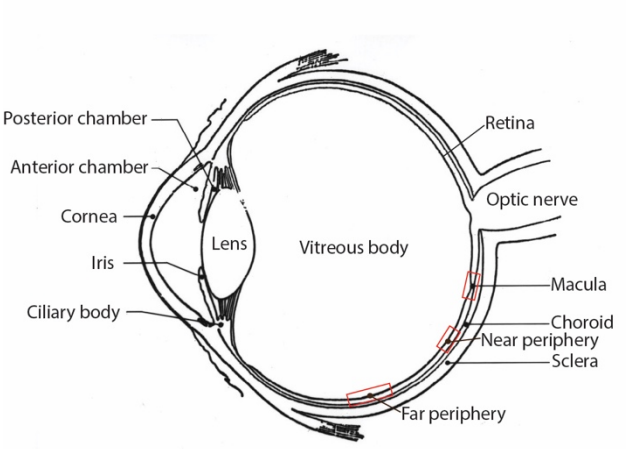

Figure 1 Anatomy of the human eye

A schematic diagram of the human eye. The eye can be subdivided into two major parts, the anterior and the posterior part. The posterior part can be subdivided into three parts: the macula, the near periphery and the far periphery (Image modified Unk, 2014).

The outer part of the eye is formed by the cornea and the sclera. In the area of the cornea, incoming light is refracted and transmitted through the anterior chamber, lens and vitreous to the retina. In addition, the cornea acts as a barrier against pathogens and structural damage, so that internal parts of the eye remain protected. The adult sclera, which consists of connective tissue fibers, withstands external and internal pressures, and is mainly responsible for shaping the eyeball. The eye is divided into the anterior segment of the eye (anterior chamber, iris, ciliary body and posterior chamber), and the posterior segment of the eye, consisting of the vitreous body, neuroretina, the retinal pigment epithelium (RPE) and the choroid. The posterior inner segment of the eye is formed by the multi-layered retina. The retina consists of the neuroretina and the single-layered RPE. The retina and the RPE form a part of the blood-retina-barrier (BRB). The BRB is subdivided into the inner BRB and outer BRB. The inner BRB is established by the tight junctions (zonulae occludents; ZO) between

neighboring retinal endothelial cells (Shakib and Cunha-Vaz, 1966). The outer BRB is established by the ZOs between neighboring RPE cells (Peyman and Bok, 1972). Two major ocular diseases, diabetic retinopathy and age-related macular degeneration (AMD), are directly associated with alterations of the BRB.

1.1.1 The anatomy of the retina

The retina is the innermost of the three layers of the posterior segment of the eye. The light, which strikes the retina, initiates a cascade of electrical and chemical events. As a part of the central nervous system (CNS) the retina can be considered brain tissue. It is the only part of the CNS that can be visualized non-invasively (Dowling, 1987). The retina consists of several layers: the nerve fiber layer (NFL), retinal ganglion cell layer (GCL), inner plexiform layer (IPL), inner nuclear layer (INL), outer plexiform layer (OPL), outer nuclear layer (ONL), the outer segment (OS), and the RPE (Trepel, 2008). The region where the optic nerves passed through the retina is called optic disk or optic nerve head. A schematic diagram of the retina-RPE complex is shown in Figure 2.

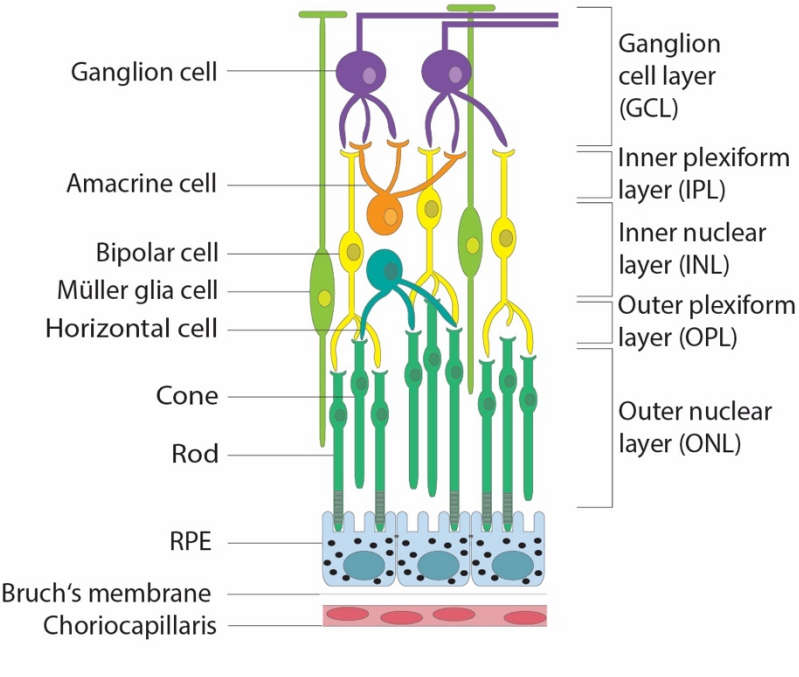

Figure 2 Structure of the retina

Diagram of the neural circuit of the retina, showing the six neuronal cell types and the two supporting cell types (Müller glia and retinal pigmented epithelium). The diagram shows the GCL, IPL, INL, OPL, ONL, RPE. Abbreviations: GCL: retinal ganglion cell layer; IPL: Inner plexiform layer; INL: Inner nuclear layer; OPL: outer plexiform layer; ONL: outer nuclear layer; RPE: retinal pigment epithelium (modified after Gramage et al., 2014)

The human macula is an oval-shaped pigmented area temporal of the optic nerve head. It consists of the perifovea, the parafovea and the fovea, which is also called

"clinical macula". The parafovea has the highest density of cones in the whole retina. The fovea is responsible for sharp central vision which is also named foveal vision (Iwasaki and Inomata, 1986). In contrast, the peripheral vision is slow and blurry (Strasburger et al., 2011). Within the fovea, an avascular zone, the foveal avascular zone is located, whereas the rest of the retina is vascularized. In the macula, the cell layers of GCL, IPL and INL are significantly reduced. This leads to the formation of the characteristic pit form of the macula. In the following Figure 3, a fundoscopy of a healthy eye with the most important characteristics is shown (A). In the histological overview, the layers of the retina are visible. Also, the reduced thickness in the pit of the GCL, IPL and INL is shown (B). The layers also presentable in an optical coherence tomography of the retina (C). The light absorption is enhanced in the macula compared to the periphery. This results in an increased energy metabolism of the cells in the retina (Wong-Riley, 2010). The macula is only present in some mammalian eyes. It is present in human eyes as well as in eyes of various monkeys, but not in rodents like mice or rats.

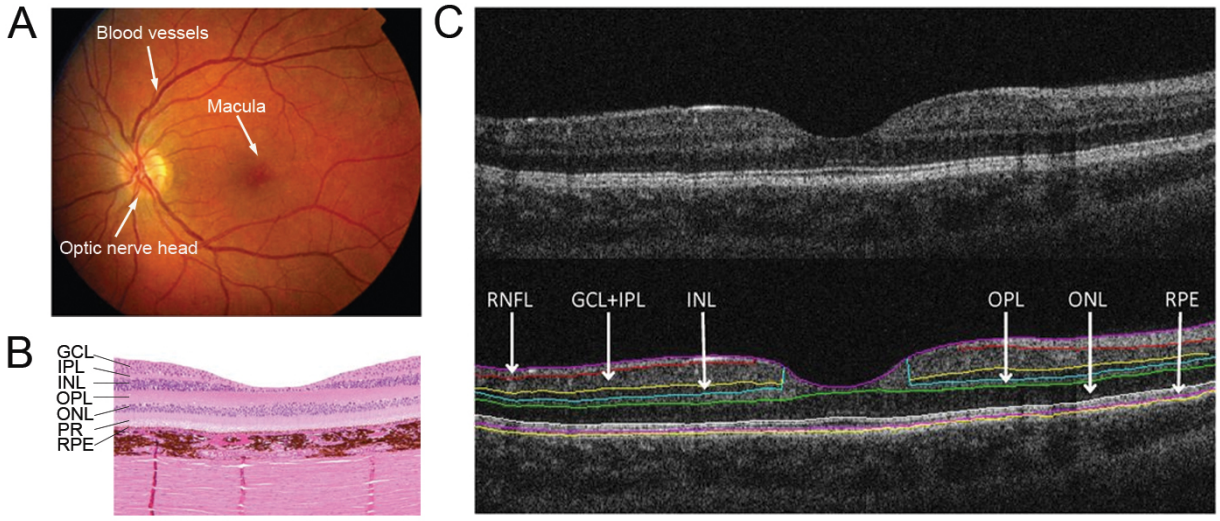

Figure 3 Different representations of the macula

(A) Fundoscopy of a healthy human eye (modified after (Herbort et al., 2011)) (B) Healthy macula in a Hematoxylin-eosin staining (modified from (Elmore et al., 2015)) (C) Macular OCT image: The image of a healthy macula (adapted from (Szigeti et al., 2015)) The layers of the retina are visible in the HE-stain as well as in the OCT scan. Abbreviations: GCL: retinal ganglion cell layer; IPL: Inner plexiform layer; INL: Inner nuclear layer; OPL: outer plexiform layer; ONL: outer nuclear layer; PR: Photoreceptors; RPE: retinal pigment epithelium; RNFL: Retinal nerve fiber layer

1.1.2 The retinal pigment epithelium

The RPE is a monolayer of melanin containing cells. The apical membrane faces the photoreceptor outer segments, whereas the basolateral membrane faces Bruch's membrane. The long apical microvilli surround the light-sensitive outer segments establishing a complex of close structural interaction. The Bruch's membrane separated the RPE from the fenestrated endothelium of the choriocapillaris (Bok, 1993). The RPE has various functions. The most important functions are summarized in Figure 4.

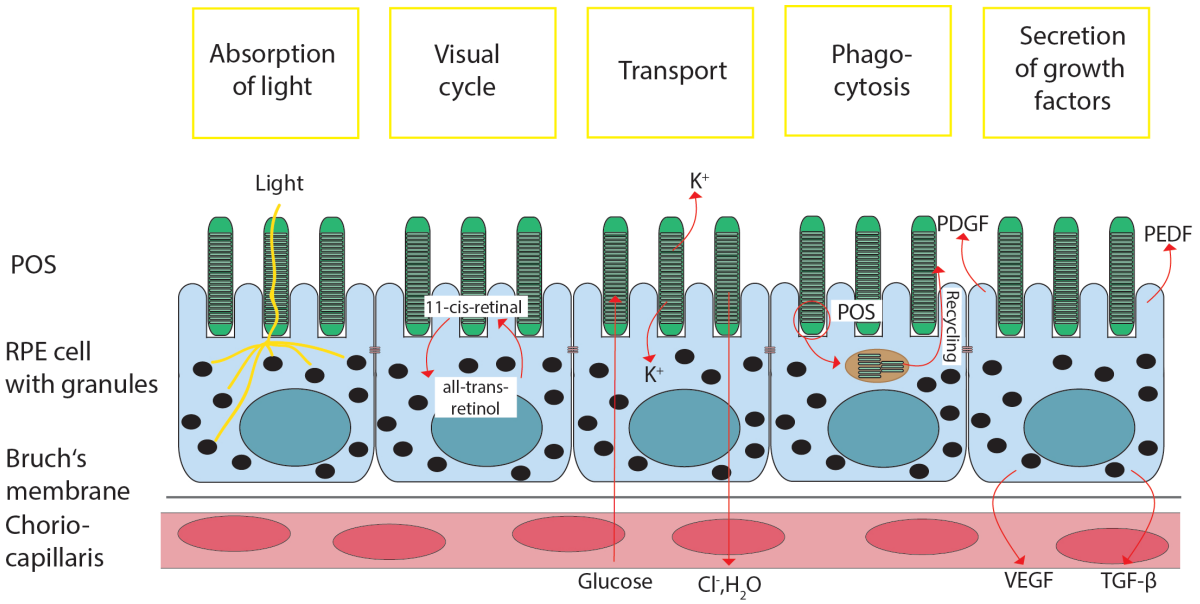

Figure 4 Summary of the functions of the retinal pigment epithelium.

Abbreviations: POS: Photoreceptor outer segments; RPE: Retinal pigment epithelium; PDGF: Platelet-derived growth factor; PEDF: pigment epithelium-derived growth factor; VEGF: vascular epithelium growth factor; TGFβ: Transforming growth factor-β. (modified after Strauss, 2005)

1.1.2.1 Absorption of light and protection

The cells of the RPE contain dark pigment granules, including melanosomes, blue light absorbing pigments and lipofuscin, which function like a wall to cover the inner bulbus with absorbing the scattered light. Besides protection of the inner bulbus from scattered light, the pigmentation is also essential for maintaining visual function as a part of the visual cycle. Additionally, the outer retina is exposed to an oxygen-rich environment. The blood perfusion of the choriocapillaris is very high (1400 ml/(min*100 g tissue)) (Alm and Bill, 1972; Alm and Bill, 1973) and it is proposed that the retina floats on the choriocapillaris, which allows photo-oxidation and subsequent oxidative damage. This

photo-oxidative activity is increased by the load of reactive oxygen species produced by phagocytosis of shed photoreceptor outer segments (Miceli et al., 1994).

The RPE has several protection mechanisms against damage from oxidative stress and toxins (Boulton and Dayhaw-Barker, 2001). The first line of defense is defined as absorption and filtering of light. For this purpose, the RPE contains a composition of various pigments that are specialized to different wavelengths and the special wavelength-dependent risks (Beatty et al., 2000). In general, light absorption is performed by melanin in melanosomes. Blue light appears to be more stressful for RPE cells in the adult eye because it permits the photo-oxidation of lipofuscin components to cell toxic substances (Ben-Shabat et al., 2001; Rozanowska et al., 1995; Rozanowska et al., 2002; Sparrow and Cai, 2001). It is absorbed by blue light absorbing pigments. However, the melanosomes and blue light absorbing pigments are only responsible for the absorption of about 60 % of light energy (Boulton, 1991). One of the pigments responsible for the absorption of the remaining 40 %, is lipofuscin. Lipofuscin accumulates in RPE cells during life and seems to reach toxic concentrations in older eyes (Delori et al., 2001). The next protection mechanism is performed by antioxidants including the enzyme superoxide dismutase (SOD) as well as some catalases. The RPE also accumulates carotenoids, like lutein and zeaxanthin (Beatty et al., 2000). A third line of protection is the cell's physiological ability to repair damaged DNA, lipids, and proteins.

As mentioned, the concentration of lipofuscin increases with age. The reduction in cell density, while the RPE is still intact, may result from apoptosis, which is caused by accumulation of toxic substances. Additionally, age leads to changes in pigmentation, including a reduction of melanosomes (Feeney, 1978; Feeney-Burns et al., 1984; Weiter et al., 1986). The increased amount of reactive oxygen species (ROS) destabilizes intracellular membrane compartments, resulting in reduced metabolic efficiency and the production of more lipofuscin and ROS.

1.1.2.2 Transepithelial transport

The RPE also transports nutrients and ions between photoreceptors and the choriocapillaris. The transepithelial transport can be distinguished between transport from the outer retina to the choriocapillaris and the transport from the choriocapillaris to the outer retina.

The RPE transports glucose and other nutrients from the choriocapillaris to the photoreceptors. To transport glucose, the RPE needs a high amount of glucose

transporters in both the apical and the basolateral membranes. The glutamate transporters GLUT1 as well as GLUT3 are highly expressed in the RPE (Ban and Rizzolo, 2000). GLUT3 mediates the basic glucose transport while GLUT1 is responsible for inducible glucose transport in response to mitogens or oncogenes, which means, it can adapt glucose transport to different metabolic demands. Another important function of the RPE is the transport of retinol to ensure the supply of retinal to the photoreceptors. The retinal is exchanged between RPE and photoreceptors during the visual cycle in which all-*trans*-retinol is taken up from photoreceptors, isomerized to 11-*cis*-retinal (Baehr et al., 2003), and redelivered to photoreceptors.

1.1.2.3 Ion Buffering

The RPE not only stabilizes the ion homeostasis in the subretinal space by transepithelial transport of ions, but it is also able to compensate for fast occurring changes in the ion composition in the subretinal space (Steinberg, 1985).

1.1.2.4 Phagocytosis

The photoreceptors contain high amounts of photosensitive molecules. As already mentioned, photoreceptors are exposed to intense levels of light. This leads to accumulation of photo-damaged proteins and lipids. In addition, retinal itself can generate photo-oxidative radicals. During each day, the concentration of light-induced toxic substances increases inside the photoreceptors (Beatty et al., 2000). The light transduction is dependent on the proper function and structure of the involved proteins, the retinal, and the membranes. To maintain the excitability of photoreceptors, the photoreceptor outer segments (POS) undergo a constant renewal process (Bok, 1993; Bok and Hall, 1971; Hall et al., 1969; Nguyen-Legros and Hicks, 2000; Young, 1967). The POS are newly built from the base of outer segments, whereas the highest concentration of radicals, photo-damaged proteins, and lipids is present in the tips. A balance between POS tip shedding and formation of new POS needs to be maintained to ensure a constant length of the POS. The shed of the POS is phagocytosed by the RPE.

1.1.2.5 Secretion of growth factors

The RPE closely interacts with photoreceptors on one side as well as with endothelial cells and cells of the immune system on the choroid side. In order to communicate with the neighboring tissues, the RPE can secrete a variety of factors as well as signaling molecules. The includes the transforming growth factor β (TGFβ) (Kvanta, 1994;

Tanihara et al., 1993), platelet-derived growth factor (PDGF) (Campochiaro et al., 1994; Campochiaro et al., 1989), vascular endothelial growth factor (VEGF) (Adamis et al., 1993; Witmer et al., 2003) and pigment epithelium-derived factor (PEDF) (Dawson et al., 1999; King and Suzuma, 2000). In the healthy eye, some of these factors are constantly released and help to maintain the structural integrity of the neighboring tissues. PEDF helps to maintain the retinal as well as the choriocapillaris structure and it was described to be neuroprotective and antiangiogenic (Cao et al., 2001; Dawson et al., 1999; King and Suzuma, 2000). Another vasoactive factor made in the RPE is VEGF, which is secreted in low concentrations by the RPE in the healthy eye (Adamis et al., 1993) where it prevents endothelial cell apoptosis and is essential for an intact endothelium of the choriocapillaris (Burns and Hartz, 1992). VEGF also acts as a permeability factor stabilizing the fenestrations of the endothelium (Roberts and Palade, 1995). Other factors are activated when the RPE is exposed to pathological conditions, e.g. hypoxia and metabolic stress. If the regulation of secretion fails under certain pathologies, the RPE will promote diseases such as choroidal neovascularization.

1.2 Aging in the neuronal system

The modern medicine increases the life span. Recently it was shown that the human lifespans are increasing by approximately three years every generation with no evidence of an impending limit (Zuo et al., 2018). But the normal, healthy aging process is often accompanied by various age-related dysfunctions, which affect many organs, including the eye.

The physiological aging process leads to alterations in the CNS, including an age-related cognitive decline and an increased appearance of neurodegenerative diseases (Bishop et al., 2010). Whereas “age” is known to be a strong cause of these conditions, the molecular mechanisms leading to the natural age-related neuronal deterioration are not well understood. The maintenance of the physiological functions with age are dependent on a response to cellular stresses, including DNA damage, loss of protein homeostasis, mitochondria dysfunction, autophagy impairment and loss of cytoskeletal integrity.

1.2.1 The aging eye

During aging process, various structures of the eye are affected. As the lens protein α-crystallin decreases with age in the human lens, there is a steady increase in the stiffness of the lens center and this loss of elasticity may account for the loss of accommodation and hence presbyopia (Glasser and Campbell, 1999). Finally, the crystallins lose transparency which leads to cataracts, a major cause of blindness worldwide. It was suggested, oxidative stress may have an important pathogenic role in the development of senile cataracts (Canadananovic et al., 2015).

1.2.1.1 The aging retina

Because of their function, retinal cells are exposed to a large amount of light throughout their lifetime, making them vulnerable to photo-induced damage. Psychophysical studies have reported age-associated declines in e.g. visual acuity and dark adaption thresholds (Weale, 1975). In the aged eye, the macular recovery after light stress is slower, potentially due to reduced efficiency of photopigment restoration (Messenio et al., 2013). This function loss might be associated with age-related structural changes, including the loss of retinal neurons (Curcio et al., 1993), RGCs (Gao and Hollyfield, 1992) and bipolar cells (Aggarwal et al., 2007). Beyond loss of retinal cells, aging is also associated with accumulation of both intracellular and extracellular deposits. However, the molecular mechanisms underlying physiological aging, which might be connected to pathologic alterations, are not well known. The cellular diversity in the retina containing over 70 subtypes is very high (Masland, 2001). The major neuronal cell types in the retina performs different functions. Amacrine, bipolar, and horizontal cells process the visual input, retinal ganglion cells transmit information to the brain (Sanes and Zipursky, 2010). During aging, the thickness of the macula decreases (Eriksson and Alm, 2009; Leung et al., 2012). The number of retinal ganglion cells and photoreceptor cells slightly declines during age, but the number of dendritic arbors of retinal ganglion cells decreases in the aged retina, explaining the changes that occur at the protein level (Samuel et al., 2011). Therefore, a detailed molecular analysis of aging is very complex.

1.2.1.2 Aging in the retinal pigment epithelium

During the aging process of the eye, morphological as well as molecular biological changes can be observed.

On a morphological basis, alterations of the intracellular granules in the RPE of postmortem human eyes were described (Ach et al., 2015; Feeney-Burns et al., 1984), including a decrease of unoccupied space in the cytoplasm of RPE cells (Feeney-Burns et al., 1984). Additionally, Ach et al. reported a lipofuscin redistribution by degranulation and aggregation in the aged human RPE, including an enlargement and thickening of the RPE cell area, the conversion from convex to irregular or concave polygons, and cytoskeleton derangement (Ach et al., 2015).

During the physiological aging process, the efficiency of some of the RPE functions described in 1.1.2 are affected. This is due to enhanced oxidative stress. Oxidative stress refers to a progressive cellular damage caused by ROS leading to protein misfolding and functional disbalance during RPE cellular senescence. The phagocytosis of POS by the RPE cells generates oxidative stress caused by ROS (Tate et al., 1995). Additionally, a high oxygen consumption and a prolonged exposure to light increases the oxidative stress to RPE cells (Beatty et al., 2000). A possible explanation for the degeneration of RPE cells is an age-related protein degradation and metabolic insufficiency. Besides the lysosomal uptake of POS, materials such as lipofuscin accumulates in the RPE cells. Although most of intracellular lipofuscin is located in the lysosomes, after inhibition of the autophagy pathway, it can accumulate also in the cytosol within the lysosomes (Hohn and Grune, 2013). Lysosomal lipofuscin appears to impair the autophagy and lysosomal degradation, resulting in increased ROS generation, protein oxidation, further aggregation, and further lipofuscin formation (Terman and Brunk, 2004). The survival of RPE cells is dependent on the removal of misfolded proteins from the cytoplasm. Several mechanisms are known to destroy aggregated proteins. First, heat-shock proteins (HSPs) work as molecular chaperones and induce the repair of misfolded proteins to prevent harmful protein aggregation (Hartl, 1996; Hartl and Hayer-Hartl, 2002). If this process is not successful, potentially toxic proteins are targeted to the proteasome machinery for degradation. Misfolded proteins are tagged with a small polypeptide ubiquitin. Polypeptide ubiquitin directs the complex to the ubiquitin/proteasomal protein degradation pathway. Other findings reveal that there is a crosstalk between HSPs, proteasomes and autophagy in the regulation of protein aggregation in RPE cells (Kaarniranta et al., 2010; Ryhanen et al., 2009). Another protein involved in the uptake of protein aggregates is *p*62. The *p*62 is a multifunctional protein adapter that has many roles in cell signaling, transcription regulation, receptor internalization and protein turnover. It is one of the most important

molecules regulating the packing and transporting of ubiquitinated, misfolded and aggregated proteins for clearance via autophagy in mammalian cells (Bjorkoy et al., 2006). The aggregated protein material is exocytosed and might be involved in the formation of chronic inflammation and the immigration of inflammatory cells like dendritic cells and macrophages. Furthermore, the material might be involved in the formation accumulation of extracellular deposits, called drusen, between the RPE and Bruch's membrane (Anderson et al., 2002). Drusen are a typical clinical sign of AMD and usually appear during all stages of the disease (Ambati et al., 2003).

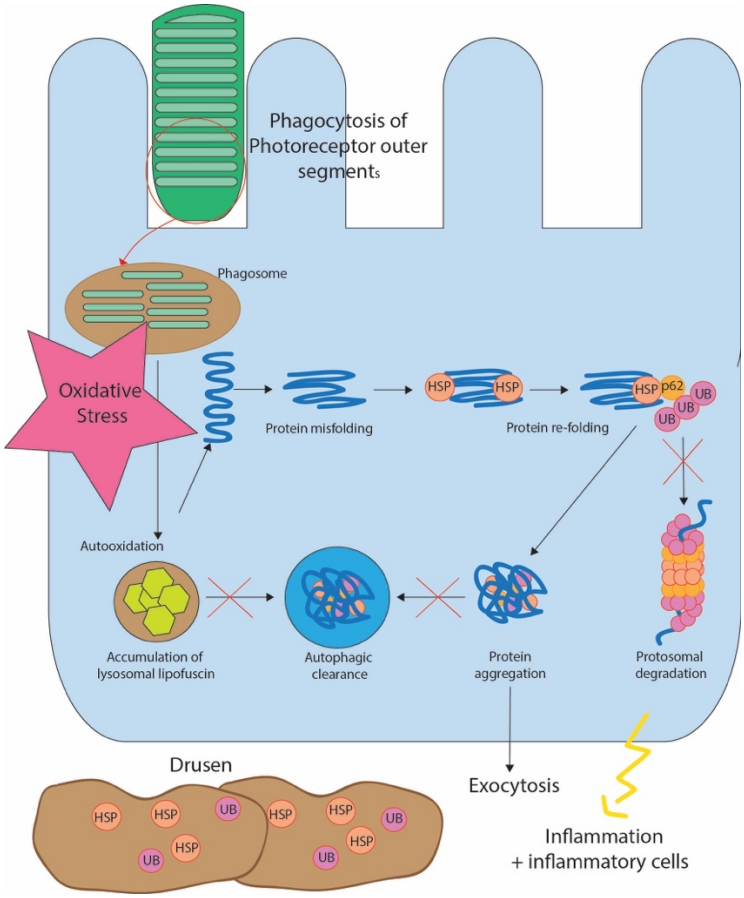

Figure 5 Schematic representation of protein aggregation in aged RPE cells

RPE cells digest POS that are endocytosed and fused with lysosomes to be degraded. In aged RPE cells, lysosomal degradation is impaired resulting in accumulation of lipofuscin, increasing oxidative stress and protein damage. HSP attempt to repair formed protein damages, but this process is estimated to be disturbed in aged cells. Simultaneously, proteasomal and autophagy protein clearance systems are not working as effectively as in young RPE cells. Thus, the efficiency of central proteolytic machines is impaired in aged cells; proteins are apparently moved via exocytosis to the outside of the RPE cells. This material might be involved in drusen formation together with chronic inflammation and inflammatory cells. (Adapted and modified from Kinnunen et al., 2012). Abbreviations: RPE: Retinal pigment epithelium; HSP: Heat shock protein; UB: Ubiquitin

1.2.1.2.1 Proteomal changes in the aging retina and RPE

To understand the cellular mechanism of retinal aging, several analyses of the proteome of the retina in aging tissue were performed. Recently, Böhm et al. performed a comparative proteomic analysis of the retinas in the common marmoset *Callithrix jacchus* (*C. jacchus*) and Sprague-Dawley rats to identify proteins for which the expression profiles are altered with maturation and aging (Böhm et al., 2013). Four proteins common in both species were found to be expressed differently in age tissue: Parkinson disease 7/DJ1, stathmin, peroxiredoxin (PRX), and β-synuclein (SNCB). This study was the first to provide evidence that the retina is physiologically characterized by specific lifelong changes in its proteome. These changes are independent of whether the retina bears a macula (Böhm et al., 2013). Additionally, those proteins are regulated in the primary somatosensory cortex and primary visual cortex of rats. Whereas the expression of PRX remains unchanged over lifetime, SNCB and DJ1 are massively increased, and stathmin is significantly reduced during lifetime (Böhm et al., 2015). Ethen et al. performed examinations of the proteome of human donor eyes with progression of AMD and found 26 proteins that showed changes at disease onset or with progression and at end-stage disease (Ethen et al., 2006), These proteins are involved in key functional pathways, such as microtubule regulation and protection from stress-induced protein unfolding. Approximately 60% of the proteins exhibited changes specific to either the macula or periphery, with the remaining 40% changing in both regions (Ethen et al., 2006). By comparing the central and peripheral parts of the retina of adult monkey eyes (*Macaca fascicularis*), Okamoto et al. identified 5 proteins (Arrestin-c, α-synuclein (SNCA), epidermal fatty acid binding protein, tropomyosin 1α chain, and heterogeneous nuclear ribonucleoproteins A2/B1) that were significantly higher expressed in the macula than in the periphery of the retina (Okamoto et al., 2010).

1.2.1.3 Animal models for aging

In addition to their phenotypical similarities, the genetic homology between humans and non-human primates is above 93 % (Tatsumoto et al., 2013). As a result, they may provide the best opportunity to study the actual mechanisms that lead to the age-related decline seen universally across species. In biomedical research, primate models were extensively used for research for diseases as well as the development of vaccinations, and advancements in organ transplant technology (Phillips et al., 2014). A contribution has been made between two commonly used nonhuman primate

species: Old World rhesus monkey and the New World marmoset. Old World monkeys originate from Africa and Asia and consists of at least 132 species, including baboons and macaques. New World monkeys originate from South America and are commonly divided into two families; the *Callitricidae* and the *Cebidae*. *Callitricidae* are the most primitive group of New World monkeys and include marmosets and tamarins. The *Cebidae* are larger and are the only monkeys with a prehensile tail. Squirrel monkeys and capuchins are two examples of monkeys in this family (Mattison and Vaughan, 2017).

One model for aging research is the common marmoset *C. jacchus*. It is a New World primate with an average lifespan of 5 to 8 years in captivity and maximum of 16.5 years in the wild. With a compressed lifespan in comparison to rhesus, marmosets are fully mature by about 2 years of age and considered aged by 8 years (Abbott et al., 2003). Marmosets are small, averaging only 350 to 400 g as adults. They live in multi-generational family units, which allows them to be easily maintained in social housing in the laboratory setting. Marmosets experience age-related pathology similar to humans. These include cancer, diabetes, chronic renal disease, and amyloidosis (Mattison and Vaughan, 2017). Due to its small size, low risk of zoonotic disease risk, reproductive efficiency, and relatively low cost to maintain in a laboratory, marmosets are becoming the preferred non-human primate for biomedical testing (Mattison and Vaughan, 2017). At 6 years of age (Abbott et al., 2003), marmosets are aged and experiencing fibrous changes in the intra-articular discs, β-amyloid deposition, reduced neurogenesis, renal pathology, weight loss, increased insulin resistance, and increased incidence of neoplasia (Tardif et al., 2011). In several non- human primates, forms of AMD have been investigated, including rhesus monkeys and cynomolgus macaques (*Macacca fascicularis*). Background findings, including drusen, were reported in 7.3 % of 1829 examined cynomolgus macaques (Pennesi et al., 2012). In contrast, only 1.2 % of 488 examined *C. jacchus* showed fundus alterations (Luetjens and Bluemel, 2015). As described in a review by Mattison and Vaughan, the common marmosets are described as a valuable model for the research in aging (Mattison and Vaughan, 2017).

1.3 Age-related macular degeneration

The importance of the understanding of the physiological aging process is underlined by the presence of AMD, which is already the leading cause of irreversible blindness

among the elderly in industrialized nations, promises to be an even greater toll with the imminent demographic right-shift (Ambati et al., 2003). In the following Figure 6, the risk factors for the development of AMD are displayed.

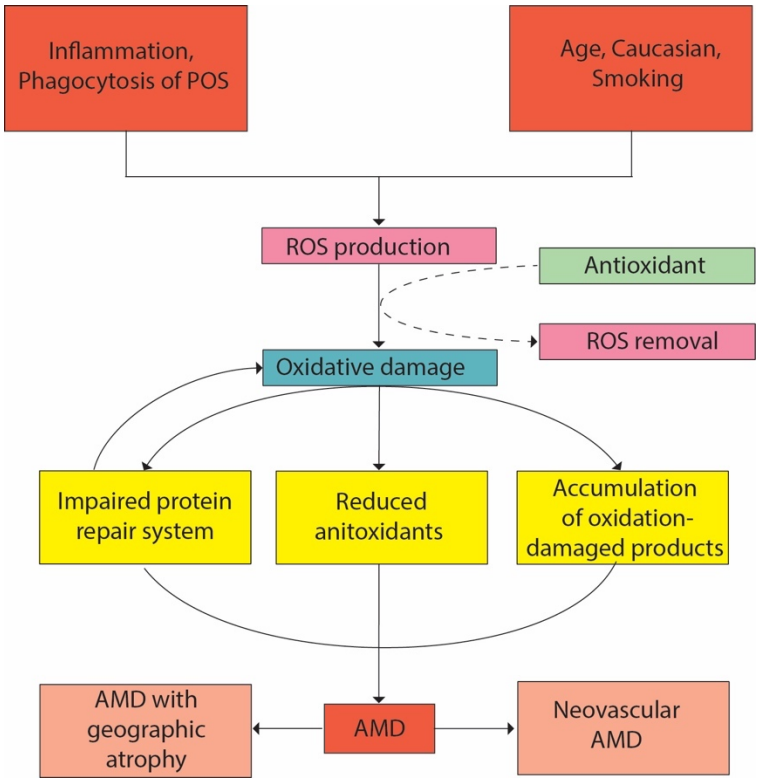

Figure 6 Risk factors for the development of age-related macular degeneration

Besides biological factors like inflammation and the phagocytosis of POS, social factors like age, ethnicity and smoking behavior are risk factors for the development of AMD. They lead to an increased oxidative damage, followed by an impaired protein repair system, reduced antioxidants and an accumulation of oxidation-damaged products, followed by a possible development of AMD. (Adapted and modified from Arslan et al., 2019) Abbreviations: POS: photoreceptor outer segments; AMD: age-related macular degeneration

Drusen are morphologically classified either as hard or soft deposits. In small numbers, they are not considered risk factors for the development of AMD, (Sarks et al., 1999) but numerous hard drusen are an independent risk factor for visual loss from AMD (Maguire et al., 1997). Soft drusen generally are larger and have indistinct edges with a tendency to become confluent. Typically, drusen are clustered in the central macula. Drusen alone do not account for a significant vision loss, however they can lead to deficits in macula function, including color contrast sensitivity, central visual field sensitivity, and spatiotemporal sensitivity (Midena et al., 1997; Stangos et al., 1995; Sunness et al., 1988; Tolentino et al., 1994).

Another clinical sign of AMD is geographic atrophy. Geographic atrophy refers to confluent areas of RPE cells death together with overlying photoreceptor atrophy (Green and Key, 1977). The visible atrophy is usually accompanied by atrophic

underlying choriocapillaris (McLeod et al., 2002) and large areas of atrophy reveal underlying choroidal blood vessels. Because the photoreceptors overlying areas of RPE atrophy are metabolically dependent on RPE cells, the geographic atrophy leads to gradual progression of visual loss (Duvall and Tso, 1985). A third clinical sign of AMD is choroidal neovascularization (CNV). CNV refers to the growth of new blood vessels from the choroid. In AMD, these vessels may remain beneath the RPE, or breach the RPE and enter the subretinal space. AMD is classified into neovascular AMD (nAMD; formerly: *wet* AMD), and AMD with geographic atrophy (gaAMD; formerly: *dry* AMD) (Ferris et al., 2013).

As described in 1.2.1.2, the appearance of drusen is a clinical hallmark of gaAMD (Gass, 1972). For patients with gaAMD, no treatment is available so far. The clinical manifestation of nAMD results from an upregulation of pro-inflammatory and angiogenic cytokines, including VEGF (Andreoli and Miller, 2007). VEGF is an important signaling protein involved in angiogenesis. In nAMD, blood vessels grow from the choroid into the subretinal or sub-RPE space (Miller, 2013). Two different types of agents against VEGF are approved by the U.S. Food and Drug Administration (FDA) so far, Ranibizumaba and Aflibercept, whereas Bevacizumab us used off-label to treat nAMD.

Figure 7 shows a schematic overview of the VEGF pathways and its inhibitors used for treatment against nAMD**.** The VEGF-related molecules placental growth factor (PGF) and VEGFB bind selectively to VEGFR-1, while VEGF binds VEGFR-1 and VEGFR-2 (Ferrara and Adamis, 2016). The heparin binding VEGF isoforms as well as PGF bind the co-receptor neuropilin 1 (NRP1) (Soker et al., 1998). However, VEGFR-1 is able to regulate the expression of a variety of genes in the endothelium, including genes with an important role in tissue homeostasis and regeneration (LeCouter et al., 2003).

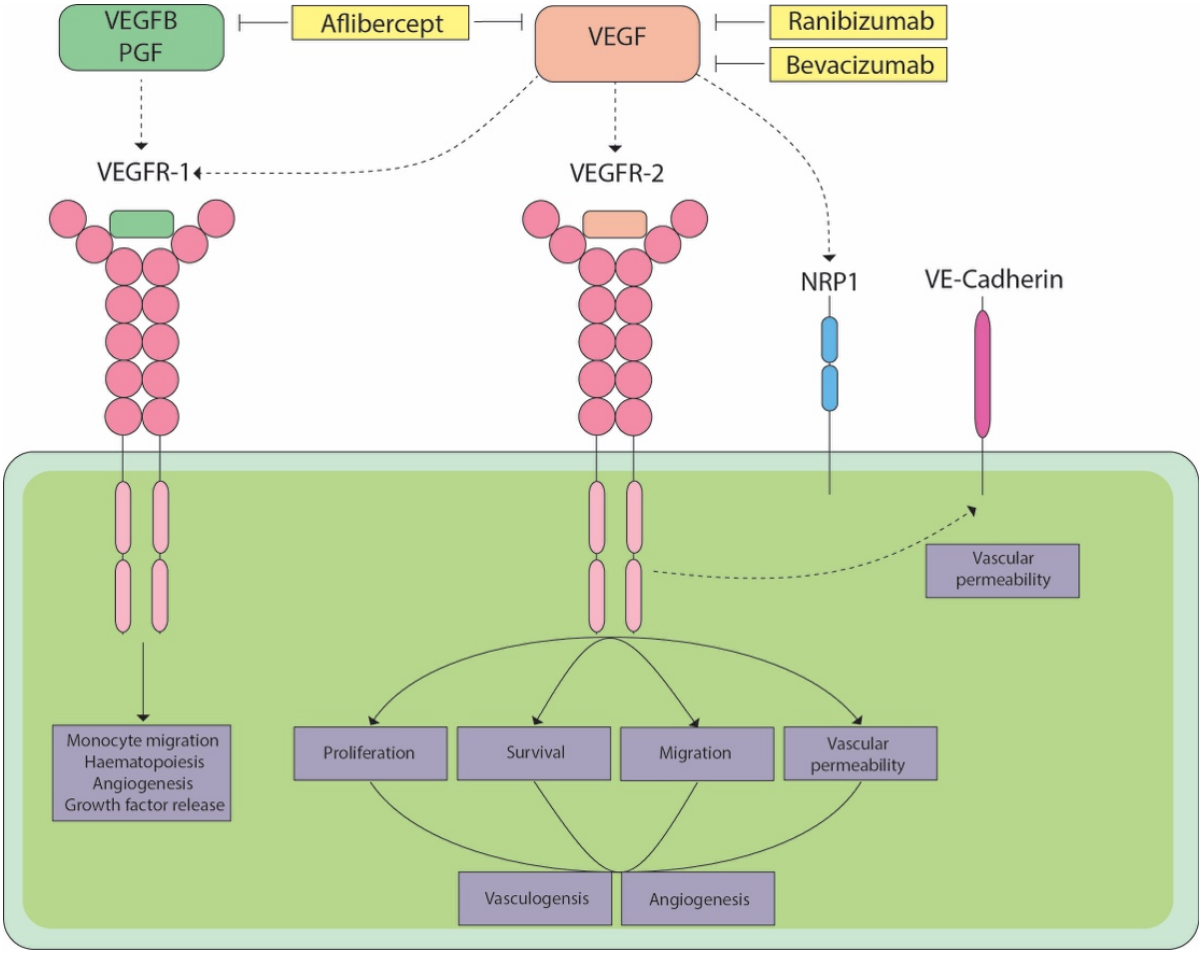

Figure 7 Schematic overview of the VEGF pathways and its inhibitors

PGF and VEGFB bind selectively to VEGFR-1, while VEGF binds VEGFR-1 and VEGFR-2. The heparin binding VEGF isoforms and PGF bind to NRP1. (Modified from (Ferrara, 2016). Abbreviations: VEGF: vascular endothelial growth factor; PGF: placental growth factor; VEGFB: vascular endothelial growth factor B; VEGFR: vascular endothelial growth factor receptor; NRP1: neuropilin 1.

1.4 β-Synuclein

One of the proteins to be found elevated in aged retinal tissue of *C. jacchus* is SNCB. Synucleins are small, soluble proteins. So far, the family includes three known proteins: SNCA, SNCB, and γ-synuclein (da Costa et al., 2003). All synucleins share a highly conserved α-helical lipid-binding motif with similarity to the class-A_2 lipid-binding domains of the exchangeable apolipoproteins. The SNCA and SNCB proteins are found primarily in brain tissue, where they are seen mainly in presynaptic terminals (Iwai et al., 1995; Nakajo et al., 1994). The γ-synuclein protein is found primarily in the peripheral nervous system and retina (Buchman et al., 1998), but its expression in breast tumors is a marker for tumor progression (Jia et al., 1999). Mutations in α-

synuclein are associated with rare familial cases of early-onset Parkinson's disease (Polymeropoulos et al., 1997), and the protein accumulates abnormally in Parkinson's disease, Alzheimer's disease, and several other neurodegenerative illnesses (Hashimoto and Masliah, 1999; Spillantini et al., 1998; Takeda et al., 1998; Wakabayashi et al., 1997). Although both proteins are localized at presynaptic terminals and are expressed at similar levels (Jakes et al., 1994), SNCB has not been implicated in the etiology of Parkinson's disease. Instead it was observed that it inhibits aggregation of SNCA both *in-vitro* (Janowska et al., 2015) and *in-vivo* (Hashimoto et al., 2001; Rockenstein et al., 2001). It was also suggested that SNCB can act as a natural inhibitor of SNCA aggregation by reducing both the initiation of its self-assembly and the proliferation of its aggregates (Brown et al., 2016).

These results suggest that SNCB can act as a natural inhibitor of SNCA aggregation by reducing both the initiation of its self-assembly and the proliferation of its aggregates.

SNCA and SNCB proteins were biochemically purified from bovine brain as constitutive inhibitors of phospholipase D2 (PLD2), an enzyme that catalyzes the hydrolysis of phosphatidylcholine to phosphatidic acid and appears to play a role in cytoskeletal reorganization and/or endocytosis at the plasma membrane (Jenco et al., 1998). The function of SNCB was shown to be related to the control of neuronal cell death, the protection of neurons from insults, and the maintenance of antiapoptotic effects in TSM-1 neurons (da Costa et al., 2003; Hashimoto et al., 2001). Recent studies show that SNCB plays a role in neurovascular units and can alter the *p*53-MDM2 (Mouse double minute 2 homolog) pathway and induce apoptosis *in-vitro* (Brockhaus et al., 2018). Less is known about the role and function of SNCB in the eye, particularly in the retina and the RPE.

2 Aim of this study

Aging is a physiological process happening in every organ and every cell. During the aging process of the eye, the physiological aging process can shift to the pathological condition of age-related macular degeneration, which can lead to blindness of the patient. The shift from the physiologic process into a pathology needs to be fully understood. This study addresses this goal and should help to understand the conversion from a physiologic to a pathologic process. Morphological and cellular changes in the RPE play an important role in the aging process, especially in the macula.

This work can be separated into three different approaches. The first approach is to study the whole transcriptome and the comparative comparison with proteomic data of the RPE in aging *C. jacchus*. Topological aspects regarding macular and peripheral parts of the RPE were considered to study age-related alterations. This data sets help to invest specific genes and proteins, up- or downregulated in aged tissue or differently regulated the macula compared to the periphery.

The second approach of the presented work contains the functional characterization of selected factors, which were found in the transcriptomal analysis described above or in previous studies regarding the aging retina of *C. jacchus*. One of these proteins is SNCB. As an antagonist of SNCA, its role in the neuronal system is partially investigated, but the role of SNCB in the aging RPE remains unclear. Therefore, the *in-vitro* role of SNCB was investigated.

During the analysis of the first approach, Cathepsin B (CTSB) was detected as a protein upregulated in aged tissue as well. As it is involved in many functions correlating with the cellular aging process, it gained further research interest in this study. Comparable to SNCB, the function of this protein is well investigated, but the role of CTSB in especially aging RPE is unknown. Therefore, the *in-vitro* role of CTSB was investigated.

In a third approach, CTSB was introduced in a premature senescence model, to study the influence of CTSB on the RPE *in-vitro*.

3 Material and Methods

3.1 Material

3.1.1 Chemicals and reagents

Chemicals/Reagents	Company
2-Methylbutan	Merck, Darmstadt
2-Propanol	AppliChem, Darmstadt
3-(4,5-Dimethylthiazol-2-yl)-2,5-Diphenyltetrazolium Bromide (MTT)	ThermoFisher Scientific, Waltham, USA
Acetic acid 100 %	Carl Roth GmbH & Co.KG, Karlsruhe
Aceton	AppliChem, Darmstadt
Acrylamide/Bisacrylamide	Carl Roth GmbH & Co.KG, Karlsruhe
Aluminum sulphate	Carl Roth GmbH & Co.KG, Karlsruhe
Ammoniumperoxodisulfat (APS)	Carl Roth GmbH & Co.KG, Karlsruhe
bisBenzimide H 33258 (Hoechst)	Sigma-Aldrich Chemie GmbH, Taufkirchen
Citrate acid	Carl Roth GmbH & Co.KG, Karlsruhe
Deoxycholic acid	Sigma-Aldrich Chemie GmbH, Taufkirchen
Diethyl dicarbonate (DEPC)	Sigma-Aldrich Chemie GmbH, Taufkirchen
Dimethyl sulfoxide (DMSO)	Sigma-Aldrich Chemie GmbH, Taufkirchen
Dithiothreitol (DTT)	Sigma-Aldrich Chemie GmbH, Taufkirchen
Eosin Y	ThermoFisher Scientific, Waltham, USA
Ethanol 70 %	Sigma-Aldrich Chemie GmbH, Taufkirchen
Ethanol absolut	AppliChem, Darmstadt

Chemicals/Reagents	Company
Ethylenediaminetetraacetic acid (EDTA)	Carl Roth GmbH & Co.KG, Karlsruhe
Fetal Calve Serum (FCS)	Sigma-Aldrich Chemie GmbH, Taufkirchen
Glycerin	Carl Roth GmbH & Co.KG, Karlsruhe
Glycin	Carl Roth GmbH & Co.KG, Karlsruhe
Hanks' Balanced Salt Solution (HBSS)	Sigma-Aldrich Chemie GmbH, Taufkirchen
Hematoxylin solution	Merck, Darmstadt
HEPES	Carl Roth GmbH & Co.KG, Karlsruhe
Hydrochloric acid (HCl)	Sigma-Aldrich Chemie GmbH, Taufkirchen
Magnesium chloride ($MgCl_2$)	Carl Roth GmbH & Co.KG, Karlsruhe
Methanol	AppliChem, Darmstadt
Milk Powder	Carl Roth GmbH & Co.KG, Karlsruhe
Mowiol	Carl Roth GmbH & Co.KG, Karlsruhe
Sodium azide (NaN_3)	Carl Roth GmbH & Co.KG, Karlsruhe
Sodium chloride (NaCl)	Carl Roth GmbH & Co.KG, Karlsruhe
Nuclear Fast Red Solution	Carl Roth GmbH & Co.KG, Karlsruhe
Paraffin Wax	TCS Bioscience, Buckingham, UK
Paraformaldehyde (PFA)	Sigma-Aldrich Chemie GmbH, Taufkirchen
Penicillin-Streptomycin (P/S)	Sigma-Aldrich Chemie GmbH, Taufkirchen
Phosphate Buffered Saline (PBS)	Sigma-Aldrich Chemie GmbH, Taufkirchen
recombinant Cathepsin B (rCTSB)	R&D Systems, Minneapolis, USA
recombinant β-Synuclein (rSNCB)	Prospec, East Brunswick, USA
Roti-Histokitt	Carl Roth GmbH & Co.KG, Karlsruhe
SERVA Blue R	SERVA Electrophoresis GmbH, Heidelberg
Sodium citrate	Carl Roth GmbH & Co.KG, Karlsruhe

Chemicals/Reagents	Company
Sodium dodecyl sulfate (SDS) Pellets	Carl Roth GmbH & Co.KG, Karlsruhe
Sucrose	Merck, Darmstadt
Tetramethylethylenediamine (TEMED)	Carl Roth GmbH & Co.KG, Karlsruhe
tert-butylhydroperoxide (*tert*-BHP)	Sigma-Aldrich Chemie GmbH, Taufkirchen
Tissue-Tek® O.C.T.™ Compound	Sakura, Alphen aan den Rijn, Netherlands
Tris base (Tris)	Carl Roth GmbH & Co.KG, Karlsruhe
Triton X-100	Carl Roth GmbH & Co.KG, Karlsruhe
Trypan blue	Sigma-Aldrich Chemie GmbH, Taufkirchen
Trypsin-EDTA (10x)	Sigma-Aldrich Chemie GmbH, Taufkirchen
Tween® 20	Carl Roth GmbH & Co.KG, Karlsruhe
Urea	Carl Roth GmbH & Co.KG, Karlsruhe
Videne Antispetic Solution	Ecolab, St. Paul, USA
Xylene	Carl Roth GmbH & Co.KG, Karlsruhe

3.1.2 Cell culture media

Cells were cultured with Dulbecco's modified Eagle's medium (DMEM).

Medium	Company
DMEM/F12	PAA Laboratories, Pasching, Austria
DMEM/F12 w/o Phenol Red	ThermoFisher Scientific, Waltham, USA

Culture Medium:	DMEM/F12 or DMEM/F12 w/o Phenol Red
containing	10 % FCS
	1 % 4-(2-hydroxyethyl)-1-piperazineethanesulfonic acid (HEPES) (0.1 M in DEPC)
	1 % P/S

3.1.3 Devices

Device	Company
7300 Real Time PCR System	Applied Biosystems; Waltham, Massachusetts, USA
Agilent Bioanalyzer RNA Nano/Pico chip	Agilent Technologies Inc., Santa Clara, USA
ApoTome 2	Carl Zeiss, Jena
Clean Bench Hera safe	Heraeus Holding GmbH, Hanau
Cryomicrotome Jung CM3000	Leica, Wetzlar
Cytoflex flow cytometer	Beckman Coulter, Inc., Brea, USA
Dewer	KGW-Isotherm GmbH, Karlsruhe
Echo Plate Reader	
Electrophoresis System	Bio-Rad Laboratories GmbH Laboratories, Hercules, USA
Embedder “Citadel”	Shandon, Cambridge, UK
Freezer -80°C	Sanyo, Osaka, Japan
Imager ChemiDoc	Bio-Rad Laboratories GmbH Laboratories, Hercules, USA
Incubator Function Line	Heraeus Holding GmbH, Hanau
Inverted Microscope	Olympus, Shinjuku, Japan
Microcentrifuge	Eppendorf AG, Wesseling-Berzdorf
NanoDrop ND-1000	Peqlab, Erlangen, Germany
Pipettes, 2.5-,10-, 200-, 1000 µl	Eppendorf AG, Wesseling-Berzdorf
Power Supply	Bio-Rad Laboratories GmbH Laboratories, Hercules, USA
Rotary microtome 2040	Reichert-Jung (Leica), Wetzlar
Scale	Sartorius GmbH & Ko. KG, Göttingen

Device	Company
StepOnePlus™ Real-Time PCR System	Applied Biosystems; Waltham, Massachusetts, USA
Thermomixer Comfort	Eppendorf AG, Wesseling-Berzdorf
Vortex Genie 2	neoLab, Heidelberg
Western Blot System	Bio-Rad Laboratories GmbH Laboratories, Hercules, USA

3.1.4 Buffers and Solutions

Buffer	Chemicals	Final concentration
Blotting buffer (10x)	30.25 g Tris 150 g Glycine ad 1 l Aq. Dest for 1x: add 10 % methanol	0.25 M 2 M 1 %
Citrate buffer	Solution A: 4.2 g Citrate acid in 200 ml A. Dest Solution B: 14.7 g Sodium Citrate in 500 ml A. Dest Working Dilution: 18 ml A + 82 ml B ad 1l Aq. Dest	10 mM
Electrophoresis Buffer (10x)	30.25 g Tris 150 g Glycine 100 ml 10 % SDS ad 1 l A. Dest	0.25 M 2 M 1 %
Nuclear Fast Red Solution	5 g Aluminium sulphate in 100 ml Aq. Dest 0.1 g Nuclear Fast Red Solution	

Buffer	Chemicals	Final concentration
Laemmli buffer	0.6 g Tris 24 g Urea 10 ml Glycine 1 g SDS 310 mg DTT 30 mg Serva Blue ad 100 ml A. Dest	50 mM 4 M 10 % 1 % 20 mM
Mowiol	12 g Mowiol 30 g Glycerin warm up to solve 30 ml A. Dest 60 ml 0.2 M Tris stir at 56 °C centrifuge 15 min at 5000xg; freeze supernatant	
PVDF-Destaining Solution	10 % Acetic acid 40 % Ethanol 50 % A. Dest	
PVDF-Staining Solution	0.075 % Serva Blue in Methanol	
RIPA Buffer	1.21 g Tris 1.75 g NaCl 0.2 g SDS 1 g Deoxycholic acid 2 g Triton X-100	50 mM1 50 mM 0.1 % 0.5 % 1 %
Separating gel buffer (4x)	180 g Tris 4 g SDS 0.02 g NaN_3 ad 1 l A. Dest pH 8.8	1.5 M 0.4 % 0.02 %
Stacking gel buffer (4x)	60 g Tris 4 g SDS 0.02 g NaN_3 ad 1 l A. Dest pH 6.8	500 mM 0.4 % 0.2 %
TBS (10x)	60.55 g Tris 85.2 g NaCl ad 1 l A. Dest pH 7.6	500 mM 1.37 M

Buffer	Chemicals	Final concentration
TBST (10x)	60.55 g Tris	500 mM
	85.2 g NaCl	1.37 M
	ad 1 l A. Dest	
	pH 7.6	
	10 ml Tween	0.1%
TE-Buffer	60 mg Tris	10 mM
	19 mg EDTA	1 mM
	ad 50 ml A. Dest	
	pH 8.0	

3.1.5 Kits and Systems

Kit/System	Company
Agilent Bioanalyzer HS DNA chips	Agilent Technologies Inc., Santa Clara, USA
ApopTag Fluorescein in Situ Apoptosis Detection Kit S7110	Merck Millipore, Burlington, Massachusetts, USA
Cell Proliferation Dye eFluor™ 670	ThermoFisher Scientific, Waltham, USA
DC Protein Assay	BioRad, München
ECL Westen Blotting detection reagent	GE Healthcare, Chicago, USA
High Capacity cDNA Reverse Transcription Kit	Applied Biosystems; Waltham, Massachusetts, USA
HiSeq 2500 High Output flow cells	Illumina, San Diego, USA
Latex beads, carboxylate-modified polystyrene, fluorescent yellow-green	Merck Millipore, Burlington, Massachusetts, USA
NEB Library Quant kit	New England Biolabs, Ipswich, USA
Ovation Human FFPE RNA-Seq Multiplex System Kit	NuGEN, Redwood City, USA
PE Annexin V Apoptosis Detection Kit I	BD Pharming
Power SYBR™ Green PCR Master Mix	Applied Biosystems; Waltham, Massachusetts, USA
QIAshredder	Qiagen, Hilden, Germany
Reactive Oxygen Species (ROS) Detection Reagents	ThermoFisher Scientific, Waltham, USA
RNeasy Mini Kit	Qiagen, Hilden, Germany
Senescence-associated β-galactosidase (SA β-gal) assay	Cell Signaling

Kit/System	Company
TaqMan™ Fast Advanced Master Mix	Applied Biosystems; Waltham, Massachusetts, USA

3.1.6 Antibodies

Antibody	Origin	IF	WB	Company
Primary Antibodies				
4-Hydroxynonenal	Mouse monoclonal	1:500		Abcam, Cambridge, UK
8-Hydroxyguanosine	Mouse monoclonal	1:500		Abcam, Cambridge, UK
ARF tumor suppressor (*p*19ARF)	Goat polyclonal	1:200		Santa Cruz Biotechnology, Dallas, USA
Cathepsin B (CTSB)	Mouse monoclonal	1:500	1:200	Abcam, Cambridge, UK
Heat shock protein 60 (HSP 60)	Goat polyclonal	1:100	1:100	Santa Cruz Biotechnology, Dallas, USA
Heat shock protein 90 (HSP 90)	Goat polyclonal	1:200	1:200	Santa Cruz Biotechnology, Dallas, USA
Heme oxygenase (decycling) 1 (HMOX1)	Mouse monoclonal	1:500		Abcam, Cambridge, UK
Mouse double minute 2 homolog (MDM2)	Mouse monoclonal	1:200		Santa Cruz Biotechnology, Dallas, USA
Nidogen 1 (NID1)	Mouse monoclonal	1:200	1:200	Santa Cruz Biotechnology, Dallas, USA
*p*53	Rabbit polyclonal	1:200		Abcam, Cambridge, UK
Parkinson disease 7/DJ1 (DJ1)	Rabbit polyclonal	1:200	1:200	Abcam, Cambridge, UK
Peroxiredoxin (PRDX)	Rabbit polyclonal	1:400	1:4000	Santa Cruz Biotechnology, Dallas, USA
Phospholipase D2 (PLD2)	Rabbit polyclonal	1:100		Sigma-Aldrich Chemie GmbH, Taufkirchen
Thrombospondin 1 (THBS1)	Mouse monoclonal	1:500	1:500	Santa Cruz Biotechnology, Dallas, USA
α-Synuclein (SNCA)	Mouse monoclonal	1:400		Abcam, Cambridge, UK

Antibody	Origin	IF	WB	Company
		Primary Antibodies		
β-synuclein (SNCB)	Rabbit monoclonal	1:400		Abcam, Cambridge, UK

Antibody	Origin	IF	WB	Company
		Secondary antibodies		
Alexa Fluor 488 Anti-Rabbit	Donkey	1:500		Jackson ImmunoResearch, Ely, UK
Alexa Fluor 488 Anti-Goat	Donkey	1:500		Jackson ImmunoResearch, Ely, UK
Alexa Fluor 488 Anti-Mouse	Donkey	1:500		Jackson ImmunoResearch, Ely, UK
Alexa Fluor 594 Anti-Rabbit	Donkey	1:500		Jackson ImmunoResearch, Ely, UK
Alexa Fluor 594 Anti-Mouse	Donkey	1:500		Jackson ImmunoResearch, Ely, UK
Anti-Mouse IgG HRP-linked	Goat		1:4000	Sigma-Aldrich Chemie GmbH, Taufkirchen
Anti-Rabbit IgG HRP-linked	Goat		1:4000	Sigma-Aldrich Chemie GmbH, Taufkirchen
Anti-Goat IgG HRP-linked	Donkey		1:0000	Invitrogen, Carlsbad, USA

3.1.7 Primer design and sequences

The synthetically prepared oligonucleotide (primer) sequences had a length of 15-25 nucleotides, a guanosine / cytosine content of 40-60%, and a melting temperature of 59-61° C. If possible, exon-spanning primers were chosen. The primer sequences of the cDNA to be amplified were taken from the online database of the National Center for Biotechnology Information, U.S. National Library of Medicine (https://www.ncbi.nlm.nih.gov/nuccore), and manufactured by the Company Biolegio (Nijmegen, The Netherlands). The lyophilized primers were dissolved in TE-buffer according to the manufacturer's instructions. Subsequently, the stock solution was diluted to a working concentration of 10 µM with DEPC water.

Amplicon		Sequence 5'→3'	Accession Number
		Human	
*p*53	FW	TGAAGCTCCCAGAATGCCAG	AB082923.1
	RV	GCTGCCCTGGTAGGTTTTCT	
MDM2	FW	AGGAGATTTGTTTGGCGTGC	NM_002392.5
	RV	TGAGTCCGATGATTCCTGCTG	
*p*14ARF	FW	TTCCCCCACTACCGTAAATG	NM_000077.4
	RV	CACTCCAGAAAACTCCAACACA	
HMOX1	FW	ACTCCCTGGAGATGACTCCC	NM_002133.2
	RV	TCAAAGAGCTGGATGTTGAGCA	
NOX4	FW	TGAACTATGAGGTCAGCCTCTG	XM_006718849.2
	RV	AAGCTTGTATGGTTTCCAGTCAT	
GCLM	FW	AGCGAGGAGGAGTTTCCAG	XM_005270754.1
	RV	CAACTGCACTTCTAGTTGATGATGA	
GCLC	FW	GTTCTCAAGTGGGGCGATGA	AB262176.1
	RV	TTCTCCCCAGACAGGACCAA	
GAPDH	FW	TGCACCACCAACTGCTTAGC	
	RV	GGCATGGACTGTGGTCATGAG	
		Sus Scofa	
*p*53	FW	TCCTCGCCAGTGCAAAAGAA	NM_213824.3
	RV	TCTCGGAACATCTCGAAGCG	
MDM2	FW	GCTGCAGGCAAATGTGCAA	NM_001105303.1
	RV	GCTGGAATCTGTGAGGTGCT	
*p*14ARF	FW	CAAGAATATGGTGCGCCGTC	NM_213735.1
	RV	CGATCTGCACCACGAAAGC	
HMOX1	FW	GTTGGAGCCACTCTTCGTTC	NM_001004027.1
	RV	TCACCCCACCTTGCTATAAAA	
NOX4	FW	TTTTGTAAACTCATGAGACAGGAAAT	XM_003357234.3
	RV	TCATGGTTCTGTGGGAGTTG	
GCLM	FW	TGACTCGTGTCTCCCTTGAA	XM_001926378.3
	RV	CGGAACATCTGCCTCAATG	
GCLC	FW	TCGAGAACTCTGCGTACGTG	XM_003482164.3
	RV	CCTTCGACAGAGGGATGAGA	

Amplicon		Sequence 5'→3'	Accession Number
		Callithrix jacchus	
LUM	FW	AACTGCCCTGAAAGCTACCC	XM_002752818.4
	RV	AGGCACCATAGGCACACTTT	
STC1	FW	CATTCGGAGGTGCTCCACTT	XM_002756834.4
	RV	CACATGTTCAGCCTGCGGTA	
CTSB	FW	GACACCCCCAAGTGTAGCAA	XM_002756787.3
	RV	ATCCGTAGTGCTTGTCCTGC	
NID1	FW	CGGAGAGGTGGAGAAAACCC	XM_008985776.2
	RV	CTCATCGCACTCAGGAACGA	
THBS1	FW	CCACGACTGCAACAAGAACG	XM_009005580.2
	RV	TTGCACTCACAGCGGTACAT	
GAPDH	FW	TAAGACCCCCTGGACCATCAGCC	XM_002759682
	RV	GGGGCAATTCGGTGTGGTGA	

The TaqMan Probes used in the study, were designed by ThermoFisher Scientific. The probes are exon spanning and design for mRNA, if applicable. No TaqMan probes specific for *C. jacchus* were available. Regarding the high homology of the genome of *C. jacchus* and the human genome, it is possible to use human TaqMan probes. The following probes were used:

Probe	Assay ID	Dye Label
BASP1	Hs00234720_g1	FAM
FMOD	Hs00157619_m1	FAM
COL4A2	Hs01098873_m1	FAM
TBP	Hs00920495_m1	FAM

3.1.8 Software

Software	Company
Adobe Illustrator CC	Adobe Systems Inc. USA
Adobe Photoshop CC2017	Adobe Systems Inc. USA
Agilent Aria Software 1.3	Agilent Technologies Inc., USA
CytExpert 1.2	Beckman Coulter, USA
EndNote X9	Thomson Reuters, USA

Software	Company
GraphPad Prism 7.0a	GraphPad, USA
Image J 2.0	Image Processing and Analysis, USA
Kaluza 1.2	Beckman Coulter, USA
Office 365 for Mac	Microsoft, USA
Molecular Signatures Database 6.0	Broad Institute, USA
PartekGS	Partek Inc, USA
Progenesis QI for proteomics	Waters, Germany
StepOne Plus Systems Software 2.3a	Applied Biosystems, USA
StrandNGS	Strand Life Sciences, India
ZEN 2 (blue Edition)	Carl Zeiss, Germany

3.2 Methods

3.2.1 Animals used in this study

In this study, eyes from cadavers from the common marmoset *Callithrix jacchus* were used. The cadaver eyes of *C. jacchus* used for other studies were kindly provided by Prof. Stefan Schlatt and Dr. Joachim Wistuba from the Centre of Reproductive Medicine and Andrology (University of Münster). The total cohort was divided as described in Table 1 into four age groups:

Table 1: Definition of the age groups used in this study

Group	Age	Number of animals
Neonatal	0-3 days	11
Adolescent	3-10 month	7
Adult	10-35 month	10
Senile	8-9 years	11

The morphology of the eyecups (in particular the retina) was determined by examination and fundoscopy. In case of corneal pathologies, like edema, artificial tear supplemental were applied to support optical transparency. Exclusion criteria for further use were any morphological, ophthalmological, or pathological condition of the

retina. As the number of donor eye is still imited, the tissue could not be used for the preparation of e.g. primary RPE cells cultures from *C. jacchus.* Due to limitations of the number of animals, no consideration could be given to the gender of the animals. The age groups were assigned in accordance with previously published literature (Ross et al., 2007; Smucny et al., 2004; Tardif et al., 2003). It is to mention that the genetic homology between human and *C. jacchus* is of over 93 % (Tatsumoto et al., 2013).
The postmortem time before the preparation was kept as short as possible (≤ 10 min). The eyecups were removed from the skull and the morphology of the eyes was determined by examination and fundoscopy immediately. In case of any abnormalities regarding the retina, the eyes were excluded from the study.
For the preparation of primary porcine RPE cell cultures (ppRPE), eyes from *Sus scrofa domesticus* (*S. scrofa*) were kindly provided from a slaughterhouse (in accordance to Regulation (EG) Nr. 1069/2009).
All animal work was conducted according to the German Animal Protection Law (TSchG) with the approval of the responsible authority (LANUV-NRW, permission numbers 39.32.7.2.1, 84.02.05.50.16014 and 84.02.005.20.12.0.18).

3.2.1.1 Isolation of total RPE from *C. jacchus*

For the preparation of the RPE from *C. jacchus* cadaver eyes, the eyecups were removed from the scull. The eyes were dissected into retina and RPE. The RPE was separated in macula and peripheral regions. For transcriptome and proteome analysis the tissue was frozen in liquid nitrogen and stored at -80 C until further use.

3.2.1.2 Isolation and cultivation of primary porcine RPE culture

For the preparing ppRPE cell cultures, *S. scrofa* eyes were obtained from a slaughterhouse and kept on ice during transport and preparation. The appendix tissue of the eyecubs was removed, cleaned with Videne Antiseptic Solution and PBS (1:5) and incubated in 0.2 mg/ml P/S for 30 min at 4 °C. Under sterile conditions, the eyes were circularly dissected underneath the *Ora serrata*. The neuroretina was removed from the subjacent RPE. RPE cells were incubated with 1 ml 10xTrypsin-EDTA for 5 min at 37°C and dissolved by pipetting up and down. Additionally, the eyecubs were washed with 1 ml PBS and placed in standard media containing FCS. The cells were centrifuged at 500 x g for 5 min and placed in culture medium.

3.2.2 Transcriptome Analysis

The transcriptome of the RPE in the aging *C. jacchus* was investigated. The RNA sequencing analysis described in 3.2.2.4 as well as the qRT-PCRs for the specific genes selected from RNA sequencing analysis (*STC1, LUM, THBS1, FMOD, BASP1, COL42A, NID1*) were performed by **PD Dr. Ludger Klein-Hitpass** (Institute for Cell Biology, Essen University Hospital, Essen, Germany; see section 3.2.2.5). The bioinformatics were performed by **Prof. Dr. Sven Rahmann** (Genome Informatics, Institute of Human Genetics, University of Duisburg-Essen) and **PD Dr. Ludger Klein-Hitpass**.

3.2.2.1 RNA-Isolation

For RNA isolation, the total RNA from ARPE-19 cells or ppRPE cells was isolated using the RNeasy Mini Kit according to the manufacturer's instructions. For the native RPE tissue from *C. jacchus*, an additional step using QIAshredder was performed before RNA isolation according to the manufacturer's instructions. The RNA was eluted in 15 µl RNase-free DEPC water. The RNA was stored at -80 °C until further use.

3.2.2.2 Quantification of RNA

The quantification of the RNA was performed using a NanoDrop spectral photometer with a wavelength of 260 nm. For the measurement, 1 µl of total RNA was used. In advance, a blank value measurement with the corresponding solvent (here: DEPC water) was performed.

3.2.2.3 cDNA-synthesis

Th cDNA was synthesized from 1 µg of total RNA using the *High Capacity cDNA Reverse Transcription* Kit according to the manufacturer's instructions. The RNA was diluted with DEPC water to 14.2 µl in total. The reactions were performed in RNAse-free 0.2 ml reaction tubes. In addition to *random* primers, which attach to random sites of RNA and represent the starting point of the cDNA synthesis, the enzyme reverse Transcriptase (RT) was added. In the presence of deoxyribonucleoside triphosphates (dNTP) the RT synthesizes the complementary cDNA strand. The components were used in the following volumes (Table 2):

Table 2: Reaction mix for cDNA synthesis

Reagent	Volume
10x RT-Puffer	2 µl
25x dNTP Mix	0.8 µl
10x Random Primer	2 µl
10x Random Primer	2 µl
Multiscribe® Reverse Transkriptase	1 µl
RNA/DEPC water mix	14.2 µl

The cDNA synthesis was performed in the Polymerase chain reaction (PCR) thermal cycler under the following conditions (Table 3):

Table 3: Temperature profile for cDNA synthesis

Step	Temperature	Time
Heat up	110 °C	
1	25 °C	10 min
2	37 °C	120 min
3	85 °C	5 min
4	4 °C	∞

The cDNA was stored at -20 °C until further use.

3.2.2.4 RNA sequencing analysis

The RNA sequencing analysis was performed by PD Dr. Ludger Klein-Hitpass. RNA-Sequencing uses the deep sequencing method Next Generation Sequencing (NGS) to reveal the presence and quantity of RNA in a biological sample and is used to reveal the whole transcriptome of the cell. The transcriptome is defined as the complete set of transcripts in a cell, and their quantity at the given time (Wang et al., 2009b). The aims of the transcriptome analysis in this study is to catalogue all transcripts of the specific RPE tissue of *C. jacchus* in different stages of age under topographical conditions. The expression patterns of each gene were compared between each group. Three biological replicates were used for each age- and topological group.

3.2.2.4.1 RNA quality control

With a bioanalyzer (Agilent Technologies GmbH) it is possible to examine the integrity of small amounts of RNA. The method determines the so-called RIN value (RNA Integrity Number) of total RNA on a scale of 1-10, with a RIN of 10, meaning a completely intact RNA, down to a RIN of 1, a nearly complete degraded RNA. In an electropherogram representing a high-quality RNA sample, different regions can be defined. The regions of the 18S and 28S-r (ribosomal) RNA fragments are of particular importance, as ribosomal RNA accounts for approximately 90% of the total RNA of a cell. From all extracted data of the electropherogram, the RIN value was determined by a mathematical algorithm (reviewed in (Schroeder et al., 2006)). In Figure 8, an example of a RIN electropherogram of control RNA is shown.

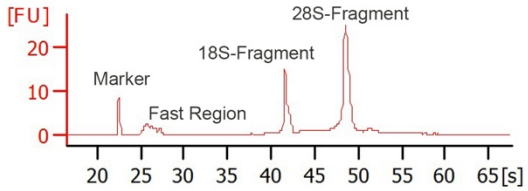

Figure 8 Electropherogram for the RIN classification of control RNA

The fluorescence-labeled control RNA is separated according to their fragment size. A peak at the level of the 18S or 28S rRNA fragment is characteristic of an intact RNA. Abscissa: run time; ordinate: fluorescence of the fragments; fluorescence units (FU)

3.2.2.4.2 Sample preparation and sequencing process

The RNA concentrations were measured by Nanodrop spectrophotometry like described in 3.2.2.2 and then analyzed on the Agilent Bioanalyzer RNA Nano/Pico chip. In total, 100 ng RNA was then processed for NGS sequencing using the Ovation Human FFPE RNA-Seq Multiplex System Kit according to the manufacturer's instructions using 15 PCR cycles. The Insert Dependent Adaptor Cleavage is used to deplete unwanted reads derived from ribosomal RNA. The "human" oligonucleotide pool for depletion was used, as *C. jacchus* shows very high sequence homology to *Homo sapiens*. The corresponding workflow is shown in Figure 9:

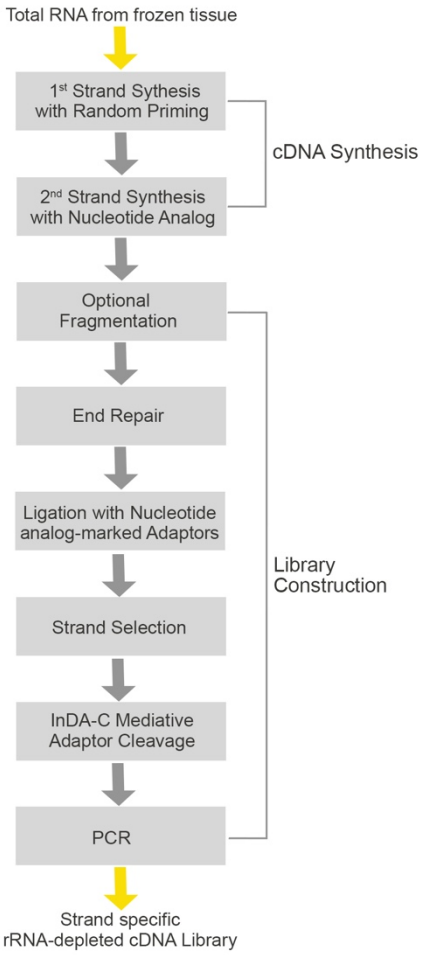

Figure 9 Ovation Human FFPE RNA-Seq Library Systems workflow

The first and second strand of cDNA was synthesized using RNA from frozen tissue with a mixture of random and poly(T) priming. To produce the final library, end repair to generate blunt ends, adaptor ligation, strand selection via nucleotide analog-targeted degradation, InDA-C-mediated adaptor cleavage and PCR amplification was performed.

3.2.2.4.3 Data processing and analysis

The size distribution of the resulting libraries was analyzed on Agilent Bioanalyzer HS DNA chips. Two library pools were generated for sequencing and quantified using the NEB Library Quant kit. The sequencing of the library pool was performed on HiSeq 2500 High Output flow cells using the paired-end mode. The paired-end sequences were aligned to the *Callithrix jacchus* ensemble genome 3.2.1.88 using the RNA aligner STAR (Dobin et al., 2013). The alignments were filtered on quality metrics in StrandNGS. For quantification of RNAs, PartekGS was used, which reports raw read counts as well as Reads Per Kilobase Million (RPKM) normalized RNA abundancies both on the gene and transcript level. Subsequently, genes expressed differently were identified using the ANOVA test. The step-up method for multiple testing correction was applied to generate corrected *p*-values. However, due to the low number of replicates, correction for multiple testing eliminates too many targets, which are likely

to be true positives. Thus, identification of genes expressed differently is based on uncorrected *p*-values ($p \leq 0.05$).

3.2.2.4.4 Gene Set Enrichment Analysis

The Gene Set Enrichment Analysis (GSEA) is an advanced computational method that determines whether an a priori defined set of genes shows statistically significant, concordant differences between two biological states using Molecular Signatures Database (MsigDB, v6.0), which contains more than 18000 gene sets for use with GSEA ordered into 8 major gene set categories. Only sets showing a False Discovery Rate (FDR) <0.25 and a Normalized Enrichment Score (NES) <-1.7 or >1.7 were considered as potentially interesting.

3.2.2.5 Quantitative Real-Time-PCR

For the investigation of gene expression alterations, quantitative Real-Time-PCR (qRT-PCR) was used. For the investigation of the expression differences of various genes in ARPE-19 cells and RPE samples from *C. jacchus* (performed by PD Dr. Ludger Klein-Hitpass), the dye SYBR Green, which binds to double stranded DNA, was used. After each cycle during qRT-PCR, the intensity of fluorescence is measured with a detector. The dye only fluoresces when bound to dsDNA. For the confirmation of the expression of selected genes after transcriptome analysis in *C. jacchus*, Singe Tube TaqMan Gene Expression probes were used additionally. TaqMan probes consist of a fluorophore, which is covalently attached to the 5'-end of the oligonucleotide probe and a quencher at the 3'-end. The quencher molecule quenches the fluorescence emitted by the fluorophore when excited by the cycler's light source via Förster resonance energy transfer (FRET). As long as the fluorophore and the quencher are in proximity, quenching inhibits any fluorescence signals. Because the genetic homology of humans and *C. jacchus* is very high (above 93 % (Tatsumoto et al., 2013)), and the TaqMan probes have a very high precision, the selection of the TaqMan probes is based on the "human" database were used for the assays. It was not possible to select TaqMan probes for all genes. Therefore, the gene expression of some genes was validated using the SYBR green method. The selection of the primers for the SYBR green method was carried out using the genome sequences of *C. jacchus*, to gain the maximal precision of this assays. In both methods, the relative expression was calculated as $2^{-\Delta Ct(\text{specific gene})}/2^{-\Delta Ct}$ mean, using a housekeeping gene as an endogenous control. For SYBR Green analysis, the housekeeping gene used

was *GAPDH*, for TaqMan-based assays, the gene used was *TBP*. The reactions were performed in specific 96-well plates. The following reaction mix (Table 4) was used for a standard reaction for PCRs using SYBR green technology:

Table 4: Reaction mix for SYBR green reactions

Reagent	Volume
SYBR Green	5 µl
DEPC water	2.1 µl
Primer Forward	0.5 µl
Primer Reverse	0.5 µl
cDNA	2.5 µl

Each gene of interest was tested three times, including the housekeeping control. A negative control using DEPC water was included for each gene of interest (GOI). A melting curve at the end of the run was included. The DNA melting temperature is specific to the amplified fragment. The results of this technique are obtained by comparing the dissociation curves of the analyzed DNA samples. The qRT-PCR was performed using the StepOnePlus™ Real-Time PCR System with the following program (Table 5):

Table 5: Temperature profile for qRT-PCR using SYBR green

Step	Temperature	Time	
Initial Step	95 °C	10 min	
Denaturation	95 °C	15 s	40 x
Primer annealing	60 °C	1 min	
Melting curve	95 °C	15 s	1 x
	65 °C	15 s	
	95 °C	15 s	
Cooling	4 °C	∞	

The following scheme was used as a standard reaction for TaqMan based assays using the TaqMan Universal PCR Master Mix for one well Table 6:

Table 6: Reaction mix for TaqMan reactions

Reagent	Volume
Master Mix	10 µl
Specific probe	1 µl
cDNA	9 µl

Each GOI was tested two times, including the housekeeping control. A negative control using DEPC water was included for each GOI. The inclusion of a melting curve is not necessary, because the probes are very specific. The qRT-PCR was performed using the Agilent Aria MX System with the following program:

Table 7: Temperature profile for TaqMan probes

Step	Temperature	Time	
Initial Step	95 °C	10 min	
Denaturation	95 °C	15 s	40 x
Probe annealing	60 °C	1 min	
Cooling	4 °C	∞	

3.2.2.6 Statistical analysis of the qRT-PCR results

The relative quantification of gene expression was compared with the comparative ΔΔCycle Threshold (C_T) method. A normalization of the gene expression of the target genes was carried out by the gene expression of the housekeeping genes (here: *GAPDH* for SYBR Green, TATA-binding protein (*TBP)* for TaqMan). The expression of each analyzed gene was normalized to the untreated sample (=100 % gene expression). For the qRT-PCR results obtained from the RPE of *C. jacchus*, the gene expression should be normalized to the gene expression in the neonatal macula sample. Three individual samples of each age and each topography was used. Hence, for each tested gene, the ΔC_T of each sample from the neonatal macula sample was calculated. In the next step, the mean of the three ΔC_T values were calculated and used for the calculations of the $\Delta\Delta C_T$values of each gene. The samples were normalized to the $\Delta\Delta C_T$ of the neonatal macula sample (=100 %). The data was analyzed with a test for two independent samples to examine for conformity with the

Gaussian distribution and processed using the independent-samples t-test with a significance of $p<0.05$.

3.2.3 Proteome Analysis

The proteome of the RPE in the aging *C. jacchus* was investigated. The proteome analysis (sections 3.2.3.1 and 3.2.3.2) was performed by **Prof. Simone König** of the Interdisciplinary center for clinical research (IZKF), Core Unit Proteomics, University of Münster. The method is described in König et at., 2018 (König et al., 2018).

3.2.3.1 Sample preparation for proteome analysis

The proteome analysis of the RPE was performed using frozen tissue from *C. jacchus*. The tissue was frozen in liquid nitrogen and grounded with a pestle, which was rinsed with 600 µl acetonitrile. Afterwards, the lysis buffer was added to the tissue. The solution was treated in an ultrasonic bath for 15 min and centrifuged with 30,000 xg for 30 min at 4 °C. The supernatant was transferred to Nanosep Omega filter units with a Molecular Weight Cut-off of 10 kDa. The sample on the filter was centrifuged with 14,000xg for 30 min at 4 °C with urea buffer. The centrifugation was followed by a reduction with 100 µl urea buffer containing 50 mM DTT for 30 min. Afterwards, the samples were centrifuged and washed with urea buffer as described above. For alkylation, the samples were vortexed for 25 min in the dark in 100 µl urea buffer containing 50 mM iodoacetamide, followed by centrifuging and incubation with 100 µl 50 mM DTT-containing urea buffer for 15 min. Afterwards, the filter unit was rinsed with 100 µl urea buffer followed by five times washing with 100 µl 50 mM NH_4HCO_3 in 5 % acetonitrile. The digestion step was performed using 40 µl trypsin solution and 60 µl Chromasolv water at 37 °C over night. Afterwards, the peptides were collected by centrifuging three times in a 100 µl of a solution containing 0.1 % formic acid containing 5 % acetonitrile. The solutions were pooled and dried.

3.2.3.2 Ion-mobility-liquid chromatography-mass spectrometry

The liquid chromatographic separation of the peptides performed using the so called “reverse phase” which is based on the interactions between the molecules. It is based on interactions between the molecules and the components of the mobile, liquid phase (polar), and solid, stationary phase (non-polar). For the analysis, the peptides were re-dissolved in 15 µl of a solution with 0.1 % formic acid containing 5 % acetonitrile. The high-definition mass spectrometry was performed using Synapt G2 Si ion mobility

mass spectrometer coupled to M-Class UPLC. The method was described in detail by Distler and colleagues in 2016 (Distler et al., 2016). The gradient was performed 90 min in a solvent system containing 100 % water versus 100 % acetonitrile, which both contained 0.1 % formic acid. The measurements were made on the following columns:
Trap column: V/M Symmetry C18 100 Å 5 µm, 180 µmÅ ~20 mm
Reversed phase column: HSS T3 1.8 µm 75µmÅ ~200 mm
with 0.5 µl injection volume.
The database-assisted analysis of the mass spectrometric data was performed with the Progenesis QI software for proteomics (non-linear dynamics) performed under the application of the protein database of *C. jacchus* at the universal protein database (UniProt), whereas special algorithms were used to compare the spectra of the fragments with the database. Proteins with an n-fold ≥2 and $p \leq 0.05$ (ANOVA) between the age- and topographic groups were considered to be potentially interesting for further analysis.

3.2.4 Microscopical techniques

3.2.4.1 Sample preparation

3.2.4.1.1 RPE-whole mount preparation

The eyecups from *C. jacchus* were removed from the skull and placed into ice-cold PBS. The ocular tissue was removed from the RPE and the RPE was flat-mounted on a nitrocellulose filter. To remove the vitreous body and the retina, fine forceps were used. For fixation, the dissected RPE was fixed in 4 % PFA in PBS at 4 °C for 30 min. After rinsing the RPE in PBS for 5 min, the tissues were transferred to 30 % sucrose and stored at 4 °C for at least 24 h. Afterwards, the fixed RPE was frozen in a mixture of 2-methylbutan and liquid nitrogen. The whole mounts were stored in PBS at 4 °C until further use.

3.2.4.1.2 Paraffin embedding of whole eye cubs of *C. jacchus*

A part of the eye cubs was kindly provided by Thekla Schokenhoff, Institute for Experimental Ophthalmology, University of Münster. The eyes of *C. jacchus* were completely removed from the skull and placed in 10 ml of 4 % PFA for fixation for at least one week. After fixation, the eyes were proceeded in a tissue embedding automat using the following protocol:

Table 8: Dehydration protocol

Reagent	Time	Repetitions
70 % Ethanol	90 min	1x
80 % Ethanol	90 min	1x
96 % Ethanol	90 min	2x
100 % Ethanol	90 min	2x
Acetone	90 min	2x
Xylene	120 min	1x
Paraffin	60 min	3x

After the proceeding, the eye cubs were placed in embedding moldings with the correct orientation to cut the eye from superior and filled with paraffin till completely covered. The preparations were kept dry at RT until further use. The section of the embedded eyes was performed on the rotary microtome with a thickness of 4 µm.

3.2.4.1.3 Cryo embedding of whole eye cubs of *C. jacchus*

The eyes of *C. jacchus* were completely removed from the skull and placed in 10 ml of 4 % PFA for fixation for at least one week. A casing made of aluminum foil with an approximate height of 2 cm is adhered on the stamper using Tissue Tek Cryo-OCT compound at -20 °C. Afterwards, the casing was filled up with Tissue Tek Cryo-OCT compound and the eye was immersed into the liquid compound. The preparation was placed at -20 °C until completely frozen and stored at -80 °C until further use. The section of the cryo-embedded eyes was performed on the cryomicrotome with a thickness of 10 µm.

3.2.4.2 Immunofluorescence Staining

For immunofluorescence staining, the RPE tissue as well as the cells needed to be fixed with either PFA or methanol, depending on the embedding method. To avoid unspecific binding, a blocking step with 10 % FCS in PBS was added to the protocol. Depending on the protocol, Triton X-100 (0.25-0.5 %) to reduce the surface tension of aqueous solutions during immunostaining, was added to the blocking solution. The primary and secondary antibodies were mixed with 10 % FCS in PBS to reach their appropriate dilution (See section 3.1.6). The embedding of the slices was performed

using the mounting medium Mowiol, containing 0.5 µg/ml Hoechst 33258 to stain the cell nuclei.

3.2.4.2.1 Immunofluorescence staining of RPE whole mounts

After whole mount preparation described in 3.2.4.1.1, the tissue was blocked with 10 % FCS+0.5 % Triton X-100 for at least 2 h at RT, followed by the incubation with the primary antibody for 72 h at 4 °C. Afterwards, the tissue was washed twice with PBS at RT for 1 h at RT. The secondary antibody was applied on the tissue and incubated for 72 h at 4 °C. After an additional washing step with PBS (2x 1 h), the RPE whole mounts were coverslipped with antifade mounting medium.

3.2.4.2.2 Immunofluorescence staining of paraffin embedded tissue

First, the slices of eye cubs of *C. jacchus* were deparaffinized using the following protocol (Table 9):

Table 9: Deparaffinizing protocol

Reagent	Time	Repetitions
Xylene	10 min	2x
99 % Ethanol	2 min	2x
96 % Ethanol	2 min	2x
70 % Ethanol	2 min	2x
Aqua Dest.	2 min	2x

After deparaffinization, the slices were heated for 3 min at 600 W in the microwave oven in citrate buffer. After cooling down to RT, the slices were washed with PBS three times for 5 min, followed by a blocking step with 10 % FCS in PBS for 30 min at RT. The primary antibody was diluted in PBS containing 10 % FCS, applied to the slices and incubated over night at 4 °C. In the following steps, the slices were washed with PBS three times for 5 min and the secondary antibodies, diluted in PBS containing 10 % FCS, were applied to the slices and incubated for 1 h at RT in the dark. After an additional washing step with PBS (3x 10 min), the slices were coverslipped with Mowiol mounting medium containing Hoechst. As a negative control, the secondary antibody was used alone.

3.2.4.2.3 Immunofluorescence staining of cryo conserved samples

After sectioning, the slices were fixed in pure methanol at -20 °C for 10 min, followed by three washing steps in PBS for 5 min each and blocking in 10 % FCS for 30 min at RT. The following steps were performed like described in 3.2.4.1.2

3.2.4.2.4 Immunofluorescence staining of ARPE-19 and ppRPE cells

The cells were seeded on round cover slips (Ø 12 mm) and grown until the desired confluence was reached. The cells were treated as necessary for the corresponding assay. After treatment, the cell culture medium was removed, and the cells were washed with PBS for 10 min followed by a fixation with PFA for 10 min. After an additional washing step with PBS for 10 min and blocking with 10 % FCS+0.25 % Triton x-100 for 2 h at RT, the primary antibodies were applied to the cover slips and incubated over night at 4 °C. After washing the cells twice with PBS for 15 min, the secondary antibodies were applied to the cells and incubated for 2 at RT in the dark. After incubation, the cells were washed with PBS three times for 15 min. For embedding, the cover slips were turned over and placed in a slide covered with Mowiol mounting medium containing Hoechst. As a negative control, the secondary antibody was used alone.

3.2.4.3 Hematoxylin and eosin staining

Selected paraffin slides were deparaffinized using the protocol described in section 3.2.4.2.2. Afterwards, the slices were treated as followed (Table 10):

Table 10: Hematoxylin and eosin staining protocol

Reagent	Time	Repetitions
Hematoxylin	4 min	1
Tab water	10 s	1
HCl/Ethanol	5 s	1
Running Tab water	5 min	1
Aq. Dest.	10 s	1
Eosin	2 min	1
70 % Ethanol	2 min	1
96 % Ethanol	2 min	2
99 % Ethanol	2 min	2
Xylene	10 min	2

Afterwards, the slices were embedded in a small drop of Roti-Histokitt and coverslipped.

3.2.5 Classifications and measurements of the RPE

The retinal sections of paraffin embedded and cryo embedded *C. jacchus* eyes were classified in three different topographical regions. The division of the region was adapted and adjusted from Ach et al. (Ach et al., 2014) and Schubert (Schubert, 2019):
(1) Macula including fovea, parafoveal area and perifoveal area,
(2) near periphery
(3) middle and far periphery (classified as far periphery)
The diameter of the RPE cell layer was measured using the straight selection in Image J. The measurements of the height in the near periphery and far periphery was normalized to heights of the cells in the macula in each sample. the intercellular distribution of pigment granule has been determined under qualitatively aspects. Ten

different points has been measured in one image. Two neonatal eyes and three adolescent and adult eyes were examined in three different slides per eye.
The measurement of the cell size of RPE cells in the wholemount was performed using Image J. The size of 20 hexagonal cells of each, macula and periphery, was measured and compared.

3.2.6 Calculation of the Cytoplasm-Nucleus Ratio

After immunofluorescence staining with antibodies detecting *p*53, MDM2, *p*14ARF (ARF tumor suppressor) and HMOX1 (heme oxygenase (decycling) 1), the quantification of the mean optical density fluorescence was accomplished by using the Image J software. The Cytoplasm-Nucleus ratio (C:N) of the control was considered to be 1. C:N ratios >1 implied an increased cytoplasmic retention, whereas C:N ratios <1 indicated increased nuclear retention (He et al., 2014; Wang et al., 2010)

3.2.7 Cell culture assays

3.2.7.1 Cell culture conditions

ARPE-19 (p30-p40) and ppRPE (p0-p2) cells were cultured in DMEM/F12 supplemented with 10 % FCS, 3.57 mg/ml HEPES, and 1 % P/S (50 µg/ml) in a humidified CO_2 atmosphere at 37 °C. The cell culture medium was replaced every 3 days to ensure the availability of nutrients and the correct pH level for the cells. Cell lines are regularly passaged to avoid overgrowing and to ensure a stable reproducible source of cells to setup experiments. To passage or collect the cells, cells were washed with 1x HBSS and incubated in 1 ml or 0.5 ml of a 0.05 % Trypsin/EDTA solution for 2-5 min at 37 °C to detach the cells from flask surface. Afterwards, cells are collected and resuspended in 10 ml supplemented growth medium. The number of cells was counted using a Neubauer Chamber. 5 µl cell suspension was diluted in 20 µl Trypane blue to avoid counting dead cells. The number of counted cells was divided by the number of counted big squares (four, respectively). This number is multiplied by 10^4 (Specific chamber factor) and by the dilution factor (five, respectively). The resulting number is the number of cells per ml. For experiments, cells were plated in either T75 or T25 flasks or in 6-well up to 96-well plates, depending on the assay. Cells used for experiments were in exponential growth phase.

3.2.7.2 Exposition of rSNCB and rCTSB to cell culture

Three different concentrations (1 ng/ml; 50 ng/ml; 500 ng/ml) of recombinant SNCB (rSNCB; rat) were used to expose ARPE-19 cells and ppRPE cells to SNCB. The homology of human SNCB to rat SNCB is 97 % (BLAST search). The used concentrations are based on results from previous studies about the role and effects of SNCB on brain microvascular endothelial cells (BMECs) which was published previously (Brockhaus et al., 2018).

ARPE-19 cells were exposed to recombinant CTSB (rCTSB; human) in three different concentrations (1 ng/ml; 10 ng/ml; 100 ng/ml). The used concentrations are based on previous experiments performed by Moon et al. (Moon et al., 2016), who worked on CTSB levels in human plasma which are correlated with fitness and hippocampus-dependent memory function.

The recombinant proteins were diluted in in culture medium to reach the desired concentration and cells were exposed to the proteins dependent of the specific assays. An overview about the incubation times is shown in the following Table 11.

Table 11: Incubation times of rSNCB and rCTSB for different assays

Application	Incubation time
MTT assay	6 h 12 h, 24 h, 48 h, 72 h
TUNEL assay	6 h 12 h, 24 h
qRT-PCR	48 h
Immunofluorescence	48 h
FACS	48 h

3.2.7.3 Cell Viability Assay

To test the viability of ARPE-19 cells and ppRPE cells treated with rSNCB and rCTSB, respectively, the MTT assay was used. It is a colorimetric assay for evaluate the metabolic activity of cells (Stocker, 1990). The NADPH-dependent cellular oxidoreductase reduces the tetrazolium dye MTT to its insoluble formazan. The cells were seeded in 48-well plates (300 µl per well, containing 2×10^4 cells/well) and treated with rSNCB and rCTSB, for 12-72 h. Afterwards, 300 µl of the MTT reagent (0.5 mg/ml in culture medium) was added to each well, and the cells were incubated for 1-2 h at 37 °C, depending on the staining of the cells. For solvation, 500 µl of isopropanol was

added to each well to dissolve the formazan. After incubating the plate for 5 min on a plate reader, the results were obtained using the microplate reader at λ=570 nm and λ=670 nm. The viability of the control samples was considered to be 100 %.

3.2.7.4 Apoptosis Assay

For detecting apoptosis in ARPE-19 cells and ppRPE cells exposed to rSNCB, a TUNEL assay was used. The terminal deoxynucleotidyl transferase dUTP nick end labeling (TUNEL) is a method for detecting DNA fragmentation by labeling the 3′-hydroxyl termini in the double-strand DNA breaks generated during apoptosis (Gorczyca et al., 1993). Therefore, the cells were seeded on round cover slips (Ø 12 mm) and grown until the desired confluence was reached followed by an exposition with the different concentrations of rSNCB for 12-72 h. Afterwards, the cells were fixed with 4 % PFA for 15 min. The ApopTag Fluorescein in Situ Apoptosis Detection Kit S7110 was used for TUNEL staining, according to the manufacturer's instructions. For embedding, the cover slips were turned over and placed in a slide covered with Mowiol mounting medium containing Hoechst. The ratio of TUNEL-positive cells and the total cell number was calculated and normalized to the untreated control.

3.2.8 Western Blot Analysis

For the detection of specific proteins from lysate of the RPE from *C. jacchus*, Western Blot analysis was used.

3.2.8.1 Preparation of protein lysates from *C. jacchus* RPE tissue

For protein isolation of RPE tissue from *C. jacchus*, the tissue was dissected on a cooled petri dish with a scalpel in small pieces. In a 1.5 ml-reaction tube, the tissue was filled up with 70-100 µl RIPA buffer for lysing the cell, depending on the size of the RPE piece, mixed and kept on ice for 30 min. Afterwards, the samples were sonicated (2x20 sec) for additional lysis, followed by a centrifugation for 20 min at 10,000xg at 4 °C. The lysate was transferred to a clean tube, whereas the pellet was discarded. The samples were kept at -20 °C until further use.

3.2.8.2 Quantification of protein concentration

The protein concentration was quantified using Bradford method. The principle of this method is based on the formation between the dye Coomassie Brilliant Blue G250 and cationic and non-polar side chains of proteins in acid solution. The complex formation

shifts the absorption maximum of λ=470 nm in the unbound dye to λ=590 nm in the complex. To determine the protein concentration, a bovine serum albumin (BSA) dilution series (standard) was used. In this study, the DC™ Protein Assay containing Reagent A and Reagent B was used. For the quantification, 5 µl of the protein sample or the standard (0 mg/ml, 0.1 mg/ml, 0.25 mg/ml, 0.5 mg/ml, 1 mg/ml, 2.5 mg/ml, 5 mg/ml, 10 mg/ml and 25 mg/ml) were mixed with 45 µl Aq. Dest. In a 96-well plate, 20 µl of each standard and sample was loaded (double determination).
10 µl of Reagent A and 75 µl of Reagent B was added to each well. The plate was incubated for 5 min at RT on a plate shaker before it was read in an ELISA reader at λ=700 nm. The protein concentrations were calculated, and 30 µg of total protein was loaded on the SDS-gel

3.2.8.3 SDS-Polyacrylamide gel electrophoresis

For the separation of proteins based on their molecular weight, a discontinues SDS-Polyacrylamide gel electrophoresis (SDS-PAGE) after Laemmli was performed (Laemmli, 1970).
In this study, separating gels with an acrylamide concentration of 10 % were used to separate the protein of interest (POI) were prepared as followed (Table 12):

Table 12: Preparation of the separating and stacking gel

	Separating gel (10 %)	Stacking gel
Acrylamide	10 ml	3 ml
Stacking gel buffer (4x)	-	5 ml
Separating gel buffer (4x)	7.5 ml	-
Aq. dest	12.5 ml	12 ml
TEMED	100 µl	50 µl
APS	100 µl	50 µl

For preparation of the protein samples, 5 µg of the protein was diluted with Aq. dest and Laemmli loading buffer was added to the sample (1:4). The samples were heated up to 95°C for 5 min to denaturize the proteins. Afterwards, 20 µl of each sample was loaded to the gel. Additionally, 5 ml of a colored standard marker for molecular weight estimation on SDS-PAGE and western blots was added. A voltage of 80 V was applied to the gel for 30 min until each sample reached the boundary of the stacking gel.

Afterwards, a voltage of 120 V was applied, and the separation was performed in the separating gel until the blue running front reached the boundary of the separating gel.

3.2.8.4 Western Blotting

After separating the proteins in the gel, they needed to be transferred to a membrane electrophoretically. In this study, the so called “wet blot” was performed.

In this study, Polyvinylidene difluoride (PVDF) membranes were used. This type membrane needs to be activated in methanol previously. The cassettes were places in the tank containing a cooling pad and filled up with blotting buffer. An electric current of 60 mA was created, and the blotting was performed at 4 °C over night. After the transfer, the efficiency of the transfer was evaluated by staining the membrane for 30s with PVDF staining solution followed by a de-stain until the bands on the membrane were clearly visible. Afterwards, the membranes were blocked with blocking buffer containing 5 % milk powder in TBS for 1 h at RT. After blocking, the membrane was cut into pieces corresponding to the molecular weight of the POI. Each strip was incubated with the respective antibody diluted in the blocking buffer for 72 h at 4 °C on a shaking device. Subsequently, the membranes were washed in TBST three times for 15 min followed by the incubation with the respective HRP-conjugated secondary antibodies (see section 3.1.6) for 2 h at RT and three additional washing steps with TBST for 15 min. For detection, the membranes were covered with ECL-Western Blotting detection reagent according to the manufacturer’s instructions and detected on the gel imaging system. The exposition time varied between 1 min and 10 min, depending on the strength of the signal.

3.2.8.5 Evaluation of protein expression

The protein expression was evaluated using Image J software. The density of each band in a gel was calculated individually. In a first step, the lanes were selected in each gel and each band in one lane was selected manually. After selection, the program provides histograms of each band (the larger the histogram, the brighter the band). To exclude unspecific signals in the background, a line across the top of the histogram must be drawn from where it first begins to drop steeply until where it levels out again. Afterwards, the “area under the curve” was calculated, which is the density of the band. This area was normalized to the density of the band of the housekeeping protein. In this study, tubulin (50 kDa) was used as a housekeeping protein. Each Western Blot was repeated three times with three individual samples of each age groups. The mean

and the standard deviation were calculated. To compare the results of protein expression, each density was normalized to the protein density of the neonatal macula sample (normalized to 1). The data was analyzed with a test for two independent samples to examine for conformity with the Gaussian distribution and processed using the independent-samples t-test with a significance of $p<0.05$.

3.2.9 Introduction of a premature senescence model *in-vitro*

The aim of introducing the cells to premature senescence was to test, if CTSB influences the premature senescence in any way. First, the systems needed to be established. Like described in the previous work (Glotin et al., 2008), APRE-19 cells were treated with, 8 mM *tert*-butyl hydroperoxide (*tert*-BHP) was for 1 h on 5 following days. In initial experiments, concentrations of 8 mM, 6 mM, 4 mM, 2 mM and 1 mM were used to expose cells. After the first day of treatment, the cells treated with higher concentrations (8 mM, 6 mM, 4 mM) were detached and dead. The concentration of *tert*-BHP and the number of treatments was decreased step by step to reach sublethal treatment conditions. The cells treated with the lower concentrations (2 mM and 1 mM) were still attached to the flask surface. The final experimental approach is shown in the following Figure 10. The cellular and molecular analysis include the experiments described in the sections 3.2.9.1 and 3.2.10.

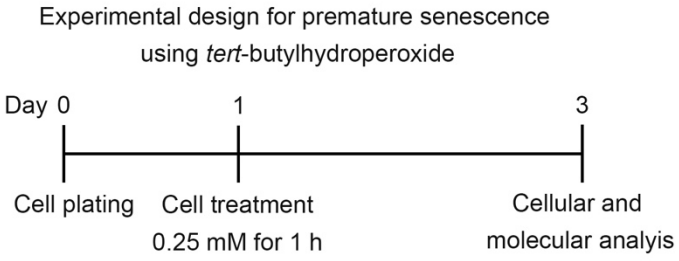

Figure 10 Experimental setup for premature senescence using *tert*-BHP.
Cells were plated at Day 0 with the appropriate cell concentration, treated on day 1 with 0.25 and 0.5 mM *tert*-butyl hydroperoxide (*tert*-BHP) for 1 h and analyzed on day 3 post treatment.

The cells were plated in a culture dish or flask with a designated cell number, depending on the final assays. The confluence of the cells at the day of treatment was about 60 %. After 24 h, the cells were treated with 0.25 mM and 0.5 mM *tert*-BHP, diluted in culture media, at 37 °C for 1 h. Afterwards, the cells were washed with HBSS and provided with fresh culture medium for 48 h to recover. After recovery, the specific assays were performed on the cells.

3.2.9.1 Analysis of senescence

To investigate the level of senescence in the cells, the senescence-associated β-galactosidase (SA β-gal) assay was used. It was shown, that several human cells express a beta-galactosidase, histochemically detectable at pH 6, upon senescence in culture. This marker is expressed by senescent, but not pre-senescent cells (Dimri et al., 1995). The cells were seeded on round cover slips (Ø 12 mm). After 24 h of cultivation, the cells were treated with 0.25 mM or 0.5 mM *tert*-BHP, respectively, for 1 h. Afterwards, the cells were washed with HBSS and recovered from treatment for 48 h, followed by the SA β-gal assay according to manufacturer's instructions. Afterwards, the cells were stained with Nuclear Fast Red Solution for 10 s and washed three times with PBS for 5 min. For embedding, the cover slips were turned over and placed in a slide covered with Mowiol mounting medium. Cells with a dark blue stain were counted to calculate the percentage of senescence. The viability of the cells was tested using a cell viability assay in accordance with the protocol described in 3.2.7.3. Additionally, the influence of *tert*-BHP on the oxidation of nucleic acids and the oxidation of lipids was investigated. For the investigation of oxidation of nucleic acids, the cells were stained with antibody against 8-Hydroxyguanosine (8-HGN). In intact animals, lesions (adducts) excised from DNA are transported from the cell through the circulation and excreted in urine. Those adducts can be assayed as a measure of oxidative damage to DNA using 8-HGN as a marker for DNA damage produced by oxidants because it represents one of the major products generated by a wide array of treatments associated with oxidant damage. In the cell, 8-HGN RNA lesions are formed by reaction with ROS generated either via normal oxidative metabolic processes, UV ionizing radiation, or exposure to oxidative agents. For the investigation of the oxidation of lipids, the cells were stained with antibody against 4-Hydroxynonenal (4-HNE). 4-HNE is an α,β-unsaturated hydroxyalkenal which is produced by lipid peroxidation in cells. Aldehydic products of lipid peroxidation, have been implicated as one of the key mediators of oxidative stress induced cell death.

3.2.10 FACS Analysis

For the investigation of the role of CTSB in senescent cells, the cells were incubated with CTSB and 0.25 mM *tert*-BHP simultaneously. On day 3, the cells were analyzed using fluorescence-activated cell sorting (FACS).
The experimental design is shown in Figure 11.

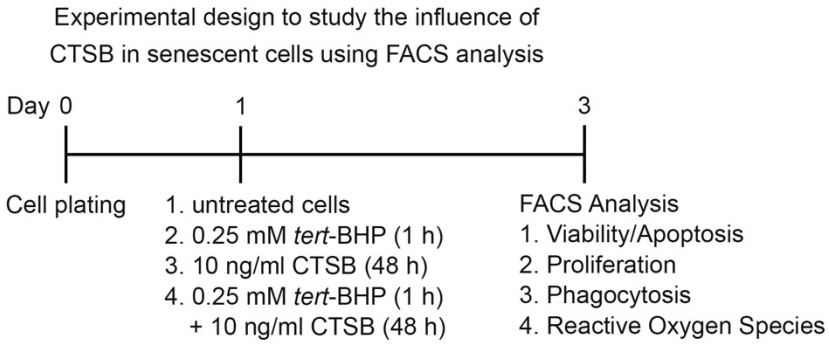

Figure 11 Experimental setup to study the influence of CTSB on senescent cells.
Cells were plated at Day 0 with the appropriate cell concentration, treated on day 1 with four different set ups: 1) untreated cells; 2) 0.25 mM *tert*-BHP for 1 h; 3) 10 ng/ml CTSB for 48 h; 4) 0.25 mM *tert*-BHP for 1 h followed by 10 ng/ml CTSB for 48 h. Cells were analyzed on day 3 post treatment.

For all experiments, cells were plated in T75 or T25 cell culture flasks with the same cell number ($1.5*10^6$ cells/T75; $5*10^5$ cells/T25) and treated as follows on day 1.

1. Untreated cell: Cells remained untreated as a control and provided with new culture medium
2. 0.25 mM *tert*-BHP: The cells were treated with the desired amount of *tert*-BHP for one hour. Afterwards, the cells were washed with HBSS and provided with new culture medium.
3. 10 ng/ml CTSB: The cells were provided with new culture medium and rCTSB was added to the medium
4. 0.25 mM *tert*-BHP + 10 ng/ml rCTSB: The cells were treated with the desired amount of *tert*-BHP for one hour. Afterwards, the cells were washed with HBSS and provided with new culture medium and rCTSB was added to the medium

FACS analysis was performed on the CytoFlex Beckman Coulter Inc, using CytoExpert Software. 50000 events were counted per experiment. The data was analyzed using Kaluza Analysis Software. The cells were initially soaked into the central measuring

capillary of the flow cytometer and passed individually through a laser beam through the process of hydrodynamic focusing in the form of a laminar particle flow. The gating strategy is explained for every staining individually. The statistical analysis was performed using One-Way ANOVA (GraphPad Prism 7.0a).

3.2.10.1.1 Analysis of viability and apoptosis

For the investigation of viability and apoptosis in cells treated with *tert*-BHP and rCTSB, the PE Annexin V Apoptosis Detection Kit was used. The loss of the plasma membrane is one of the earliest events in apoptosis. In apoptotic cells, the plasma membrane phospholipid phosphatidylserine is translocated from the inner to the outer layer, which exposes phosphatidylserine to the external cellular environment. Annexin V has a high affinity for PS, which leads to a binding to phosphatidylserine exposed cells. Annexin V is conjugated to the fluorochrome Phycoerythrin (PE). PE Annexin V staining precedes the loss of membrane integrity which accompanies the latest stages of cell death resulting from either apoptotic or necrotic processes. Therefore, the staining is typically used in combination with the vital dye 7-Amino-Actinomycin (7AAD) to allow the investigator to identify early apoptotic cells. Viable cells with intact membranes exclude 7AAD, whereas the membranes of dead and damaged cells are permeable to 7AAD (Vermes et al., 1995). For the staining, the cells were detached from the flask with Trypsin-EDTA, and the cells of each condition were divided into four parts. The cells were washed twice with PBS and re-suspended in ice cold 200 µl 1x Annexin V Binding buffer. The cells were stained which 5 µl PE Annexin V and 5 µl 7AAD using the following scheme for each condition (Table 13):

Table 13: Sample scheme for Annexin V-7AAD assay

Probe	PE Annexin V	7AAD
1	-	-
2	-	+
3	+	-
4	+	+

The gating strategy is described in the following Figure 12. First, all detected cells were plotted in a dot plot. The side scatter height (SSC-H) was plotted against the forward scatter height (FSC-H). To discriminate between singlets and doublets single, the side scatter area (SSC-A) was plotted against the SSC-H. The single cells were gated (Gate

A). In the next step, the height signal of 7AAD (7AAD-H) was plotted against the height signal of PE Annexin V to discriminate the single cells in their different states. Therefore, the plot was gated into four quadrants. Cells which are negative for 7AAD as well as PE Annexin V staining (Gate B--) are viable cells. 7AAD positive and PE Annexin V negative cells (Gate B-+) are necrotic whereas 7AAD negative and PE Annexin V positive cells (Gate B+-) are in early apoptosis. Cells which are positive for both, 7AAD and PE Annexin V (Gate B++), are cells in apoptosis. The value for each gate was given in percent.

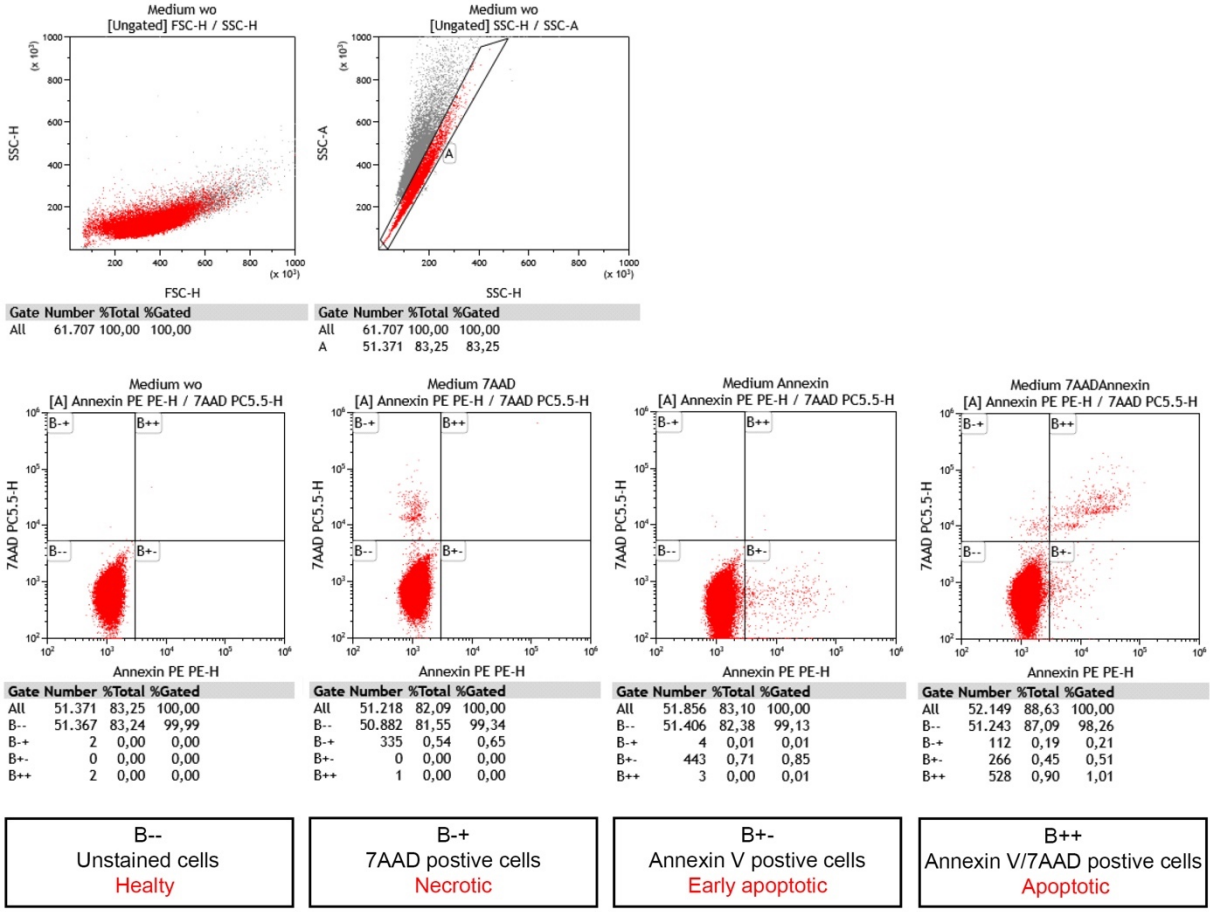

Figure 12 Gating strategy for the analysis of viability and apoptosis

The side scatter height (SSC-H) was plotted against the forward scatter height (FSC-H). The side scatter area (SSC-A) was plotted against the SSC-H To discriminate between single and clustered cells. The single cells were gated (Gate A). The height signal of 7AAD (7AAD-H) was plotted against the height signal of PE Annexin V to discriminate the single cells in their different states. Negative for 7AAD and PE Annexin V staining (Gate B--): viable cells. 7AAD positive and PE Annexin V negative (Gate B-+): necrotic cells. 7AAD negative and PE Annexin V positive cells (Gate B+-): early apoptosis. 7AAD and PE Annexin V positive (Gate B++): apoptotic cells. The information for each gate was given in percent.

3.2.10.1.2 Proliferation assay

To investigate the cell proliferation, the cells were stained with Cell Proliferation Dye eFluor™ 670. It is a red fluorescent dye that can be used to monitor individual cell divisions. The dye binds to any primary amine in cells and as the cell divides, the dye is equally distributed between the daughter cells. The dye was reconstituted as described in the manufacturer's manual. The staining took place before any treatment of the cells. For the staining, $3*10^6$ cells were used and diluted in 2 ml PBS. The dye was diluted in 2 ml PBS (1:2000) and both initial solutions were mixed and incubated for 10 min at RT in the dark. Afterwards, the cells were washed twice with ice-cold HBSS containing 10 % FCS. The cells were counted again and seeded with a density of $5*10^5$ cells/T25 and treated in the following days as described above. For FACS, the cells were detached from the flask with Trypsin-EDTA, and the cells of each condition were divided into two parts. The cells were washed twice with PBS and re-suspended in 200 µl PBS. As a control, unstained cells were used. To ensure only viable cells were counted, the cells were additionally stained with 7AAD as described above. The following scheme was used for each condition for the measurement (Table 14):

Table 14: Sample scheme for the proliferation assay

Sample	7AAD	eFluor™ 670
1	+	-
2	+	+

The gating strategy is described in the following Figure 13. First, all detected cells were plotted in a dot plot. The SSC-H was plotted against the FSC-H. To discriminate between single cells and clustered cells, the SSC-A was plotted against the SSC-H. The single cells were gated (Gate A/D). In the next step, the SSC-H was plotted against 7AAD-H to gate the viable cells (Gate B/E). In the following step, the count of the measured events /cells was plotted against the height of the eFluor™ 670 dye in a histogram. The geometric mean (X-Gmean) of the untreated controls was compared to the X-Gmean of the samples. A reduced X-Gmean implies an increase in proliferation. The overlay histogram shows the histogram of an unstained control compared to the stained untreated control.

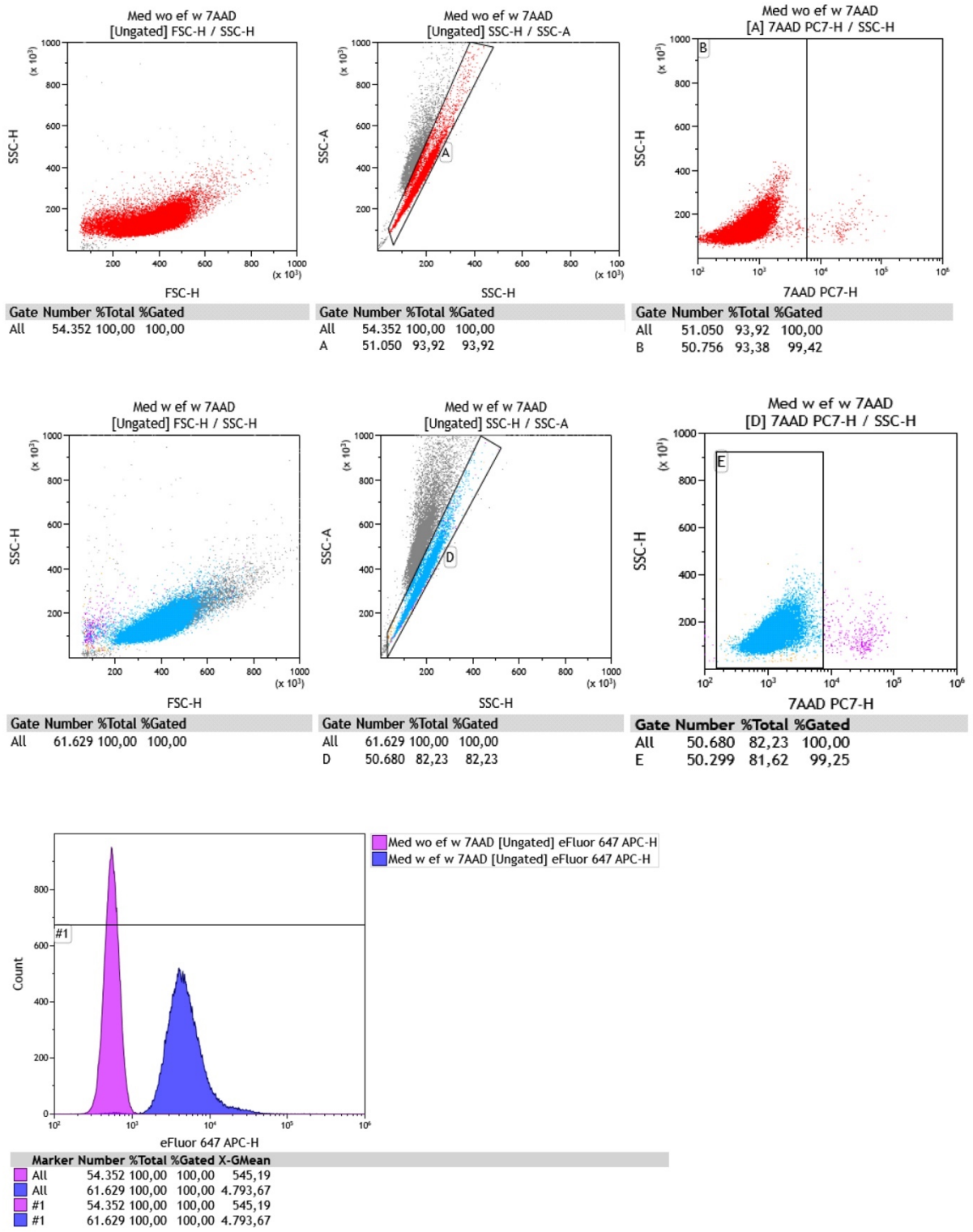

Figure 13 Gating Strategy for the Proliferation Assay

The side scatter height (SSC-H) was plotted against the forward scatter height (FSC-H). The side scatter area (SSC-A) was plotted against the SSC-H To discriminate between single and clustered cells. The single cells were gated (Gate A7D). SSC-H was plotted against 7AAD-H to gate the viable cells (Gate B/E). Count of the cells was plotted against the height of the eFluor™ 670 dye in a histogram. The geometric mean (X-Gmean) of the untreated controls was compared to the X-Gmean of the samples. The overlay histogram shows the histogram of an unstained control compared to the stained untreated control.

3.2.10.1.3 Phagocytosis assay

To investigate whether *tert*-BHP or CTSB have an influence on phagocytosis, the cells were incubated with carboxylate-modified polystyrene Latex beads, which are yellow green fluorescent. The particle size of the latex beads was 1 µm. After *tert*-BHP or rCTSB treatment, the cells were incubated with 20 µl of the aqueous latex bead suspension to gain a final concentration of $8*10^8$ beads per flask for 120 min at 37 °C. Afterwards, the cells were washed twice with PBS and re-suspended in 200 µl PBS. As a control, unstained cells were used. To be sure, only events of viable cells were counted, the cells were additionally stained with 7AAD as described above. The following scheme was used for each condition for the measurement (Table 15):

Table 15: Sample scheme for the phagocytosis assay

Sample	7AAD	Latex beads
1	+	-
2	+	+

The gating strategy is described in the following Figure 14. First, all detected cells were plotted in a dot plot. The SSC-H was plotted against the FSC-H. To distinguish between single cells and clustered cells and to exclude the unbound beads, the SSC-A was plotted against the SSC-H. The single cells were gated (A/C). In the next step, the SSC-H was plotted against 7AAD-H to gate the viable cells (E/F). In the following step, the count of the cells was plotted against the height of the Latex beads (Beads-H) in a histogram. All cells within the gates were positive for phagocytosed latex beads (B/D). The percentage of gated cells is used to compare the phagocytosis rate of the different treated cells.

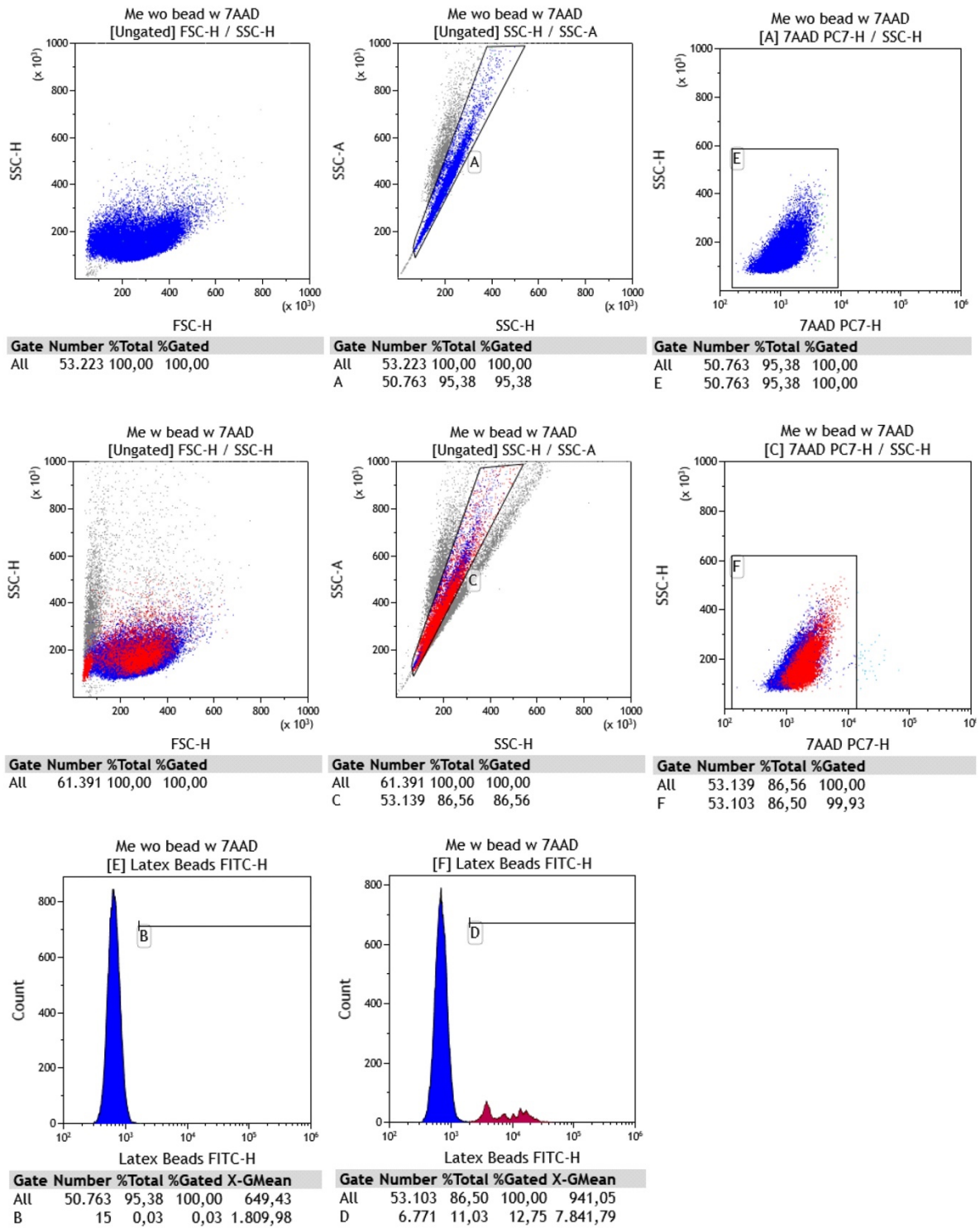

Figure 14 Gating Strategy for the Phagocytosis Assay

The side scatter height (SSC-H) was plotted against the forward scatter height (FSC-H). The side scatter area (SSC-A) was plotted against the SSC-H To discriminate between single and clustered cells. The single cells were gated (Gate A/C). SSC-H was plotted against 7AAD-H to gate the viable cells (E/F). In the following step, the count of the cells was plotted against the height of the Latex beads (Beads-H) in a histogram. All cells within the gates phagocytosed beads (B/D). The percentage of gated cells is used to compare the phagocytosis rate of the different treated cells

3.2.10.1.4 Intracellular ROS level

To investigate the intracellular ROS level after *tert*-BHP and rCSTB treatment, the cells were incubated with the ROS Detection Reagents 2',7'-dichlordihydrofluorescein-diacetat (H_2DCFDA). Chemically reduced and acetylated forms of 2',7'-dichlorofluorescein (DCF) are non-fluorescent until the acetate groups are removed by intracellular esterases and oxidation occurs within the cell. The oxidation of these probes can be detected by monitoring the increase in fluorescence. The following Figure 15 shows the reaction equation from H_2DCFDA to the deacetylated, oxidized DCF with the help of the esterase.

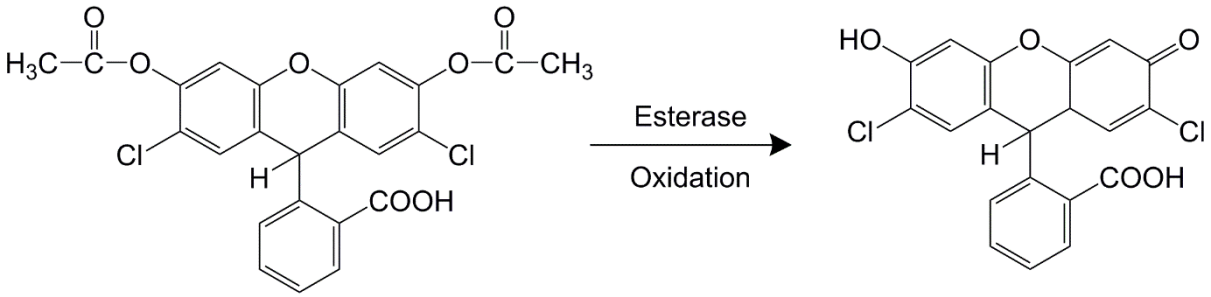

Figure 15 Reaction equation from H_2DCFDA to the deacetylated, oxidized DCF

H_2DCFDA is non-fluorescent until the acetate groups are removed by intracellular esterases and oxidation occurs within the cell. The result of the reaction is the fluorescent and oxidized DCF. Oxidation of these probes can be detected by monitoring the increase in fluorescence with a flow cytometer, fluorometer, microplate reader, or fluorescence microscope, using excitation sources and filters appropriate for fluorescein (FITC).

An important difference to other FACS assays is, that the cells need to be cultured in culture medium without phenol red as the dye may disturb the signal in the FACS analysis. Apart from that the cells were treated as described above. After treatment, the cells were washed twice with PBS, divided into two parts and re-suspended in 1000 µl PBS. The cells were incubated with 1 µM of H_2DCFDA for 15 min at 37 °C. As a control, unstained cells were used. Afterwards, the cells were washed twice again and re-suspended in 200 µl PBS. Dead cells were excluded via 7AAD staining. The following scheme was used for each condition for the measurement (Table 16)

Table 16: Sample scheme for ROS assay

Probe	7AAD	H_2DCFDA
1	+	-
2	+	+

The gating strategy is described in the following Figure 16. First, all detected cells were plotted in a dot plot. The SSC-H was plotted against the FSC-H. To discriminate between single cells and clustered cells, the side scatter area (SSC-A) was plotted against the SSC-H. The single cells were gated (Gate A). In the next step, the SSC-H was plotted against 7AAD-H to gate the viable cells (Gate B). In the following step, the Count of the cells was plotted against the height of the ROS dye (ROS-H) in a histogram. ROS is present in each cell. The mean fluorescent intensity is used to calculate the ROS level of the cells after treatment.

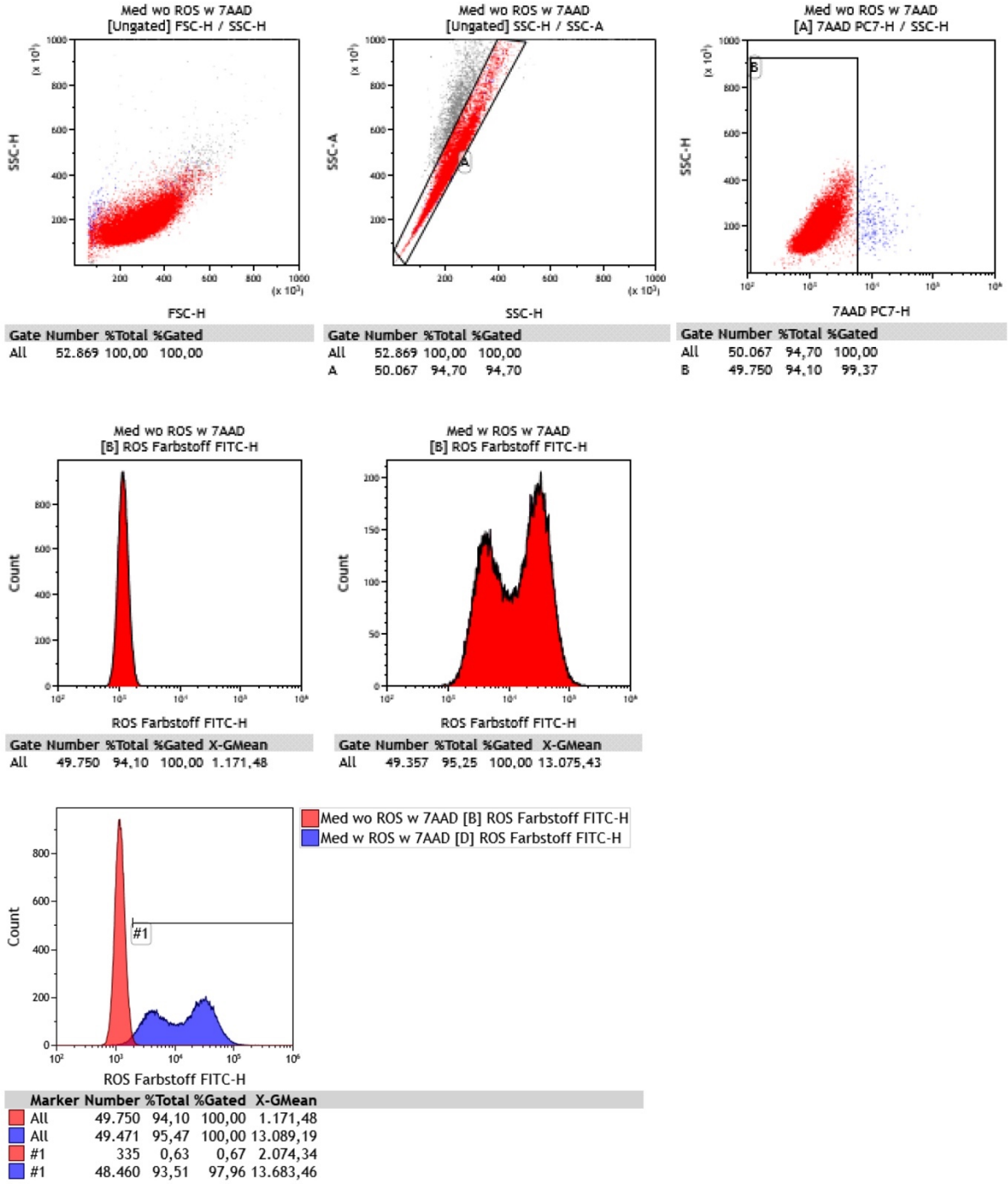

Figure 16 Gating strategy for ROS Assay

The SSC-H was plotted against the FSC-H. The SSC-A was plotted against the SSC-H To discriminate between single and clustered cells. The single cells were gated (Gate A). SSC-H was plotted against 7AAD-H to gate the viable cells (B).

4 Results

4.1 Histological characterization of aging RPE

The results of this chapter are published in Hadrian et al., 2019 (Hadrian et al., 2019)
The histological analysis of the RPE in retinal sections of *C. jacchus* was performed to reveal morphological alterations in RPE, regarding age and topography. The results of the HE-staining are shown in Figure 17. Alterations of the distribution of intracellular pigmentation in RPE cells, depending on the age and topography, have been found. Independently of the topographical localization, the granules were equally distributed in the cells in neonatal tissue. In the macula and near periphery regions of the adolescent RPE, the intracellular pigment granules shifted towards the apical side of the RPE. In the far periphery the granules are equally distributed. The pigment granules in aged tissue were located on the apical side. Regarding macular and peripheral regions, the pigment granules were equally distributed. Next to changes in the location of the pigmentation, changes in morphological characteristics (shape, respectively), of the granules are detected. In neonatal animals the granule pigments appear elliptical with no morphological variations. In macular and near peripheral region, the pigment granules appeared more circular in adolescent and adult animals. In contrast, the pigments granules appeared elliptical in far peripheral cells (Figure 17).

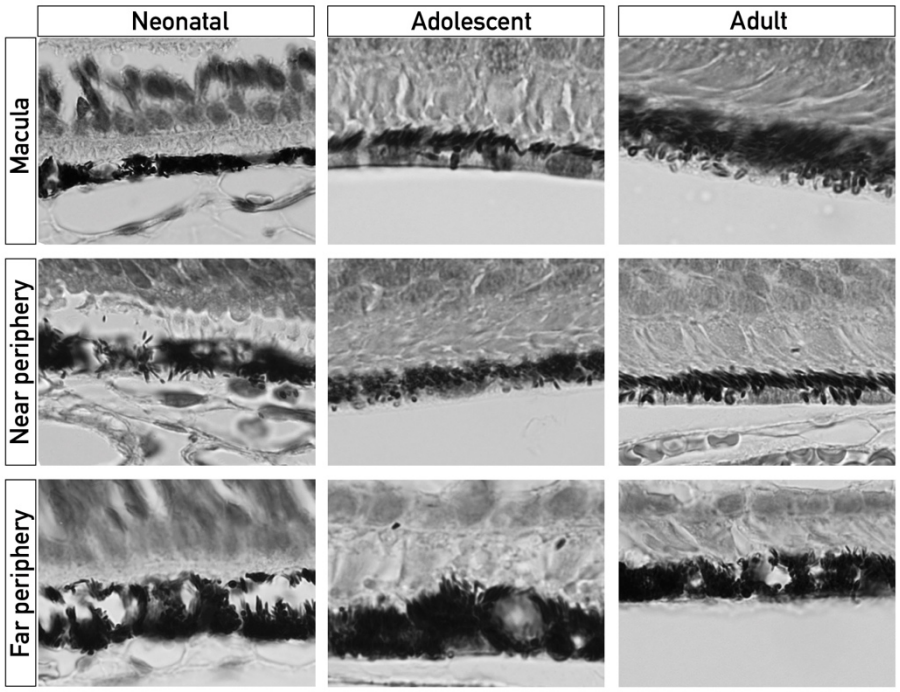

Figure 17 Histological characterization of the RPE in *C. jacchus* over lifetime

HE-stain of paraffin retinal section of *C jacchus* at different ages: neonatal, adolescent, and adult. Retinal sections were divided into different regions: macula, near periphery, and far periphery. All pictures are shown with a 100x magnification. (Adapted from Hadrian et al., 2019) Abbreviations: RPE: Retinal pigment epithelium; *C. jacchus: Callithrix jacchus*; HE: Hematoxylin and Eosin

For a quantitative analysis, the height of the single-layer RPE was examined. The analysis of the heights of the cells is shown Figure 18. The height of the RPE differed between the age-stages. The cell height was normalized to the arithmetic mean. In the macula, the height of the RPE cells increases with age (neonatal: 0.68±0.12; adult: 1.27±0.14, p=0.001). The heights remained unchanged in the near periphery and decreases in the far periphery (neonatal: 1.46±0.07; adult: 1.05±0.17, p=0.02). The height of the RPE cells increased significantly from the macula to the far periphery in neonatal RPE (Macula: 0.68±0.12; Near periphery: 0.95±0.09, p=0.02; Far periphery: 1.46±0.07, p=<0.001). The height of the RPE is significantly increased in the far periphery in adolescent tissue (Macula: 0.82±0.11; Far periphery: 1.43±0.04, p=0.002), whereas it decreases significantly between the macula and the near periphery. In adult tissue, the height of the RPE decreases significantly between the macula and the near periphery (Macula: 1.27±0.14; Near periphery: 0.93±0.12, p=0.02).

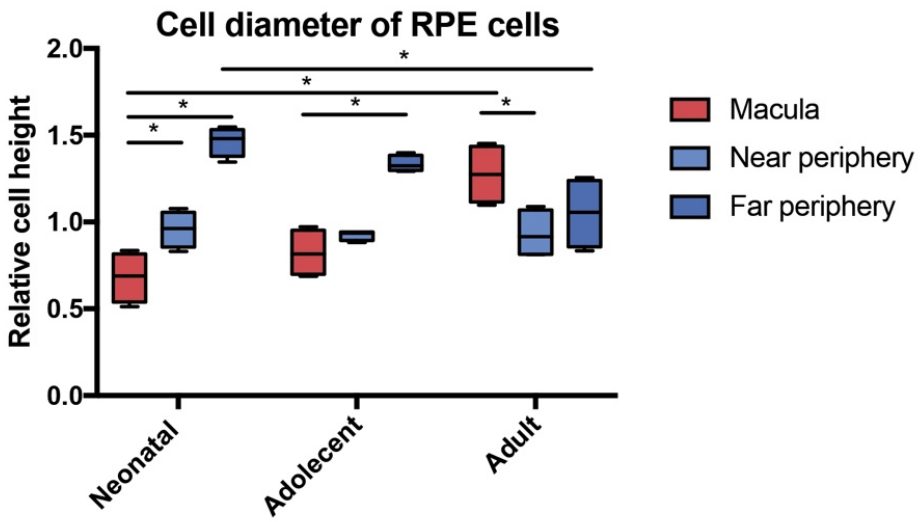

Figure 18 Cell diameter of RPE cells regarding age and topography

Relative height of RPE cells in retinal sections of paraffin-embedded eyes in different ages and different regions of the RPE of *C. jacchus*. (Adapted from Hadrian et al., 2019) * $p<0.05$ indicating statistical significance; Abbreviations: RPE: Retinal pigment epithelium; *C. jacchus: Callithrix jacchus*

The differential distribution of the pigment granules described above, is schematically shown in Figure 19.

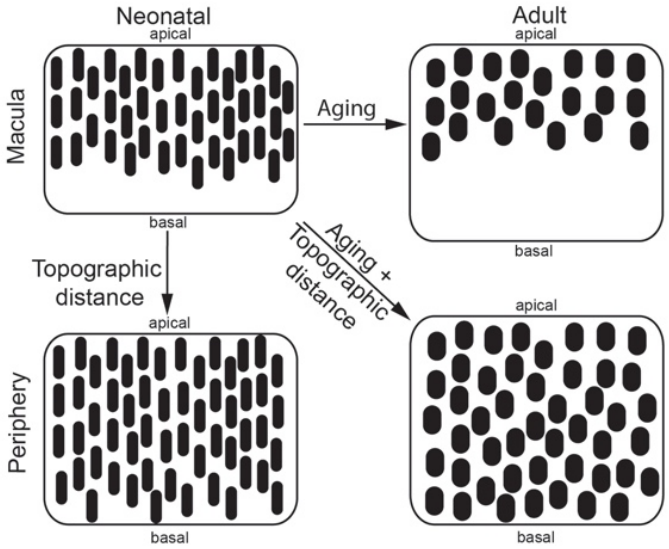

Figure 19 Schematic topology of pigment granules

Schematic topology of pigment granules depending the age and the region in the RPE of *C. jacchus*. (Adapted from Hadrian et al., 2019) Abbreviations: RPE: Retinal pigment epithelium; *C. jacchus: Callithrix jacchus*

4.2 Transcriptome analysis of the RPE from *C. jacchus*

The RNA sequencing analysis were performed by **PD Dr. Ludger Klein-Hitpass**. The bioinformatics were performed by **Prof. Dr. Sven Rahmann** and **PD Dr. Ludger Klein-Hitpass**.

The transcriptome of the RPE of *C. jacchus* was compared under consideration of age and topography. Figure 20 displays the total number of differently expressed genes in the transcriptome.

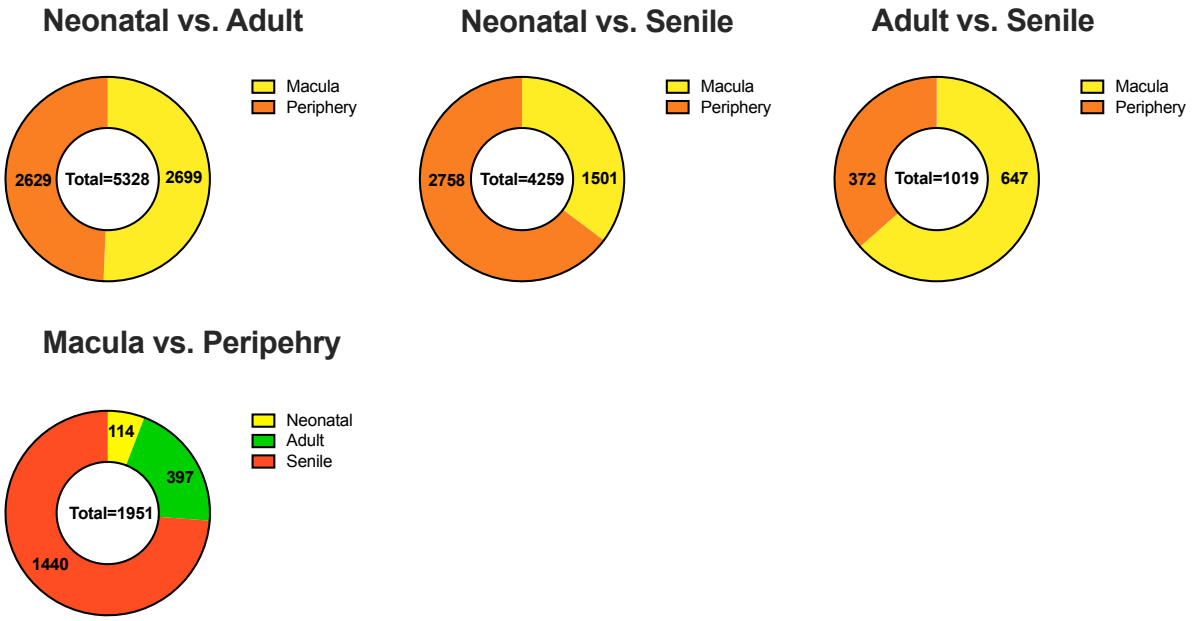

Figure 20 Summary of Transcriptome Analysis

The numbers display the count of significant differently expressed genes between the stages of age and the topographic groups.

The gene numbers were analyzed under age-related conditions. In neonatal compared to adult tissue 2699 genes in the macula and 2629 genes in the periphery were expressed differently in neonatal tissue compared to adult tissue. In neonatal vs. senile tissue, 1501 genes in the macula and 2758 genes in the periphery were expressed differently. In adult vs. senile tissue, this number in the macula was 647 genes and the periphery 372 genes. Under topography conditions, in the neonate tissue 114 genes, in the adult tissue 397 genes, and in the aged tissue 1440 genes were expressed differently in the macula compared to periphery.

Then, the complete data set were analyzed using GSEA. GSEA revealed the alterations of related functions under consideration of enriched or depleted genes. In the following Figure 21, an example of a GSEA is shown. It shows all gene sets with

genes expressed significantly different in adult peripheral samples compared to neonatal peripheral samples. The nine subgroups were analyzed in a comparative manner.

	GS follow link to MSigDB	GS DETAILS	SIZE	ES	NES	NOM p-val	FDR q-val	FWER p-val	RANK AT MAX	LEADING EDGE
1	HALLMARK_INTERFERON_GAMMA_RESPONSE	Details ...	152	-0.71	-3.15	0.000	0.000	0.000	2116	tags=66%, list=15%, signal=77%
2	HALLMARK_INTERFERON_ALPHA_RESPONSE	Details ...	71	-0.73	-2.92	0.000	0.000	0.000	2092	tags=70%, list=15%, signal=83%
3	HALLMARK_IL6_JAK_STAT3_SIGNALING	Details ...	64	-0.74	-2.85	0.000	0.000	0.000	1585	tags=61%, list=12%, signal=69%
4	HALLMARK_TNFA_SIGNALING_VIA_NFKB	Details ...	164	-0.59	-2.67	0.000	0.000	0.000	2175	tags=50%, list=16%, signal=59%
5	HALLMARK_MYC_TARGETS_V1	Details ...	138	-0.57	-2.53	0.000	0.000	0.000	4169	tags=70%, list=30%, signal=99%
6	HALLMARK_EPITHELIAL_MESENCHYMAL_TRANSITION	Details ...	164	-0.55	-2.49	0.000	0.000	0.000	2790	tags=49%, list=20%, signal=60%
7	HALLMARK_INFLAMMATORY_RESPONSE	Details ...	147	-0.52	-2.31	0.000	0.000	0.000	2655	tags=48%, list=19%, signal=58%
8	HALLMARK_E2F_TARGETS	Details ...	147	-0.50	-2.20	0.000	0.000	0.000	3258	tags=48%, list=24%, signal=62%
9	HALLMARK_G2M_CHECKPOINT	Details ...	158	-0.48	-2.18	0.000	0.000	0.000	3272	tags=42%, list=24%, signal=55%
10	HALLMARK_IL2_STAT5_SIGNALING	Details ...	161	-0.46	-2.08	0.000	0.000	0.000	2137	tags=34%, list=16%, signal=40%
11	HALLMARK_MTORC1_SIGNALING	Details ...	169	-0.45	-2.04	0.000	0.000	0.000	3399	tags=44%, list=25%, signal=57%
12	HALLMARK_APOPTOSIS	Details ...	131	-0.45	-1.98	0.000	0.000	0.000	2770	tags=44%, list=20%, signal=54%
13	HALLMARK_ALLOGRAFT_REJECTION	Details ...	131	-0.45	-1.97	0.000	0.000	0.000	2157	tags=34%, list=16%, signal=40%
14	HALLMARK_UNFOLDED_PROTEIN_RESPONSE	Details ...	92	-0.47	-1.96	0.000	0.000	0.000	3404	tags=50%, list=25%, signal=66%
15	HALLMARK_MYC_TARGETS_V2	Details ...	46	-0.53	-1.93	0.000	0.000	0.000	4298	tags=63%, list=31%, signal=91%
16	HALLMARK_COMPLEMENT	Details ...	154	-0.41	-1.86	0.000	0.000	0.001	3305	tags=43%, list=24%, signal=56%
17	HALLMARK_UV_RESPONSE_UP	Details ...	117	-0.42	-1.80	0.002	0.001	0.010	2454	tags=34%, list=18%, signal=41%
18	HALLMARK_ANGIOGENESIS	Details ...	28	-0.55	-1.78	0.000	0.001	0.013	1127	tags=39%, list=8%, signal=43%
19	HALLMARK_OXIDATIVE_PHOSPHORYLATION	Details ...	137	-0.40	-1.75	0.000	0.002	0.018	5532	tags=64%, list=40%, signal=105%
20	HALLMARK_ESTROGEN_RESPONSE_LATE	Details ...	155	-0.38	-1.69	0.000	0.003	0.038	1543	tags=24%, list=11%, signal=27%
21	HALLMARK_REACTIVE_OXIGEN_SPECIES_PATHWAY		37	-0.48	-1.67	0.002	0.004	0.049	1940	tags=27%, list=14%, signal=31%
22	HALLMARK_CHOLESTEROL_HOMEOSTASIS		60	-0.43	-1.66	0.007	0.004	0.060	2562	tags=40%, list=19%, signal=49%
23	HALLMARK_HYPOXIA		149	-0.37	-1.65	0.000	0.005	0.069	2385	tags=29%, list=17%, signal=35%
24	HALLMARK_KRAS_SIGNALING_UP		152	-0.36	-1.63	0.000	0.006	0.085	2371	tags=28%, list=17%, signal=33%

Figure 21 Example of a GSEA: All hallmarks detected in this gene set

The hallmark list shows all gene sets with significant differently expressed genes in adult peripheral samples compared to neonatal peripheral samples. Only sets with an FDR q-value <0.25 and a NES <-1.7 or >1.7 were included in the study. Abbreviations: GSEA: Gene set enrichment analysis; FDR: False Discovery Rate; NES: Normalized Enrichment Score

As an example, the gene set “Hallmark Angiogenesis” including the heat map is displayed in Figure 22. Three to four sample were included, depending on the availability. The samples of the adult peripheral group are displayed in grey, whereas the samples of the peripheral neonatal samples are displayed in orange. Red squares indicate a high gene expression, whereas blue squares indicate a low gene expression. The color intensity also indicates the expression difference. The genes are ordered by their significance in gene expression difference starting with a high expression to a low expression in adult peripheral samples.

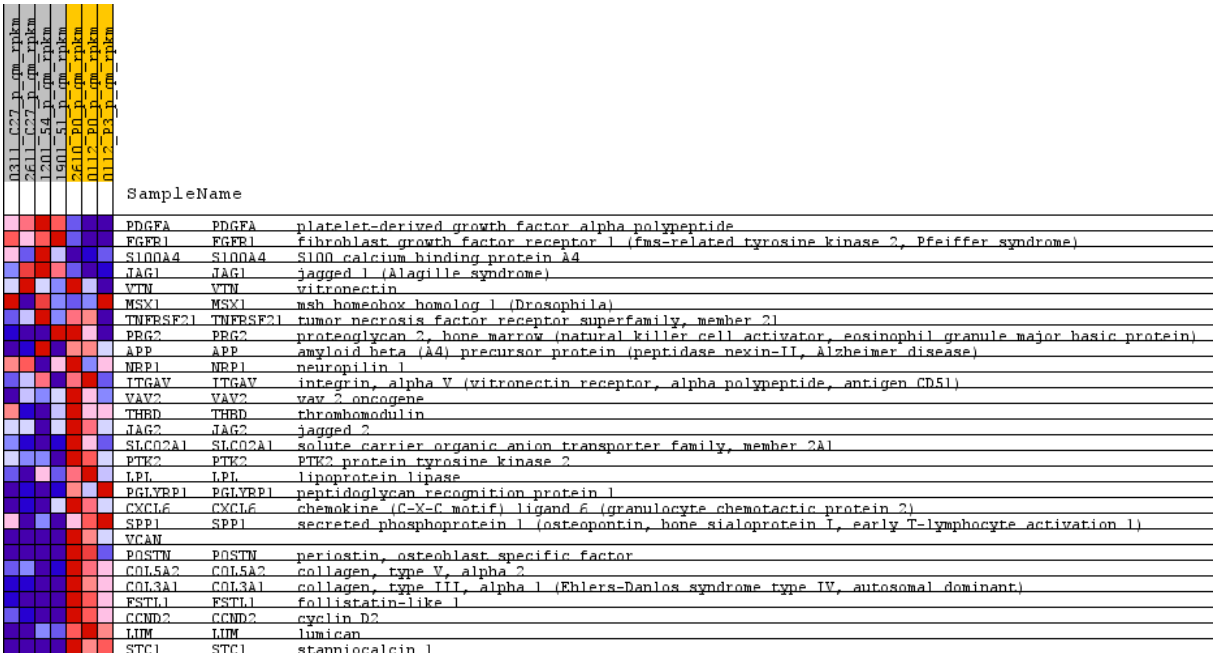

Figure 22 Exemplary list of genes found in the hallmark

Samples of the adult peripheral group are displayed in grey; peripheral neonatal samples are displayed in orange. Red squares indicate a high gene expression; blue squares indicate a low gene expression. The genes are ordered by their significance in gene expression difference starting with a high expression to a low expression in adult peripheral samples.

Figure 23 shows selected enrichment plots. The primary result of the gene set enrichment analysis is the enrichment score, which reflects the degree to which a gene set is overrepresented at the top or bottom of a ranked list of genes. A positive enrichment score indicates gene set enrichment at the top of the ranked list; a negative enrichment score indicates gene set enrichment at the bottom of the ranked list. The enrichment plot provides a graphical view of the enrichment score for a gene set. The top portion of the plot shows the running enrichment score for the gene set as the analysis walks down the ranked list. The score at the peak of the plot is the enrichment score for the gene set. Gene sets with a distinct peak at the beginning or end of the ranked list are generally the most interesting.

Figure 23 A shows selected enrichment plots of hallmarks containing genes downregulated in the neonate macula compared to the senile macula, considering age-related conditions. It includes “unfolded protein response”, “reactive oxygen species” and “epithelial–mesenchymal transition”. The enrichment plots indicate that the majority of the genes in these gene sets are downregulated in the neonate macular compared to the senile macula, having a negative enrichment score. Figure 23 B shows selected enrichment plots of hallmarks containing genes upregulated in the senile macula compared to the adult macula, considering age-related conditions as

well. It includes “inflammatory response”, “IL6 JAK STAT 3 signaling” and “*Myc* Targets”. The enrichment plots indicate that the majority of the genes in these gene sets are upregulated in the macula of the senile RPE compared to the macula of the adult RPE, having a positive enrichment score. Figure 23 C shows selected enrichment plots of hallmarks containing genes upregulated in the senile macula compared to the senile periphery, considering topography-related conditions. It includes “epithelial–mesenchymal transition”, “angiogenesis” and “*Myc* Targets”. The enrichment plots indicate that the majority of the genes in these gene sets are upregulated in the macula of the senile RPE compared to the periphery, having a positive enrichment score. The selected genes out of these plots are most likely from the peaked region of the enrichment plots.

A: Downregulated in the neonate macula compared to the senile macula

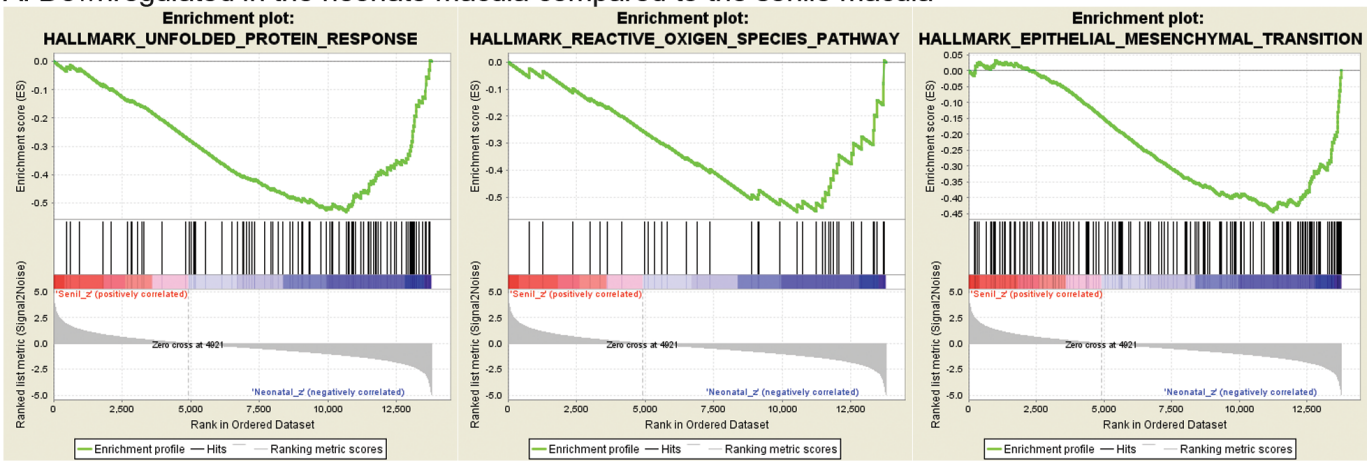

B: Upregulated in the senile macula compared to the adult macula

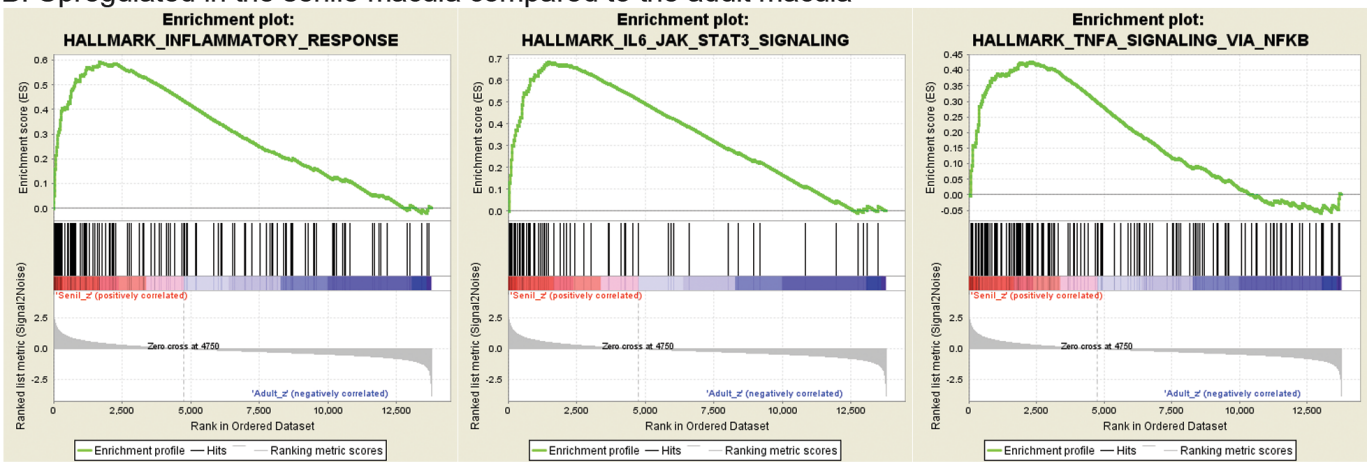

C: Upregulated in the senile macula compared to the senile periphery

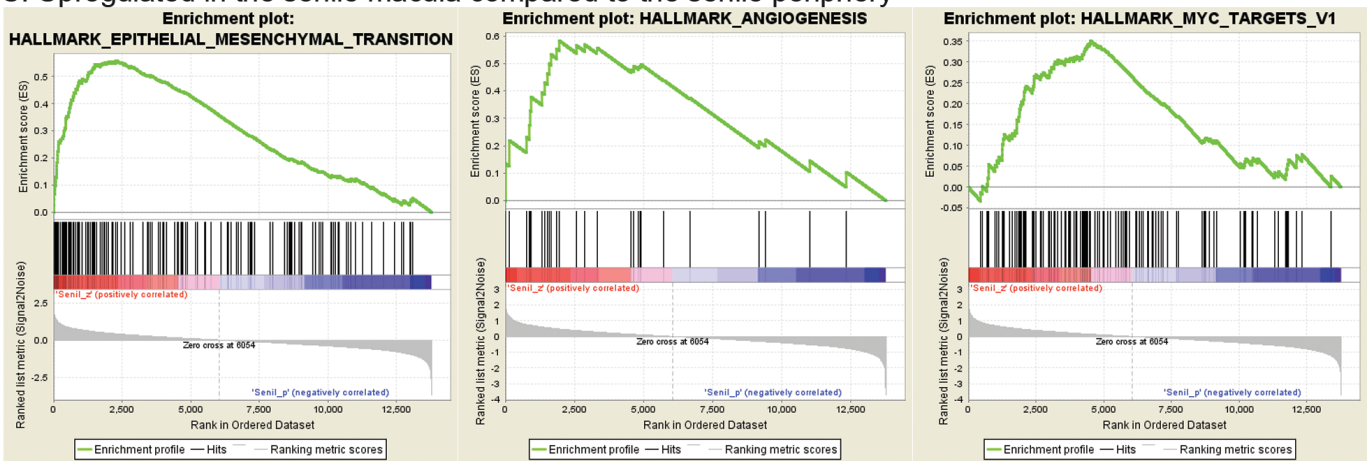

Figure 23 Enrichment Plot of the hallmark

The ES reflects the degree to which a gene set is overrepresented at the top or bottom of a ranked list of genes. A positive ES indicates gene set enrichment at the top of the ranked list; a negative ES indicates gene set enrichment at the bottom of the ranked list.

4.2.1 Gene Set Enrichment analysis

In the GSEA, eight different hallmarks were chosen to be further investigated and potentially interesting genes were listed.

- Angiogenesis
- Epithelial-mesenchymal transition (EMT)
- IL6 JAK STAT 3 signaling
- Unfolded protein response
- Inflammatory response
- Reactive oxygen species (ROS)
- Tumor necrosis factor α
- *Myc* targets

4.2.1.1 Hallmark angiogenesis

In the following Table 17, a selection of genes which are associate with angiogenesis and neovascularization and significant differently expressed in aged tissue compared to neonatal tissue is shown.

Table 17: Hallmark Angiogenesis

Genes selected from the Hallmark Angiogenesis. Abbreviations: nm: neonatal macula; np: neonatal periphery; am: adult macula; ap: adult periphery; sm: senile macula; sp: senile periphery; FDR: False Discovery Rate; NES: Normalized Enrichment Score

Gene	Protein	FDR	NES	Regulation
STC1	Stanniocalcin 1	0.001	-1.75	nm/np ↑ sz/sp am/ap
LUM	Lumican	0.001	-1.75	nm/np ↑ sm/sp am/ap
FSTL1	Follistatin-related protein 1	0	-1.75	nm/np ↑ sm/sp am/ap
APP	Amyloid-Precursor-Protein	0	-2.1	np ↑ sp

4.2.1.2 Hallmark epithelial-mesenchymal transition

EMT and its reverse process, epithelial-mesenchymal- transition are critical for development of many tissues and organs in the developing embryo, and numerous embryonic events such as neural crest formation, heart valve formation, and myogenesis (Thiery et al., 2009). In the following Table 18, a selection of genes is

shown which are associated with epithelial-mesenchymal transition and are expressed significantly different in aged tissue compared to neonatal tissue.

Table 18: Hallmark epithelial–mesenchymal transition

Genes selected from the Hallmark Epithelial–mesenchymal transition. Abbreviations: nm: neonatal macula; np: neonatal periphery; am: adult macula; ap: adult periphery; sm: senile macula; sp: senile periphery; FDR: False Discovery Rate; NES: Normalized Enrichment Score

Gene	Protein	FDR	NES	Regulation
THBS1	Thrombospondin 1	-1.77	0	nm ↓ sm/am
THBS2	Thrombospondin 2	-1.77	0	nm ↑ sm/am
MATN2	Matrilin 2	-1.77	0	np ↑ sp/ap
MATN3	Matrilin 3	-1.77	0	np ↑ sp/ap
FBN1	Fibrillin-1	-1.77	0	np ↑ sp/ap
FMOD	Fibromodulin	-1.77	0	nm/np ↓ sm/sp az/ap
FBLN2	Fibulin-2	-1.77	0	nm/np ↑ sm/sp am/ap
BASP1	Brain Abundant Membrane Attached Signal Protein 1	-1.77	0	nm/np ↑ sm/sp
TNC	Tenascin C	-1.77	0	nm ↓ np; np ↑ sp/ap
NID1	Nidogen 1	-1.77	0	nm/np ↑ sm/sp/ap
COL42A	Collagen Typ IV, α2	-2.5	0.001	nm/np ↑ sm/sp am/ap

4.2.1.3 Hallmark IL6 JAK STAT 3 signaling

Signal Transducers and Activators of Transcription 3 (STAT3) activity is critical for a wide range of functions in various cell types, including cellular differentiation, cell-cycle progression, proliferation, and survival (Akira, 2000; Barry et al., 2009; Fragoso et al., 2012; Haricharan and Li, 2014; Nichane et al., 2010; Xiong et al., 2008). In Table 19, a selection of genes is shown which are associated with STAT3 signaling and are expressed significantly different in aged tissue compared to neonatal tissue.

Table 19: Hallmark IL6 JAK STAT 3 signaling

Genes selected from the Hallmark IL6 JAK STAT 3 Signaling. Abbreviations: nm: neonatal macula; np: neonatal periphery; am: adult macula; ap: adult periphery; sm: senile macula; sp: senile periphery; FDR: False Discovery Rate; NES: Normalized Enrichment Score

Gene	Protein	FDR	NES	Regulation
HMOX1	heme oxygenase (decycling) 1	-1.9	0	nm/np ↑ sm/sp am/ap
TNFA	Tumor necrosis factor alpha	-1.9	0	np ↑ sp/ap
FAS	Tumor Necrosis Factor Receptor Superfamily, Member 6	-2.4	0	am ↓ ap

4.2.1.4 Hallmark unfolded protein response

In response to stress, cells have evolved an intricate set of signaling pathways named the unfolded protein response to restore the homeostasis of the endoplasmatic reticulum. In the following Table 20, a selection of genes is shown which are associated with unfolded protein response and expressed significantly different in aged tissue compared to neonatal tissue.

Table 20: Hallmark unfolded protein response

Genes selected from the Hallmark Unfolded Protein Response. Abbreviations: nm: neonatal macula; np: neonatal periphery; am: adult macula; ap: adult periphery; sm: senile macula; sp: senile periphery; FDR: False Discovery Rate; NES: Normalized Enrichment Score

Gene	Protein	FDR	NES	Regulation
XBP1	X-box binding protein 1	-1.8	0	np ↑ sp/ap
HSP90	Heat shock protein 90	-1.8	0	np ↑ sp

4.2.1.5 Hallmark Inflammatory response

Stress factors that can induce inflammation in aged RPE cells are an increased oxidative stress, reduced proteostasis, and increasing dysfunctionality (Kauppinen et al., 2016). In Table 21, a selection of genes is shown which are associated with inflammation and inflammatory response and significant differently expressed in aged tissue compared to neonatal tissue.

Table 21: Hallmark Inflammatory response

Genes selected from the Hallmark Inflammatory Response. Abbreviations: nm: neonatal macula; np: neonatal periphery; am: adult macula; ap: adult periphery; sm: senile macula; sp: senile periphery; FDR: False Discovery Rate; NES: Normalized Enrichment Score

Gene	Protein	FDR	NES	Regulation
PROK2	Prokineticin 2	-1.77	0.004	nm/np ↑ sm/sp am/ap
PSEN1	Presenilin-1	-1.77	0.004	np ↑ sp

4.2.1.6 Hallmark Reactive oxygen species

The ROS are products which are present under normal physiological conditions due to the partial reduction of molecular oxygen in cells.

In the following Table 22, a selection of genes is shown which are associated with ROS and ROS production and expressed significantly different in aged tissue compared to neonatal tissue.

Table 22: Hallmark reactive oxygen species

Genes selected from the Hallmark Reactive Oxygen Species. Abbreviations: nm: neonatal macula; np: neonatal periphery; am: adult macula; ap: adult periphery; sm: senile macula; sp: senile periphery; FDR: False Discovery Rate; NES: Normalized Enrichment Score

Gene	Protein	FDR	NES	Regulation
SOD2	Superoxidedismutase 2	-1.8	0.0001	nm/np ↑ sm/sp am/ap
PRDX6	Peroxiredoxin 6	-1.8	0.0001	nm/np ↑ sm/sp am/ap
TXN	Thioredoxin	-1.8	0.0001	nm/np ↑ sm/sp am/ap
CTSB	Cathepsin B	-1.8	0.0001	nm ↓ sm

4.2.1.7 Hallmark Tumor necrosis factor α

TNFα is a potent inflammatory cytokine, mainly produced by activated macrophages and T-cells, with a broad range of biological activities (Sedger and McDermott, 2014). In the following Table 23, a selection of genes is shown which are associated with TNFα and expressed significantly different in aged tissue compared to neonatal tissue.

Table 23: Hallmark TNFα

Signaling Genes selected from the Hallmark TNFα signaling. Abbreviations: nm: neonatal macula; np: neonatal periphery; am: adult macula; ap: adult periphery; sm: senile macula; sp: senile periphery; FDR: False Discovery Rate; NES: Normalized Enrichment Score

Gene	Protein	FDR	NES	Regulation
EDN1	Endothelin 1	-1.77	0.001	nm/np ↑ sm/sp am/ap
TNFA	Tumor necrosis facotor alpha	-1.77	0.001	np ↑ sp/ap
TNF	Tumor necrosis facotor	-1.77	0.001	nm ↓ np
RPE65	Retinal pigment epithelium-specific 65 kDa protein	-1.77	0.001	am ↑ ap; np ↓ ap/sp

4.2.1.8 Hallmark *Myc* targets

The *Myc* transcription factor is highly conserved in metazoans (Meyer and Penn, 2008). Increased expression of the MYC protein strongly promotes cell proliferation and has been documented as a frequent event in a wide variety of human cancers. In the following Table 24, a selection of genes which are associated with *Myc* targets and expressed significantly different in aged tissue compared to neonatal tissue.

Table 24: Hallmark *Myc* Targets

Genes selected from the Hallmark *Myc* Targets Abbreviations: nm: neonatal macula; np: neonatal periphery; am: adult macula; ap: adult periphery; sm: senile macula; sp: senile periphery; FDR: False Discovery Rate; NES: Normalized Enrichment Score

Gene	Protein	FDR	NES	Regulation
LPL	Lipoprotein lipase	-1.77	0	nm ↑ sm
HSPD1	Heat Shock Protein Family D (Hsp60) Member 1	-2.09	0	np ↑ sp
ADAMTSL4	ADAMTS-like protein 4	-1.77	0	sm ↓ sp; np ↑ sp/ap
PDGFA	Platelet-Derived Growth Factor A	-1.77	0	nm/np ↓ ap/am sm/sp

4.2.2 Selection of genes and validation of gene expression

Out of genes listed in the section 4.2.1 above, eight genes were selected for further validation.

- Stanniocalin (*STC1*)
- Lumican (*LUM*)
- Thrombospondin 1 (*THBS1*)
- Fibromodulin (*FMOD*)
- Brain Abundant Membrane Attached Signal Protein 1 (*BASP1*)
- Collagen Type 4, subunit alpha (*COL4A2*)
- Nidogen 1 (*NID1*)
- Cathepsin B (*CTSB*)

The mRNA expression levels were studied by qRT-PCR. The justification for the selection of the genes is given in each section.

4.2.2.1 Stanniocalcin 1

In Figure 24, the gene expression of *STC1* is shown. The gene expression of *STC1* was significantly downregulated in adult and senile macular and peripheral samples compared to the macular and peripheral samples in neonatal RPE. This finding was confirmed using qRT-PCR (Neonate m: 126%53%, p=0.58; Adult m: 16%±9%, p=0.005; Adult p: 20%±4%, p=0.001; Senile m: 33%±28%, p=0.08; Senile p: 16%±6%, p=0.002).

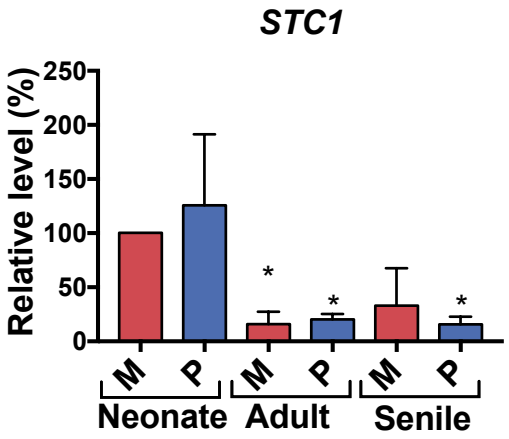

Figure 24 Gene expression of *STC1*

The gene expression of *STC1* relative to the gene expression in neonatal macula tissue; *indicating $p \leq 0.05$ Abbreviations: M: Macula; P: Periphery

4.2.2.2 Lumican

The gene expression of *LUM* was significantly downregulated in adult and senile macular and peripheral samples compared to the macular and peripheral samples in neonatal RPE. This finding was confirmed for adult peripheral and senile macular and peripheral samples using qRT-PCR (Neonate p: 74%±11%, p=0.08; Adult m: 64%±51%, p=0.42; Adult p: 31%±11%, p=0.01; Senile m: 35%±17%, p=0.03; Senile p: 47%±19%, p=0.05) (Figure 25).

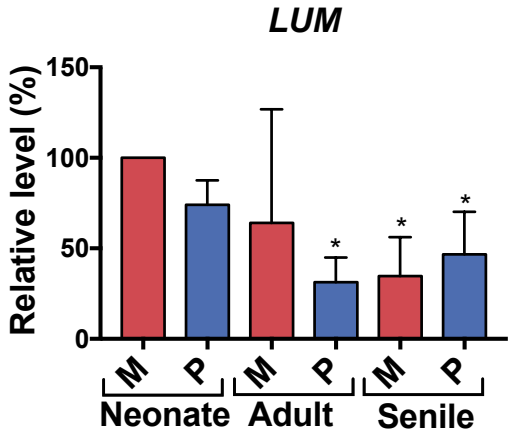

Figure 25 Gene expression of *LUM*

The gene expression of *LUM* relative to the gene expression in neonatal macula tissue; *indicating $p \leq 0.05$ Abbreviations: M: Macula; P: Periphery

4.2.2.3 Thrombospondin 1

The gene expression of *THBS1* was significantly upregulated in adult and senile macular samples compared to the macular samples in neonatal RPE. This finding was not confirmed for in the qRT-PCR, but the trend in the results was similar to the findings in the transcriptomal analysis (Figure 26) (Neonate p: 57%±25%, p=0.13; Adult m: 447%±269%, p=0.21; Adult p: 241%±55%, p=0.06; Senile m: 316%±156%, p=0.20; Senile p: 230%±171%, p=0.39).

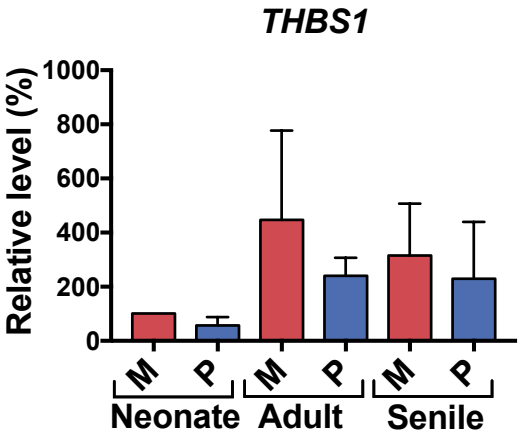

Figure 26 Gene expression of *THBS1*

The gene expression of *THBS1* relative to the gene expression in neonatal macula tissue; *indicating $p \leq 0.05$
Abbreviations: M: Macula; P: Periphery

4.2.2.4 Fibromodulin

The gene expression of *FMOD* was significantly upregulated in adult and senile macular and peripheral samples compared to the macular and peripheral samples in neonatal RPE. This finding was confirmed only for senile samples using qRT-PCR (Figure 27) (Senile m: 525%±135%, p=0.04; Senile p: 220%±32%, p=0.03). In contrast, the gene expression in the peripheral sample of the adult tissue is significantly decreased (Adult p: 65%±6%, p=0.01). The expression of the neonate peripheral sample and adult macula sample remained unchanged (Neonate p: 81%±23%, p=0.36; Adult m: 106%±24%, p=0.77).

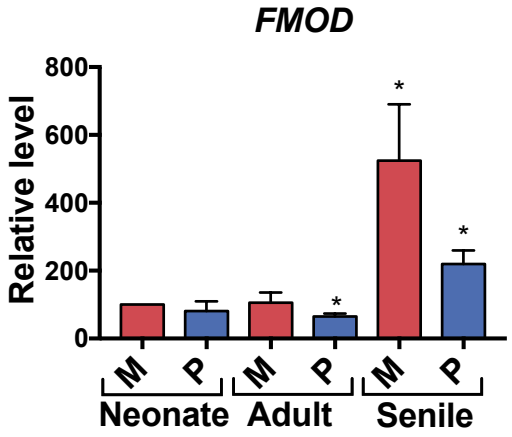

Figure 27 Gene expression of *FMOD*

The gene expression of *FMOD* relative to the gene expression in neonatal macula tissue; *indicating $p \leq 0.05$
Abbreviations: M: Macula; P: Periphery

4.2.2.5 Brain Abundant Membrane Attached Signal Protein 1

The gene expression of *BASP1* was significantly downregulated in senile macular and peripheral samples compared to the macular and peripheral samples in neonatal RPE. This finding was confirmed only for senile samples using qRT-PCR (Figure 28) (Senile z: 35%±112%, p=0.01; Senile p: 19%±6%, p=0.003). Additionally, the gene expression in the peripheral sample of the adult tissue was significantly decreased as well (Adult p: 31%±9%, p=0.008). The expression of the neonate peripheral sample and adult macula sample remained unchanged (Neonate p: 111%±21%, p=0.53; Adult m: 83%±71%, p=0.77).

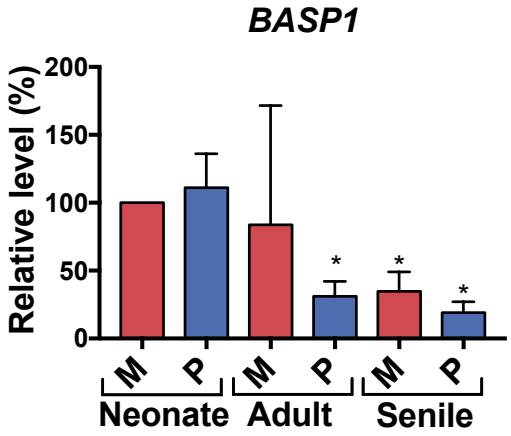

Figure 28 Gene expression of *BASP1*

The gene expression of *BASP1* relative to the gene expression in neonatal macula tissue; *indicating $p \leq 0.05$ Abbreviations: M: Macula; P: Periphery

4.2.2.6 Collagen Type 4, subunit alpha

The gene expression of *COL4A2* was significantly downregulated in adult and senile macular and peripheral samples compared to the macular and peripheral samples in neonatal RPE. This finding was confirmed using qRT-PCR (Neonate p: 92%±16%, p=0.55; Adult m: 23%±13%, p=0.01; Adult p: 15%±2%, p=0.0002; Senile m: 13%±4%, p=0.001; Senile p: 8%±2%, p=0.0002) (Figure 29).

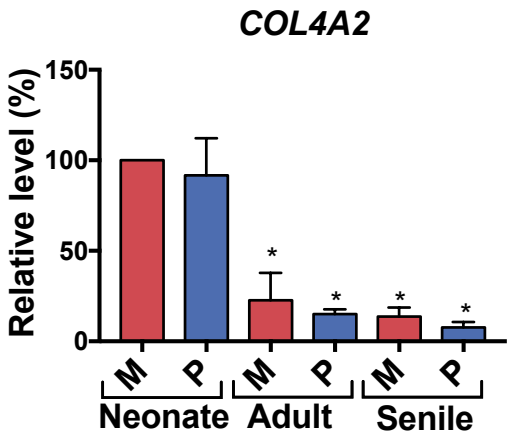

Figure 29 Gene expression of *COL4A2*

The gene expression of *COL4A2* relative to the gene expression in neonatal macula tissue; *indicating $p \leq 0.05$ Abbreviations: M: Macula; P: Periphery

4.2.2.7 Nidogen 1

In this study, a significant downregulation of *NID1* was found in aged tissue, which was confirmed using qRT-PCR (Neonate p: 80%±27%, p=0.41; Adult m: 63%±8%, p=0.02; Adult p: 59%±7%, p=0.01; Senile m: 55%±1%, p=0.02; Senile p: 35%±11%, p=0.01).

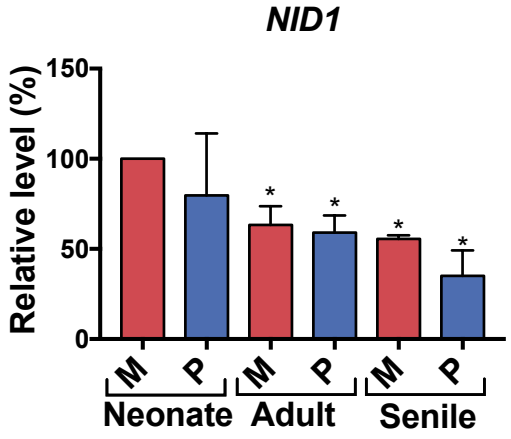

Figure 30 Gene expression of *NID1*

The gene expression of *NID1* relative to the gene expression in neonatal macula tissue; *indicating $p \leq 0.05$ Abbreviations: M: Macula; P: Periphery

4.2.2.8 Cathepsin B

The transcriptome study shows an upregulation of *CTSB*. The qRT-PCR results showed the same trend, although the results were not significant (Figure 31) (Neonate p: 84%±31%, p=0.54; Adult m: 146%±21%, p=0.09; Adult p: 130%±16%, p=0.12; Senile m: 245%±56%, p=0.06; Senile p: 193%±93%, p=0.29).

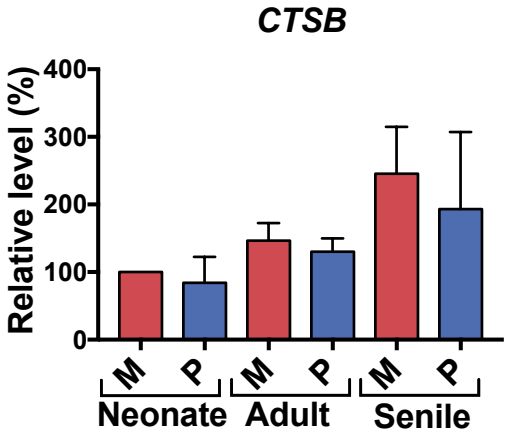

Figure 31 Gene expression of *CTSB*

The gene expression of *CTSB* relative to the gene expression in neonatal macula tissue; *indicating $p \leq 0.05$ Abbreviations: M: Macula; P: Periphery

4.3 Proteomic analysis of the RPE from *C. jacchus*

The results of this chapter are published in König et al., 2018 (König et al., 2018). The proteome analysis was performed by **Prof. Simone König**.

RPE proteins from the macula and the periphery were analyzed. Three samples of each age group were used. The identification of the proteins was performed using the UniProt database for human and *C. jacchus*. At the point of analysis, the database for *C. jacchus* contained a high number of unreviewed entries, which means many proteins were unassigned. Depending on the bioinformatics tool, it is difficult to perform pathway analysis using the *C. jacchus* accession numbers. Therefore, the experiments were firstly analyzed using the human database, followed by a re-analysis for *C. jacchus*. The prospective function of unknown proteins was specified by sequence comparison (Blast tool in UniProt.org).

4.3.1 Principle component analysis

To visualize the assembly of the proteins, a principle component analysis (PCA) was performed. PCA is a commonly used algorithm that reduces the dimensions of a data set. The PCA results in simplified data sets without losing the variances. That involves the generation of artificial variables. These artificial variables are called principal components (PC) and capture most of the variances within the dataset. The PCA of this study is shown in Figure 32. The x-axis is the component that captures most of the variance within the dataset (here: 48.57 %) and forms the first major component (PC1). The orthogonal y-axis is the second major component (PC2), accounting for 13.48 % of the variance in the dataset. Thus, the two major components accounted for approximately 62 % of the total variance of the data set and formed the framework for positioning the analyzed samples in a 2-dimensional coordinate system. The samples formed two major cluster: macula and periphery. Within the major clusters, each age group forms a sub-cluster. The neonatal samples were well differentiated from aged samples in both, macula and periphery. The neonate samples (marked as p0) from macula and periphery slightly overlap, whereas the adult and senile samples from macula and periphery form completely isolated clusters.

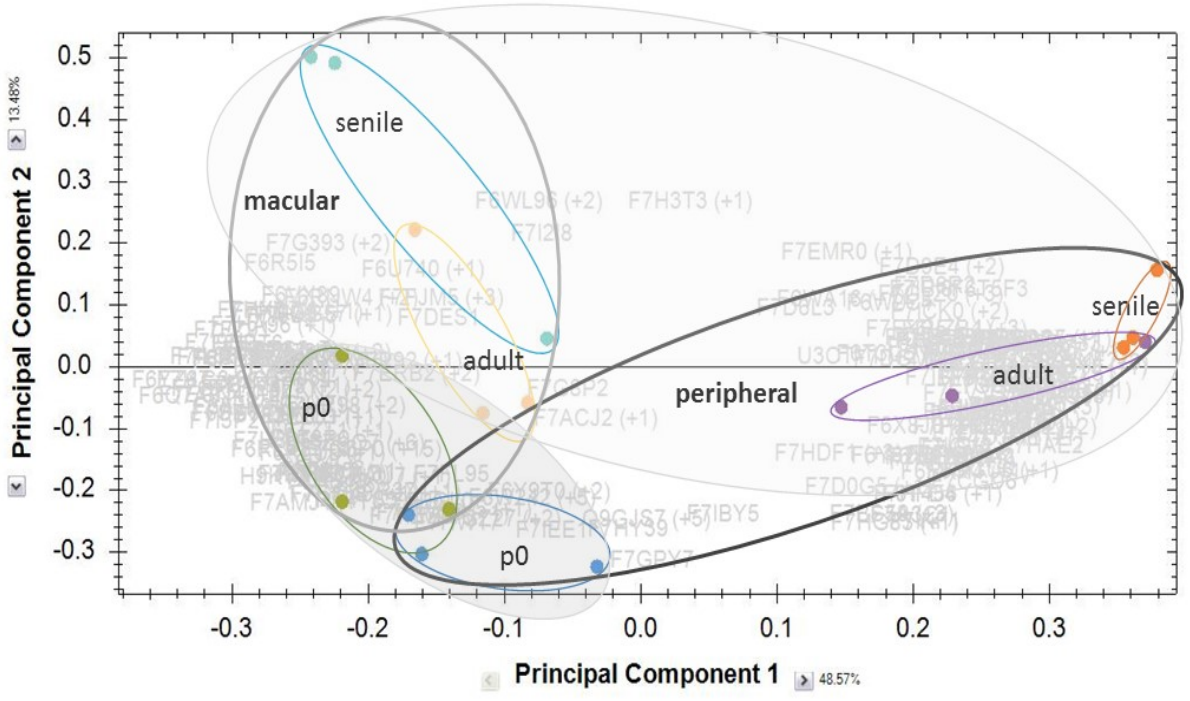

Figure 32 Principle component analysis

The abscissa (Principle Component 1) records 48.57 % of the variance within the data set. The ordinate (Principle Component 1) recorded 13.48 % of the variance of the data set. The samples were clearly separated into two clusters. The proteins were filtered to $p \leq 0.05$ (adapted from König et al., 2018(König et al., 2018))

4.3.2 Selection of proteins and validation of protein expression

The morphological distribution and expression pattern of selected proteins were performed using immunofluorescence and Western Blot analysis with the RPE tissue from *C. jacchus*. For an overview about the staining intensities of the specific proteins, images of the whole eye cub of neonatal and senile eyes are shown for each staining.

- Cathepsin B (CTSB)
- Heat Shock Protein 60 (HSP60)
- Heat Shock Protein 90 (HSP90)
- Nidogen 1 (NID1)
- Peroxiredoxin (PRDX)
- Thrombospondin 1 (THBS1)

The justification for the selection of each protein is given in the according section.

4.3.2.1 Cathepsin B

As described in section 4.2.2.8, CTSB is a promising protein in the context of the aging RPE. Regarding the proteome analysis, CTSB was elevated in aged tissue. The densiometric analysis showed an increase in the densiometric measurement for macular and peripheral tissue in senile RPE (Senile m: 11.48±3.65; p=0.01; Senile p: 9.33±1.79; p=0.002) compared to neonatal macular tissue, whereas no expression difference was shown between neonatal and adult samples (Neonate p: 2.22±0.88; p=0.16; Adult m: 3.14±1.27; p=0.07; Adult p: 3.89±2.10; p=0.12). No difference between macular and peripheral samples was detectable at any age. The comparison of the neonatal and senile staining from CTSB, shows an increased fluorescence intensity, and therefore a supposedly increased expression of CTSB in the senile RPE (Figure 33).

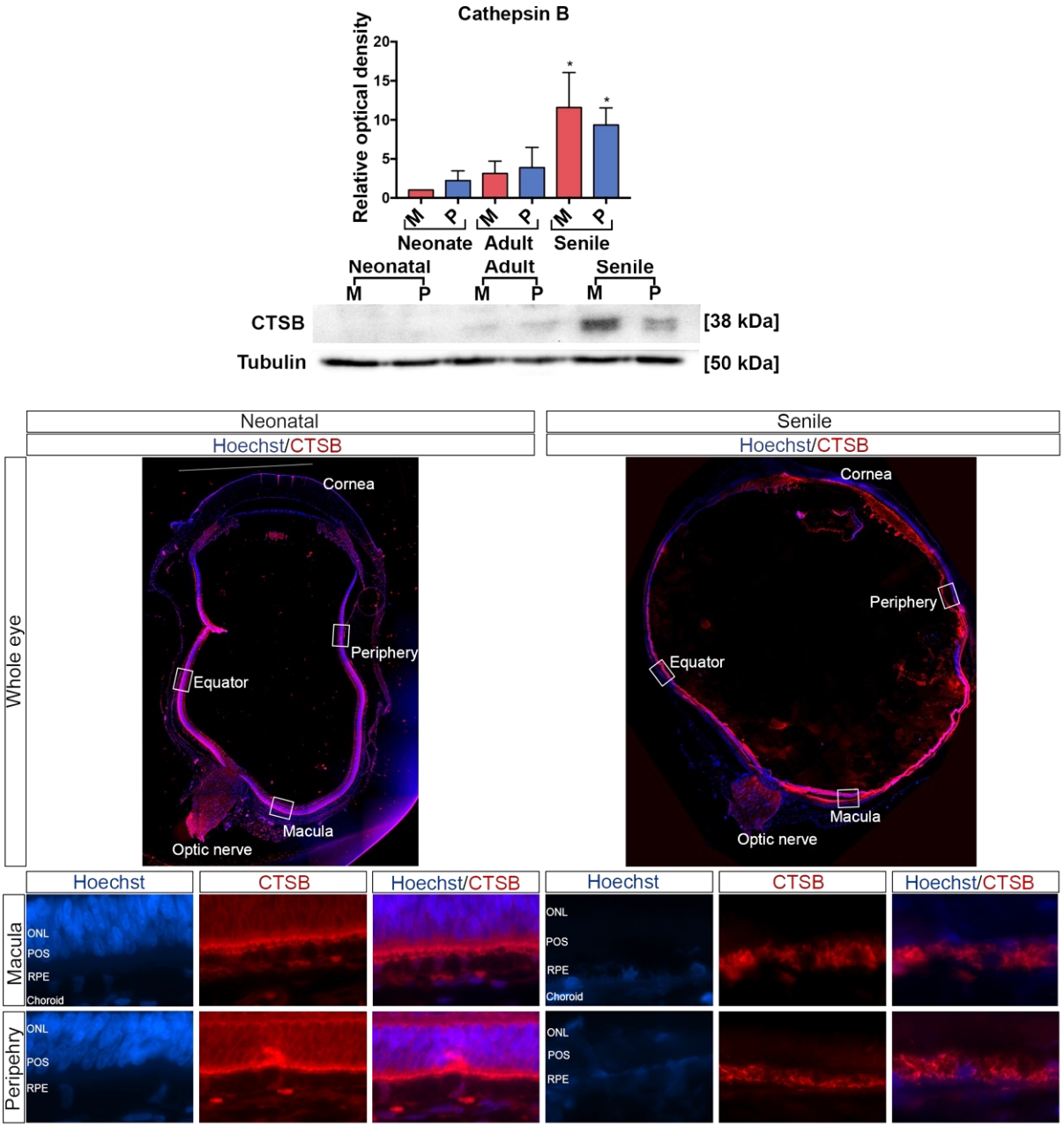

Figure 33 Protein expression of CTSB

RPE of *C. jacchus* was investigated, separated in M and periphery P of neonatal, adult and senile tissue. Densiometric analysis of the Western Blot is shown. Three samples were investigated for each tissue for Western Blot. *indicating $p \leq 0.05$ IF shows the staining of paraffin-embedded sections (neonatal) and cryo-embedded sections (senile) of CTSB in the macula and the periphery. As secondary antibody Alexa-594 (red) was used to visualize the staining; Magnification: 63x; Negative control was performed with the secondary antibody alone (not shown). Abbreviations: *C. jacchus*: *Callithrix jacchus*; RPE: Retinal Pigment Epithelium; CTSB: Cathepsin B; M: Macula; P: Periphery; ONL: Outer Nuclear Layer; POS: Photoreceptor Outer segments

4.3.2.2 Heat Shock Protein 60

In the proteomic analysis, it was proposed that HSP60 is upregulated in aged tissue. In Figure 34, the densiometric analysis of HSP60 shows the same trend as the mass spectrometry, but no significant increase between neonate, adult and senile tissue. Nevertheless, the expression was significantly increased in neonatal peripheral tissue compared to the macula (2.17±0.25; p=0.04). No expression difference is shown in adult and senile samples (Adult m: 1.80±0.54; p=0.16; Adult p: 2.25±1.0; p=0.13; Senile m: 2.50±1.85; p=0.31; Senile p: 4.33±2.10; p=0.89). The comparison of the neonatal and senile staining from HSP60 showed an increased fluorescence intensity, and therefore a supposedly increased expression of HSP60 in the senile RPE.

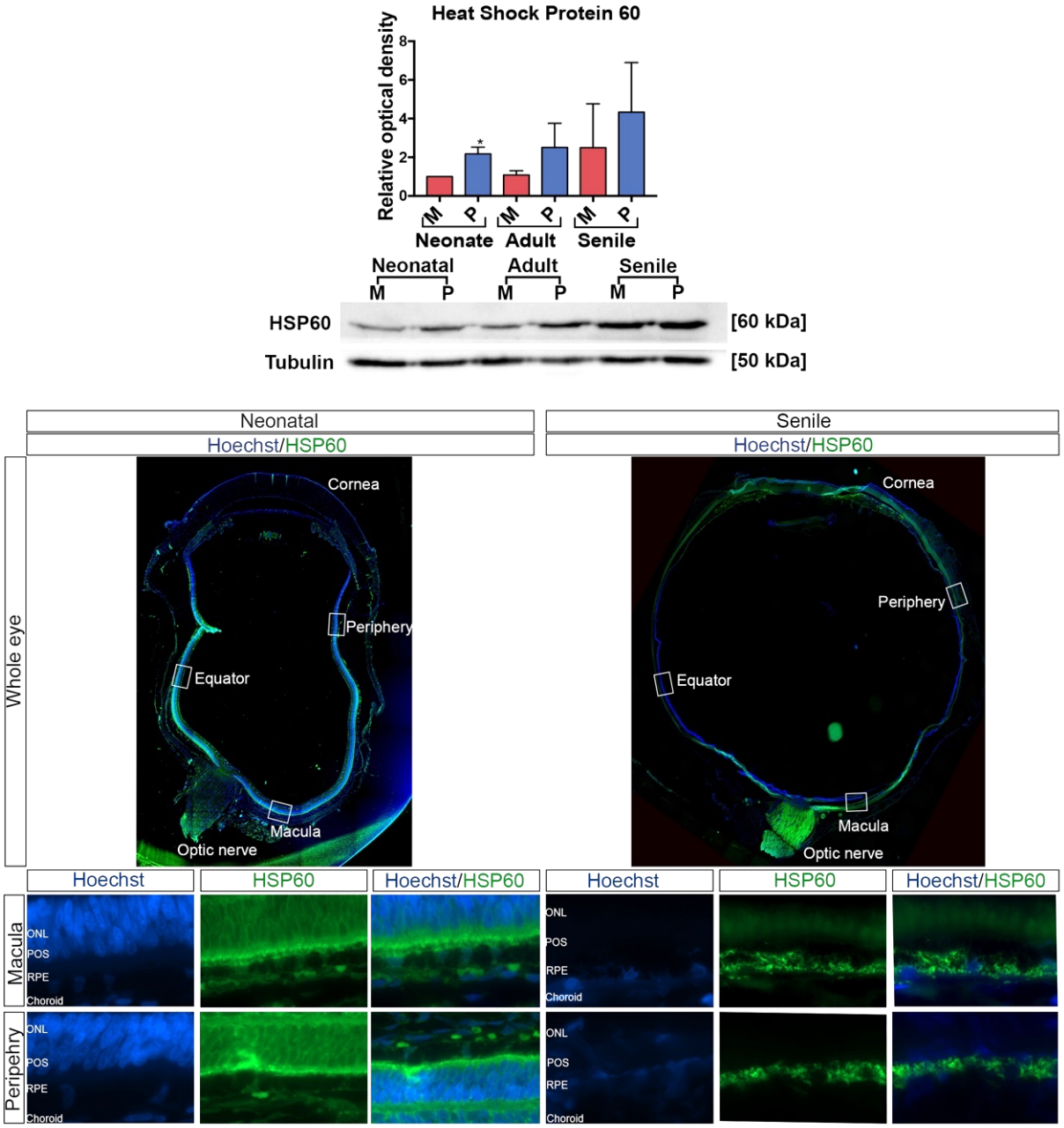

Figure 34 Protein expression of HSP60

RPE of *C. jacchus* was investigated, separated in M and periphery P of neonatal, adult and senile tissue. Densiometric analysis of the Western Blot is shown. Three samples were investigated for each tissue for Western Blot. *indicating $p \leq 0.05$ IF shows the staining of paraffin-embedded sections (neonatal) and cryo-embedded sections (senile) of CTSB in the macula and the periphery. As secondary antibody Alexa-594 (red) was used to visualize the staining; Magnification: 63x; Negative control was performed with the secondary antibody alone (not shown). Abbreviations: *C. jacchus*: *Callithrix jacchus*; RPE: Retinal Pigment Epithelium; HSP: Heat shock protein; M: Macula; P: Periphery; ONL: Outer Nuclear Layer; POS: Photoreceptor Outer segments

4.3.2.3 Heat Shock Protein 90

The results of the mass spectrometry showed an increase of the β-subunit of HSP90 in aged tissue. In contrast, the densiometric analysis (Figure 35) showed a significantly decreased expression of the protein (Neonate p: 0.66±0.17; p=0.07; Adult m:

0.39±0.25; *p*=0.03; Adult p: 0.37±0.22; *p*=0.02; Senile m: 0.24±0.19; *p*=0.005; Senile p: 0.29±0.21; *p*=0.009). No difference between macular and peripheral samples was detectable at any age. The fluorescence intensity of HSP90 was very low in both, neonatal and senile RPE.

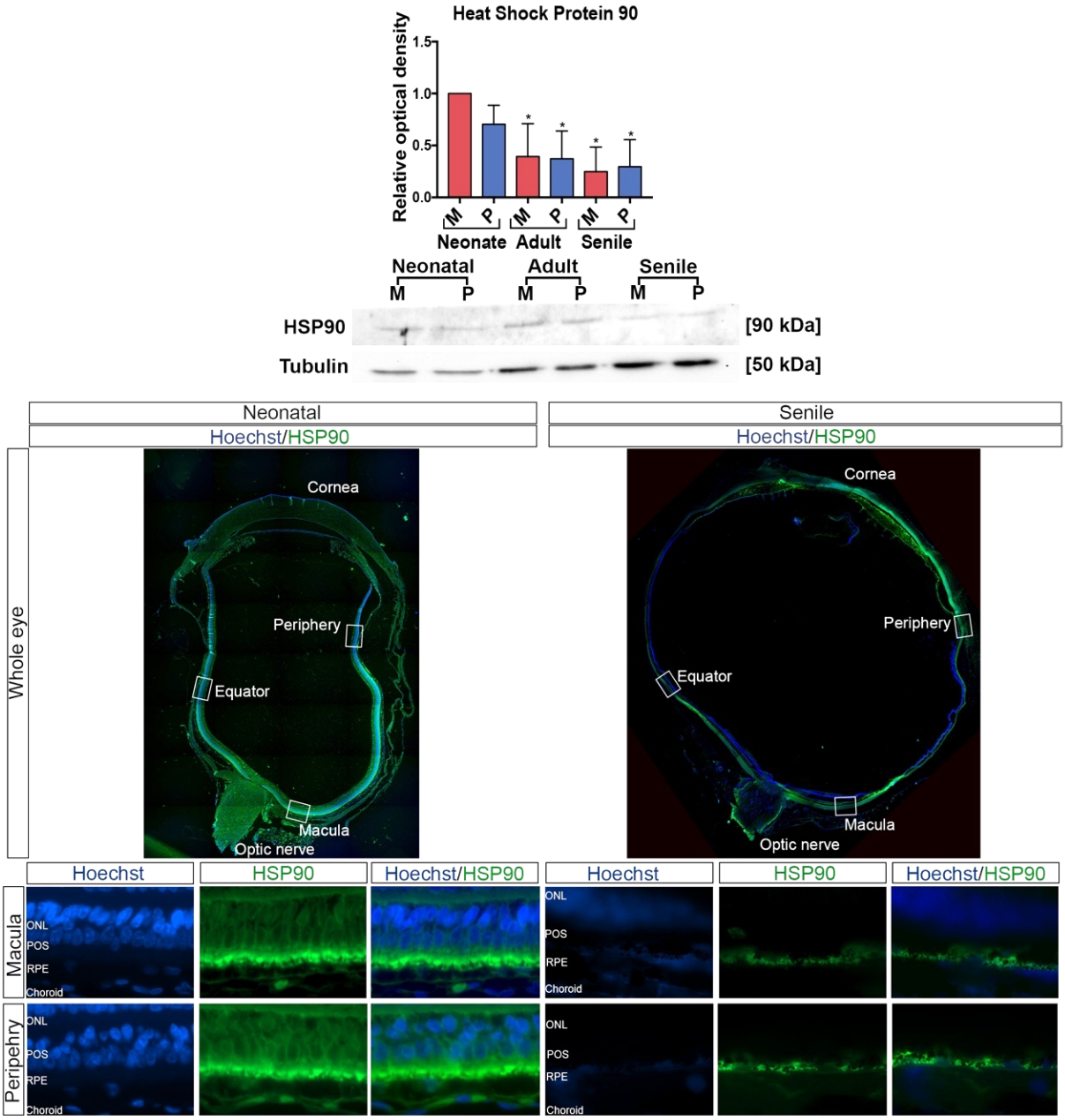

Figure 35 Protein expression of HSP90

RPE of *C. jacchus* was investigated, separated in M and periphery P of neonatal, adult and senile tissue. Densiometric analysis of the Western Blot is shown. Three samples were investigated for each tissue for Western Blot. *indicating $p \leq 0.05$ IF shows the staining of paraffin-embedded sections (neonatal) and cryo-embedded sections (senile) of CTSB in the macula and the periphery. As secondary antibody Alexa-594 (red) was used to visualize the staining; Magnification: 63x; Negative control was performed with the secondary antibody alone (not shown). Abbreviations: *C. jacchus*: *Callithrix jacchus*; RPE: Retinal Pigment Epithelium; HSP: Heat shock protein; M: Macula; P: Periphery; ONL: Outer Nuclear Layer; POS: Photoreceptor Outer segments

4.3.2.4 Nidogen 1

The densiometric analysis of the Western Blots of NID1 showed a decreased protein expression in aged tissue and is significant for peripheral adult tissue (0.39±0.21; p=0.01) and adult senile tissue (0.18±0.19; p=0.004), whereas the expression in macular tissue remained unchanged (Figure 36) (Neonate p: 1.83±0.44; p=0.08; Adult m: 0.47±0.37; p=0.12; Senile m: 0.57±0.58; p=0.36). No difference between macular and peripheral samples was detectable at any age. These results are comparable to the results of the mass spectrometry. The fluorescence intensity of NID1 was very low in both, neonatal and senile RPE, whereas the Western Blot analysis shows a decreased expression.

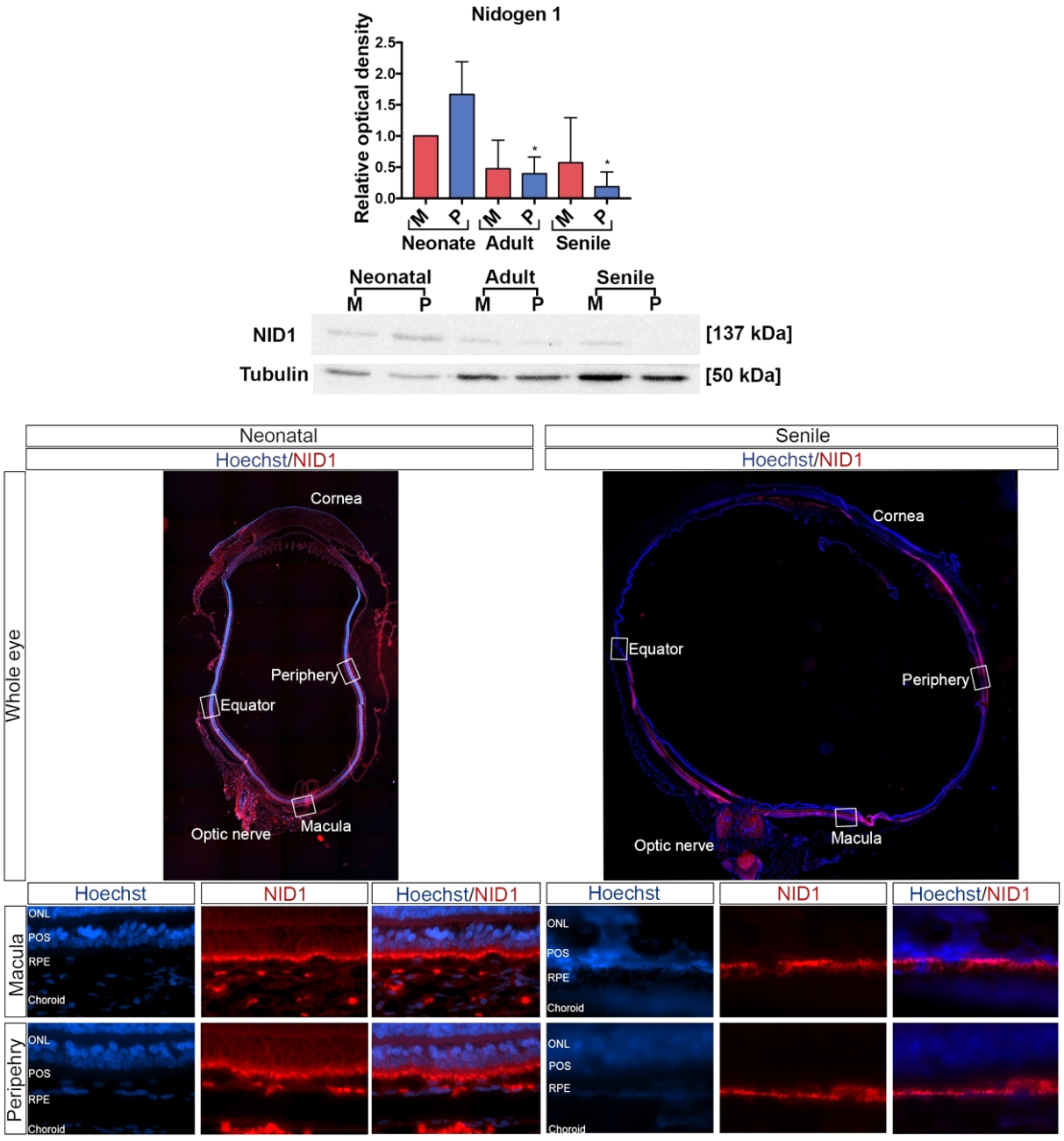

Figure 36 Protein expression of NID1

RPE of *C. jacchus* was investigated, separated in M and periphery P of neonatal, adult and senile tissue. Densiometric analysis of the Western Blot is shown. Three samples were investigated for each tissue for Western Blot. *indicating $p \leq 0.05$ IF shows the staining of paraffin-embedded sections (neonatal) and cryo-embedded sections (senile) of CTSB in the macula and the periphery. As secondary antibody Alexa-594 (red) was used to visualize the staining; Magnification: 63x; Negative control was performed with the secondary antibody alone (not shown). Abbreviations: *C. jacchus*: *Callithrix jacchus*; RPE: Retinal Pigment Epithelium; NID1 Nidogen 1; M: Macula; P: Periphery; ONL: Outer Nuclear Layer; POS: Photoreceptor Outer segments

4.3.2.5 Peroxiredoxin

In the mass spectrometry, PRDX was elevated in aged samples. The same expression pattern is shown in the Western Blot analysis (Neonate p: 1.11±0.4; p=0.73; Adult m: 4.66±1.0; p=0.007; Adult p: 5.87±3.54; p=012; Senile m: 6.33±1.46; p=0.006; Senile p: 3.13±0.61; p=0.007). The mass spectrometry also showed an increase in PRDX expression in peripheral tissue. In contrast, the Western Blot analysis shows a decreased expression in peripheral tissue (3.13±0.61; p=0.04) compared to macular tissue. For PRDX, the fluorescence intensity was very low in the neonatal RPE and is highly increased in senile RPE. The results are shown in Figure 37.

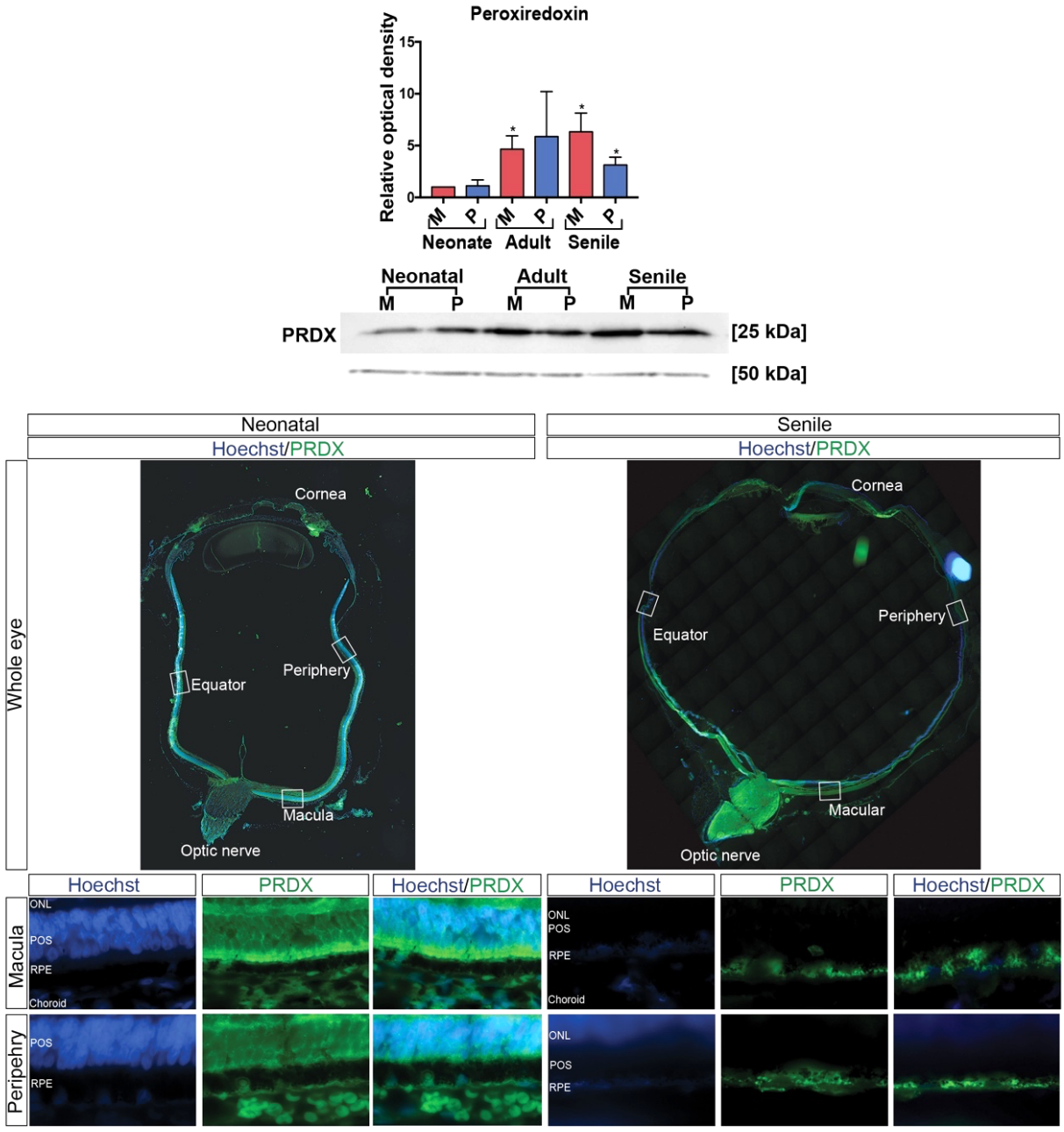

Figure 37 Protein expression of PRDX

RPE of *C. jacchus* was investigated, separated in M and periphery P of neonatal, adult and senile tissue. Densiometric analysis of the Western Blot is shown. Three samples were investigated for each tissue for Western Blot. *indicating $p \leq 0.05$ IF shows the staining of paraffin-embedded sections (neonatal) and cryo-embedded sections (senile) of CTSB in the macula and the periphery. As secondary antibody Alexa-594 (red) was used to visualize the staining; Magnification: 63x; Negative control was performed with the secondary antibody alone (not shown). Abbreviations: *C. jacchus*: *Callithrix jacchus*; RPE: Retinal Pigment Epithelium; PRDX: Peroxiredoxin; M: Macula; P: Periphery; ONL: Outer Nuclear Layer; POS: Photoreceptor Outer segments

4.3.2.6 Thrombospondin 1

The mass spectrometry results showed a significantly higher protein expression in neonatal tissue. In contrast, shown in Figure 38, the densiometric results showed a

significant increase in aged tissue (Neonate p: 1.64±0.63; p=0.42; Adult m: 35.11±11.48; p=0.04; Adult p: 26.75±17.98; p=0.28; Senile m: 27.57±11.43; p=0.08; Senile p: 16.44±1.12; p=0.005). The fluorescence intensity for THBS1 was very low in the neonatal RPE and is highly increased in senile RPE.

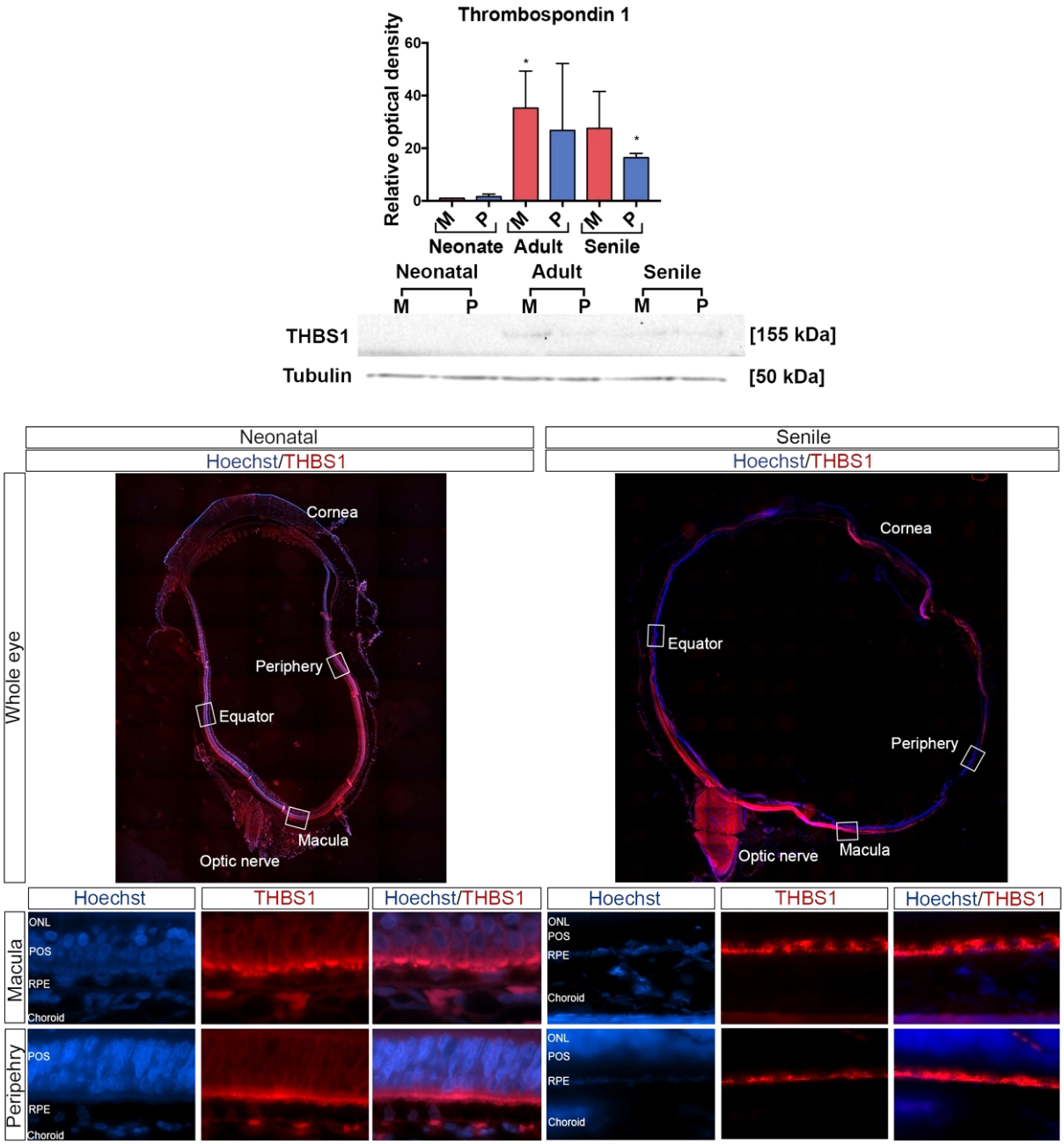

Figure 38 Protein expression of THBS1

RPE of *C. jacchus* was investigated, separated in M and periphery P of neonatal, adult and senile tissue. Densiometric analysis of the Western Blot is shown. Three samples were investigated for each tissue for Western Blot. *indicating $p \leq 0.05$ IF shows the staining of paraffin-embedded sections (neonatal) and cryo-embedded sections (senile) of CTSB in the macula and the periphery. As secondary antibody Alexa-594 (red) was used to visualize the staining; Magnification: 63x; Negative control was performed with the secondary antibody alone (not shown). Abbreviations: *C. jacchus*: *Callithrix jacchus*; RPE: Retinal Pigment Epithelium; THBS1: Thrombospondin 1; M: Macula; P: Periphery; ONL: Outer Nuclear Layer; POS: Photoreceptor Outer segments.

4.4 Functional characterization of selected factors

4.4.1 *In-vitro* characterization of β-Synuclein

The results of this chapter are published in Hadrian et al., 2019 (Hadrian et al., 2019).

4.4.1.1 Expression of β-Synuclein in native RPE from *C. jacchus*

The intracellular distribution and topographical localization of SNCA and SNCB were examined using immunofluorescence in RPE wholemounts as well as in paraffin-embedded sections of the RPE from *C. jacchus*.

4.4.1.1.1 Expression of β-Synuclein in neonatal RPE

To analyze the expression pattern in neonatal RPE, a wholemount preparation was performed and the tissue was analyzed using immunofluorescence (Figure 39). The analysis of neonatal RPE wholemount shows both SNCA and SNCB in cell membranes in the area around the macular. In some cells, SNCB was present in the cytoplasm, whereas SNCA was exclusively present in the cell membranes in all cells. In the peripheral regions, the presence of SNCB shifted mainly to the nucleus and the cytoplasm. In the periphery, SNCA was present in the nucleus and the cell membranes, but not in the cytoplasm.

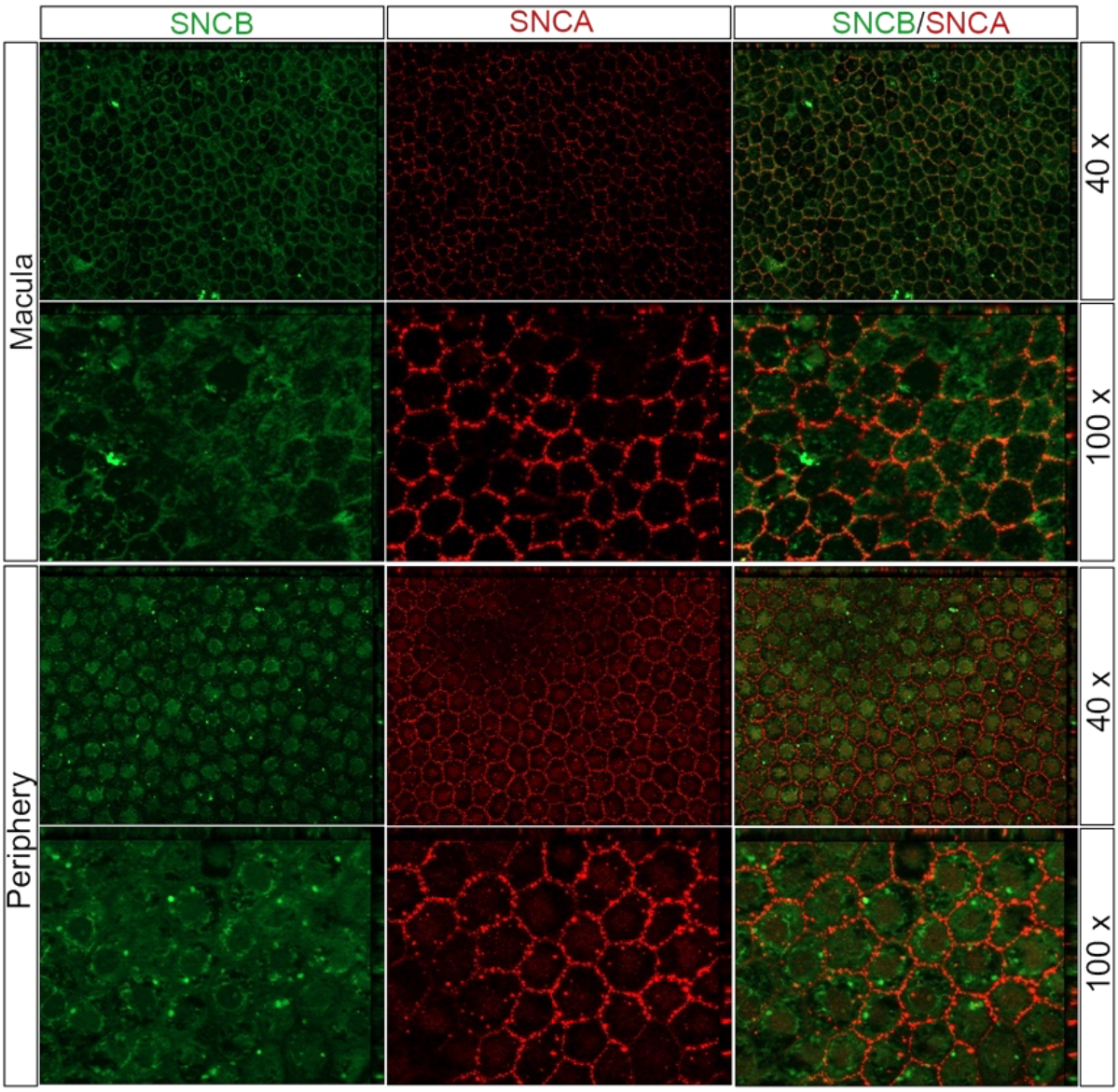

Figure 39 Protein expression of SNCA and SNCB of neonate *C. jacchus*

The protein expression of SNCA and SNCB in RPE whole mounts of neonate *C. jacchus* staining of SNCB (green) and SNCA (red) is shown. Secondary antibodies (green, Alexa 488; red, Alexa 594) were used to visualize antigen staining; Magnification: 40x and 100x); Negative control was performed with the secondary antibody alone (not shown). Abbreviations: SNCA: α-synuclein; SNCB: β-synuclein; RPE: retinal pigment epithelium; *C. jacchus*: *Callithrix jacchus*

As an additional quantification, the area of the cells was measured in the macula and in the periphery (Figure 40). The area of cells in the proximal periphery (1.04±0.13) was comparable to that in the macula, while it was significantly larger in the distant periphery (1.97±0.331, $p<0.001$) than in the macula.

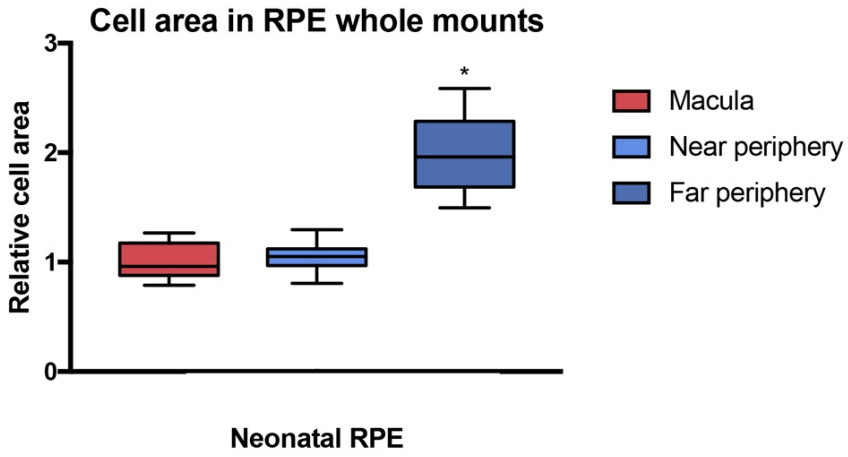

Figure 40 Cell areas in RPE wholemounts

Relative cell area of cells in the macula, near periphery and far periphery, normalized to the cell area in the macula.

* $p \leq 0.05$ indicating statistical significance. Abbreviations: RPE: Retinal pigment epithelium

4.4.1.1.2 Expression of β-Synuclein in aging RPE

For the analysis of the age-related expression of SNCB and SNCA in the RPE from *C. jacchus*, paraffin slices from neonatal, adolescent and adult animals were used for immunofluorescences staining (Figure 41). SNCA and SNCB was hardly detectable in the RPE of neonatal tissue in macula and periphery. In adolescent tissue, the fluorescence intensity was slightly higher for both SNCB and SNCA. The fluorescence intensity of SNCA in the macula was higher than in the periphery. In adult tissue, the fluorescence intensity of SNCB increased in the macula and remained the same in the periphery. For SNCA, the fluorescence intensity increased a lot in the macula and remained unchanged in the periphery.

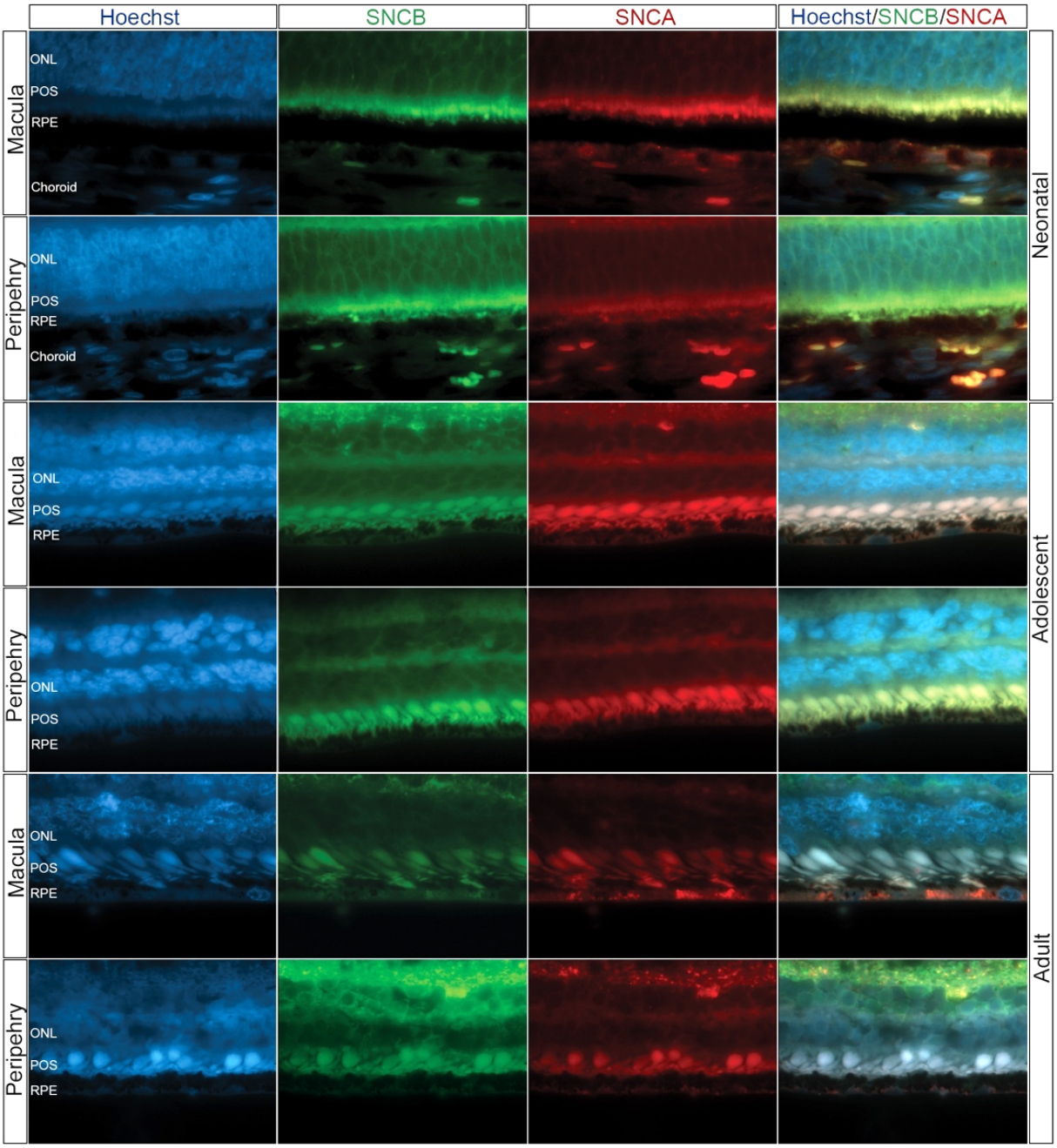

Figure 41 Protein expression of SNCA and SNCB in retinal sections

Expression of SNCA and SNCB in retinal sections of paraffin embedded eyecups of *C. jacchus* RPE in neonatal, adolescent and adult tissue. Immunofluorescence staining of SNCB (green) and SNCA (red); Hoechst (blue) was used to visualize cell nuclei. Secondary antibodies (green, Alexa 488; red, Alexa 594) were used to visualize antigen staining. Magnification: 100x. Negative control was performed with the secondary antibody alone (not shown). Abbreviations: SNCA: α-Synuclein; SNCB: β-Synuclein; RPE: retinal pigment epithelium; *C. jacchus*: *Callithrix jacchus*

4.4.1.2 *In-vitro* characterization of β-Synuclein

For the characterization of SNCB *in-vitro*, the secondary cell line ARPE-19 was used. As described in 3.2.7.2, the cells were incubated with different concentrations of recombinant SNCB and analyzed afterwards.

4.4.1.2.1 Expression of β-Synuclein in ARPE-19 cells

In a first step, the expression pattern of SNCB and SNCA was evaluated in untreated ARPE-19 cells. The distribution of the both proteins is shown in Figure 42.

In untreated ARPE-19 cells, the fluorescence intensity of SNCA was the highest in the nucleus and cell membrane, while SNCB was mainly present in the nucleus of the cells and the cytoplasm close to the nucleus. SNCA and SNCB showed comparable intracellular distribution patterns to periphery-located RPE cells in *C. jacchus*. No staining of SNCB was visible in the cell membranes. The main fluorescence appeared in the nucleus and in the cytosol close to the nucleus. SNCA was mainly present in the cell membranes and the nucleus of the cells.

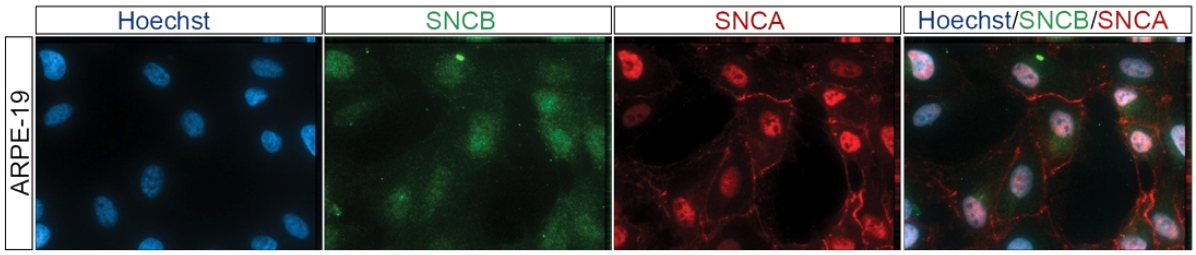

Figure 42 Expression of SNCA and SNCB in ARPE-19 cells

Immunofluorescence staining of SNCB (green) and SNCA (red) in ARPE-19 cells. Hoechst (blue) was used to stain cell nuclei. Secondary antibodies (green, Alexa 488; red, Alexa 594) were used to visualize antigen staining. Magnification: 63x. Negative control was performed with the secondary antibody alone (not shown). Abbreviations: SNCA: α-Synuclein; SNCB: β-Synuclein

4.4.1.2.2 Influence of rSNCB on viability and apoptosis

To study the influence of rSNCB on viability and apoptosis, the cells were treated with rSNCB for 6 h, 12 h and 24 h. The viability of the cells was investigated using MTT assay. The results of the MTT test are shown in Figure 43. The viability of ARPE-19 cells after exposure to rSNCB was not significantly altered compared to the untreated control (6 h: 1 ng/ml: 89.36±16.41%, p=0.35; 50 ng/ml: 83.57±19.01% p=0.29; 500 ng/ml: 95.78±20.56%, p=0.65; 12 h: 1 ng/ml: 94.09±2.16%, p=0.66; 50 ng/ml: 93.39±10.59%, p=0.44; 500 ng/ml: 97.15±6.97%, p=0.22; 24 h: 1 ng/ml: 97.16±4.45%, p=0.39; 50 ng/ml: 90.58±14.58%, p=0.37; 500 ng/ml: 73.56±32.61%, p=0.29).

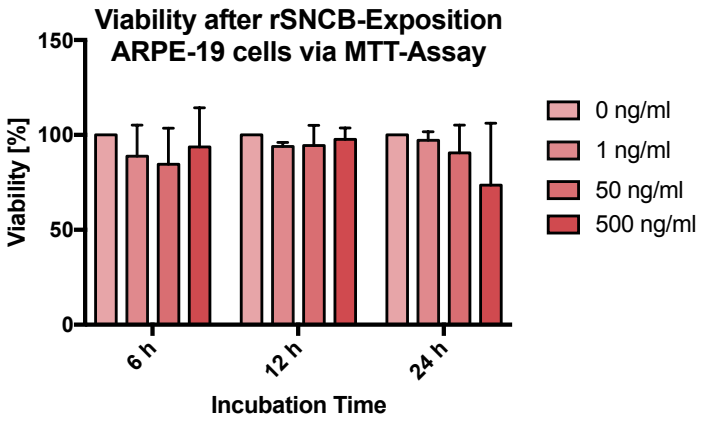

Figure 43 Viability of rSNCB-treated ARPE-19 cells

Viability of the ARPE-19 cells following the treatment with rSNCB was determined using the MTT assay. The viability of untreated cells was set to be 100 %. Abbreviations: rSNCB: recombinant β-Synuclein; MTT: 3-(4,5-Dimethylthiazol-2-yl)-2,5-Diphenyltetrazolium Bromide

The apoptosis of ARPE-19 cells treated with rSNCB was investigated using TUNEL assay. The results of the TUNEL assay are shown in Figure 44. A significant decrease in apoptotic cells was observed in ARPE-19 cells exposed to rSNCB at the lower concentration of 1 ng/ml after 6 h (78±11%, p=0.004) compared to untreated cells. After exposure to higher concentrations of rSNCB, the number of apoptotic cells increased significantly (500 ng/ml: 135±30%, p=0.032). After 12 h of exposure, the number of TUNEL-positive cells was significantly decreased compared to controls (1 ng/ml: 53±19%, p=0.002; 50 ng/ml: 36±15%, $p \leq 0.001$; 500 ng/ml: 26±13%, $p \leq 0.001$). No alterations of TUNEL-positive cells have been found in after 24 h (1 ng/ml: 98±19%; 50 ng/ml: 113±56%; 500 ng/ml: 100±31%).

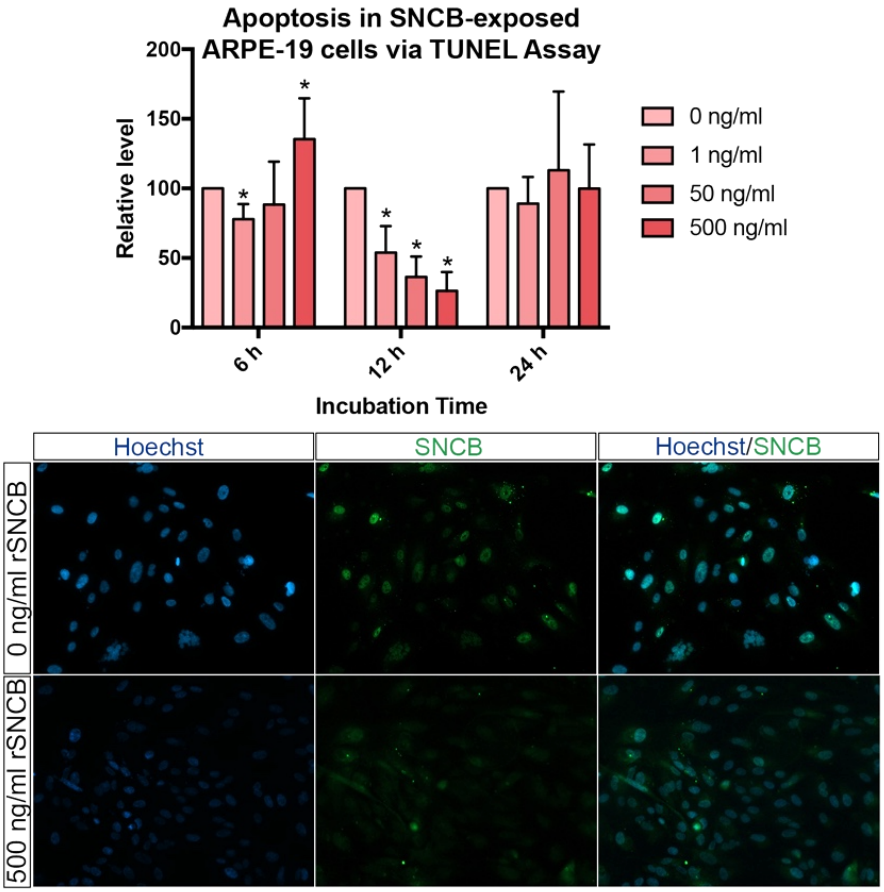

Figure 44 Apoptosis of rSNCB-treated ARPE-19 cells

Rate of apoptosis revealed by TUNEL assay of rSNCB-exposed ARPE-19 cells. Hoechst (blue) was used to stain cell nuclei. The survival of untreated cells was set to be 100 %; * indicates $p \leq 0.05$, compared with the untreated control. Abbreviations: rSNCB: recombinant β-Synuclein; TUNEL: terminal deoxynucleotidyl transferase dUTP nick end labeling

4.4.1.2.3 Influence of rSNCB on *p*53 signaling cascade

The *p*53-MDM2 signal pathway, which includes *p*53, MDM2, *p*14ARF and PLD2 was examined in rSNCB-exposed ARPE-19 cells using immunofluorescence (Figure 45) and mRNA-expression analysis (Figure 47). The main alterations of the fluorescent intensity in rSNCB-exposed ARPE-19 cells were found after 72 h of incubation with rSNCB. The fluorescence intensity of *p*53 was slightly increased in rSNCB-exposed ARPE-19 cells compared to untreated controls. In untreated ARPE-19 cells, the main fluorescence was detectable in the nucleus, whereas the fluorescence intensity increases in the cytoplasm after treatment with high concentrations of rSNCB. The intensity of fluorescence staining of MDM2 was higher in the nucleus of ARPE-19 cells and is slightly increased in the cytoplasm after exposure to higher concentrations rSNCB. The general fluorescence intensity of *p*14ARF in ARPE-19 cells did not change after rSNCB exposure compared to controls. The influence of PLD2 in SNCB-exposed

ARPE-19 cells showed an increase expression in cell membranes of SNCB-exposed cells compared to untreated control. The intensity increaseed mainly in the cell nucleus but is also present in the cytoplasm of the cells.

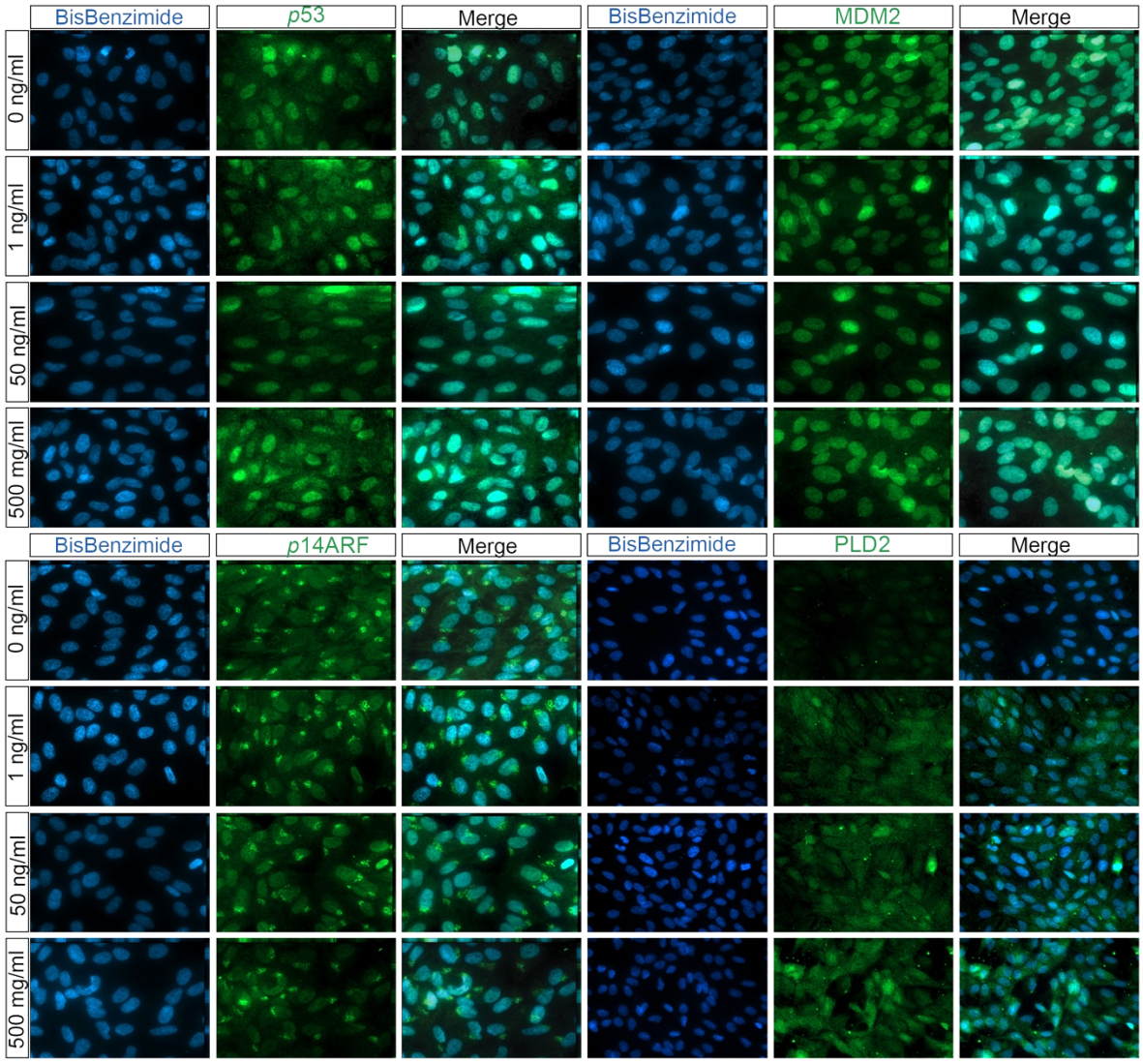

Figure 45 *p*53-MDM2 cascade in rSNCB exposed ARPE-19 cells

ARPE-19 cells were treated with rSNCB (1, 50 and 500 ng/ml) *in-vitro* for 24-48 hours, followed by analysis IF *p*53 and MDM2 and *p*14ARF (green) staining in ARPE-19 cells. Hoechst (blue) was used to visualize cell nuclei. Secondary antibody (green, Alexa 488) was used to visualize antigen staining. Magnification: 63x. Negative control was performed with the secondary antibody only (not shown). Abbreviations: rSNCB: recombinant β-Synuclein; MDM2: Mouse double minute 2 homolog; *p*14ARF: ARF tumor suppressor; PLD2: Phospholipase D2

To quantify the changes in fluorescence intensity, the C:N ratio was calculated for each image (Figure 46). For *p*53, the C:N ratio was unchanged after treatment with high concentrations of rSNCB (1 ng/ml 0.87±0.24, p=0.16; 50 ng/ml: 1.15±0.24, p=0.09; 500 ng/ml: 0.81±0.30, p=0.09). For MDM2, the C:N ratio did not show any shift from the nucleus into the cytoplasm (1 ng/ml: 0.84±0.1, p=0.03; 50 ng/ml: 0.72±0.23,

p=0.004; 500 ng/ml: 1.10±0.15, *p*=0.16). A decrease in the C:N ratio indicate the shifting of *p*14ARF into the nucleus (1 ng/ml: 0.76±0.13, *p*=0.001; 50 ng/ml: 0.60±0.14, *p*<0.001; 500 ng/ml: 0.69±0.18, *p*<0.001). A decrease in the C:N ratio of PLD2 indicates its shifting into the nucleus (1 ng/ml: 0.80±0.13, *p*=0.54; 50 ng/ml: 0.51±0.11, *p*<0.001; 500 ng/ml: 0.82±0.09, *p*=0.84).

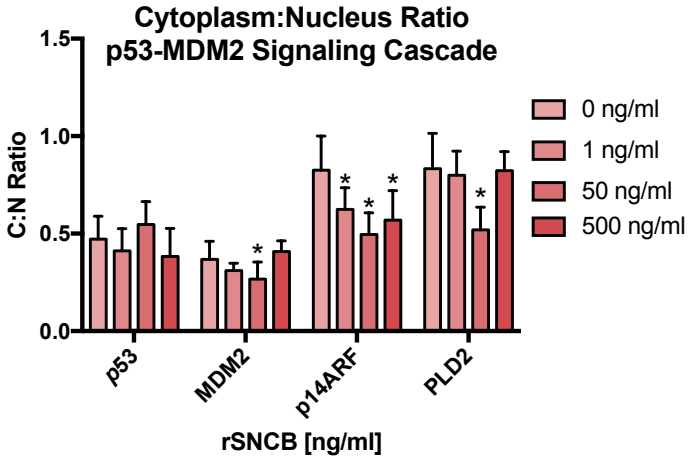

Figure 46 C:N ratio of *p*53, MDM2 and *p*14ARF

C:N ratio revealed by fluorescence intensities of p53, MDM2, *p*14ARF, and PLD2 using immunofluorescence. * indicates *p*≤0.05, compared with the untreated control. Abbreviations: C:N: Cytoplasm:Nucleus; rSNCB: recombinant β-Synuclein; MDM2: Mouse double minute 2 homolog; *p*14ARF: ARF tumor suppressor; PLD2: Phospholipase D2

For an expression comparison of the factors of the *p*53 signaling cascade, qRT-PCR was performed, and the mRNA expression level of the genes was investigated (Figure 47). The mRNA level of *p*53 was not altered in rSNCB-exposed ARPE-19 cells compared to controls (1 ng/ml: 1.05±0.30, *p*=0.72; 50 ng/ml: 1.17±0.17, *p*=0.13; 500 ng/ml: 1.00±0.13, *p*=0.95). The mRNA level of MDM2 showed a significant decrease after exposure to higher concentrations of rSNCB (1 ng/ml 0.98±0.09, *p*=0.72; 50 ng/ml: 0.94±0.12, *p*=0.43); 500 ng/ml: 0.81±0.13, *p*=0.06). The mRNA level of *p*14ARF decreased significantly after exposure to 50 ng/ml rSNCB (0.42±0.25, *p*=0.05) and 500 ng/ml rSNCB (0.61±0.17, *p*=0.06) compared to controls but no significant change after treatment with 1 ng/ml (0.59±0.27; *p*=0.13) could be observed. The mRNA level of PLD2 was significantly increased after exposure to 1 ng/ml rSNCB (1.30±0.08 *p*=0.02) and 50 ng/ml rSNCB (1.35±0.1, *p*=0.02) compared to controls (500 ng/ml: 1.04±0.14 *p*=0.72).

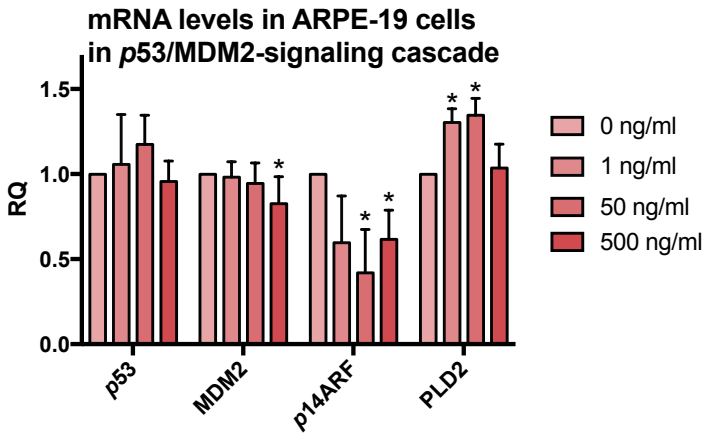

Figure 47 *p*53-MDM2 cascade in rSNCB exposed ARPE-19 cells

*p*53, MDM2 and p14ARF mRNA levels in rSNCB-treated ARPE-19 cells, compared with those in the untreated control. * indicates $p \leq 0.05$, compared with the untreated control. Abbreviations rSNCB: recombinant β-Synuclein; MDM2: Mouse double minute 2 homolog; *p*14ARF: ARF tumor suppressor; PLD2: Phospholipase D2

4.4.1.2.4 Influence of rSNCB on inflammation and oxidation

For the investigation of the inflammatory responses in rSNCB-exposed ARPE-19 cells, alterations in immunofluorescence staining (Figure 48) and mRNA levels of HMOX1 (Figure 49) were measured in ARPE-19 cells exposed to increasing concentrations of rSNCB. The fluorescence intensity of HMOX1 increased after treatment with rSNCB. The fluorescence intensity was higher in the nucleus in the untreated control, whereas the intensity of HMOX 1 in cells exposed to rSNCB is increased in the cytoplasm.

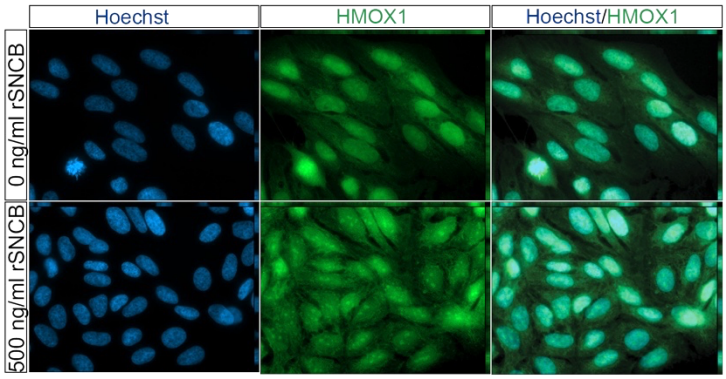

Figure 48 Inflammatory stress response in rSNCB exposed ARPE-19 cells

Immunofluorescence of HMOX1 (green) staining of rSNCB-treated ARPE-19 cells. Hoechst (blue) was used to visualize cell nuclei. Secondary antibody (green, Alexa 488) was used to visualize antigen staining. Negative control was performed with the secondary antibody alone (not shown). Magnification: 63x. Abbreviations: rSNCB: recombinant β-Synuclein; HMOX1: Heme oxygenase (decycling) 1

An increase in the expression level of HMOX1 mRNA was found for the exposure to 50 ng/ml rSNCB (1 ng/ml: 1.45±0.25, p=0.09; 50 ng/ml: 1.80±0.23; p=0.02; 500 ng/ml: 1.29±0.23; p=0.16). The antioxidative properties in rSNCB-exposed ARPE-19 cells

were assessed by measuring the mRNA expression levels of NOX4, GCLM and GCLC (Figure 49). The mRNA expression levels of NOX4 were significantly increased in rSNCB-exposed APRE-19 cells (1 ng/ml: 1.49±0.28, p=0.04; 50 ng/ml: 2.09±0.89, p=0.002; 500 ng/ml: 1.43±0.21, p=0.02), whereas the mRNA expression levels of GCLM (1 ng/ml: 0.94±0.17; p=0.57; 50 ng/ml 1.13±0.18; p=0.23; 500 ng/ml 0.99±0.84; p=0.93) and GCLC (1 ng/ml: 0.86±0.16; p=0.15; 50 ng/ml 148±0.50; p=0.27; 500 ng/ml 0.92±0.05; p=0.13) were not altered in rSNCB-exposed ARPE-19 cells compared to untreated controls.

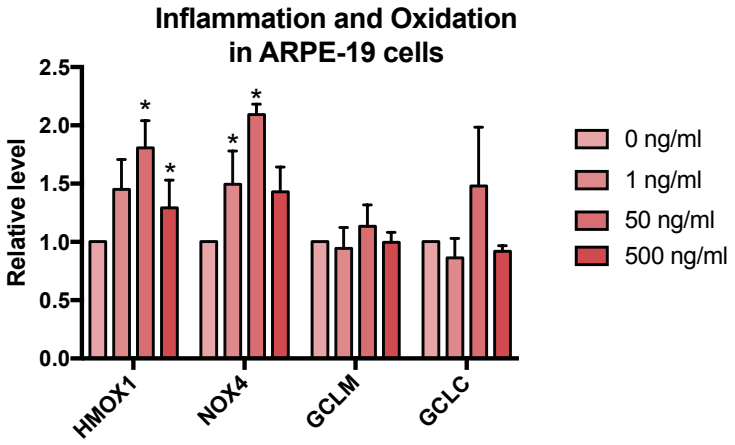

Figure 49 Inflammatory and oxidative stress response in rSNCB exposed ARPE-19 cells

HMOX1, NOX4, GCLM and GCLC mRNA levels in rSNCB-treated ARPE-19 cells, relative to those in the untreated control. * indicates $p \leq 0.05$, compared with the untreated control. Abbreviations: rSNCB: recombinant β-Synuclein; HMOX1: Heme oxygenase (decycling) 1; NOX4: Nicotinamide adenine dinucleotide phosphate oxidase 4; GCLM: Glutamate-cysteine ligase catalytic subunit; GCLC: Glutamate-cysteine ligase regulatory subunit

4.4.1.3 Characterization in primary porcine RPE

To confirm the results of a secondary, immortalized cell line like ARPE-19 cells, a primary cell line was used for the same experiments as described above. For the primary cell line, RPE cells from *Sus scofa domesticus* were used. The bioavailability of eyes from *S. scofa* is very high, the anatomy of the eye and the genetic homology compared to the human eye is high and the eye cubs are large, having a high number of cells. The SNCA and SNCB expression levels, viability, apoptosis, *p*53-MDM2 signaling cascade, and inflammation were studied in rSNCB-exposed ppRPE cells. In contrast to the experiments with ARPE-19 cells, the results are mainly based on qRT-PCR, because as a primary cell line, ppRPE cells do not grow very well on glass cover slips used for immunofluorescence. Growing on glass changes the morphology of the cells and slows down cell growth significantly.

4.4.1.3.1 Expression of β-Synuclein in ppRPE cells

SNCB and SNCA was endogenously expressed in ppRPE-cells (Figure 50). SNCB was mainly present in the nucleus of the cells and in the cytoplasm close to the nucleus. The fluorescence intensity for SNCA was the highest in the nucleus and cell membrane.

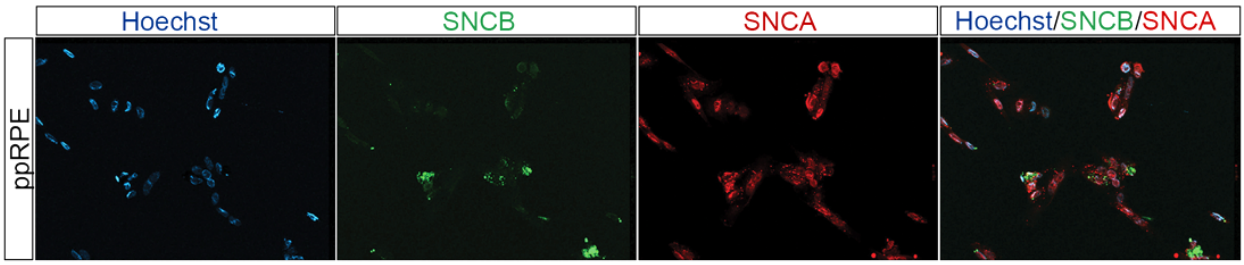

Figure 50 Expression of SNCA and SNCB in ppRPE cells

Immunofluorescence staining of SNCB (green) and SNCA (red) in ppRPE cells. Hoechst (blue) was used to stain cell nuclei. Secondary antibodies (green, Alexa 488; red, Alexa 594) were used to visualize antigen staining. Magnification: 63x. Negative control was performed with the secondary antibody alone (not shown); Abbreviations: SNCA: α-Synuclein; SNCB: β-Synuclein

4.4.1.3.2 Influence of rSNCB on viability and apoptosis

To study the influence of rSNCB on viability and apoptosis, the cells were treated with rSNCB for 6 h, 12 h and 24 h. The viability of the cells was investigated using the MTT assay (Figure 51). The analysis of viability did not reveal any alterations in rSNCB-exposed ppRPE cells after 12 h (1 ng/ml: 132.0±9.9 %, p=0.14; 50 ng/ml: 131.2±7.0 %, p=0.09; 500 ng/ml: 118.8±7.3 %, p=0.16) or 24 h (24 h: 1 ng/ml: 110.0±2.0 %, p=0.08; 50 ng/ml: 109.33±6.76 %, p=0.29; 500 ng/ml: 118.2±1.4 %, p=0.05) compared to controls.

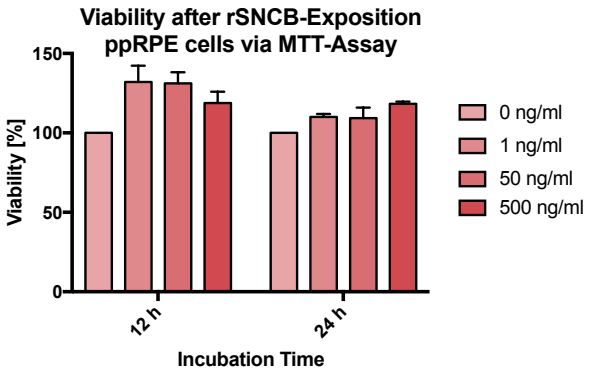

Figure 51 Viability of rSNCB-treated ppRPE cells

Viability of the ppRPE cells following the treatment with rSNCB was determined using the MTT assay. The viability of untreated cells was set to be 100 %; Abbreviations: rSNCB: recombinant β-Synuclein; MTT: 3-(4,5-Dimethylthiazol-2-yl)-2,5-Diphenyltetrazolium Bromide

In contrast, the TUNEL assays (Figure 52) showed a significant decrease in TUNEL-positive cells compared to untreated controls after 12 h in ppRPE exposed to rSNCB at higher concentrations (50 ng/ml: 73±8 %, p=0.03; 500 ng/ml: 47±9 %, p=0.01). The number of TUNEL-positive cells remained constant after treatment with lower concentrations. The number of TUNEL-positive ppRPE cells did not changed after 6 h (1 ng/ml: 105±22 %, p=0.75; 50 ng/ml: 113±26 %, p=0.49; 500 ng/ml: 131±36 %, p=0.27) and 24h (1 ng/ml: 90±54 %, p=0.78; 50 ng/ml: 88±43 %, p=0.66; 500 ng/ml: 59±30 %, p=0.13).

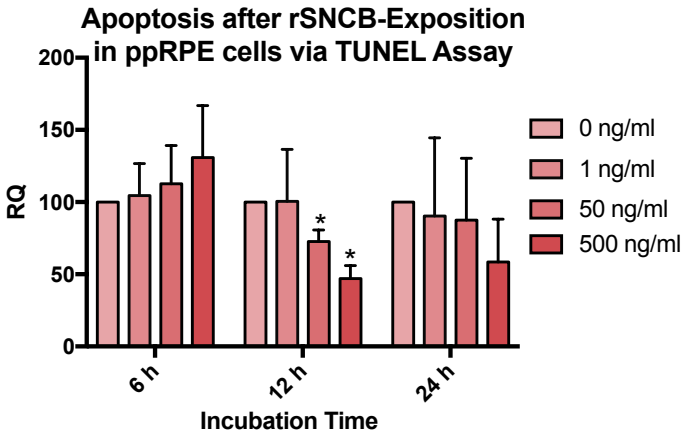

Figure 52 Apoptosis of rSNCB-treated ARPE-19 cells

Rate of apoptosis revealed by TUNEL assay of rSNCB-exposed ARPE-19 cells; the survival of untreated cells was set to be 100 %; * indicates $p \leq 0.05$, compared with the untreated control. Abbreviations: rSNCB: recombinant β-Synuclein; TUNEL: terminal deoxynucleotidyl transferase dUTP nick end labeling

4.4.1.3.3 Influence of rSNCB on *p*53 signaling cascade

The *p*53-MDM2 signaling cascade in the rSNCB-exposed ppRPE was investigated using qRT-PCR (Figure 53). The mRNA level of *p*53 did not changed in rSNCB-exposed ppRPE cells compared to controls (1 ng/ml: 1.10±0.17, p=0.54; 50 ng/ml: 1.06±0.05, p=0.72; 500 ng/ml: 0.97±0.16 p=0.83. The mRNA levels of MDM2 (0.70±0.06, p=0.01) and *p*14ARF (0.75±0.07, p=0.02) decreased significantly after exposure to rSNCB at 500 ng/ml, but not at lower concentrations (MDM2: 1 ng/ml: 1.03±0.11, p=0.71; 50 ng/ml: 0.86±0.18, p=0.31; *p*14ARF : 1 ng/ml: 1.14±0.30, p=0.49; 50 ng/ml: 0.75±0.06, p=0.07).

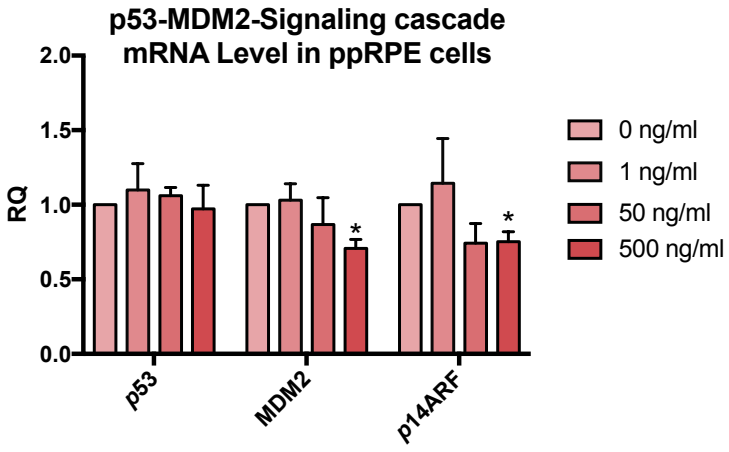

Figure 53 *p*53-MDM2 cascade rSNCB exposed ppRPE cells

*p*53, MDM2 and p14ARF mRNA levels in rSNCB-treated ppRPE cells, compared with those in the untreated control. * indicates $p \leq 0.05$, compared with the untreated control. Abbreviations rSNCB: recombinant β-Synuclein; MDM2: Mouse double minute 2 homolog; *p*14ARF: ARF tumor suppressor

4.4.1.3.4 Influence of rSNCB on inflammation and oxidation

The anti-inflammatory properties of rSNCB were examined analyzing HMOX1 in ppRPE cells. The exposure of rSNCB to ppRPE did not change the mRNA expression level of HMOX1 (1 ng/ml: 1.28±0.28, p=0.16; 50 ng/ml: 1.39±0.35, p=0.17; 500 ng/ml: 1.29±0.23, p=0.25). The results of the mRNA analysis are shown in Figure 54. An increase in the mRNA expression of NOX4 was found in rSNCB-exposed ppRPE cells (1 ng/ml: 1.78±0.50, p=0.15; 50 ng/ml: 1.47±0.10, p=0.11; 500 ng/ml: 1.24±0.06, p=0.10), whereas the mRNA expression levels of GCLM (1 ng/ml: 1.24±0.45, p=0.32; 50 ng/ml: 0.91±0.33, p=0.73; 500 ng/ml: 0.92±0.31, p=0.25) and GCLC (1 ng/ml: 1.08±0.24, p=0.42; 50 ng/ml: 0.92±0.07, p=0.17; 500 ng/ml: 1.03±0.13, p=0.87) remained unchanged after rSNCB exposure.

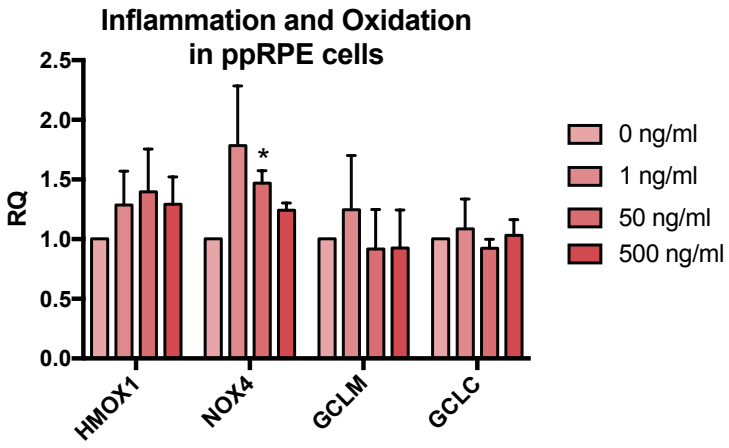

Figure 54 Inflammatory and oxidative stress response in rSNCB exposed ppRPE cells

HMOX1, NOX4, GCLM and GCLC mRNA levels in rSNCB-treated ppRPE cells, relative to those in the untreated control. * indicates $p \leq 0.05$, compared with the untreated control. Abbreviations: rSNCB: recombinant β-Synuclein; HMOX1: Heme oxygenase (decycling) 1; NOX4: Nicotinamide adenine dinucleotide phosphate oxidase 4; GCLM: Glutamate-cysteine ligase catalytic subunit; GCLC: Glutamate-cysteine ligase regulatory subunit

4.4.2 *In-vitro* characterization of Cathepsin B

4.4.2.1 Influence of rCTSB on ARPE-19 cells

The potential influence of CTSB was studied in CTSB-exposed ARPE-19 cells using different concentrations of recombinant CTSB. First, the viability of the cells was investigated after treatment with rCTSB for 24 h (Figure 55). After treatment with 1 ng/ml rCTSB, the viability of the cells remained unchanged (98.22±12.24 %, p=0.082). The viability was significantly reduced after treatment with 10 ng/ml rCTSB (85.34±1.46 %, p=0.004) and 100 ng/ml (81.86±2.26 %, p=0.008).

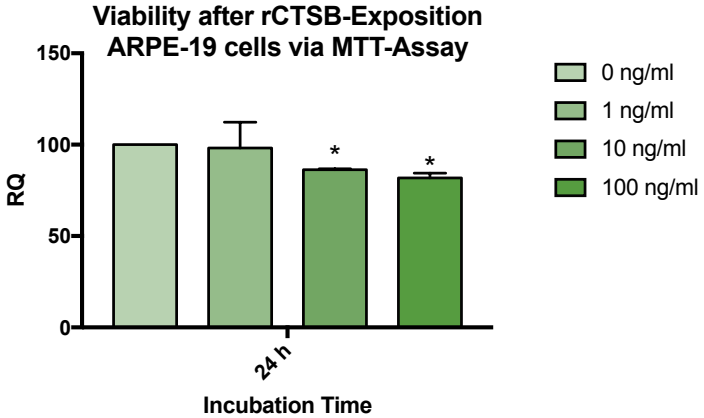

Figure 55 Viability of rCTSB-treated ARPE-19 cells

Viability of the ARPE-19 cells following the treatment with rCTSB was determined using the MTT assay. The viability of untreated cells was set to be 100 %; * indicates $p \leq 0.05$, compared with the untreated control. Abbreviations: rCTSB: recombinant Cathepsin B; MTT: 3-(4,5-dimethylthiazol-2-yl)-2,5-diphenyltetrazolium Bromide

To investigate the influence of CTSB on the extracellular matrix, the expression pattern of the tight-junction proteins ZO-1 and Occludin was investigated using immunofluorescence (Figure 56). In the untreated control, ZO-1 was mainly present in the nucleus of the cells and in the cell membrane, whereas Occludin was mainly present in the cytoplasm and in the cell membrane. In the membrane, the proteins appeared highly ordered to form tight junctions between the cells and to maintain the cellular communication. After treatment with rCTSB, the cells showed disrupted tight junction proteins and reduced cell-cell contacts with increased free space between the cells.

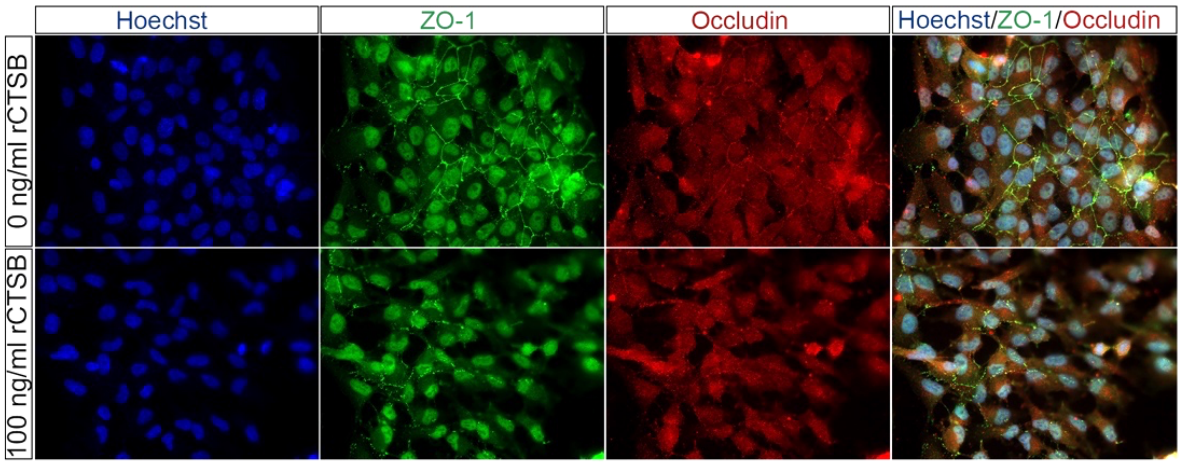

Figure 56 Protein expression of ZO-1 and Occludin in rCTSB exposed ARPE-19 cells
Immunofluorescence staining of ZO-1 (green) and Occludin (red) in ARPE-19 cells. Hoechst (blue) was used to stain cell nuclei. Secondary antibodies (green, Alexa 488; red, Alexa 594) were used to visualize antigen staining. Magnification: 63x. Negative control was performed with the secondary antibody alone (not shown). Abbreviations: rCTSB: recombinant Cathepsin B; ZO-1: zonulae occludents 1

The *p*53-MDM2 signal pathway was examined in rCTSB-exposed ARPE-19 cells using immunofluorescence (Figure 57) and mRNA-expression analysis (Figure 58).
The fluorescence intensity of *p*53 was increased in several cells compared to untreated controls. In untreated ARPE-19 cells, *p*53 fluorescence was mainly detected in the nucleus, whereas the fluorescence intensity increaseed in the cytoplasm in the affected cells after treatment rCTSB. The intensity of fluorescence staining of MDM2 does not change after rCTSB exposure compared to controls.

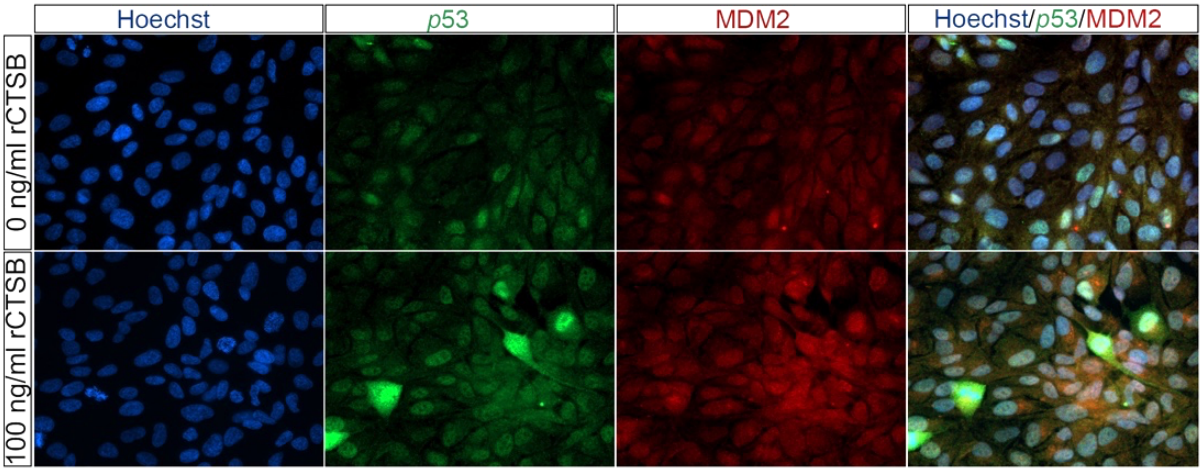

Figure 57 Protein expression of the *p*53-MDM2 cascade in rCTSB exposed ARPE-19 cells

ARPE-19 cells were treated with rCTSB (1, 10 and 100 ng/mL) for 48 hours, followed by analysis IF *p*53 (green) and MDM2 (red) staining in ARPE-19 cells. Hoechst (blue) was used to visualize cell nuclei. Secondary antibody (green, Alexa 488; red, Alexa 594) was used to visualize antigen staining. Magnification: 63x. Negative control was performed with the secondary antibody only (not shown). Abbreviations: rCTSB: recombinant Cathepsin B; MDM2: Mouse double minute 2 homolog

The mRNA level of *p*53 is significant increased after exposure of ARPE 19 cells with 100 ng/ml CTSB (1 ng/ml: 1.71±0.67, p=0.27; 10 ng/ml: 1.36±0.30, p=0.23; 100 ng/ml: 5.75±1.54, p=0.02). The mRNA expression levels of MDM2 showed a significant decrease after exposure to rCTSB (1 ng/ml: 0.26±0.18, p=0.03; 10 ng/ml: 0.27±0.17, p=0.03; 100 ng/ml: 0.40±0.28, p=0.09). The mRNA level of *p*14ARF did not alter after treatment with rCTSB compared to the controls (1 ng/ml: 1.40±0.31, p=0.21; 10 ng/ml: 0.67±0.21, p=0.35; 100 ng/ml: 1.69±0.83, p=0.35).

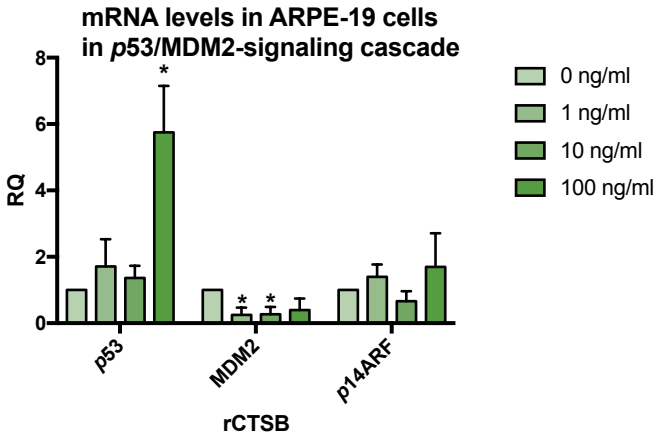

Figure 58 *p*53-MDM2 cascade within rCTSB exposed ARPE-19 cells

*p*53, MDM2 and p14ARF mRNA levels in rCTSB treated ARPE-19 cells, compared with those in the untreated control. * indicates $p \leq 0.05$, compared with the untreated control. Abbreviations: rCTSB: recombinant Cathepsin B; MDM2: Mouse double minute 2 homolog; *p*14ARF: ARF tumor suppressor

To study the influence of CTSB on the expression pattern of VEGF, immunofluorescence was used after incubating ARPE-19 cells with rCTSB (Figure 59). The highest fluorescence intensity of VEGF was located in the cytoplasm close to the nucleus. This fluorescence intensity was increased after treatment with rCTSB.

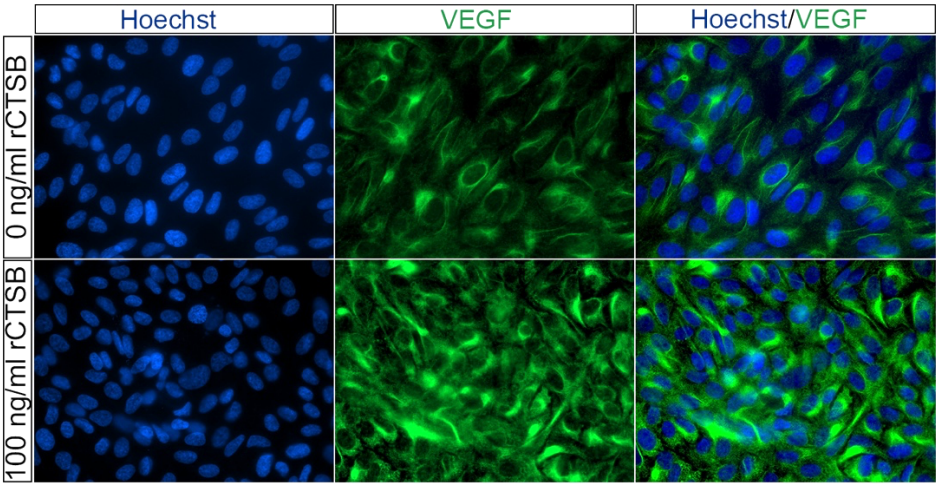

Figure 59 Protein expression of VEGF within rCTSB exposed ARPE-19 *in-vitro*

Immunofluorescence staining of VEGF (green) in ARPE-19 cells. Hoechst (blue) was used to stain cell nuclei. Secondary antibodies (green, Alexa 488) were used to visualize antigen staining. Magnification: 63x. Negative control was performed with the secondary antibody alone (not shown); Abbreviations: rCTSB: recombinant Cathepsin B; VEGF: vascular endothelial growth factor

CTSB is endogenously expressed in ARPE-19 cells at a low level. The exposure to rCTSB also increased the intracellular expression of CTSB significantly. This is shown in the immunofluorescence staining (Figure 60). Additionally, the analysis of the mRNA of CTSB showed increased mRNA levels (1 ng/ml: 11.24±0.25, p=0.01; 10 ng/ml: 14.03±11.08, p=0.23; 100 ng/ml: 7.82±2.76, p=0.05)

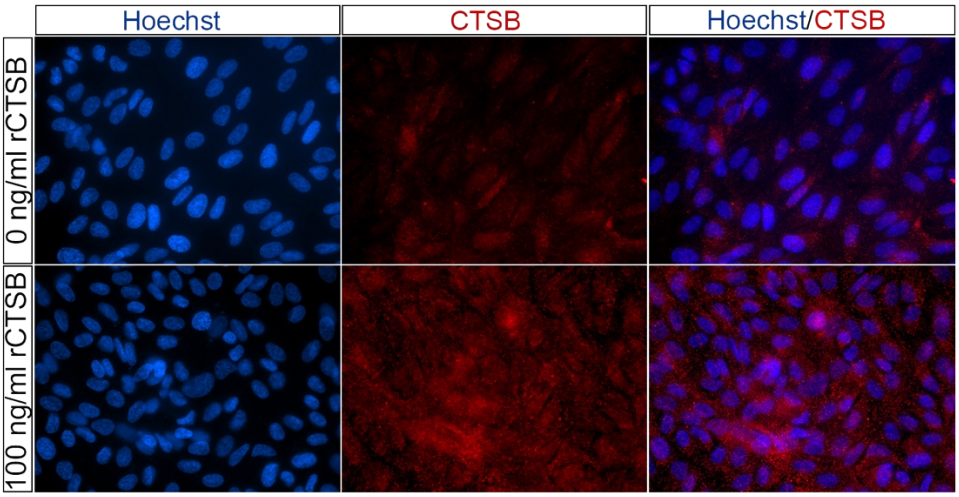

Figure 60 Protein expression of CTSB within rCTSB exposed ARPE-19 *in-vitro*

Immunofluorescence staining of CTSB (red) in ARPE-19 cells. Hoechst (blue) was used to stain cell nuclei. Secondary antibodies (red, Alexa 594) were used to visualize antigen staining. Magnification: 63x. Negative control was performed with the secondary antibody alone (not shown); Abbreviations: rCTSB: recombinant Cathepsin B; CTSB: Cathepsin B

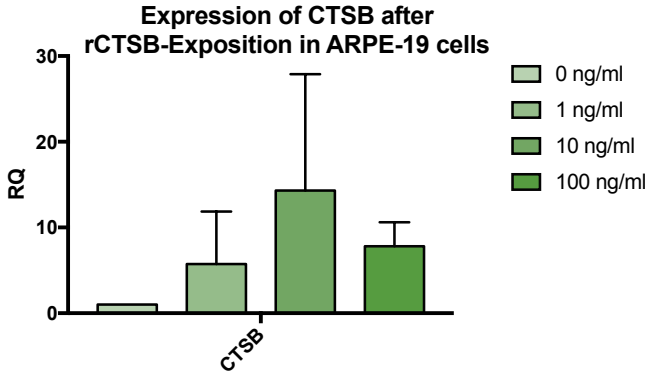

Figure 61 Gene expression of CTSB within rCTSB exposed ARPE-19 *in-vitro* on mRNA level

mRNA levels of CTSB in rCTSB treated ARPE-19 cells, compared with those in the untreated control. * indicates $p \leq 0.05$, compared with the untreated control. Abbreviations: rCTSB: recombinant Cathepsin B; CTSB: Cathepsin B

4.4.2.2 Establishment of an *in-vitro* senescence model

For the establishment of the *in-vitro* senescence model, accordingly to the described model by Glotin et al., was used (Glotin et al., 2008). A β-galactosidase assay was performed to evaluate the level of senescence. The cells showed no staining at all, which indicates that those cells were not alive. In the following steps, the concentration was reduced to 0.5 mM and 0.25 mM *tert*-BHP and the cells were treated for one hour, the medium was changed, and the cells had a recovery time of 24 h before analysis. The number of β-galactosidase positive cells was significantly increased after

treatment with 0.25 mM *tert*-BHP (46.63±1.24 %, $p<0.0001$) and 0.5 mM *tert*-BHP (58.67±2.72 %, $p<0.0001$).

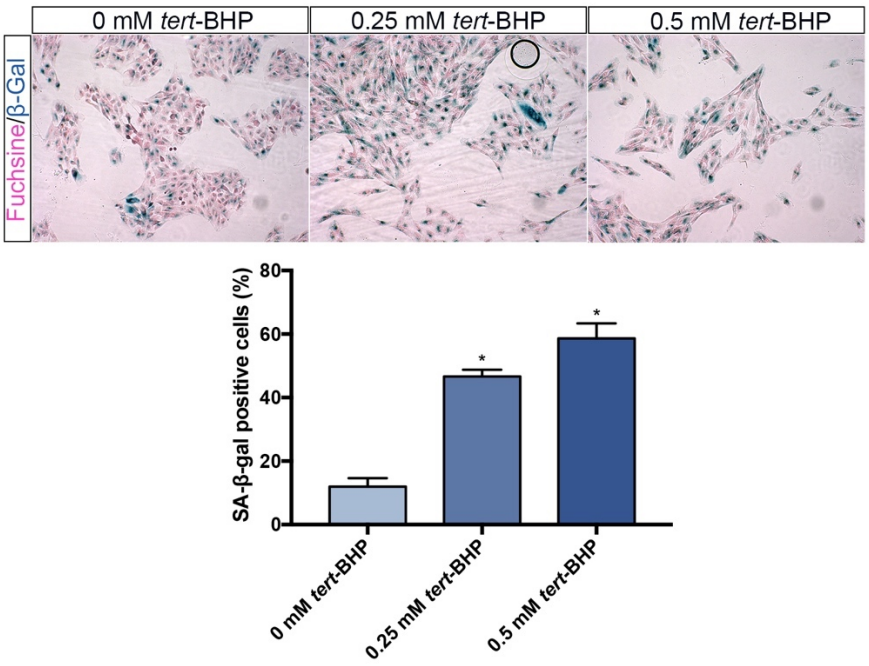

Figure 62 β-galactosidase assay on ARPE-19 cells treated with *tert*-BHP

ARPE-19 cells were treated with 0.25 mM and 0.5 mM *tert*-BHP for 1 h. To enhance visibility, the cells were stained with Fuchsine (pink). * indicates $p \leq 0.05$, compared with the untreated control. Magnification: 20x; Abbreviations: *tert*-BHP: *tert*-butylhydroperoxide

To study the influence of *tert*-BHP on ARPE-19 cells, the viability of the cells was investigated after treatment with 0.25 mM and 0.5 mM for one hour (Figure 63). After treatment with 0.25 mM *tert*-BHP, the viability of the cells remained unchanged (92.22±4.06 %, $p=0.06$). The viability was significantly reduced after treatment with 0.5 mM *tert*-BHP (80.26±8.45 %, $p=0.02$).

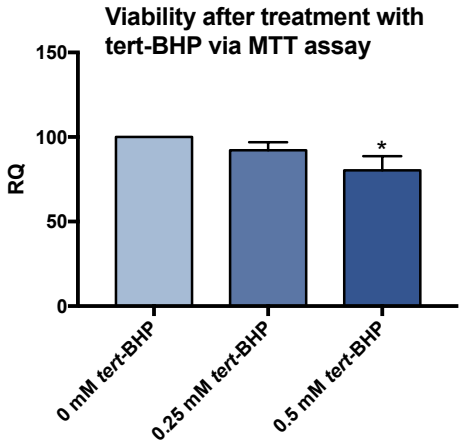

Figure 63 Viability of ARPE-19 cells after treatment with *tert*-BHP

Viability of the ARPE-19 cells following the treatment with *tert*-BHP was determined using the MTT assay. The viability of untreated cells was set to be 100 %; * indicates $p \leq 0.05$, compared with the untreated control. Abbreviations: *tert*-BHP: *tert*-butylhydroperoxide; MTT: 3-(4,5-Dimethylthiazol-2-yl)-2,5-Diphenyltetrazolium Bromide

To study the influence of *tert*-BHP on the oxidation of nucleic acids, the cells were stained with antibody against 8-HGN (Figure 64). Without treatment, the cells showed a slight staining of the nucleus. After treatment with 0.25 mM *tert*-BHP, the cells showed an increased fluorescence intensity in the nucleus. After treatment with 0.5 mM *tert*-BHP, the cells showed increased fluorescence intensity in the nucleus compared to untreated cells, but the signal is diffuse.

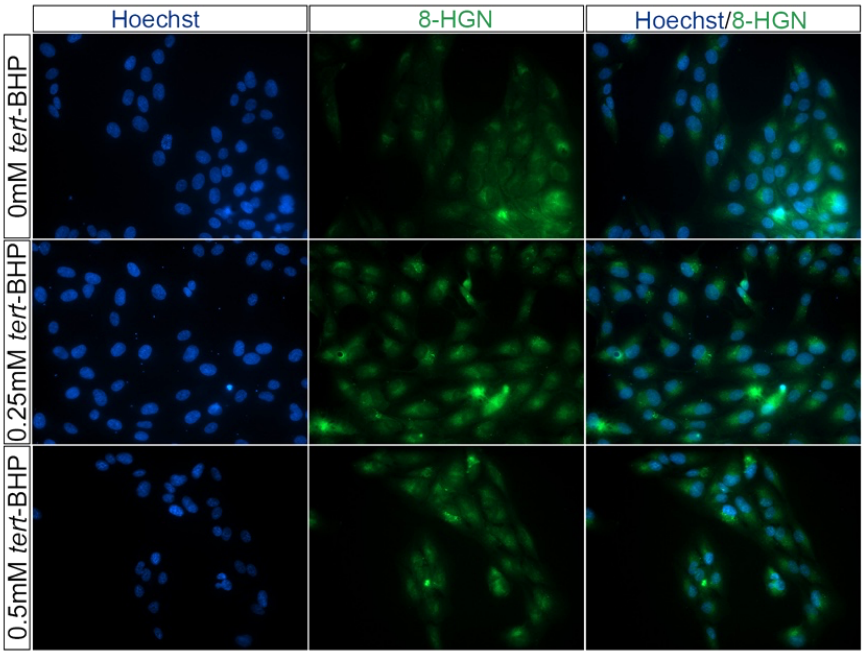

Figure 64 Protein expression of 8-HNG after treatment with *tert*-BHP

The cells were treated with 0.25 mM and 0.5 mM *tert*-BHP and stained with anti-8HNG to determine the level of the oxidation of the nucleic acids. Hoechst (blue) was used to stain cell nuclei. Secondary antibody (green, Alexa 488) were used to visualize antigen staining. Magnification: 40x. Negative control was performed with the secondary antibody alone (not shown); Abbreviations: *tert*-BHP: *tert*-butylhydroperoxide; 8-HGN: 8-Hydroxyguanosine

To study the influence of *tert*-BHP on the oxidation of lipids, the cells were stained with antibody against 4-HNE (Figure 65). After treatment with 0.25 mM *tert*-BHP and 0.5 mM *tert*-BHP, the cells showed an increased fluorescence intensity in the cytoplasm.

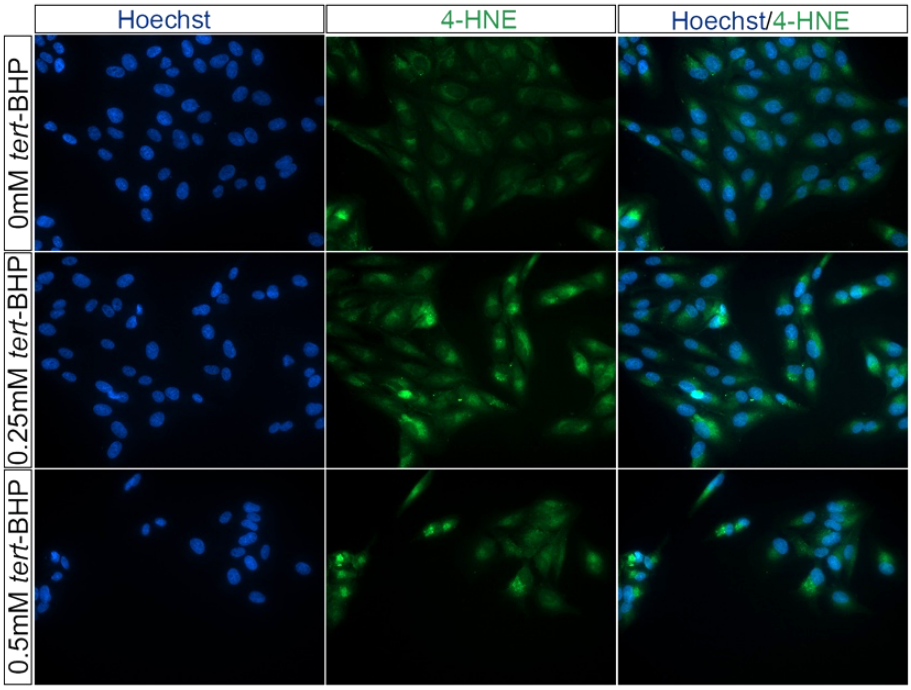

Figure 65 Protein expression of 4-HNE after treatment with *tert*-BHP

The cells were treated with 0.25 mM and 0.5 mM *tert*-BHP and stained with anti-4-HNE to determine the level of the oxidation of lipids. Hoechst (blue) was used to stain cell nuclei. Secondary antibody (green, Alexa 488) were used to visualize antigen staining. Magnification: 40x. Negative control was performed with the secondary antibody alone (not shown). Abbreviations: *tert*-BHP: *tert*-butylhydroperoxide; 4 HNE: 4-Hydroxynonenal

Comparing the results of cells treated with 0.25 mM and 0.5 mM *tert*-BHP, both concentrations lead the cells into premature senescence. The effects of both treatments were comparable regarding the effects on protein expressions, but the viability was significantly reduced in cells treated with 0.5 mM *tert*-BHP. For further use of the premature senescence model, the cells were treated with 0.25 mM *tert*-BHP.

4.4.2.3 Influence of CTSB on premature cellular senescence

To study the influence of CTSB on premature senescent cells, the cells were treated as described 3.2.7.2. First, the viability and apoptosis of the cells was investigated using PE Annexin V/7AAD staining. In further steps, the proliferation of the cells was investigated using Cell Proliferation Dye eFluor™ 670. Additionally, the phagocytosis rate was tested after additional treatment of the cells with fluorescent latex beads, which were incorporated into the cells. Finally, the influence of the treatment with tert-BHP and CTSB on the intracellular ROS levels was investigated using H_2DCFDA as a dye. The oxidized form is fluorescent.

4.4.2.3.1 Viability and apoptosis

To study viability and apoptosis of the cells after treatment with *tert*-BHP, the cells were stained with PE Annexin V and 7AAD and analyzed via FACS. The result of this analysis is shown in Figure 66. The results show that in all treatments more than 90 % of the cells were alive. Only a very small number (~1 % of the cells) were necrotic. The number of cells in early apoptosis was slightly higher in cells treated with *tert*-BHP (3.32±2.28 %) and *tert*-BHP/CTSB (3.02±2.00 %) compared to untreated cells (0.76±0.43 %). Furthermore, the number of cells already in apoptosis was slightly higher in treated cells (*tert*-BHP: 4.02±1.63 %; CTSB: 2.58±1.88 %; *tert*-BHP/CTSB: 3.38±1.59 %) compared to untreated cells (1.91±0.65 %) with no significant differences. The results are summarized in the following Table 25

Table 25: Summary of analysis of viability and apoptosis

SD: Standard deviation, $p \leq 0.05$ indicates as significant compared to untreated control. Abbreviations: *tert*-BHP: *tert*-butylhydroperoxide; SD: Standard deviation; CTSB: Cathepsin B

	Treatment	Value [%]	±SD [%]	*p* value
Alive	Untreated	96.91	0.92	
	tert-BHP	92.43	3.48	0.07
	CTSB	95.87	2.65	0.90
	tert-BHP/CTSB	93.56	3.24	0.23
Necrotic	Untreated	0.40	0.23	
	tert-BHP	0.71	0.46	0.62
	CTSB	0.62	0.42	0.79
	tert-BHP/CTSB	0.82	0.48	0.40
Early apoptotic	Untreated	0.76	0.43	
	tert-BHP	3.28	2.29	0.06
	CTSB	0.92	0.78	0.99
	tert-BHP/CTSB	3.02	2.00	0.10
Apoptotic	Untreated	1.91	0.66	
	tert-BHP	4.03	1.64	0.18
	CTSB	2.59	1.89	0.86
	tert-BHP/CTSB	3.38	1.59	0.44

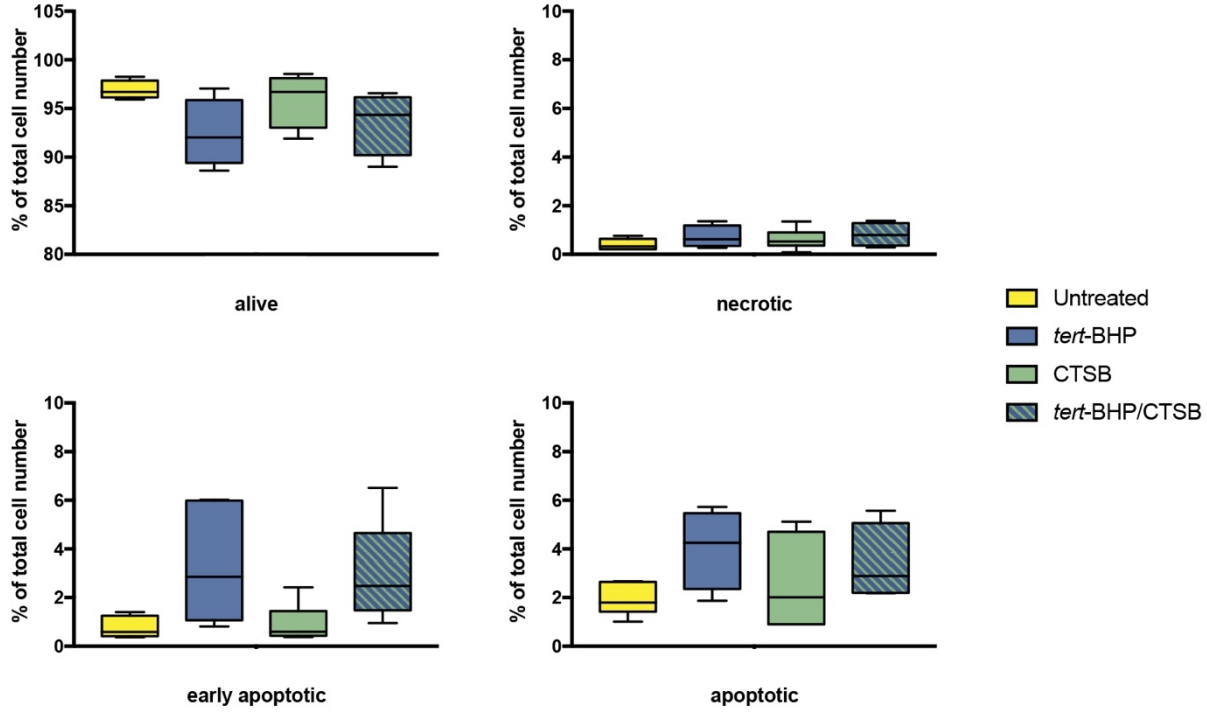

Figure 66 Analysis of viability and apoptosis of *tert*-BHP and rCTSB treated ARPE-19 cells

ARPE-19 cells were treated with of *tert*-BHP and rCTSB as described above. Viability and apoptosis were investigated using PE Annexin V/7AAD staining for FACS to visualize living, necrotic, early apoptotic and apoptotic cells. Abbreviations: *tert*-BHP: *tert*-butylhydroperoxide; rCTSB: recombinant Cathepsin B; FACS: Fluorescence-activated cell sorting; 7AAD: 7-Amino-Actinomycin

4.4.2.3.2 Proliferation

The results of the analysis of proliferation are shown in Figure 67. The geometric mean of cells treated with *tert*-BHP (15987.48±413577, p=0.0004) and *tert*-BHP/CTSB (16941.92±5632.37, p=0.0001) was significantly higher than the geometric mean of untreated cells (5235.26±2086.38) and cells treated only with CTSB (5336.65±1848.14). The geometric mean was about three times higher in samples treated with *tert*-BHP, which means that the untreated cells proliferated 1.5 more often than treated cells.

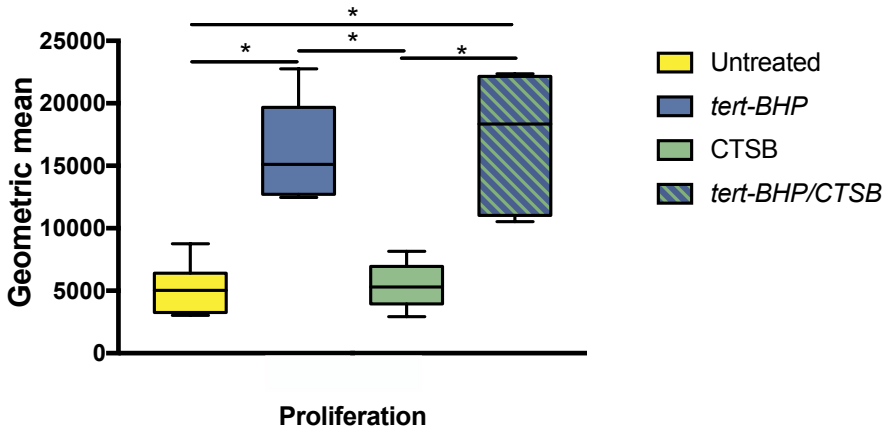

Figure 67 Analysis of proliferation of *tert*-BHP and rCTSB treated ARPE-19 cells

ARPE-19 cells were treated with of *tert*-BHP and rCTSB as described above. Proliferation was investigated using eFluor™ 670 staining for FACS to visualize the differences in cell division; * indicates $p \leq 0.05$, compared with the untreated control; Abbreviations: *tert*-BHP: *tert*-butylhydroperoxide; rCTSB: recombinant Cathepsin B; FACS: Fluorescence-activated cell sorting

4.4.2.3.3 Phagocytosis

The results of the phagocytosis assay are shown in Figure 68. The phagocytosis rate significantly increased in cells treated with *tert*-BHP (50.46±8.77 %, p=0.017) and *tert*-BHP/CTSB (66.58±10.87 %, p=0.0001) compared to the untreated control (32.08±10.12 %). The phagocytosis rate did not change with cells treated with CTSB (33.82±8.68 %). Additionally, the phagocytosis rate was significantly increased in cells treated with *tert*-BHP/CTSB compared to cells treated only with *tert*-BHP (p=0.04).

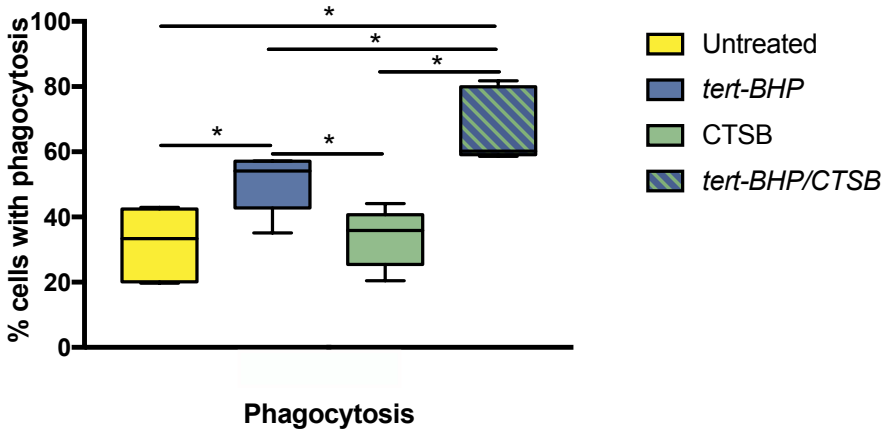

Figure 68 Analysis of phagocytosis of *tert*-BHP and rCTSB treated ARPE-19 cells

ARPE-19 cells were treated with of *tert*-BHP and rCTSB as described above. Phagocytosis of the cells was investigated feeding the cells with fluorescent latex beads. * indicates $p \leq 0.05$, compared with the untreated control. Abbreviations: *tert*-BHP: *tert*-butylhydroperoxide; rCTSB: recombinant Cathepsin B

4.4.2.3.4 ROS levels

The median of the fluorescence intensity showed the intracellular ROS level. The results are summarized in Figure 69. The observed changes in the ROS level between different treatments were not significant. Although the treatment with *tert*-BHP (17721.67±6788.09) seems to increase the level of intracellular ROS. The treatment with CTSB (12234.29±3539.12) and *tert*-BHP/CTSB (13273.29±2987.59) did not seem to increase the ROS level compared to the untreated control (14255.00±1967.25).

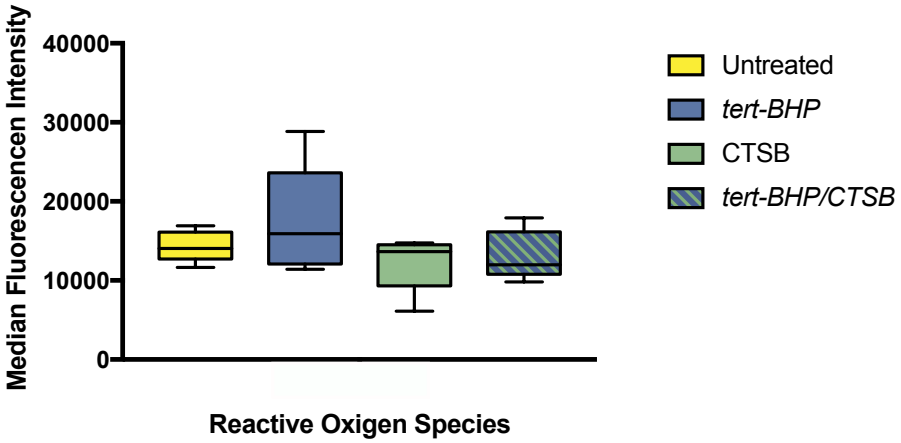

Figure 69 Analysis of intracellular ROS level of *tert*-BHP and rCTSB treated ARPE-19 cells

ARPE-19 cells were treated with of *tert*-BHP and rCTSB as described above. Intracellular ROS level was investigated using H_2DCFDA as a dye. Abbreviations: *tert*-BHP: *tert*-butylhydroperoxide; rCTSB: recombinant Cathepsin B; ROS: Reactive oxygen species

5 Discussion

Alterations in the physiological aging process can lead to severe pathologies. There are alterations in the retina, as well as in the RPE during the aging process which are not fully understood. That includes the conversion from the aging process into a severe pathology.

In many cases in medical research, mouse or rat models are used to achieve a better understanding of the current situation and to find possible treatment options. As the macula is a key player in the physiological aging process as wells as in pathologies. Therefore, the use of mouse or rat models is not suitable for this study as these animals do not have a macula. In a comparative proteomic analysis of the retinas of C. *jacchus* and Sprague-Dawley rats, proteins were identified which's expression profiles are altering with maturation and aging (Böhm et al., 2013). These changes are independent of whether the retina bears a macula (Böhm et al., 2013). In prior studies it was also shown, that the proteome of human eyes changes with progression of AMD (Ethen et al., 2006). Ideally, the changes in the proteome and additionally the transcriptome of the RPE from young age to senile should be investigated in human RPE. Despite the possible use of cadaver eyes from an eye bank, it is very difficult to collect a cohort from different stages of live, because the majority of eye donors is >70 years old.

To circumvent this problem, donor eyes from *C. jacchus* from all stages of life were used. The development of the eye as well as the anatomy and genetic homology of the eye is very comparable with humans. The donor eyes from monkey used for other studies were kindly provided by Prof. Stefan Schlatt and Dr. Joachim Wistuba from the Centre of Reproductive Medicine and Andrology (University of Münster). AMD was not observed in *C. jacchus* yet and only 1.2 % of 488 examined animals showed fundus alterations, but forms of AMD have been investigated in several other non-human primates (Pennesi et al., 2012).

The findings of this study can be divided in three main parts, including (1) the histological alterations of the aging RPE of *C. jacchus*, the (2) molecular changes in the aging RPE of *C. jacchus* on gene and protein level as well as (3) the investigation of the function of SNCB and CTSB in the RPE.

The major findings of the study are:

1. The distribution and shape of pigment granules change in the RPE of *C. jacchus* over lifetime.
2. The results from the gene analysis are comparable to the results from the proteome analysis
3. The number of genes and proteins expressed significantly different between macula and periphery increases with age
4. The obtained differences in the distribution of SNCB in primate RPE along with alterations of cellular functions in rSNCB-exposed RPE cells support SNCB-related effects like inflammatory response and stress-related properties on RPE over lifetime.
5. The overabundance of CTSB influences the RPE regarding several cellular functions, including cell-cell-contacts via tight junctions and the expression level of the proangiogenic factor VEGF
6. CTSB influences senescent RPE cells especially in the phagocytosis rate

5.1 Morphological changes in the aging RPE

To gain an overview about morphological changes in the aging RPE, a histological characterization of the aging RPE of *C. jacchus* was performed (Figure 17). The results of the histological characterization of aging RPE showed a change in the distribution and shape of pigment granules over lifetime. As described above, the pigment granules are capable of various functions, including the absorption of light and the protection against oxygen, ROS and metal ions such as iron (Sparrow et al., 2010). It was found, that the quantity of pigment granules decreases during lifetime, which is comparable to described alterations of intracellular granules in the RPE of postmortem human eyes published previously (Ach et al., 2015; Feeney-Burns et al., 1984). Additionally, the age-related alterations of the intracellular localization of pigmented granules towards the apical side of the RPE cells of *C. jacchus* (Figure 19) are similar to the results in previously published studies (Feeney, 1978; Feeney-Burns et al., 1984). The described findings may indicate the decreased potential of light absorption, and increased ROS due to extensive light exposure. The decrease in number of pigment granules and the concurrent decrease in free cytoplasmatic space may be explained by the increase of the pigment granules in volume and size. It was previously shown that lipofuscin redistributes by the degranulation and aggregation in the aged

human RPE (Ach et al., 2015). Furthermore, an enlargement and thickening of the RPE cell area combined with a transformation from convex to irregular or concave polygons and as well as derangement of the cytoskeleton was described (Ach et al., 2015). A possible explanation for the observed changes might be the increased association of pigment granules with melanosomes. In previous studies it was reported, that the quantity of granules is increased as well as reduced in postmortem eyes (Ach et al., 2014; Gao and Hollyfield, 1992; Ts'o and Friedman, 1968; Watzke et al., 1993), due to the use of different analysis techniques and varieties in postmortem times (Böhm, 2017). The presented age- as well as localization-related distribution of intracellular pigment granules may reflect the age-related increase of metabolic- and stress related conditions. The increased differences in the topographical distribution and intracellular localization of pigmented granules during lifetime, might be explained by the different metabolic requirements of macula and periphery, such as the greater light exposure in the central region compared to the peripheral region causing elevated inflammatory responses (Bone et al., 2012; Wellen and Hotamisligil, 2005).

5.2 Transcriptome analysis

The RNA sequencing analysis were performed by **PD Dr. Ludger Klein-Hitpass**. The bioinformatics were performed by **Prof. Dr. Sven Rahmann** and **PD Dr. Ludger Klein-Hitpass**.

To gain a complete overview of the changes in the genome of the aging RPE of *C. jacchus*, NGS was performed with the collected RPE samples of different ages and topographic conditions. NGS is a very sensitive method compared to traditional Sanger sequencing (Chin et al., 2013). This increased sensitivity is necessary if the amount of available RNA/cDNA is limited.

The total amounts of genes expressed significantly different varies between the age groups (Figure 20). The comparison between neonatal and adult tissue resulted in more than 5000 genes, of which about 50% could be found in the macula while the other half was found in the periphery. The comparison of neonatal with senile tissue led to more than 4000 genes, of which only 35 % were expressed differently in the macula. The number of genes expressed differently in tissue from adult RPE compared with senile RPE is reduced to 1000 genes with 63 % of the genes found in the macula.

In neonatal tissue, the number of genes differently expressed in the macula compared to the periphery, was very low and about 10 times higher in senile tissue.
This is consistent with the hypothesis, that the macula and the peripheral parts of the RPE age differently, due to an increased light exposure and an increased energy metabolism of the cells in the macula (Cheung and Wong, 2016; Wong-Riley, 2010). During the growth of the animal until sexual maturity (~477 days for a female, ~382 day for a male animal) (Weigl, 2005), the genome of macula and periphery changes significantly. The number of changes in the transcriptome is significantly reduced when comparing adult and senile tissue, indicating, that most changes are completed during the first year of life. The high percentage of genes expressed differently in the macula in senile tissue compared to adult tissue indicate the aging process of the macula and may indicate first signs of the development of an age-related pathology like the development of drusen as it is already known, that various monkey species can develop drusen during life (Gouras et al., 2008; Hope et al., 1992; Nicolas et al., 1996). The GSEA and its enrichment plots revealed several cellular functions which include significant up- or downregulated genes in the aging RPE. Out of these, eight different GSEA were chosen to be further investigated. The justification for the selection of these particular gene sets is given in the following sections 5.2.1 to 5.2.8

5.2.1 Angiogenesis

Angiogenesis is an important process during embryogenic development. The cardiovascular system is the first functional organ to develop in the vertebrate embryo. It forms through several distinct, but parallel, processes. The primordial vascular system is defined by vasculogenesis (Risau and Flamme, 1995). While the embryonic vascular system develops in anticipation of the demands of the growing embryo for oxygen and nutrients, angiogenesis in the adult organism occurs in response to the metabolical requirements of tissues and is efficiently triggered by hypoxia. A variety of diseases are associated with either insufficient or excess blood vessel growth (Breier, 2000). VEGF is responsible the stimulation of endothelial cell survival in newly formed blood vessels (Alon et al., 1995; Benjamin and Keshet, 1997). Additionally, VEGF is a key factor for induction and maintenance of the ingrowth of the blood vessel in the retina and is expressed by RGC during development (Pierce et al., 1996; Stone et al., 1996; Stone et al., 1995). Furthermore, it inhibits the migration of astrocytes and endothelial cells into the macula (Sandercoe et al., 2003). However, angiogenesis is

regulated by various inhibitors and initiators. In homeostasis, the amount of pro- and anti-angiogenetic factors is balanced. The results of the transcriptome analysis showed pro- and anti-angiogenetic factors expressed significantly different in aged RPE. Besides nAMD, angiogenesis and neovascularization are prominent signs for diseases including retinopathy of prematurity (Chen and Smith, 2007), diabetic retinopathy (Tremolada et al., 2012) and retinal vein occlusion (Campa et al., 2016). It also takes place in eyes with myopic maculopathy, which occurs in patients with high myopic eyes (Hotchkiss and Fine, 1981; Ikuno, 2017).

5.2.2 Epithelial-mesenchymal transition

EMT is a process in which epithelial cells lose their differentiated phenotypes and become mesenchymal-like cells. It plays a is crucial role during embryogenesis, organ development, wound healing and tissue generation (Kalluri and Weinberg, 2009). In proliferative vitreoretinopathy, the detachment of the retina, followed by a loss of cell-cell contacts of the RPE, initiates EMT and proliferation (Tamiya et al., 2010). The EMT is an essential process for tissue fibrogenesis during normal aging as well as during the development of an age-related pathology. Higher levels of EMT proteins in aged tissues support the involvement of EMT as a possible cause and/or consequence of aging (Santos et al., 2019). During CNV in AMD, immature choroidal vessels break through the RPE into the subretinal space and cause fibrous scarring as a result of blood and plasma leakage. In late AMD forms, photoreceptors die because of a progressive atrophy of the RPE and of the choriocapillaris. At sites of choroidal neovascularization, the RPE loses its barrier function and transdifferentiates from its epithelial structure to a myofibroblast-like mesenchymal phenotype (Guidry et al., 2002; Hirasawa et al., 2011; Lopez et al., 1996; Watanabe et al., 2005). This may facilitate CNV.

5.2.3 IL6 JAK STAT 3 signaling

The Janus kinase/signal transducers and activators of transcription (JAK/STAT) pathway is used to transduce a multitude of signals for development and homeostasis. In mammals, the JAK/STAT pathway is the principal signaling mechanism for cytokines and growth factors. The activation of JAK stimulates cell proliferation, differentiation, migration and apoptosis (Rawlings et al., 2004). It was shown, that the JAK pathway is activated more in tissue of older animals and in senescent cells compared to non-

senescent cells (Xu et al., 2015). STAT3 also plays roles in regulating immune response and inflammation (Aggarwal et al., 2009). Within the eye, STAT3 plays an important role in the development of many ocular structures, including lens and retina. Zhang et al. examined the expression of different STATs throughout the developing mouse eye (Zhang et al., 2003). STAT3 has been implicated as a regulator of the inflammatory response in the RPE (Chou et al., 2012) and protects the RPE from oxidative stress (Fragoso et al., 2012; Patel and Hackam, 2013). STAT3 is also associated with CNV in AMD. It is a critical transcriptional mediator of the angiogenic factor VEGF (Xu et al., 2005b).

5.2.4 Unfolded protein response

If unfolded protein response fails, endoplasmic reticulum stress will activate the apoptotic cascades followed by cell death (Xu et al., 2005a). A variety of endoplasmic reticulum stress-related genes are involved in apoptosis (Oyadomari and Mori, 2004). The deletion of those proteins protects cells from ER stress-induced apoptosis in various disease models (Oyadomari et al., 2002; Tamaki et al., 2008). The loss of the X-box binding protein 1 (XBP1), a master regulator of the adaptive unfolded protein response, impairs cell death. In addition, Zhong et al. implied XBP1 in redox regulation and cell survival in the RPE (Zhong et al., 2012). Conditional knockout of XBP1 gene in RPE cells resulted in increased oxidative stress and apoptosis in the RPE, accompanied by a mild cone photoreceptor loss and defects in retinal function (Zhong et al., 2012). These findings suggest that the UPR signaling may be implicated in RPE degeneration during AMD.

5.2.5 Inflammatory response

It is believed, that the process of inflammation is an important component that contributes various pathogenesis and that aging can cause inflammatory changes. Inflammation can be caused by infection or injury as well as by tissue stress and malfunction. The latter was described as para-inflammation (Medzhitov, 2008). One of the main factors which may increase tissue stress and malfunction is aging. As already described in 1.2.1.1 and 5.1, certain characteristic changes occur in the retina and RPE cells with age (Gao and Hollyfield, 1992), including the accumulation of lipofuscin and the deposition of waste materials in the basal lamina. In addition, increased levels of oxidative stress and the accumulation of oxidized materials may stimulate RPE cells

to produce inflammatory cytokines and chemokines (Xu et al., 2009). After exposure to oxidative stress, RPE cells can – amongst others – produce. the inflammatory cytokine IL-8 (Higgins et al., 2003), leading to the assumption that the aging RPE participates in para-inflammation during the aging process (Gao and Hollyfield, 1992). Additionally, the deposition of waste materials in the basal lamina may lead to drusen in the Bruch's membrane. Drusen are the first clinical signs detectable in AMD patients (Kaarniranta et al., 2013) and are known to contain many potentially damaging constituents including lipids, lipoproteins, RPE-derived cellular debris, e.g. melanin granules, and lipofuscin, amyloid-β, and oxidation by-products, as well as numerous inflammation-related factors, such as complement components, and acute phase proteins like vitronectin and fibrinogen (Anderson et al., 2004; Ebrahimi and Handa, 2011; Hageman et al., 1999; Ishibashi et al., 1986). Isolated drusen material has also been proven to be pro-inflammatory through the activation of both traditional and the more recently discovered signaling systems, such as NF-κB and the inflammasome pathway (Doyle et al., 2012; Liu et al., 2015; Liu et al., 2013; Liu et al., 2014).

5.2.6 Reactive oxygen species

ROS for example originate as a product of the respiratory chain in mitochondria, in photochemical and enzymatic reactions, exposure to UV light or ionizing radiation (Nita and Grzybowski, 2016). Low levels of ROS production are required to maintain physiological functions, including proliferation, host defense, signal transduction and gene expression (Droge, 2002). During the physiological aging process, it was shown, that the efficiency of some of the RPE functions is affected, due to enhanced oxidative stress. The phagocytosis of POS by the RPE cells generates oxidative stress caused by ROS (Tate et al., 1995). Additionally, a high oxygen consumption and a prolonged exposure to light increases the oxidative stress to RPE cells (Beatty et al., 2000). ROS levels increase in the aging retina, although the retina and RPE cells are rich in both enzymatic and nonenzymic antioxidants. Increased levels of ROS and reduced antioxidant cell defense systems lead to oxidative stress and result in damage of photoreceptors, RPE cells and choriocapillaris in the apoptosis process (Lu et al., 2006; Zarbin, 2004). Chronic elevated ROS levels and oxidative stress, para-inflammation as well as long term hypoxia decrease the ability of RPE cells to remove damaged and nonfunctional proteins via the lysosomal clearance system (Blasiak et al., 2014). The excessive accumulation together with the oxidative stress seems to

play an important role in the AMD pathogenesis and RPE cells are critical site of injury in AMD (Kaarniranta et al., 2009).

5.2.7 TNFα-signaling

Aging is associated with increased inflammatory activity in the blood. This inflammatory activity includes increased levels of circulating TNFα (Bruunsgaard et al., 1999; Paolisso et al., 1998). The increased inflammatory activity in the elderly may reflect age-related pathological processes. Chronic exposure of TNFα is sufficient to alter the morphology of the RPE and disturb the main features that define the differentiated state of RPE cells. These alterations are similar to the alterations observed in neurodegenerative diseases such as AMD (Touhami et al., 2018). It could be shown, that macrophages, which mainly produce TNFα, accumulate on the apical site of the RPE, adjacent to the atrophic zones, CNV and around large drusen in intermediate AMD (Combadiere et al., 2007; Guillonneau et al., 2017; Gupta et al., 2003; Lad et al., 2015; Levy et al., 2015; Sennlaub et al., 2013). A possible role of TNFα in age RPE, as well as in AMD is also suggested by the observation that plasmatic TNFα concentrations increase with age (Bruunsgaard et al., 2000; Paolisso et al., 1998). It was shown, that a chronic exposure of TNFα to primary RPE cells, increases the size of RPE cells and leads to polynucleation. It decreases the gene expression of genes correlated to the visual cycle and disables the formation of RPE tight-junctions and transepithelial resistance. Furthermore, it decreases the immunosuppressive capacities of the RPE (Touhami et al., 2018).

5.2.8 *Myc* Targets

By conservative estimates, 15–20% of all genes are directly regulated by MYC, including genes that play key roles in metabolism, ribosome biogenesis, cell cycle, apoptosis, differentiation, and stem cell maintenance (Dang, 2012). While age does not have a significant effect on *Myc* expression in any mouse tissue examined (Zahn et al., 2007), many of the biological processes regulated by MYC have also been implicated in aging and age-associated diseases. MYC overexpression results in an increase in ROS and DNA damage (Vafa et al., 2002), which are believed to contribute to the progression of aging (Hoeijmakers, 2009). It may also affect the inflammatory state that accompanies aging, since it directly regulates expression of some cytokines

(Whitfield and Soucek, 2012). It was suggested, that increased MYC activity promotes several processes that have been connected with aging and age-associated diseases.

5.3 Verification of gene expression

Out of the hallmarks described in 4.2.1 and 5.2,, several genes were selected. The functions of all genes in the eye and in the RPE were researched. The functions of many selected genes are well known in the RPE, whereas some genes were not described in the RPE at all. Out of the large number of genes with significantly different expression in the aged RPE compared to neonatal RPE, eight genes were chosen to be further investigated. The number of selected genes is only a very small part of the potentially interesting genes found in this study. This study revealed thousands of genes with different expression levels in the aging RPE of *C. jacchus* with the regard of their topology within the RPE. Because of the high homology between humans and *C. jacchus*, the majority of the findings should be also true for the aging RPE from humans. However, the comparison with human tissue will not be possible in further studies, regarding the lack of neonatal and adult human RPE tissue. Nevertheless, senile RPE tissue obtained from an eye bank should be investigated regarding expression differences between macula and periphery in aged eyes.
Eight genes were selected for validation. The justification for the selection of this gene is given in the following sections 5.3.1-5.3.8.

5.3.1 Stanniocalcin 1

STC1 is a secreted glycoprotein which was initially discovered in bony fish as a Calcium-reducing factor for calcium-phosphate regulation in the fish gill (Lafeber et al., 1988; Wagner et al., 1986). STC1 was found to be upregulated in the neonatal macula and periphery compared to aged samples. This upregulation was also confirmed in the qRT-PCR. STC1 is also expressed in human tissues and organs, including the endocrine and paracrine system (Ishibashi and Imai, 2002). Previous studies have suggested various roles for STC1 in developmental and pathophysiological processes, including the modulation of angiogenesis. It was shown, that STC1 promotes tumor angiogenesis through up-regulation of VEGF in gastric cancer cells (He et al., 2011) and angiogenic sprouting in Human umbilical vein endothelial cells (HUVECs) via VEGF/VEGFR2 and angiopoietin signaling pathways (Law and Wong, 2013).

Furthermore, it was shown, that STC1 reduces ROS and the resulting apoptosis and necrosis as well as the inflammatory response (Wang et al., 2009a). It was also demonstrated, that intravitreal administration of STC1 rescued photoreceptors from degeneration (Roddy et al., 2012). A recent study also reported, that intravitreal STC1 enhances new blood vessel growth in a rat model of laser induced CNV (Zhao et al., 2018).

5.3.2 Lumican

The expression of LUM is downregulated in aged macular and peripheral samples compared to the neonatal samples in NGS as well as in the qRT-PCR. LUM is an extracellular matrix protein of the small leucine rich proteoglycans (SLRPs). Decorin, fibromodulin, biglycan, and keratocan are also parts of the SLRP family (Hardingham and Fosang, 1992). Lumican was first characterized as a corneal keratan sulfate proteoglycan in chick cornea (Blochberger et al., 1992). Lumican is critical for corneal clarity by maintaining the strict collagen architecture of the cornea (Chakravarti et al., 2000; Maurice, 1957). It has been implicated in regulating aqueous humor outflow. In primary open angle glaucoma, the expression of lumican was doubled in the trabecular meshwork compared to healthy eyes (Diskin et al., 2006). Lumican has also been documented as an inhibitor of tumor angiogenesis (Diskin et al., 2006; Kresse et al., 1993; Maurice, 1957), but it does not suppress angiogenesis in non-pathological settings including healing wounds, cultures of aortic rings, and basement membrane matrix (Amjadi et al., 2013).

5.3.3 Thrombospondin 1

In the proteome of neonate tissue of *C. jacchus*, THBS1 was found to be upregulated in neonate RPE of *C. jacchus* (König et al., 2018), whereas it is upregulated in aged tissue on gene level, shown by NGS and qRT-PCR. THBS1 is an extracellular matrix protein which participate in cell-to-cell and cell-to- matrix communication. THBS1 is a binding partner of several structural proteins and regulates the availability of growth factors in the ECM. It acts as a potent inhibitor of angiogenesis via the inhibition of endothelial cells. This type of proteins is essential in the BM to suppress choroidal vessel overgrowth (Lawler, 2000; Lawler and Lawler, 2012). Reduced expression of THBS1 in AMD is associated with drusen formation, inflammation and the development of CNV (Housset and Sennlaub, 2015).

5.3.4 Fibromodulin

FMOD is upregulated in aged tissue on gene level, shown by NGS and qRT-PCR. Like lumican, FMOD is a member of the SLRP-family (Hardingham and Fosang, 1992). It is mainly expressed in mesenchymal connective tissue and involved in a series of biological and pathophysiological processes (Jan et al., 2016; Schaefer and Iozzo, 2008). FMOD was reported to play important roles in modulating ECM organization and binds to the same collagen type as lumican (Svensson et al., 2000). It is a regulator for cell reprogramming (Frikeche et al., 2016). A knockdown of FMOD in RPE cells downregulates the expression of VEGF and VEGFR2, which leads to an inhibition of the signaling pathway of the AKT phosphorylation. Consequently, the proliferation and migration of RPE cells is inhibited (Hu et al., 2018).

5.3.5 Brain Abundant Membrane Attached Signal Protein 1

It was shown, that BASP1 is downregulated in aged tissue. Not much is known about BASP1, especially in the eye. BASP1 was originally identified as a membrane and cytoplasmic protein that sequesters lipids through an N-terminal myristoyl motif (Mosevitsky, 2005). BASP1 is also present in the nucleus and can function as a transcriptional corepressor for the Wilms' tumor 1 protein (Toska and Roberts, 2014).

5.3.6 Type IV collagen A2

COL4A2 was found to be downregulated in aged samples, confirmed by NGS and qRT-PCR. It is composed of six distinct gene products, which are named α1-α6 (Prockop and Kivirikko, 1995). Two of those isoforms (α1 and α2) are ubiquitously present in human basement membranes Type IV collagen promotes cell adhesion, migration and differentiation (Paulsson, 1992). The C-terminal part of the α2 isoform is known as canstatin. The ability of canstatin to inhibit specifically endothelial cell proliferation, migration, and tube formation strongly suggests that it is an anti-angiogenic agent and inhibits tumor growth (Kamphaus et al., 2000). It was also shown, that canstatin inhibits hypoxia-induces apoptosis through activating integrins in cardiomyoblasts (Kanazawa et al., 2017).

5.3.7 Nidogen 1

In the proteome of neonate tissue of *C. jacchus*, NID1 was found to be upregulated in aged RPE of *C. jacchus* (König et al., 2018), as well as in the NGS and qRT-PCR NID1 is an essential component of the basement membrane besides other components like type IV collagen, proteoglycans, laminin (Smith and Ockleford, 1994) and fibronectin (Ockleford et al., 1993). NID1 acts as a linker between laminins, collagens and proteoglycans in the ECM and binds to cell surface integrins, involving it in establishing and maintaining the basement membrane and tissue architecture. Therefore, it prevents CNV and acts as an anti-angiogenic protein. The loss of NID1 may increase vessel leakage and facilitates the migration of endothelial cells into the CNV area (Semkova et al., 2014). It also interacts with cell receptor molecules and controls cell polarization, migration, and invasion (Kohling et al., 2006; Miosge et al., 2001).

5.3.8 Cathepsin B

As in the RPE of the proteome of *C. jacchus* (König et al., 2018), the NGS and qRT-PCR shows an increased expression of CTSB in aged RPE tissue. CTSB is a lysosomal cysteine protease and plays an important role in intracellular proteolysis. Cathepsins are multifunctional enzymes which are involved in tumor growth, migration, invasion, metastasis, and angiogenesis (Mohamed and Sloane, 2006). In tumors, the CTSB expression correlates with tumor angiogenesis and is believed to promote the remodeling of the extracellular matrix to permit neovascularization (Buck et al., 1992; Mai et al., 2002). It plays a role in the induction of Alzheimer's disease (Wu et al., 2017) and is works as a trypsinogen (Halangk et al., 2000). It was also shown, that CTSB is implicated in TNFα-induced apoptosis (Guicciardi et al., 2000). Upregulation of CTSB is trigged by oxidative stress. This upregulation leads to angiogenesis and a remodeling of the extracellular matrix of the cells (Im et al., 2005), which may lead to CNV in the mammalian eye. In a Cathepsin B/Cathepsin Z double knockout mouse it was shown, that the laser induced CNV formation is reduced, whereas the single knock out mice do not show any changes in CNV formation compared to wildtype mice (Buhler et al., 2013).

5.4 Proteome analysis

The study design of the proteome analysis is identical to the transcriptome analysis. The study was performed using the sensitive method of Ion-mobility-liquid chromatography-mass spectrometry. The proteome analysis was performed by **Prof. Simone König**. Parts of this discussion are already published in König et al., 2018 (König et al., 2018).

As described in section 4.3.1, the detected protein profiles partially separated all sample groups in the PCA (Figure 32). The neonatal samples were well differentiated from aged samples in both, macula and periphery. The neonate samples from macula and periphery slightly overlap, whereas the adult and senile samples from macula and periphery form completely isolated clusters. These results reflect the major molecular changes in the developing eye. In comparison to the results from the NGS, the PCA shows, that in neonatal samples the number of proteins expressed differently is lower compared to the samples from aged donor animals.
Out of the large number of proteins expressed significantly different in the aged RPE compared to neonatal RPE, six proteins were chosen to be further investigation using Western Blot methods as well as immunofluorescence. Three proteins – CTSB, NID1 and THBS1 – were also investigated in the transcriptome analysis.

5.4.1 Heat shock protein 60

The heat shock protein 60 (HSP60) is a molecular chaperon. HSP60 is implicated in mitochondrial protein import and macromolecular assembly. It may facilitate the correct folding of imported proteins and may also prevent misfolding and promote the refolding and proper assembly of unfolded polypeptides generated under stress conditions in the mitochondrial matrix (Gupta, 1995). HSP60 was linked to cardiovascular diseases, stress response, cancer and certain types of immunological disorders (Pockley and Henderson, 2018). Ethen et al. detected the expression of HSP60 within the central and peripheral neuroretina of AMD-diseased human eyes (Ethen et al., 2006). Immunization studies within the experimental autoimmune glaucoma model associated it within neurodegenerative diseases of the retina (Joachim et al., 2010) however, nothing is known about its role within the RPE. For HSP60, the same trend revealed

by mass spectrometry, Western Blot analysis and immunofluorescence (Figure 34)
Heat shock protein 90

Heat shock protein 90 (HSP90) is a molecular chaperone known to be responsible for the correct folding of newly synthesized proteins and denaturation of misfolded proteins by chaperone cycle (Csermely et al., 1998; Pratt, 1993). Because overexpression or accumulation of misfolded proteins is responsible for diseases such as Alzheimer's disease, Parkinson's disease, and multiple sclerosis, HSP90 inhibitors might be promising chemotherapeutic (Buchner, 1999). HSP90 has also multiple roles in the retina. HSP90 inhibitors prevent retinal degeneration in models of retinitis pigmentosa (Aguila et al., 2014) and AMD. Cell death and functional abnormalities in the RPE conduce to the development of AMD and is associated with increased oxidative stress (Jarrett and Boulton, 2012). In RPE cells, the expression increases during the progression of AMD (Decanini et al., 2007). It was also suggested, that HSP90 expressed from necrotic RPE cells may cause the inflammatory responses RPE cells (Qin et al., 2011). For HSP90, an increase in the protein expression is shown in the proteome analysis, whereas the Western Blot analysis revealed a significant decreased protein expression (Figure 35). The antibody against HSP90 which was used for validation in this study, was directed against both the α- and β- subunit of HSP90. The proteome analysis suggested an increased expression of the β-subunit of HSP90 during lifetime. It was shown, that the α-subunit and the β-subunit of HSP90 act similar in cases of a hypoxia and nutrient paucity stress-response mechanism during wound healing (Jayaprakash et al., 2015), but a differing behavior of the protein subunits is not unusual in other cases.

5.4.2 Peroxiredoxin

The family of peroxiredoxins (PRDX) consists of six members in humans, which are distributed in cytosol, mitochondria, peroxisome, and plasma and are involved in various cellular activities, such as cellular defense against reactive oxygen species, receptor signaling, gene regulation, and apoptosis in ocular tissues (Rhee et al., 2005; Singh and Shichi, 2001). Oxidative stress may trigger a para-inflammatory response, resulting in alterations in vascular permeability or breakdown of the blood brain barrier (Chen and Xu, 2015). Moreover, PRDX may be also be associated with the stress response in the RPE-Choroid complex and therefore be involved in maintaining the hemostasis of the integrity of the BRB, Bruch's membrane and extracellular matrix.

The expression pattern revealed in the mass spectrometry analysis was confirmed with Western Blot methods as well as immunofluorescence (Figure 37).

5.4.3 Cathepsin B, Nidogen 1 and Thrombospondin 1

The justification for CTSB, NID1 and THBS1 is given in the sections 5.3.3, 5.3.7, and 5.3.8. The expression pattern revealed in the mass spectrometry analysis was confirmed for CTSB (Figure 33) and NID1 (Figure 36). These results indicate, that the regulation of this proteins is happening on both gene and protein level.
For THBS1, the mass spectrometry analysis revealed a decreased expression in aged compared to neonatal RPE, which indicate a higher risk to develop age-related disturbances of the RPE/choroid complex. In contrast, the Western Blot analysis, immunofluorescence analysis (Figure 38) as well as the transcriptome analysis with the corresponding qRT-PCR (Figure 26) show a significant increase of both protein and gene expression in aged tissue. As the expression levels in the aged samples compared to the neonatal samples of THBS1 is equivalent in the Western Blot, the immunofluorescence, transcriptome analysis and the qRT-PCR, it may be, that the results of the expression pattern given by the mass spectrometry are wrong.

5.5 *In-vitro* characterization of β-Synuclein

The discussion of this chapter is published in Hadrian et al., 2019 (Hadrian et al., 2019). The role of SNCB in the RPE is not known yet. Therefore, the lifetime expression of SNCB and its antagonist SNCA was investigated in the RPE of *C. jacchus*. In the following steps, the potential role of SNCB in ARPE-19 and native ppRPE cells *in-vitro* was investigated. For this approach, the cells were incubated with recombinant SNCB. The highest concentration of rSNCB (500 ng/ml) was used to reflect the described accumulation of SCNB in the neurovascular unit and visual system (Böhm et al., 2018; Böhm et al., 2015; Böhm et al., 2013; Brockhaus et al., 2018). The accumulation of SNCB in the visual system, together with the differential dose-depended results, may justify the presentation of the complete data set.

5.5.1 Differential distributions of SNCA and SNCB in the RPE of *C. jacchus*

Both SNCA and SNCB were detectable in the primate RPE and showed different age- and topography-related distributions. The expression levels of SNCA and SNCB in native tissues of *C. jacchus* were not measured during all stages of life due to the limited availability of native tissues. Especially for the preparation of RPE whole mounts, no tissue of older animal was available. Also, the postmortem time to preparation was kept as short as possible, but it may have differed between the analyzed samples. The protein expression of SNCA and SNCB in RPE whole mounts of neonate *C. jacchus* (Figure 39) showed different distributions between macular and peripheral tissue. Especially SNCB is mainly present in the cell membrane in the macula, whereas analysis of the periphery shows the main fluorescence intensity in the cytoplasm. This may lead to the assumption, that the function of the proteins differs between macula and periphery.

In the paraffin-embedded tissue of *C. jacchus* (Figure 41), it was shown, that the fluorescence intensity and therefore the concentration of both SNCA and SNCA in the macula increases with age. The physiological aging process is associated with an ongoing degeneration of the RPE (Ach et al., 2014; König et al., 2018; Watzke et al., 1993). As described above, the age-related impairment of the RPE to phagocyte degraded POS, result in an accumulation of iron-loaded photoreceptors (Frost et al., 2014). It was described, that an increased accumulation of SNCA takes place in the entire neuroretina, including the RPE over lifetime (Surguchov et al., 2001). This may be explained by the ongoing degradation of SNCA by lysosomes and its positive loop-triggered inhibition of lysosomal activity (Baksi et al., 2016). The expression patterns of SNCB in parts of the visual system, like neuroretina, ascending visual pathway as well as visual cortex has been investigated in previous studies (Böhm et al., 2018; Böhm et al., 2015; Böhm et al., 2013) whereas this study focused in the increased SNCB expression in the RPE over lifetime. By promoting neuroprotective properties via Akt-signaling cascade and *p*53/MDM2-mediated apoptosis rates in vascular endothelial cells, SNCB has been proposed as a physiological competitor to SNCA, (Brockhaus et al., 2018; Snyder et al., 2005). In this study, the increased accumulation of SNCA is shown in the central RPE. It was also shown, that the SNCB expression level was lower in the macula compared to the periphery. The increased accumulation of SCNA, which acts cytotoxically, together with lower expression of SNCB, which acts

neuroprotective, in central regions, support the ongoing secondary cytotoxicity effects of SNCA. Additionally, the different metabolic conditions in the macular region support the predominantly onset of age-related diseases in the macular area.

5.5.2 Viability and apoptosis in rSNCB-exposed ARPE-19 cells

This study shows, that the addition of rSNCB to ARPE-19 cells alters the apoptosis of the cells time- and dose-dependently (Figure 44). The initially pro-survival effects were found after a short incubation time, while secondary effects promote the switch into a pro-apoptotic state after longer incubation times. As SNCB did not alter viability (Figure 43), it decreased apoptosis in ARPE-19 cells. The dose-dependent effect on apoptosis in rSNCB-treated BMECs occurred when rSNCB was present at higher concentrations, with an inverse correlation between the rSNCB concentration and apoptosis (Brockhaus et al., 2018). Anti-apoptotic effects in SNCB-exposed RPE cells were found after an exposure with rSNCB for 12 h. This supports the protective concept of SNCB in early stages of SNCB exposure (Hashimoto et al., 2004), whereas the apoptosis levels did not change significantly after exposures for 24 h. To sum it up, the presented data implied dose-depended and time-dependent effects of SNCB on RPE cells. These data suggest that further studies are essential towards understanding the mechanisms of SNCB effects.

5.5.3 Induction of the *p*53 signal pathway in rSNCB-exposed ARPE-19 cells

The increase PDL2 levels together with stabilization of *p*53 and an enhanced shifting of *p*14ARF into the nucleus together with the decrease of MDM2 indicates a PLD2-mediated activation of *p*53 in rSNCB-exposed ARPE-19 cells. Severe oxidative stress results in the *p*53 induced apoptosis and cellular senescence via the generation of ROS (Rufini et al., 2013). It was shown, that the presence of SNCB reduced the activity of *p*53 in neuroblastoma cells and primary cortical neurons (Hashimoto et al., 2004). Recent results show, that the presence of SNCB activated *p*53 in BMECs, which indicated the alterations of the neurovascular unit (Brockhaus et al., 2018). In this study evidences about a SNCB-mediated activation of PLD2 and the activation of *p*53 in accompanied by reduced MDM2 activity in ARPE-19 cells was provided. That may also be case in this study. The decreased levels of *p*14ARF indicate a negative feedback of the activation of *p*53. Recent studies reported about analogous SNCB-related PLD2

activation and further *p*53 stabilization by an inhibition of MDM2 resulting in pro-survival signaling (Hui et al., 2004). The interaction between the SNCB-mediated activation of PLD2 and the *p*53-signaling cascade may play a role in the premature cellular senescence of the RPE.

5.5.4 Inflammatory and oxidative stress response in rSNCB-exposed ARPE-19 cells

Increases in NOX4 and HMOX1 imply increased oxidative stress and inflammatory responses in rSNCB-exposed ARPE-19 cells. The stress response in SNCB-related ARPE-19 cells was investigated using HMOX1 and NOX4. This response might be potential *p*53-mediated. Previous studies revealed an antioxidative role of SNCB in BMECs (Brockhaus et al., 2018). This study shows a significant upregulation of HMOX1 (Figure 48), and of NOX4 (Figure 49) in APRE-19 cells. These findings indicate, that SNCB induces oxidative stress and inflammation in RPE cells. This upregulation might also protect RPE cells from further damage (Gambino et al., 2013). GCLC and HMOX1 are involved in redox protection, acting as a target of associated stress response (Magne et al., 2011). In the aging retina, oxidative stress is the main initial factor for the para-inflammatory responses (Xu et al., 2009). In this study, no alteration in the mRNA expression of GCLC and GCLM (Figure 49) after exposure to rSNCB was observed. That may indicate, that the rSNCB-induced stress response may result in HMOX1 overexpression and is therefore not related to changes GCLC or GCLM expression. This excludes an involvement pf SNCB in alterations of the glutathione synthesis.

5.5.5 Comparable responses of core cellular functions in ppRPE cells exposed to rSNCB

Due to limitations in the availability of primary human RPE cells, validation experiments were performed with ppRPE cells. Those are established as cellular source of e.g., primary RPE cells in AMD research (Klettner and Miura, 2019). For this study primary porcine RPE cells were used to compare the results of ARPE-19 cells to primary cells. The pig retina maintains the structure of ten layers, the same as in the human retina because the embryonic development is similar (Gu et al., 2007). There is a depressed central area, rich in cones, that is comparable to the human macula (Bertschinger et

al., 2008; Gu et al., 2007). It has the shape of a horizontal band called the foveal streak (Kiilgaard et al., 2007), which is placed over the optic nerve head (Voss Kyhn et al., 2007). The proportion of cones and rods is similar to the human retina, and the paramacular density of cones is also similar (Gu et al., 2007). In this study, comparable results related to viability, apoptosis, *p*53 activity, and inflammatory and stress responses were found in the native ppRPE (Figure 53, Figure 54). The less conclusive results of the ppRPE compared to the results of ARPE-19 cells might be explained by native cells being less homogeneous than ARPE-19 cells. Furthermore, the study with ppRPE cells is also limited by the reduced capabilities of ppRPE cells to grow on glass slides for immunofluorescence. As shown in Figure 50, the density of the cells is very low, even after a long growing period, which makes is difficult to perform experiments regarding the expression patterns of proteins.

5.6 *In-vitro* characterization of Cathepsin B

5.6.1 Viability in rCTSB-exposed ARPE-19 cells

As the function of CTSB in the (aging) RPE remain actual unclear, this part of the study investigated the role and function of CTSB *in-vitro*. Therefore, ARPE-19 cells were exposed to recombinant CTSB. The used concentrations are based on previous experiments performed by Moon et al. (Moon et al., 2016). As Moon et al. did not investigate the influence of the cell viability after treatment, MTT tests were performed in this study. As the viability of the cells was only slightly influenced, the proposed concentrations for the treatment were suitable for further experiments

5.6.2 Influence of rCTSB on the expression pattern of tight-junction proteins

To investigate the influence of CTSB on the extracellular matrix, the expression pattern of the tight-junction proteins ZO-1 and Occludin was investigated. The integrity of the epithelial cell layers is maintained by intercellular junctional complexes composed of tight junctions, adherens junctions, and desmosomes (Schneeberger and Lynch, 2004). Tight junctions (*zonulae occludentes*) form a continuous, circumferential, belt-like structure at the boundary between the apical and the basolateral membrane

domains in epithelial and endothelial cells (Forster, 2008). Tight junctions form separate compartments and are crucial for the exchange of substances between the internal and external cellular environment by the expression of tissue-specific transport proteins and channels and function as barriers (Staehelin, 1973). The transmembrane proteins constituting the tight junctions are attached to the cytoskeleton, thereby linking cell–cell and cell–substrate adhesion sites (Forster, 2008). In previous studies it was shown, that a blockade of CTSB significantly abolished palmitate-induced activation of Nlrp3 inflammasomes, which leads to a down-regulation of ZO-1/ZO-2, and enhanced permeability in microvascular endothelial cells (Wang et al., 2016). It was also suggested, that aging in rats may alter the molecular anatomy of the blood-brain-barrier by reducing the expression of ZO-1 (Mooradian et al., 2003). In this study, the presence of rCTSB in the cell culture medium influences the arrangement of ZO-1 and occludin in the cell membranes of ARPE-19 cells. In the untreated control, the tight-junction proteins were well arranged in the cell membranes, whereas the distribution of the proteins was fragmentary in the cells treated with rCTSB, even with very low concentration. The immunofluorescence images did not show levels in the expression differences of the two proteins after exposure to rCTSB. Furthermore, the presence of rCTSB increased the free space between the cells. This might be caused by the disturbed arrangement of the tight-junction proteins. Similar results have been reported previously (Porter et al., 2013).

5.6.3 Influence of rCTSB on the *p*53-MDM2 signaling cascade

The influence of CTSB on the *p*53-MDM2 signaling cascade was investigated on protein- as well as gene level. Both methods showed an increase of the expression of *p*53 in ARPE 19 cells after exposure to 100 ng/ml rCTSB. On gene level, a significant decrease of the expression of MDM2 after exposure to rCTSB was shown, whereas the expression level of *p*14ARF did not change. The upregulation of *p*53 and the corresponding downregulation of the negative regulator MDM2 results in a stabilization of *p*53 and an activation of the *p*53-related cascades. Those include growth arrest, DNA repair and apoptosis, and the inhibition of angiogenesis (Teodoro et al., 2007). One of the proteins downregulated by *p*53 is VEGF (Pal et al., 2001). Additionally, the increased expression of *p*53 upregulates the expression of THBS1 (Dameron et al., 1994) and COL4A2, because *p*53 transcriptionally activates the promoter for the COL4A2 gene (Bian and Sun, 1997). COL4A2 is downregulated in the aged RPE of *C.*

jacchus (see also section 5.3.6), whereas CTSB is upregulated. The upregulation of CTSB may influence the activity of *p*53. The detected upregulation seems to be influenced by age; however, it may not influence the COL4A2 promotor. Several mechanisms are involved in the complex cascades. The presented data provide additional aspects in the multifactorial aging mechanisms.

5.6.4 Influence of rCTSB on the expression of VEGF

CTSB is known to be a likely contributor to neuronal diseases and tumor angiogenesis (Buck et al., 1992; Mackay et al., 1997; Qian et al., 1989). To our knowledge, the associated cell types and molecular targets modulated by CTSB have not been identified yet. First, retinal endothelia cells may produce pro- and antiangiogenic factors in a CTSB-regulated manner (Im et al., 2005). An overexpression suppresses *in-vitro* VEGF-dependent tube formation (Im et al., 2005). Second, the stimulation of lung endothelial cells with VEGF resulted in an upregulation of proteases, including CTSB (Dao et al., 2018). In the neuroepithelial cells, which were used in this study, the increased amount of rCTSB in the medium may lead to a higher expression of VEGF in the cells. However, the expression level of VEGF induced by an oversupply of CTSB is not transferable from endothelial cells to epithelial cells.

5.6.5 Influence of rCTSB on the expression of CTSB

The treatment of ARPE-19 cells with rCTSB resulted in an overexpression of CTSB on protein- as wells as on gene level. As already mentioned, the expression of CTSB is related on the oxidative stress of cells (Im et al., 2005). The presence of recombinant CTSB in the cell culture medium may increase the oxidative stress, which can lead to an overexpression of CTSB in the cells. As described in section 4.4.2.1, the stimulation of endothelial cells with VEGF resulted in an upregulation of CTSB (Dao et al., 2018). The presence of CTSB in the medium induced the expression of VEGF in epithelial cells. That may induce a feedback loop in which the increased expression of VEGF also induces the expression of CTSB in the cells.

5.7 Senescence model

Senescence is widely used term in context of biological aging. In the current literature two definitions exist of the term “senescence”: 1. The irreversible growth arrest triggered by telomere shortening counting cell generations 2. Any kind of irreversible arrest of proliferative cell types which is induced by damaging agents or cell cycle deregulations after overexpression of proto-oncogenes (de Magalhaes et al., 2002). Senescent cells are not stimulated to divide by serum or passage in culture, and senescence invokes a specific cell cycle profile that differs from most damage-induced arrest processes or contact inhibition (Sherwood et al., 1988). The cellular senescence can be triggered by a number of cellular stresses, which includes oxidative stress, telomere dysfunction, non-telomeric DNA damage, and oncogenic activation. It is a potent tumor suppression mechanism named oncogene-induced senescence. Senescent cells are also seen in aged or damaged tissues, and they may reduce tissue regeneration capacity with age (Collado et al., 2007).

5.7.1 Establishment of a premature senescence model

To study mechanisms of aging *in-vitro*, a premature senescence model needs to be introduced. Those models simulating senescence of cells *in-vitro* using various techniques and underlying mechanisms. Those include physical processes to induce aging by using e.g UV-light (Chainiaux et al., 2002) or chemical processes using e.g peroxide (de Magalhaes et al., 2004; de Magalhaes et al., 2002). The senescence model used in this study is based on the model described by Glotin et al. (Glotin et al., 2008). To establish the model in the presented approach, the cells were treated as follows: Exposition of the cells with 8 mM *tert*-BHP for each 1 h on 5 following days. However, the cells were necrotic after the first day of exposition. Therefore, the concentrations were decreased step by step to reach sublethal treatment conditions, ending on 0.25 mM and 0.5 mM *tert*-BHP for 1 h. In the presented approach a discrepancy between the used concentrations and number of treatments compared to the published model (Glotin et al., 2008) has been found. In another study performed by de Magalhaes and colleagues (de Magalhaes et al., 2004), cells were treated with 1.2 mM H_2O_2 for 2 h to induce cellular senescence. Both chemicals, H_2O_2 and *tert*-BHP, are peroxides, therefore their mechanism of action seems to be very similar. This concentration is close to the concentrations of *tert*-BHP used in this study.

With the used concentrations as described in the approach, the β-galactosidase assay was performed successfully (Figure 62). The results showed a significant increase in β-galactosidase positive cells, indicated by blue color. β-galactosidase is a biomarker for senescent cells as it is expressed by senescent cells but not in pre-senescent or immortal cells (Dimri et al., 1995).

A further indication for cell in a senescent state is the oxidation status of nucleic acids and lipids. In animals, lesions excised from DNA are transported from the cell through the circulation and excreted in urine. Those adducts can be assayed as a measure of oxidative damage to DNA using 8-HGN as a marker for DNA damage produced by oxidants because it represents one of the major products generated by a wide array of treatments associated with oxidant damage. In the cell, 8-HGN RNA lesions are formed by reaction with ROS generated either via normal oxidative metabolic processes, UV ionizing radiation, or exposure to oxidative agents. 4-HNE is an α,β-unsaturated hydroxyalkenal which is produced by lipid peroxidation in cells. Aldehydic products of lipid peroxidation, have been implicated as one of the key mediators of oxidative stress induced cell death.

The increased fluorescent intensity (Figure 64, Figure 65) in this study indicates increased oxidative damage of the nucleic acids as well as lipids. These results are comparable to the results in the study performed by Glotin and colleagues (Glotin et al., 2008). In the retina of patients with AMD, an increased oxidative damage on nucleic acids and lipids was demonstrated before (Shen et al., 2007).

5.7.2 Influence of Cathepsin B on premature senescent cells

After the introducing the premature senescence model in APRE-19 cells, the influence of CTSB on premature senescent cells was investigated. CTSB is increasingly expressed in aged RPE tissue (König et al., 2018), indicating an important role in the physiological aging process of the RPE. However, the role of CTSB especially in the aging RPE is actual unknown.

Initially, the influence of CTSB on apoptosis on *tert*-BHP induced senescent cells was investigated (Figure 66). No influence of CTSB on *tert*-BHP induced senescent cells regarding the rate of viable, apoptotic and necrotic cells have been found. Furthermore, the treatment with *tert*-BHP to induce premature senescence did not influence the rate of viable, apoptotic and necrotic cells significantly.

A crucial step in various forms of cell death including apoptosis and necrosis is the loss of the lysosomal integrity and therefore the releases of proteases into the cytoplasm (Boya and Kroemer, 2008; Cesen et al., 2012; Guicciardi et al., 2004). CTSB is present in lysosomes in the cells. The unaltered apoptosis rate of the cells after treatment with CTSB may lead to the assumption, that the increased amount of intracellular CTSB may not influence the internal integrity of lysosomes in the cells, neither does *tert*-BHP. A decreased proliferation of cells treated with *tert*-BHP (Figure 67) to introduce the senescence shows a decreased proliferation by a rate of 1.5. That means, *tert*-BHP treated cells divided 1.5 less often than untreated cells. In recent studies, *tert*-BHP treated ARPE-19 cells were not able to proliferate after serum stimulation. Additionally, that the number of cells treated with *tert*-BHP in the S phase of the cell cycle was significantly lower compared to untreated cells, whereas most of the cells treated with *tert*-BHP were in G1 phase (Glotin et al., 2008). Senescent cells are irreversibly arrested at the G1 phase of the cell cycle and do not respond to various external stimuli, but they remain metabolically active (Collado et al., 2007; Hoare et al., 2010). These results promote the theory, that *tert*-BHP treated cells are in a senescent state. The presence of CTSB did not influence the proliferation rate of the cells, whether treated with *tert*-BHP or not. Previous studies reported, that the downregulation of CTSB in endometrial cancer and pancreatic islet cell carcinogenesis inhibits the cell proliferation (Bao et al., 2013; Gocheva et al., 2006). The presented data did not confirm the opposite proliferation behavior of the cells. The overabundance of CTSB does not lead to an increased proliferation of ARPE-19 cells.

The phagocytosis rate was increased in cells treated with *tert*-BHP and *tert*-BHP/CTSB compared to the untreated control (Figure 68). In contrast, the phagocytosis rate did not change in cells treated with CTSB alone. As mentioned in section 1.1.2.4, phagocytosis is an important mechanism of RPE cells to digest photoreceptor outer segments. Senescent cells may increase their ability to phagocyte. The apoptosis of cells leads to a rapid elimination of dysfunctional cells by phagocytosis in a manner that does not stimulate an inflammatory response (Erwig and Henson, 2008). As shown before, the number of early apoptotic or apoptotic cells after treatment with *tert*-BHP is not significantly higher (Figure 66), however the interquartile range of apoptotic and early apoptotic cells is higher compared to the untreated control, indicating a higher number of early apoptotic or apoptotic cells. That can promote a phagocytotic response of the viable cells.

The link between the phagocytosis and CTSB was already shown previously. Prior studies showed, that cells of the trabecular meshwork which were phagocytically challenged, show an upregulation of CTSB (Porter et al., 2013). In addition, the lysosomal rupture and cytoplasmic release of CTSB triggered by the phagocytosis of crystals leads to an activation of the NLRP3 inflammasome and maturation of the proinflammatory cytokines IL-1β and IL-18 (Halle et al., 2008). Those factors are linked to the development of and Alzheimer's disease (Halle et al., 2008). It was also shown, that CTSB is involved in the presence autophagosomes. It provides a signal to control the expression of lysosomal and autophagy-related proteins by maintaining the population and size of lysosomes and autophagosomes within a cell (Man and Kanneganti, 2016). The overabundance of CTSB may increase the number of lysosomes and autophagosomes (Man and Kanneganti, 2016). Recent studies also indicate, that different subcellular localization patterns of STAT3 affect autophagy in various ways, including nuclear STAT3 fine-tunes autophagy via the transcriptional regulation of several autophagy-related genes such as CTSB (You et al., 2015). A study shows, that autophagy enhances the rate of neutrophil phagocytosis of pneumococci in neutrophils (Ullah et al., 2017), while other studies show that the autophagy reduces the phagocytosis rate of particles and mycobacteria in macrophages (Bonilla et al., 2013; Lima et al., 2011). In the present study, the overabundance of CTSB in senescent cells, but not in untreated cells, increased the phagocytosis rate significantly. It may be hypothesized, that the senescent cells reverse the dependency between phagocytosis and CTSB and therefore, the presence of CTSB increases the phagocytosis rate. Additionally, it may influence the presence and number of autophagosomes in the senescent RPE, leading to an increased phagocytosis rate.

Lastly, the intracellular ROS production was investigated (Figure 69). The free radical theory of aging discusses the role of ROS-induced cellular damage in aging (Hekimi et al., 2011). Low intracellular ROS levels improve defense mechanisms of the by inducing adaptive responses, contributing stress resistance and longevity, while high intracellular ROS levels induce insufficient adaptive responses, contributing aging onset and progression (Yan, 2014). A basal level of ROS and oxidative stress is essential for cell survival (Janssen-Heininger et al., 2008; Sena and Chandel, 2012), whereas severe oxidative stress impairs the cell self-repair ability and may lead to cell death. Additionally, age-related changes in cells are associated with decreased

mitochondrial function, accompanied by increased ROS (Chan, 2006). A recent study showed, that the ROS levels increased in H_2O_2 treated cells, whereas the activity of CTSB decreased (Tai et al., 2017). In in the initial study of *tert*-BHP-induced senescence in ARPE-19 cells, Glotin et. al. showed, that the intracellular ROS level was increased by a factor of 13 after treatment with 8 mM *tert*-BHP (Glotin et al., 2008). In the present study, the observed changes in the ROS level between different treatments were not significant, whereas the senescent state of the cells has been shown by the β-Gal staining (Figure 62) for both concentrations. However, the results of the investigation of the intracellular ROS production indicate, that a higher amount of *tert*-BHP is needed to increase the intracellular ROS level in senescent cells.

5.8 Outlook

Summarized, this study gives a closer insight in the molecular aging process of the aging RPE in *C. jacchus* on gene as well as on protein level. By the number of significant differently expressed genes, it is possible to conclude, that the macula ages different than the periphery, indicating, that the functions of the single proteins involved in the aging process may differ between macula and periphery. Moreover, the functions of most of those proteins is unclear. This study gives an insight into the function of SNCB and CTSB in the (aging) RPE. Further studies are obligated to get a deeper knowledge about the function of SNCB, CTSB and other relevant proteins in the aging RPE. Additionally, the findings in the aging RPE of *C. jacchus* need to be validated in the RPE of human eyes to get a deep understanding of the physiological aging. This can help to find therapeutic approaches to prevent the conversion into a severe pathology.

6 References

Abbott, D.H., D.K. Barnett, R.J. Colman, M.E. Yamamoto, and N.J. Schultz-Darken. 2003. Aspects of common marmoset basic biology and life history important for biomedical research. *Comp Med*. 53:339-350.

Ach, T., C. Huisingh, G. McGwin, Jr., J.D. Messinger, T. Zhang, M.J. Bentley, D.B. Gutierrez, Z. Ablonczy, R.T. Smith, K.R. Sloan, and C.A. Curcio. 2014. Quantitative autofluorescence and cell density maps of the human retinal pigment epithelium. *Invest Ophthalmol Vis Sci*. 55:4832-4841.

Ach, T., E. Tolstik, J.D. Messinger, A.V. Zarubina, R. Heintzmann, and C.A. Curcio. 2015. Lipofuscin redistribution and loss accompanied by cytoskeletal stress in retinal pigment epithelium of eyes with age-related macular degeneration. *Invest Ophthalmol Vis Sci*. 56:3242-3252.

Adamis, A.P., D.T. Shima, K.T. Yeo, T.K. Yeo, L.F. Brown, B. Berse, P.A. D'Amore, and J. Folkman. 1993. Synthesis and secretion of vascular permeability factor/vascular endothelial growth factor by human retinal pigment epithelial cells. *Biochem Biophys Res Commun*. 193:631-638.

Aggarwal, B.B., A.B. Kunnumakkara, K.B. Harikumar, S.R. Gupta, S.T. Tharakan, C. Koca, S. Dey, and B. Sung. 2009. Signal transducer and activator of transcription-3, inflammation, and cancer: how intimate is the relationship? *Ann N Y Acad Sci*. 1171:59-76.

Aggarwal, P., T.C. Nag, and S. Wadhwa. 2007. Age-related decrease in rod bipolar cell density of the human retina: an immunohistochemical study. *J Biosci*. 32:293-298.

Aguila, M., D. Bevilacqua, C. McCulley, N. Schwarz, D. Athanasiou, N. Kanuga, S.S. Novoselov, C.A. Lange, R.R. Ali, J.W. Bainbridge, C. Gias, P.J. Coffey, P. Garriga, and M.E. Cheetham. 2014. Hsp90 inhibition protects against inherited retinal degeneration. *Hum Mol Genet*. 23:2164-2175.

Akira, S. 2000. Roles of STAT3 defined by tissue-specific gene targeting. *Oncogene*. 19:2607-2611.

Alm, A., and A. Bill. 1972. The oxygen supply to the retina. II. Effects of high intraocular pressure and of increased arterial carbon dioxide tension on uveal and retinal blood flow in cats. A study with radioactively labelled microspheres including flow determinations in brain and some other tissues. *Acta Physiol Scand*. 84:306-319.

Alm, A., and A. Bill. 1973. Ocular and optic nerve blood flow at normal and increased intraocular pressures in monkeys (Macaca irus): a study with radioactively labelled microspheres including flow determinations in brain and some other tissues. *Exp Eye Res*. 15:15-29.

Alon, T., I. Hemo, A. Itin, J. Pe'er, J. Stone, and E. Keshet. 1995. Vascular endothelial growth factor acts as a survival factor for newly formed retinal vessels and has implications for retinopathy of prematurity. *Nat Med*. 1:1024-1028.

Ambati, J., B.K. Ambati, S.H. Yoo, S. Ianchulev, and A.P. Adamis. 2003. Age-related macular degeneration: etiology, pathogenesis, and therapeutic strategies. *Surv Ophthalmol*. 48:257-293.

Amjadi, S., K. Mai, P. McCluskey, and D. Wakefield. 2013. The role of lumican in ocular disease. *ISRN Ophthalmol*. 2013:632302.

Anderson, D.H., R.F. Mullins, G.S. Hageman, and L.V. Johnson. 2002. A role for local inflammation in the formation of drusen in the aging eye. *Am J Ophthalmol*. 134:411-431.

Anderson, D.H., K.C. Talaga, A.J. Rivest, E. Barron, G.S. Hageman, and L.V. Johnson. 2004. Characterization of beta amyloid assemblies in drusen: the deposits associated with aging and age-related macular degeneration. *Exp Eye Res*. 78:243-256.

Andreoli, C.M., and J.W. Miller. 2007. Anti-vascular endothelial growth factor therapy for ocular neovascular disease. *Curr Opin Ophthalmol*. 18:502-508.

Arslan, S., S. Kadayifcilar, and G. Samur. 2019. The Potential Role of Dietary Antioxidant Capacity in Preventing Age-Related Macular Degeneration. *J Am Coll Nutr*. 38:424-432.

Baehr, W., S.M. Wu, A.C. Bird, and K. Palczewski. 2003. The retinoid cycle and retina disease. *Vision Res*. 43:2957-2958.

Baksi, S., A.K. Tripathi, and N. Singh. 2016. Alpha-synuclein modulates retinal iron homeostasis by facilitating the uptake of transferrin-bound iron: Implications for visual manifestations of Parkinson's disease. *Free Radic Biol Med*. 97:292-306.

Ban, Y., and L.J. Rizzolo. 2000. Regulation of glucose transporters during development of the retinal pigment epithelium. *Brain Res Dev Brain Res*. 121:89-95.

Bao, W., Q. Fan, X. Luo, W.W. Cheng, Y.D. Wang, Z.N. Li, X.L. Chen, and D. Wu. 2013. Silencing of Cathepsin B suppresses the proliferation and invasion of endometrial cancer. *Oncol Rep*. 30:723-730.

Barry, S.P., P.A. Townsend, J. McCormick, R.A. Knight, T.M. Scarabelli, D.S. Latchman, and A. Stephanou. 2009. STAT3 deletion sensitizes cells to oxidative stress. *Biochem Biophys Res Commun*. 385:324-329.

Beatty, S., H. Koh, M. Phil, D. Henson, and M. Boulton. 2000. The role of oxidative stress in the pathogenesis of age-related macular degeneration. *Surv Ophthalmol*. 45:115-134.

Ben-Shabat, S., C.A. Parish, M. Hashimoto, J. Liu, K. Nakanishi, and J.R. Sparrow. 2001. Fluorescent pigments of the retinal pigment epithelium and age-related macular degeneration. *Bioorg Med Chem Lett*. 11:1533-1540.

Benjamin, L.E., and E. Keshet. 1997. Conditional switching of vascular endothelial growth factor (VEGF) expression in tumors: induction of endothelial cell shedding and regression of hemangioblastoma-like vessels by VEGF withdrawal. *Proc Natl Acad Sci U S A*. 94:8761-8766.

Bertschinger, D.R., E. Beknazar, M. Simonutti, A.B. Safran, J.A. Sahel, S.G. Rosolen, S. Picaud, and J. Salzmann. 2008. A review of in vivo animal studies in retinal prosthesis research. *Graefes Arch Clin Exp Ophthalmol*. 246:1505-1517.

Bian, J., and Y. Sun. 1997. Transcriptional activation by p53 of the human type IV collagenase (gelatinase A or matrix metalloproteinase 2) promoter. *Mol Cell Biol*. 17:6330-6338.

Bishop, N.A., T. Lu, and B.A. Yankner. 2010. Neural mechanisms of ageing and cognitive decline. *Nature*. 464:529-535.

Bjorkoy, G., T. Lamark, and T. Johansen. 2006. p62/SQSTM1: a missing link between protein aggregates and the autophagy machinery. *Autophagy*. 2:138-139.

Blasiak, J., G. Petrovski, Z. Vereb, A. Facsko, and K. Kaarniranta. 2014. Oxidative stress, hypoxia, and autophagy in the neovascular processes of age-related macular degeneration. *Biomed Res Int*. 2014:768026.

Blochberger, T.C., J.P. Vergnes, J. Hempel, and J.R. Hassell. 1992. cDNA to chick lumican (corneal keratan sulfate proteoglycan) reveals homology to the small interstitial proteoglycan gene family and expression in muscle and intestine. *J Biol Chem*. 267:347-352.

Böhm, M. 2017. [Methodological limitations in the use of human donor eyes exemplified by age-related alterations in cell density of the retinal pigment epithelium]. *Ophthalmologe*. 114:671-672.

Böhm, M.R., K. Hadrian, K. Brockhaus, H. Melkonyan, and S. Thanos. 2018. Age-Related Expression of Beta-Synuclein in the Ascending Visual Pathway and Comparative Analysis of its Function within the Neuroretina and Cerebral Cortex in-vitro. *J Alzheimers Dis Parkinsonism*. Vol 8(1):427.

Böhm, M.R., H. Melkonyan, and S. Thanos. 2015. Life-time expression of the proteins peroxiredoxin, beta-synuclein, PARK7/DJ-1, and stathmin in the primary visual and primary somatosensory cortices in rats. *Front Neuroanat*. 9:16.

Böhm, M.R., S. Mertsch, S. König, T. Spieker, and S. Thanos. 2013. Macula-less rat and macula-bearing monkey retinas exhibit common lifelong proteomic changes. *Neurobiol Aging*. 34:2659-2675.

Bok, D. 1993. The retinal pigment epithelium: a versatile partner in vision. *J Cell Sci Suppl*. 17:189-195.

Bok, D., and M.O. Hall. 1971. The role of the pigment epithelium in the etiology of inherited retinal dystrophy in the rat. *J Cell Biol*. 49:664-682.

Bone, R.A., J.C. Gibert, and A. Mukherjee. 2012. Light distributions on the retina: relevance to macular pigment photoprotection. *Acta Biochim Pol*. 59:91-96.

Bonilla, D.L., A. Bhattacharya, Y. Sha, Y. Xu, Q. Xiang, A. Kan, C. Jagannath, M. Komatsu, and N.T. Eissa. 2013. Autophagy regulates phagocytosis by modulating the expression of scavenger receptors. *Immunity*. 39:537-547.

Boulton, M. 1991. Ageing of the retinal pigment epithelium. *Progress in Retinal Research* 11:125-151.

Boulton, M., and P. Dayhaw-Barker. 2001. The role of the retinal pigment epithelium: topographical variation and ageing changes. *Eye (Lond)*. 15:384-389.

Boya, P., and G. Kroemer. 2008. Lysosomal membrane permeabilization in cell death. *Oncogene*. 27:6434-6451.

Breier, G. 2000. Angiogenesis in embryonic development--a review. *Placenta*. 21 Suppl A:S11-15.

Brockhaus, K., M.R.R. Böhm, H. Melkonyan, and S. Thanos. 2018. Age-related Beta-synuclein Alters the p53/Mdm2 Pathway and Induces the Apoptosis of Brain Microvascular Endothelial Cells In Vitro. *Cell Transplant*:963689718755706.

Brown, J.W., A.K. Buell, T.C. Michaels, G. Meisl, J. Carozza, P. Flagmeier, M. Vendruscolo, T.P. Knowles, C.M. Dobson, and C. Galvagnion. 2016. beta-Synuclein suppresses both the initiation and amplification steps of alpha-synuclein aggregation via competitive binding to surfaces. *Sci Rep*. 6:36010.

Bruunsgaard, H., K. Andersen-Ranberg, B. Jeune, A.N. Pedersen, P. Skinhoj, and B.K. Pedersen. 1999. A high plasma concentration of TNF-alpha is associated with dementia in centenarians. *J Gerontol A Biol Sci Med Sci*. 54:M357-364.

Bruunsgaard, H., P. Skinhoj, A.N. Pedersen, M. Schroll, and B.K. Pedersen. 2000. Ageing, tumour necrosis factor-alpha (TNF-alpha) and atherosclerosis. *Clin Exp Immunol*. 121:255-260.

Buchman, V.L., H.J. Hunter, L.G. Pinon, J. Thompson, E.M. Privalova, N.N. Ninkina, and A.M. Davies. 1998. Persyn, a member of the synuclein family, has a distinct pattern of expression in the developing nervous system. *J Neurosci*. 18:9335-9341.

Buchner, J. 1999. Hsp90 & Co. - a holding for folding. *Trends Biochem Sci*. 24:136-141.

Buck, M.R., D.G. Karustis, N.A. Day, K.V. Honn, and B.F. Sloane. 1992. Degradation of extracellular-matrix proteins by human cathepsin B from normal and tumour tissues. *Biochem J*. 282 (Pt 1):273-278.

Buhler, A., S. Berger, F. Bengsch, G. Martin, H. Han, S. Vierkotten, A. Pielen, D. Boehringer, G. Schlunck, S. Fauser, H.T. Agostini, T. Reinheckel, and A. Stahl. 2013. Cathepsin proteases promote angiogenic sprouting and laser-induced choroidal neovascularisation in mice. *Exp Eye Res*. 115:73-78.

Burns, M.S., and M.J. Hartz. 1992. The retinal pigment epithelium induces fenestration of endothelial cells in vivo. *Curr Eye Res*. 11:863-873.

Campa, C., G. Alivernini, E. Bolletta, M.B. Parodi, and P. Perri. 2016. Anti-VEGF Therapy for Retinal Vein Occlusions. *Curr Drug Targets*. 17:328-336.

Campochiaro, P.A., S.F. Hackett, S.A. Vinores, J. Freund, C. Csaky, W. LaRochelle, J. Henderer, M. Johnson, I.R. Rodriguez, Z. Friedman, and et al. 1994. Platelet-derived growth factor is an autocrine growth stimulator in retinal pigmented epithelial cells. *J Cell Sci*. 107 (Pt 9):2459-2469.

Campochiaro, P.A., R. Sugg, G. Grotendorst, and L.M. Hjelmeland. 1989. Retinal pigment epithelial cells produce PDGF-like proteins and secrete them into their media. *Exp Eye Res*. 49:217-227.

Canadananovic, V., S. Latinovic, S. Barisic, N. Babic, and S. Jovanovic. 2015. Age-related changes of vitamin C levels in aqueous humour. *Vojnosanit Pregl*. 72:823-826.

Cao, W., J. Tombran-Tink, R. Elias, S. Sezate, D. Mrazek, and J.F. McGinnis. 2001. In vivo protection of photoreceptors from light damage by pigment epithelium-derived factor. *Invest Ophthalmol Vis Sci*. 42:1646-1652.

Cesen, M.H., K. Pegan, A. Spes, and B. Turk. 2012. Lysosomal pathways to cell death and their therapeutic applications. *Exp Cell Res*. 318:1245-1251.

Chainiaux, F., J.P. Magalhaes, F. Eliaers, J. Remacle, and O. Toussaint. 2002. UVB-induced premature senescence of human diploid skin fibroblasts. *Int J Biochem Cell Biol*. 34:1331-1339.

Chakravarti, S., W.M. Petroll, J.R. Hassell, J.V. Jester, J.H. Lass, J. Paul, and D.E. Birk. 2000. Corneal opacity in lumican-null mice: defects in collagen fibril structure and packing in the posterior stroma. *Invest Ophthalmol Vis Sci*. 41:3365-3373.

Chan, D.C. 2006. Mitochondria: dynamic organelles in disease, aging, and development. *Cell*. 125:1241-1252.

Chen, J., and L.E. Smith. 2007. Retinopathy of prematurity. *Angiogenesis*. 10:133-140.

Chen, M., and H. Xu. 2015. Parainflammation, chronic inflammation, and age-related macular degeneration. *J Leukoc Biol*. 98:713-725.

Cheung, C.M., and T.Y. Wong. 2016. Clinical Relevance and Application of the Age-Related Eye Disease Study Severity Scale for Age-Related Macular Degeneration. *JAMA Ophthalmol*. 134:1047-1048.

Chin, E.L., C. da Silva, and M. Hegde. 2013. Assessment of clinical analytical sensitivity and specificity of next-generation sequencing for detection of simple and complex mutations. *BMC Genet*. 14:6.

Chou, W.W., Y.S. Wang, K.C. Chen, J.M. Wu, C.L. Liang, and S.H. Juo. 2012. Tannic acid suppresses ultraviolet B-induced inflammatory signaling and complement factor B on human retinal pigment epithelial cells. *Cell Immunol*. 273:79-84.

Collado, M., M.A. Blasco, and M. Serrano. 2007. Cellular senescence in cancer and aging. *Cell*. 130:223-233.

Combadiere, C., C. Feumi, W. Raoul, N. Keller, M. Rodero, A. Pezard, S. Lavalette, M. Houssier, L. Jonet, E. Picard, P. Debre, M. Sirinyan, P. Deterre, T. Ferroukhi, S.Y. Cohen, D. Chauvaud, J.C. Jeanny, S. Chemtob, F. Behar-Cohen, and F. Sennlaub. 2007. CX3CR1-dependent subretinal microglia cell accumulation is associated with cardinal features of age-related macular degeneration. *J Clin Invest*. 117:2920-2928.

Csermely, P., T. Schnaider, C. Soti, Z. Prohaszka, and G. Nardai. 1998. The 90-kDa molecular chaperone family: structure, function, and clinical applications. A comprehensive review. *Pharmacol Ther*. 79:129-168.

Curcio, C.A., C.L. Millican, K.A. Allen, and R.E. Kalina. 1993. Aging of the human photoreceptor mosaic: evidence for selective vulnerability of rods in central retina. *Invest Ophthalmol Vis Sci*. 34:3278-3296.

da Costa, C.A., E. Masliah, and F. Checler. 2003. Beta-synuclein displays an antiapoptotic p53-dependent phenotype and protects neurons from 6-hydroxydopamine-induced caspase 3 activation: cross-talk with alpha-synuclein and implication for Parkinson's disease. *J Biol Chem*. 278:37330-37335.

Dameron, K.M., O.V. Volpert, M.A. Tainsky, and N. Bouck. 1994. The p53 tumor suppressor gene inhibits angiogenesis by stimulating the production of thrombospondin. *Cold Spring Harb Symp Quant Biol*. 59:483-489.

Dang, C.V. 2012. MYC on the path to cancer. *Cell*. 149:22-35.

Dao, D.T., J.T. Vuong, L. Anez-Bustillos, A. Pan, P.D. Mitchell, G.L. Fell, M.A. Baker, D.R. Bielenberg, and M. Puder. 2018. Intranasal delivery of VEGF enhances compensatory lung growth in mice. *PLoS One*. 13:e0198700.

Dawson, D.W., O.V. Volpert, P. Gillis, S.E. Crawford, H. Xu, W. Benedict, and N.P. Bouck. 1999. Pigment epithelium-derived factor: a potent inhibitor of angiogenesis. *Science*. 285:245-248.

de Magalhaes, J.P., F. Chainiaux, F. de Longueville, V. Mainfroid, V. Migeot, L. Marcq, J. Remacle, M. Salmon, and O. Toussaint. 2004. Gene expression and regulation in H2O2-induced premature senescence of human foreskin fibroblasts expressing or not telomerase. *Exp Gerontol*. 39:1379-1389.

de Magalhaes, J.P., F. Chainiaux, J. Remacle, and O. Toussaint. 2002. Stress-induced premature senescence in BJ and hTERT-BJ1 human foreskin fibroblasts. *FEBS Lett*. 523:157-162.

Decanini, A., C.L. Nordgaard, X. Feng, D.A. Ferrington, and T.W. Olsen. 2007. Changes in select redox proteins of the retinal pigment epithelium in age-related macular degeneration. *Am J Ophthalmol*. 143:607-615.

Delori, F.C., D.G. Goger, and C.K. Dorey. 2001. Age-related accumulation and spatial distribution of lipofuscin in RPE of normal subjects. *Invest Ophthalmol Vis Sci*. 42:1855-1866.

Dimri, G.P., X. Lee, G. Basile, M. Acosta, G. Scott, C. Roskelley, E.E. Medrano, M. Linskens, I. Rubelj, O. Pereira-Smith, and et al. 1995. A biomarker that identifies senescent human cells in culture and in aging skin in vivo. *Proc Natl Acad Sci U S A*. 92:9363-9367.

Diskin, S., J. Kumar, Z. Cao, J.S. Schuman, T. Gilmartin, S.R. Head, and N. Panjwani. 2006. Detection of differentially expressed glycogenes in trabecular meshwork of eyes with primary open-angle glaucoma. *Invest Ophthalmol Vis Sci*. 47:1491-1499.

Distler, U., J. Kuharev, P. Navarro, and S. Tenzer. 2016. Label-free quantification in ion mobility-enhanced data-independent acquisition proteomics. *Nat Protoc*. 11:795-812.

Dobin, A., C.A. Davis, F. Schlesinger, J. Drenkow, C. Zaleski, S. Jha, P. Batut, M. Chaisson, and T.R. Gingeras. 2013. STAR: ultrafast universal RNA-seq aligner. *Bioinformatics*. 29:15-21.

Dowling, J.E. 1987. The Retina, an approachable part of the brain. Harvard University Press, Cambridge.

Doyle, S.L., M. Campbell, E. Ozaki, R.G. Salomon, A. Mori, P.F. Kenna, G.J. Farrar, A.S. Kiang, M.M. Humphries, E.C. Lavelle, L.A. O'Neill, J.G. Hollyfield, and P. Humphries. 2012. NLRP3 has a protective role in age-related macular degeneration through the induction of IL-18 by drusen components. *Nat Med*. 18:791-798.

Droge, W. 2002. Free radicals in the physiological control of cell function. *Physiol Rev*. 82:47-95.

Duvall, J., and M.O. Tso. 1985. Cellular mechanisms of resolution of drusen after laser coagulation. An experimental study. *Arch Ophthalmol*. 103:694-703.

Ebrahimi, K.B., and J.T. Handa. 2011. Lipids, lipoproteins, and age-related macular degeneration. *J Lipids*. 2011:802059.

Elmore, S.A., M.C. Cora, M.M. Gruebbel, S.A. Hayes, J.S. Hoane, H. Koizumi, R. Peters, T.J. Rosol, B.P. Singh, and K.A. Szabo. 2015. Proceedings of the 2014 National Toxicology Program Satellite Symposium. *Toxicol Pathol*. 43:10-40.

Eriksson, U., and A. Alm. 2009. Macular thickness decreases with age in normal eyes: a study on the macular thickness map protocol in the Stratus OCT. *Br J Ophthalmol*. 93:1448-1452.

Erwig, L.P., and P.M. Henson. 2008. Clearance of apoptotic cells by phagocytes. *Cell Death Differ*. 15:243-250.

Ethen, C.M., C. Reilly, X. Feng, T.W. Olsen, and D.A. Ferrington. 2006. The proteome of central and peripheral retina with progression of age-related macular degeneration. *Invest Ophthalmol Vis Sci*. 47:2280-2290.

Feeney, L. 1978. Lipofuscin and melanin of human retinal pigment epithelium. Fluorescence, enzyme cytochemical, and ultrastructural studies. *Invest Ophthalmol Vis Sci*. 17:583-600.

Feeney-Burns, L., E.S. Hilderbrand, and S. Eldridge. 1984. Aging human RPE: morphometric analysis of macular, equatorial, and peripheral cells. *Invest Ophthalmol Vis Sci*. 25:195-200.

Ferrara, N. 2016. VEGF and Intraocular Neovascularization: From Discovery to Therapy. *Transl Vis Sci Technol*. 5:10.

Ferrara, N., and A.P. Adamis. 2016. Ten years of anti-vascular endothelial growth factor therapy. *Nat Rev Drug Discov*. 15:385-403.

Ferris, F.L., 3rd, C.P. Wilkinson, A. Bird, U. Chakravarthy, E. Chew, K. Csaky, S.R. Sadda, and C. Beckman Initiative for Macular Research Classification. 2013. Clinical classification of age-related macular degeneration. *Ophthalmology*. 120:844-851.

Forster, C. 2008. Tight junctions and the modulation of barrier function in disease. *Histochem Cell Biol*. 130:55-70.

Fragoso, M.A., A.K. Patel, R.E. Nakamura, H. Yi, K. Surapaneni, and A.S. Hackam. 2012. The Wnt/beta-catenin pathway cross-talks with STAT3 signaling to regulate survival of retinal pigment epithelium cells. *PLoS One*. 7:e46892.

Frikeche, J., G. Maiti, and S. Chakravarti. 2016. Small leucine-rich repeat proteoglycans in corneal inflammation and wound healing. *Exp Eye Res*. 151:142-149.

Frost, L.S., C.H. Mitchell, and K. Boesze-Battaglia. 2014. Autophagy in the eye: implications for ocular cell health. *Exp Eye Res*. 124:56-66.

Gambino, V., G. De Michele, O. Venezia, P. Migliaccio, V. Dall'Olio, L. Bernard, S.P. Minardi, M.A. Della Fazia, D. Bartoli, G. Servillo, M. Alcalay, L. Luzi, M. Giorgio, H. Scrable, P.G. Pelicci, and E. Migliaccio. 2013. Oxidative stress activates a specific p53 transcriptional response that regulates cellular senescence and aging. *Aging Cell*. 12:435-445.

Gao, H., and J.G. Hollyfield. 1992. Aging of the human retina. Differential loss of neurons and retinal pigment epithelial cells. *Invest Ophthalmol Vis Sci*. 33:1-17.

Gass, J.D. 1972. Drusen and disciform macular detachment and degeneration. *Trans Am Ophthalmol Soc*. 70:409-436.

Glasser, A., and M.C. Campbell. 1999. Biometric, optical and physical changes in the isolated human crystalline lens with age in relation to presbyopia. *Vision Res*. 39:1991-2015.

Glotin, A.L., F. Debacq-Chainiaux, J.Y. Brossas, A.M. Faussat, J. Treton, A. Zubielewicz, O. Toussaint, and F. Mascarelli. 2008. Prematurely senescent ARPE-19 cells display features of age-related macular degeneration. *Free Radic Biol Med*. 44:1348-1361.

Gocheva, V., W. Zeng, D. Ke, D. Klimstra, T. Reinheckel, C. Peters, D. Hanahan, and J.A. Joyce. 2006. Distinct roles for cysteine cathepsin genes in multistage tumorigenesis. *Genes Dev*. 20:543-556.

Gorczyca, W., F. Traganos, H. Jesionowska, and Z. Darzynkiewicz. 1993. Presence of DNA strand breaks and increased sensitivity of DNA in situ to denaturation in abnormal human sperm cells: analogy to apoptosis of somatic cells. *Exp Cell Res*. 207:202-205.

Gouras, P., L. Ivert, N. Landauer, J.A. Mattison, D.K. Ingram, and M. Neuringer. 2008. Drusenoid maculopathy in rhesus monkeys (Macaca mulatta): effects of age and gender. *Graefes Arch Clin Exp Ophthalmol*. 246:1395-1402.

Gramage, E., J. Li, and P. Hitchcock. 2014. The expression and function of midkine in the vertebrate retina. *Br J Pharmacol*. 171:913-923.

Green, W.R., and S.N. Key, 3rd. 1977. Senile macular degeneration: a histopathologic study. *Trans Am Ophthalmol Soc*. 75:180-254.

Gu, P., L.J. Harwood, X. Zhang, M. Wylie, W.J. Curry, and T. Cogliati. 2007. Isolation of retinal progenitor and stem cells from the porcine eye. *Mol Vis*. 13:1045-1057.

Guicciardi, M.E., J. Deussing, H. Miyoshi, S.F. Bronk, P.A. Svingen, C. Peters, S.H. Kaufmann, and G.J. Gores. 2000. Cathepsin B contributes to TNF-alpha-mediated hepatocyte apoptosis by promoting mitochondrial release of cytochrome c. *J Clin Invest*. 106:1127-1137.

Guicciardi, M.E., M. Leist, and G.J. Gores. 2004. Lysosomes in cell death. *Oncogene*. 23:2881-2890.

Guidry, C., N.E. Medeiros, and C.A. Curcio. 2002. Phenotypic variation of retinal pigment epithelium in age-related macular degeneration. *Invest Ophthalmol Vis Sci*. 43:267-273.

Guillonneau, X., C.M. Eandi, M. Paques, J.A. Sahel, P. Sapieha, and F. Sennlaub. 2017. On phagocytes and macular degeneration. *Prog Retin Eye Res*. 61:98-128.

Gupta, N., K.E. Brown, and A.H. Milam. 2003. Activated microglia in human retinitis pigmentosa, late-onset retinal degeneration, and age-related macular degeneration. *Exp Eye Res*. 76:463-471.

Gupta, R.S. 1995. Evolution of the chaperonin families (Hsp60, Hsp10 and Tcp-1) of proteins and the origin of eukaryotic cells. *Mol Microbiol*. 15:1-11.

Hadrian, K., H. Melkonyan, S. Schlatt, J. Wistuba, S. Wasmuth, A. Heiligenhaus, S. Thanos, and M.R.R. Böhm. 2019. Age-related distribution and potential role of SNCB in topographically different retinal areas of the common marmoset Callithrix jacchus, including the macula. *Exp Eye Res*. 185:107676.

Hageman, G.S., R.F. Mullins, S.R. Russell, L.V. Johnson, and D.H. Anderson. 1999. Vitronectin is a constituent of ocular drusen and the vitronectin gene is expressed in human retinal pigmented epithelial cells. *FASEB J*. 13:477-484.

Halangk, W., M.M. Lerch, B. Brandt-Nedelev, W. Roth, M. Ruthenbuerger, T. Reinheckel, W. Domschke, H. Lippert, C. Peters, and J. Deussing. 2000. Role of cathepsin B in intracellular trypsinogen activation and the onset of acute pancreatitis. *J Clin Invest*. 106:773-781.

Hall, M.O., D. Bok, and A.D. Bacharach. 1969. Biosynthesis and assembly of the rod outer segment membrane system. Formation and fate of visual pigment in the frog retina. *J Mol Biol*. 45:397-406.

Halle, A., V. Hornung, G.C. Petzold, C.R. Stewart, B.G. Monks, T. Reinheckel, K.A. Fitzgerald, E. Latz, K.J. Moore, and D.T. Golenbock. 2008. The NALP3 inflammasome is involved in the innate immune response to amyloid-beta. *Nat Immunol*. 9:857-865.

Hardingham, T.E., and A.J. Fosang. 1992. Proteoglycans: many forms and many functions. *FASEB J*. 6:861-870.

Haricharan, S., and Y. Li. 2014. STAT signaling in mammary gland differentiation, cell survival and tumorigenesis. *Mol Cell Endocrinol*. 382:560-569.

Hartl, F.U. 1996. Molecular chaperones in cellular protein folding. *Nature*. 381:571-579.

Hartl, F.U., and M. Hayer-Hartl. 2002. Molecular chaperones in the cytosol: from nascent chain to folded protein. *Science*. 295:1852-1858.

Hashimoto, M., P. Bar-On, G. Ho, T. Takenouchi, E. Rockenstein, L. Crews, and E. Masliah. 2004. Beta-synuclein regulates Akt activity in neuronal cells. A possible mechanism for neuroprotection in Parkinson's disease. *J Biol Chem*. 279:23622-23629.

Hashimoto, M., and E. Masliah. 1999. Alpha-synuclein in Lewy body disease and Alzheimer's disease. *Brain Pathol*. 9:707-720.

Hashimoto, M., E. Rockenstein, M. Mante, M. Mallory, and E. Masliah. 2001. beta-Synuclein inhibits alpha-synuclein aggregation: a possible role as an anti-parkinsonian factor. *Neuron*. 32:213-223.

He, L.F., T.T. Wang, Q.Y. Gao, G.F. Zhao, Y.H. Huang, L.K. Yu, and Y.Y. Hou. 2011. Stanniocalcin-1 promotes tumor angiogenesis through up-regulation of VEGF in gastric cancer cells. *J Biomed Sci*. 18:39.

He, X., X.M. Zhang, J. Wu, J. Fu, L. Mou, D.H. Lu, Y. Cai, X.G. Luo, A. Pan, and X.X. Yan. 2014. Olfactory experience modulates immature neuron development in postnatal and adult guinea pig piriform cortex. *Neuroscience*. 259:101-112.

Hekimi, S., J. Lapointe, and Y. Wen. 2011. Taking a "good" look at free radicals in the aging process. *Trends Cell Biol*. 21:569-576.

Herbort, C.P., M. Papadia, and P. Neri. 2011. Myopia and inflammation. *J Ophthalmic Vis Res*. 6:270-283.

Higgins, G.T., J.H. Wang, P. Dockery, P.E. Cleary, and H.P. Redmond. 2003. Induction of angiogenic cytokine expression in cultured RPE by ingestion of oxidized photoreceptor outer segments. *Invest Ophthalmol Vis Sci*. 44:1775-1782.

Hirasawa, M., K. Noda, S. Noda, M. Suzuki, Y. Ozawa, K. Shinoda, M. Inoue, Y. Ogawa, K. Tsubota, and S. Ishida. 2011. Transcriptional factors associated with epithelial-mesenchymal transition in choroidal neovascularization. *Mol Vis*. 17:1222-1230.

Hoare, M., T. Das, and G. Alexander. 2010. Ageing, telomeres, senescence, and liver injury. *J Hepatol*. 53:950-961.

Hoeijmakers, J.H. 2009. DNA damage, aging, and cancer. *N Engl J Med*. 361:1475-1485.

Hohn, A., and T. Grune. 2013. Lipofuscin: formation, effects and role of macroautophagy. *Redox Biol*. 1:140-144.

Hope, G.M., W.W. Dawson, H.M. Engel, R.J. Ulshafer, M.J. Kessler, and M.B. Sherwood. 1992. A primate model for age related macular drusen. *Br J Ophthalmol*. 76:11-16.

Hotchkiss, M.L., and S.L. Fine. 1981. Pathologic myopia and choroidal neovascularization. *Am J Ophthalmol*. 91:177-183.

Housset, M., and F. Sennlaub. 2015. Thrombospondin-1 and Pathogenesis of Age-Related Macular Degeneration. *J Ocul Pharmacol Ther*. 31:406-412.

Hu, H., S. Li, J. Li, C. Huang, F. Zhou, L. Zhao, W. Yu, and X. Qin. 2018. Knockdown of Fibromodulin Inhibits Proliferation and Migration of RPE Cell via the VEGFR2-AKT Pathway. *J Ophthalmol*. 2018:5708537.

Hui, L., T. Abbas, R.M. Pielak, T. Joseph, J. Bargonetti, and D.A. Foster. 2004. Phospholipase D elevates the level of MDM2 and suppresses DNA damage-induced increases in p53. *Mol Cell Biol*. 24:5677-5686.

Ikuno, Y. 2017. Overview of the Complications of High Myopia. *Retina*. 37:2347-2351.

Im, E., A. Venkatakrishnan, and A. Kazlauskas. 2005. Cathepsin B regulates the intrinsic angiogenic threshold of endothelial cells. *Mol Biol Cell*. 16:3488-3500.

Ishibashi, K., and M. Imai. 2002. Prospect of a stanniocalcin endocrine/paracrine system in mammals. *Am J Physiol Renal Physiol*. 282:F367-375.

Ishibashi, T., R. Patterson, Y. Ohnishi, H. Inomata, and S.J. Ryan. 1986. Formation of drusen in the human eye. *Am J Ophthalmol*. 101:342-353.

Iwai, A., E. Masliah, M. Yoshimoto, N. Ge, L. Flanagan, H.A. de Silva, A. Kittel, and T. Saitoh. 1995. The precursor protein of non-A beta component of Alzheimer's disease amyloid is a presynaptic protein of the central nervous system. *Neuron*. 14:467-475.

Iwasaki, M., and H. Inomata. 1986. Relation between superficial capillaries and foveal structures in the human retina. *Invest Ophthalmol Vis Sci*. 27:1698-1705.

Jakes, R., M.G. Spillantini, and M. Goedert. 1994. Identification of two distinct synucleins from human brain. *FEBS Lett*. 345:27-32.

Jan, A.T., E.J. Lee, and I. Choi. 2016. Fibromodulin: A regulatory molecule maintaining cellular architecture for normal cellular function. *Int J Biochem Cell Biol*. 80:66-70.

Janowska, M.K., K.P. Wu, and J. Baum. 2015. Unveiling transient protein-protein interactions that modulate inhibition of alpha-synuclein aggregation by beta-synuclein, a pre-synaptic protein that co-localizes with alpha-synuclein. *Sci Rep*. 5:15164.

Janssen-Heininger, Y.M., B.T. Mossman, N.H. Heintz, H.J. Forman, B. Kalyanaraman, T. Finkel, J.S. Stamler, S.G. Rhee, and A. van der Vliet. 2008. Redox-based regulation of signal transduction: principles, pitfalls, and promises. *Free Radic Biol Med*. 45:1-17.

Jarrett, S.G., and M.E. Boulton. 2012. Consequences of oxidative stress in age-related macular degeneration. *Mol Aspects Med*. 33:399-417.

Jayaprakash, P., H. Dong, M. Zou, A. Bhatia, K. O'Brien, M. Chen, D.T. Woodley, and W. Li. 2015. Hsp90alpha and Hsp90beta together operate a hypoxia and nutrient paucity stress-response mechanism during wound healing. *J Cell Sci*. 128:1475-1480.

Jenco, J.M., A. Rawlingson, B. Daniels, and A.J. Morris. 1998. Regulation of phospholipase D2: selective inhibition of mammalian phospholipase D isoenzymes by alpha- and beta-synucleins. *Biochemistry*. 37:4901-4909.

Jia, T., Y.E. Liu, J. Liu, and Y.E. Shi. 1999. Stimulation of breast cancer invasion and metastasis by synuclein gamma. *Cancer Res*. 59:742-747.

Joachim, S.C., M.B. Wax, P. Seidel, N. Pfeiffer, and F.H. Grus. 2010. Enhanced characterization of serum autoantibody reactivity following HSP 60 immunization in a rat model of experimental autoimmune glaucoma. *Curr Eye Res*. 35:900-908.

Kaarniranta, K., J. Hyttinen, T. Ryhanen, J. Viiri, T. Paimela, E. Toropainen, I. Sorri, and A. Salminen. 2010. Mechanisms of protein aggregation in the retinal pigment epithelial cells. *Front Biosci (Elite Ed)*. 2:1374-1384.

Kaarniranta, K., A. Salminen, E.L. Eskelinen, and J. Kopitz. 2009. Heat shock proteins as gatekeepers of proteolytic pathways-Implications for age-related macular degeneration (AMD). *Ageing Res Rev*. 8:128-139.

Kaarniranta, K., D. Sinha, J. Blasiak, A. Kauppinen, Z. Vereb, A. Salminen, M.E. Boulton, and G. Petrovski. 2013. Autophagy and heterophagy dysregulation leads to retinal pigment epithelium dysfunction and development of age-related macular degeneration. *Autophagy*. 9:973-984.

Kalluri, R., and R.A. Weinberg. 2009. The basics of epithelial-mesenchymal transition. *J Clin Invest*. 119:1420-1428.

Kamphaus, G.D., P.C. Colorado, D.J. Panka, H. Hopfer, R. Ramchandran, A. Torre, Y. Maeshima, J.W. Mier, V.P. Sukhatme, and R. Kalluri. 2000. Canstatin, a novel matrix-derived inhibitor of angiogenesis and tumor growth. *J Biol Chem*. 275:1209-1215.

Kanazawa, H., K. Imoto, M. Okada, and H. Yamawaki. 2017. Canstatin inhibits hypoxia-induced apoptosis through activation of integrin/focal adhesion kinase/Akt signaling pathway in H9c2 cardiomyoblasts. *PLoS One*. 12:e0173051.

Kauppinen, A., J.J. Paterno, J. Blasiak, A. Salminen, and K. Kaarniranta. 2016. Inflammation and its role in age-related macular degeneration. *Cell Mol Life Sci*. 73:1765-1786.

Kiilgaard, J.F., J.U. Prause, M. Prause, E. Scherfig, M.H. Nissen, and M. la Cour. 2007. Subretinal posterior pole injury induces selective proliferation of RPE cells in the periphery in in vivo studies in pigs. *Invest Ophthalmol Vis Sci*. 48:355-360.

King, G.L., and K. Suzuma. 2000. Pigment-epithelium-derived factor--a key coordinator of retinal neuronal and vascular functions. *N Engl J Med*. 342:349-351.

Kinnunen, K., G. Petrovski, M.C. Moe, A. Berta, and K. Kaarniranta. 2012. Molecular mechanisms of retinal pigment epithelium damage and development of age-related macular degeneration. *Acta Ophthalmol*. 90:299-309.

Klettner, A., and Y. Miura. 2019. Porcine RPE/Choroidal Explant Cultures. *Methods Mol Biol*. 1834:109-118.

Kohling, R., R. Nischt, A. Vasudevan, M. Ho, M. Weiergraber, T. Schneider, and N. Smyth. 2006. Nidogen and nidogen-associated basement membrane proteins and neuronal plasticity. *Neurodegener Dis*. 3:56-61.

König, S., K. Hadrian, S. Schlatt, J. Wistuba, S. Thanos, and M.R.R. Böhm. 2018. Topographic protein profiling of the age-related proteome in the retinal pigment epithelium of Callithrix jacchus with respect to macular degeneration. *J Proteomics*.

Kresse, H., H. Hausser, and E. Schonherr. 1993. Small proteoglycans. *Experientia*. 49:403-416.

Kvanta, A. 1994. Expression and secretion of transforming growth factor-beta in transformed and nontransformed retinal pigment epithelial cells. *Ophthalmic Res*. 26:361-367.

Lad, E.M., S.W. Cousins, J.S. Van Arnam, and A.D. Proia. 2015. Abundance of infiltrating CD163+ cells in the retina of postmortem eyes with dry and neovascular age-related macular degeneration. *Graefes Arch Clin Exp Ophthalmol*. 253:1941-1945.

Laemmli, U.K. 1970. Cleavage of structural proteins during the assembly of the head of bacteriophage T4. *Nature*. 227:680-685.

Lafeber, F.P., R.G. Hanssen, Y.M. Choy, G. Flik, M.P. Herrmann-Erlee, P.K. Pang, and S.E. Bonga. 1988. Identification of hypocalcin (teleocalcin) isolated from trout Stannius corpuscles. *Gen Comp Endocrinol*. 69:19-30.

Law, A.Y., and C.K. Wong. 2013. Stanniocalcin-1 and -2 promote angiogenic sprouting in HUVECs via VEGF/VEGFR2 and angiopoietin signaling pathways. *Mol Cell Endocrinol*. 374:73-81.

Lawler, J. 2000. The functions of thrombospondin-1 and-2. *Curr Opin Cell Biol*. 12:634-640.

Lawler, P.R., and J. Lawler. 2012. Molecular basis for the regulation of angiogenesis by thrombospondin-1 and -2. *Cold Spring Harb Perspect Med*. 2:a006627.

LeCouter, J., D.R. Moritz, B. Li, G.L. Phillips, X.H. Liang, H.P. Gerber, K.J. Hillan, and N. Ferrara. 2003. Angiogenesis-independent endothelial protection of liver: role of VEGFR-1. *Science*. 299:890-893.

Leung, C.K., M. Yu, R.N. Weinreb, C. Ye, S. Liu, G. Lai, and D.S. Lam. 2012. Retinal nerve fiber layer imaging with spectral-domain optical coherence tomography: a prospective analysis of age-related loss. *Ophthalmology*. 119:731-737.

Levy, O., B. Calippe, S. Lavalette, S.J. Hu, W. Raoul, E. Dominguez, M. Housset, M. Paques, J.A. Sahel, A.P. Bemelmans, C. Combadiere, X. Guillonneau, and F. Sennlaub. 2015. Apolipoprotein E promotes subretinal mononuclear phagocyte survival and chronic inflammation in age-related macular degeneration. *EMBO Mol Med*. 7:211-226.

Lima, J.G., C. de Freitas Vinhas, I.N. Gomes, C.M. Azevedo, R.R. dos Santos, M.A. Vannier-Santos, and P.S. Veras. 2011. Phagocytosis is inhibited by autophagic induction in murine macrophages. *Biochem Biophys Res Commun*. 405:604-609.

Liu, C., L. Cao, S. Yang, L. Xu, P. Liu, F. Wang, and D. Xu. 2015. Subretinal injection of amyloid-beta peptide accelerates RPE cell senescence and retinal degeneration. *Int J Mol Med*. 35:169-176.

Liu, R.T., J. Gao, S. Cao, N. Sandhu, J.Z. Cui, C.L. Chou, E. Fang, and J.A. Matsubara. 2013. Inflammatory mediators induced by amyloid-beta in the retina and RPE in vivo: implications for inflammasome activation in age-related macular degeneration. *Invest Ophthalmol Vis Sci*. 54:2225-2237.

Liu, R.T., A. Wang, E. To, J. Gao, S. Cao, J.Z. Cui, and J.A. Matsubara. 2014. Vinpocetine inhibits amyloid-beta induced activation of NF-kappaB, NLRP3 inflammasome and cytokine production in retinal pigment epithelial cells. *Exp Eye Res*. 127:49-58.

Lopez, P.F., B.D. Sippy, H.M. Lambert, A.B. Thach, and D.R. Hinton. 1996. Transdifferentiated retinal pigment epithelial cells are immunoreactive for vascular endothelial growth factor in surgically excised age-related macular degeneration-related choroidal neovascular membranes. *Invest Ophthalmol Vis Sci*. 37:855-868.

Lu, L., S.F. Hackett, A. Mincey, H. Lai, and P.A. Campochiaro. 2006. Effects of different types of oxidative stress in RPE cells. *J Cell Physiol*. 206:119-125.

Luetjens, C.M.K., and J.K. Bluemel. 2015. Consideration the Use of Callithrix Jacchus. *In* The Nonhuman Primate in Nonclinical Drug Development and Safety Assessment. J.K. Bluemel, S. Korte, E. Schenck, and G. Weinbauer, editors. Elsevier, London. pp. 448-449.

Mackay, E.A., A. Ehrhard, M. Moniatte, C. Guenet, C. Tardif, C. Tarnus, O. Sorokine, B. Heintzelmann, C. Nay, J.M. Remy, J. Higaki, A. Van Dorsselaer, J. Wagner, C. Danzin, and P. Mamont. 1997. A possible role for cathepsins D, E, and B in the processing of beta-amyloid precursor protein in Alzheimer's disease. *Eur J Biochem*. 244:414-425.

Magne, L., E. Blanc, B. Legrand, D. Lucas, R. Barouki, H. Rouach, and M. Garlatti. 2011. ATF4 and the integrated stress response are induced by ethanol and cytochrome P450 2E1 in human hepatocytes. *J Hepatol*. 54:729-737.

Maguire, M., S. Bressler, N. Bressler, J. Alexander, C. Hiner, N. Javornik, D. Phillips, M. Marsh, B. Hawkins, D. Burgess, S. Chandra, M. Klein, D. Orth, T. Stevens, and S.L. Fine. 1997. Risk factors for choroidal neovascularization in the second eye of patients with juxtafoveal or subfoveal choroidal neovascularization secondary to age-related macular degeneration. Macular Photocoagulation Study Group. *Arch Ophthalmol*. 115:741-747.

Mai, J., M. Sameni, T. Mikkelsen, and B.F. Sloane. 2002. Degradation of extracellular matrix protein tenascin-C by cathepsin B: an interaction involved in the progression of gliomas. *Biol Chem*. 383:1407-1413.

Man, S.M., and T.D. Kanneganti. 2016. Regulation of lysosomal dynamics and autophagy by CTSB/cathepsin B. *Autophagy*. 12:2504-2505.

Masland, R.H. 2001. The fundamental plan of the retina. *Nat Neurosci*. 4:877-886.

Mattison, J.A., and K.L. Vaughan. 2017. An overview of nonhuman primates in aging research. *Exp Gerontol*. 94:41-45.

Maurice, D.M. 1957. The structure and transparency of the cornea. *J Physiol*. 136:263-286.

McLeod, D.S., M. Taomoto, T. Otsuji, W.R. Green, J.S. Sunness, and G.A. Lutty. 2002. Quantifying changes in RPE and choroidal vasculature in eyes with age-related macular degeneration. *Invest Ophthalmol Vis Sci*. 43:1986-1993.

Medzhitov, R. 2008. Origin and physiological roles of inflammation. *Nature*. 454:428-435.

Messenio, D., G. Marano, S. Gerosa, F. Iannelli, and E.M. Biganzoli. 2013. The influence of age on the recovery of the ERG photostress test. *Doc Ophthalmol*. 126:87-97.

Meyer, N., and L.Z. Penn. 2008. Reflecting on 25 years with MYC. *Nat Rev Cancer*. 8:976-990.

Miceli, M.V., M.R. Liles, and D.A. Newsome. 1994. Evaluation of oxidative processes in human pigment epithelial cells associated with retinal outer segment phagocytosis. *Exp Cell Res*. 214:242-249.

Midena, E., C. Degli Angeli, M.C. Blarzino, M. Valenti, and T. Segato. 1997. Macular function impairment in eyes with early age-related macular degeneration. *Invest Ophthalmol Vis Sci*. 38:469-477.

Miller, J.W. 2013. Age-related macular degeneration revisited--piecing the puzzle: the LXIX Edward Jackson memorial lecture. *Am J Ophthalmol*. 155:1-35 e13.

Miosge, N., S. Holzhausen, C. Zelent, P. Sprysch, and R. Herken. 2001. Nidogen-1 and nidogen-2 are found in basement membranes during human embryonic development. *Histochem J*. 33:523-530.

Mohamed, M.M., and B.F. Sloane. 2006. Cysteine cathepsins: multifunctional enzymes in cancer. *Nat Rev Cancer*. 6:764-775.

Moon, H.Y., A. Becke, D. Berron, B. Becker, N. Sah, G. Benoni, E. Janke, S.T. Lubejko, N.H. Greig, J.A. Mattison, E. Duzel, and H. van Praag. 2016. Running-Induced Systemic Cathepsin B Secretion Is Associated with Memory Function. *Cell Metab*. 24:332-340.

Mooradian, A.D., M.J. Haas, and J.M. Chehade. 2003. Age-related changes in rat cerebral occludin and zonula occludens-1 (ZO-1). *Mech Ageing Dev*. 124:143-146.

Mosevitsky, M.I. 2005. Nerve ending "signal" proteins GAP-43, MARCKS, and BASP1. *Int Rev Cytol*. 245:245-325.

Nakajo, S., S. Shioda, Y. Nakai, and K. Nakaya. 1994. Localization of phosphoneuroprotein 14 (PNP 14) and its mRNA expression in rat brain determined by immunocytochemistry and in situ hybridization. *Brain Res Mol Brain Res*. 27:81-86.

Nguyen-Legros, J., and D. Hicks. 2000. Renewal of photoreceptor outer segments and their phagocytosis by the retinal pigment epithelium. *Int Rev Cytol*. 196:245-313.

Nichane, M., X. Ren, and E.J. Bellefroid. 2010. Self-regulation of Stat3 activity coordinates cell-cycle progression and neural crest specification. *EMBO J*. 29:55-67.

Nicolas, M.G., K. Fujiki, K. Murayama, M.T. Suzuki, R. Mineki, M. Hayakawa, Y. Yoshikawa, F. Cho, and A. Kanai. 1996. Studies on the mechanism of early onset macular degeneration in cynomolgus (Macaca fascicularis) monkeys. I. Abnormal concentrations of two proteins in the retina. *Exp Eye Res*. 62:211-219.

Nita, M., and A. Grzybowski. 2016. The Role of the Reactive Oxygen Species and Oxidative Stress in the Pathomechanism of the Age-Related Ocular Diseases and Other Pathologies of the Anterior and Posterior Eye Segments in Adults. *Oxid Med Cell Longev*. 2016:3164734.

Ockleford, C., N. Bright, A. Hubbard, C. D'Lacey, J. Smith, L. Gardiner, T. Sheikh, M. Albentosa, and K. Turtle. 1993. Micro-trabeculae, macro-plaques or mini-basement membranes in human term fetal membranes? *Philos Trans R Soc Lond B Biol Sci*. 342:121-136.

Okamoto, H., S. Umeda, T. Nozawa, M.T. Suzuki, Y. Yoshikawa, E.T. Matsuura, and T. Iwata. 2010. Comparative proteomic analyses of macular and peripheral retina of cynomolgus monkeys (Macaca fascicularis). *Exp Anim*. 59:171-182.

Oyadomari, S., A. Koizumi, K. Takeda, T. Gotoh, S. Akira, E. Araki, and M. Mori. 2002. Targeted disruption of the Chop gene delays endoplasmic reticulum stress-mediated diabetes. *J Clin Invest*. 109:525-532.

Oyadomari, S., and M. Mori. 2004. Roles of CHOP/GADD153 in endoplasmic reticulum stress. *Cell Death Differ*. 11:381-389.

Pal, S., K. Datta, and D. Mukhopadhyay. 2001. Central role of p53 on regulation of vascular permeability factor/vascular endothelial growth factor (VPF/VEGF) expression in mammary carcinoma. *Cancer Res*. 61:6952-6957.

Paolisso, G., M.R. Rizzo, G. Mazziotti, M.R. Tagliamonte, A. Gambardella, M. Rotondi, C. Carella, D. Giugliano, M. Varricchio, and F. D'Onofrio. 1998. Advancing age and insulin resistance: role of plasma tumor necrosis factor-alpha. *Am J Physiol*. 275:E294-299.

Patel, A.K., and A.S. Hackam. 2013. Toll-like receptor 3 (TLR3) protects retinal pigmented epithelium (RPE) cells from oxidative stress through a STAT3-dependent mechanism. *Mol Immunol*. 54:122-131.

Paulsson, M. 1992. Basement membrane proteins: structure, assembly, and cellular interactions. *Crit Rev Biochem Mol Biol*. 27:93-127.

Pennesi, M.E., M. Neuringer, and R.J. Courtney. 2012. Animal models of age related macular degeneration. *Mol Aspects Med*. 33:487-509.

Peyman, G.A., and D. Bok. 1972. Peroxidase diffusion in the normal and laser-coagulated primate retina. *Invest Ophthalmol*. 11:35-45.

Phillips, K.A., K.L. Bales, J.P. Capitanio, A. Conley, P.W. Czoty, B.A. t Hart, W.D. Hopkins, S.L. Hu, L.A. Miller, M.A. Nader, P.W. Nathanielsz, J. Rogers, C.A. Shively, and M.L. Voytko. 2014. Why primate models matter. *Am J Primatol*. 76:801-827.

Pierce, E.A., E.D. Foley, and L.E. Smith. 1996. Regulation of vascular endothelial growth factor by oxygen in a model of retinopathy of prematurity. *Arch Ophthalmol*. 114:1219-1228.

Pockley, A.G., and B. Henderson. 2018. Extracellular cell stress (heat shock) proteins-immune responses and disease: an overview. *Philos Trans R Soc Lond B Biol Sci*. 373.

Polymeropoulos, M.H., C. Lavedan, E. Leroy, S.E. Ide, A. Dehejia, A. Dutra, B. Pike, H. Root, J. Rubenstein, R. Boyer, E.S. Stenroos, S. Chandrasekharappa, A. Athanassiadou, T. Papapetropoulos, W.G. Johnson, A.M. Lazzarini, R.C. Duvoisin, G. Di Iorio, L.I. Golbe, and R.L. Nussbaum. 1997. Mutation in the alpha-synuclein gene identified in families with Parkinson's disease. *Science*. 276:2045-2047.

Porter, K., Y. Lin, and P.B. Liton. 2013. Cathepsin B is up-regulated and mediates extracellular matrix degradation in trabecular meshwork cells following phagocytic challenge. *PLoS One*. 8:e68668.

Pratt, W.B. 1993. The role of heat shock proteins in regulating the function, folding, and trafficking of the glucocorticoid receptor. *J Biol Chem*. 268:21455-21458.

Prockop, D.J., and K.I. Kivirikko. 1995. Collagens: molecular biology, diseases, and potentials for therapy. *Annu Rev Biochem*. 64:403-434.

Qian, F., A.S. Bajkowski, D.F. Steiner, S.J. Chan, and A. Frankfater. 1989. Expression of five cathepsins in murine melanomas of varying metastatic potential and normal tissues. *Cancer Res*. 49:4870-4875.

Qin, S., M. Ni, X. Wang, F. Maurier-Mahe, D.L. Shurland, and G.A. Rodrigues. 2011. Inhibition of RPE cell sterile inflammatory responses and endotoxin-induced uveitis by a cell-impermeable HSP90 inhibitor. *Exp Eye Res*. 93:889-897.

Rawlings, J.S., K.M. Rosler, and D.A. Harrison. 2004. The JAK/STAT signaling pathway. *J Cell Sci*. 117:1281-1283.

Rhee, S.G., K.S. Yang, S.W. Kang, H.A. Woo, and T.S. Chang. 2005. Controlled elimination of intracellular H(2)O(2): regulation of peroxiredoxin, catalase, and glutathione peroxidase via post-translational modification. *Antioxid Redox Signal*. 7:619-626.

Risau, W., and I. Flamme. 1995. Vasculogenesis. *Annu Rev Cell Dev Biol*. 11:73-91.

Roberts, W.G., and G.E. Palade. 1995. Increased microvascular permeability and endothelial fenestration induced by vascular endothelial growth factor. *J Cell Sci*. 108 (Pt 6):2369-2379.

Rockenstein, E., L.A. Hansen, M. Mallory, J.Q. Trojanowski, D. Galasko, and E. Masliah. 2001. Altered expression of the synuclein family mRNA in Lewy body and Alzheimer's disease. *Brain Res*. 914:48-56.

Roddy, G.W., R.H. Rosa, Jr., J.Y. Oh, J.H. Ylostalo, T.J. Bartosh, Jr., H. Choi, R.H. Lee, D. Yasumura, K. Ahern, G. Nielsen, M.T. Matthes, M.M. LaVail, and D.J. Prockop. 2012. Stanniocalcin-1 rescued photoreceptor degeneration in two rat models of inherited retinal degeneration. *Mol Ther*. 20:788-797.

Ross, C.N., J.E. Fite, H. Jensen, and J.A. French. 2007. Demographic review of a captive colony of callitrichids (Callithrix kuhlii). *Am J Primatol*. 69:234-240.

Rozanowska, M., J. Jarvis-Evans, W. Korytowski, M.E. Boulton, J.M. Burke, and T. Sarna. 1995. Blue light-induced reactivity of retinal age pigment. In vitro generation of oxygen-reactive species. *J Biol Chem*. 270:18825-18830.

Rozanowska, M., W. Korytowski, B. Rozanowski, C. Skumatz, M.E. Boulton, J.M. Burke, and T. Sarna. 2002. Photoreactivity of aged human RPE melanosomes: a comparison with lipofuscin. *Invest Ophthalmol Vis Sci*. 43:2088-2096.

Rufini, A., P. Tucci, I. Celardo, and G. Melino. 2013. Senescence and aging: the critical roles of p53. *Oncogene*. 32:5129-5143.

Ryhanen, T., J.M. Hyttinen, J. Kopitz, K. Rilla, E. Kuusisto, E. Mannermaa, J. Viiri, C.I. Holmberg, I. Immonen, S. Meri, J. Parkkinen, E.L. Eskelinen, H. Uusitalo, A. Salminen, and K. Kaarniranta. 2009. Crosstalk between Hsp70 molecular chaperone, lysosomes and proteasomes in autophagy-mediated proteolysis in human retinal pigment epithelial cells. *J Cell Mol Med*. 13:3616-3631.

Samuel, M.A., Y. Zhang, M. Meister, and J.R. Sanes. 2011. Age-related alterations in neurons of the mouse retina. *J Neurosci*. 31:16033-16044.

Sandercoe, T.M., S.F. Geller, A.E. Hendrickson, J. Stone, and J.M. Provis. 2003. VEGF expression by ganglion cells in central retina before formation of the foveal depression in monkey retina: evidence of developmental hypoxia. *J Comp Neurol*. 462:42-54.

Sanes, J.R., and S.L. Zipursky. 2010. Design principles of insect and vertebrate visual systems. *Neuron*. 66:15-36.

Santos, F., C. Moreira, S. Nobrega-Pereira, and B. Bernardes de Jesus. 2019. New Insights into the Role of Epithelial(-)Mesenchymal Transition during Aging. *Int J Mol Sci*. 20.

Sarks, S.H., J.J. Arnold, M.C. Killingsworth, and J.P. Sarks. 1999. Early drusen formation in the normal and aging eye and their relation to age related maculopathy: a clinicopathological study. *Br J Ophthalmol*. 83:358-368.

Schaefer, L., and R.V. Iozzo. 2008. Biological functions of the small leucine-rich proteoglycans: from genetics to signal transduction. *J Biol Chem*. 283:21305-21309.

Schneeberger, E.E., and R.D. Lynch. 2004. The tight junction: a multifunctional complex. *Am J Physiol Cell Physiol*. 286:C1213-1228.

Schroeder, A., O. Mueller, S. Stocker, R. Salowsky, M. Leiber, M. Gassmann, S. Lightfoot, W. Menzel, M. Granzow, and T. Ragg. 2006. The RIN: an RNA integrity number for assigning integrity values to RNA measurements. *BMC Mol Biol*. 7:3.

Schubert, H. 2019. Structure of the Neural Retina. *In* Ophthalmology. M. Yanoff and J.S. Duker, editors. Elsevier Saunders, Edinburgh. 419-422.

Sedger, L.M., and M.F. McDermott. 2014. TNF and TNF-receptors: From mediators of cell death and inflammation to therapeutic giants - past, present and future. *Cytokine Growth Factor Rev*. 25:453-472.

Semkova, I., N. Kociok, D. Karagiannis, R. Nischt, N. Smyth, M. Paulsson, O. Strauss, and A.M. Joussen. 2014. Anti-angiogenic effect of the basement membrane protein nidogen-1 in a mouse model of choroidal neovascularization. *Exp Eye Res*. 118:80-88.

Sena, L.A., and N.S. Chandel. 2012. Physiological roles of mitochondrial reactive oxygen species. *Mol Cell*. 48:158-167.

Sennlaub, F., C. Auvynet, B. Calippe, S. Lavalette, L. Poupel, S.J. Hu, E. Dominguez, S. Camelo, O. Levy, E. Guyon, N. Saederup, I.F. Charo, N.V. Rooijen, E. Nandrot, J.L. Bourges, F. Behar-Cohen, J.A. Sahel, X. Guillonneau, W. Raoul, and C. Combadiere. 2013. CCR2(+) monocytes infiltrate atrophic lesions in age-related macular disease and mediate photoreceptor degeneration in experimental subretinal inflammation in Cx3cr1 deficient mice. *EMBO Mol Med*. 5:1775-1793.

Shakib, M., and J.G. Cunha-Vaz. 1966. Studies on the permeability of the blood-retinal barrier. IV. Junctional complexes of the retinal vessels and their role in the permeability of the blood-retinal barrier. *Exp Eye Res*. 5:229-234.

Shen, J.K., A. Dong, S.F. Hackett, W.R. Bell, W.R. Green, and P.A. Campochiaro. 2007. Oxidative damage in age-related macular degeneration. *Histol Histopathol*. 22:1301-1308.

Sherwood, S.W., D. Rush, J.L. Ellsworth, and R.T. Schimke. 1988. Defining cellular senescence in IMR-90 cells: a flow cytometric analysis. *Proc Natl Acad Sci U S A*. 85:9086-9090.

Singh, A.K., and H. Shichi. 2001. Peroxiredoxin in bovine ocular tissues: immunohistochemical localization and in situ hybridization. *J Ocul Pharmacol Ther*. 17:279-286.

Smith, J., and C.D. Ockleford. 1994. Laser scanning confocal examination and comparison of nidogen (entactin) with laminin in term human amniochorion. *Placenta*. 15:95-106.

Smucny, D.A., D.H. Abbott, K.G. Mansfield, N.J. Schultz-Darken, M.E. Yamamoto, A.I. Alencar, and S.D. Tardif. 2004. Reproductive output, maternal age, and survivorship in captive common marmoset females (Callithrix jacchus). *Am J Primatol*. 64:107-121.

Snyder, H., K. Mensah, C. Hsu, M. Hashimoto, I.G. Surgucheva, B. Festoff, A. Surguchov, E. Masliah, A. Matouschek, and B. Wolozin. 2005. beta-Synuclein reduces proteasomal inhibition by alpha-synuclein but not gamma-synuclein. *J Biol Chem*. 280:7562-7569.

Soker, S., S. Takashima, H.Q. Miao, G. Neufeld, and M. Klagsbrun. 1998. Neuropilin-1 is expressed by endothelial and tumor cells as an isoform-specific receptor for vascular endothelial growth factor. *Cell*. 92:735-745.

Sparrow, J.R., and B. Cai. 2001. Blue light-induced apoptosis of A2E-containing RPE: involvement of caspase-3 and protection by Bcl-2. *Invest Ophthalmol Vis Sci*. 42:1356-1362.

Sparrow, J.R., D. Hicks, and C.P. Hamel. 2010. The retinal pigment epithelium in health and disease. *Curr Mol Med*. 10:802-823.

Spillantini, M.G., R.A. Crowther, R. Jakes, N.J. Cairns, P.L. Lantos, and M. Goedert. 1998. Filamentous alpha-synuclein inclusions link multiple system atrophy with Parkinson's disease and dementia with Lewy bodies. *Neurosci Lett*. 251:205-208.

Staehelin, L.A. 1973. Further observations on the fine structure of freeze-cleaved tight junctions. *J Cell Sci*. 13:763-786.

Stangos, N., S. Voutas, F. Topouzis, and V. Karampatakis. 1995. Contrast sensitivity evaluation in eyes predisposed to age-related macular degeneration and presenting normal visual acuity. *Ophthalmologica*. 209:194-198.

Steinberg, R.H. 1985. Interactions between the retinal pigment epithelium and the neural retina. *Doc Ophthalmol*. 60:327-346.

Stocker, R. 1990. Induction of haem oxygenase as a defence against oxidative stress. *Free Radic Res Commun*. 9:101-112.

Stone, J., T. Chan-Ling, J. Pe'er, A. Itin, H. Gnessin, and E. Keshet. 1996. Roles of vascular endothelial growth factor and astrocyte degeneration in the genesis of retinopathy of prematurity. *Invest Ophthalmol Vis Sci*. 37:290-299.

Stone, J., A. Itin, T. Alon, J. Pe'er, H. Gnessin, T. Chan-Ling, and E. Keshet. 1995. Development of retinal vasculature is mediated by hypoxia-induced vascular endothelial growth factor (VEGF) expression by neuroglia. *J Neurosci*. 15:4738-4747.

Strasburger, H., I. Rentschler, and M. Juttner. 2011. Peripheral vision and pattern recognition: a review. *J Vis*. 11:13.

Strauss, O. 2005. The retinal pigment epithelium in visual function. *Physiol Rev*. 85:845-881.

Sunness, J.S., M.A. Johnson, R.W. Massof, and S. Marcus. 1988. Retinal sensitivity over drusen and nondrusen areas. A study using fundus perimetry. *Arch Ophthalmol*. 106:1081-1084.

Surguchov, A., B. McMahan, E. Masliah, and I. Surgucheva. 2001. Synucleins in ocular tissues. *J Neurosci Res*. 65:68-77.

Svensson, L., I. Narlid, and A. Oldberg. 2000. Fibromodulin and lumican bind to the same region on collagen type I fibrils. *FEBS Lett*. 470:178-182.

Szigeti, A., E. Tatrai, B.E. Varga, A. Szamosi, D.C. DeBuc, Z.Z. Nagy, J. Nemeth, and G.M. Somfai. 2015. The Effect of Axial Length on the Thickness of Intraretinal Layers of the Macula. *PLoS One*. 10:e0142383.

Tai, H., Z. Wang, H. Gong, X. Han, J. Zhou, X. Wang, X. Wei, Y. Ding, N. Huang, J. Qin, J. Zhang, S. Wang, F. Gao, Z.M. Chrzanowska-Lightowlers, R. Xiang, and H. Xiao. 2017. Autophagy impairment with lysosomal and mitochondrial dysfunction is an important characteristic of oxidative stress-induced senescence. *Autophagy*. 13:99-113.

Takeda, A., M. Hashimoto, M. Mallory, M. Sundsumo, L. Hansen, A. Sisk, and E. Masliah. 1998. Abnormal distribution of the non-Abeta component of Alzheimer's disease amyloid precursor/alpha-synuclein in Lewy body disease as revealed by proteinase K and formic acid pretreatment. *Lab Invest*. 78:1169-1177.

Tamaki, N., E. Hatano, K. Taura, M. Tada, Y. Kodama, T. Nitta, K. Iwaisako, S. Seo, A. Nakajima, I. Ikai, and S. Uemoto. 2008. CHOP deficiency attenuates cholestasis-induced liver fibrosis by reduction of hepatocyte injury. *Am J Physiol Gastrointest Liver Physiol*. 294:G498-505.

Tamiya, S., L. Liu, and H.J. Kaplan. 2010. Epithelial-mesenchymal transition and proliferation of retinal pigment epithelial cells initiated upon loss of cell-cell contact. *Invest Ophthalmol Vis Sci*. 51:2755-2763.

Tanihara, H., M. Yoshida, M. Matsumoto, and N. Yoshimura. 1993. Identification of transforming growth factor-beta expressed in cultured human retinal pigment epithelial cells. *Invest Ophthalmol Vis Sci*. 34:413-419.

Tardif, S.D., K.G. Mansfield, R. Ratnam, C.N. Ross, and T.E. Ziegler. 2011. The marmoset as a model of aging and age-related diseases. *ILAR J*. 52:54-65.

Tardif, S.D., D.A. Smucny, D.H. Abbott, K. Mansfield, N. Schultz-Darken, and M.E. Yamamoto. 2003. Reproduction in captive common marmosets (Callithrix jacchus). *Comp Med*. 53:364-368.

Tate, D.J., Jr., M.V. Miceli, and D.A. Newsome. 1995. Phagocytosis and H2O2 induce catalase and metallothionein gene expression in human retinal pigment epithelial cells. *Invest Ophthalmol Vis Sci*. 36:1271-1279.

Tatsumoto, S., N. Adati, Y. Tohtoki, Y. Sakaki, T. Boroviak, S. Habu, H. Okano, H. Suemizu, E. Sasaki, and M. Satake. 2013. Development and characterization of cDNA resources for the common marmoset: one of the experimental primate models. *DNA Res*. 20:255-262.

Teodoro, J.G., S.K. Evans, and M.R. Green. 2007. Inhibition of tumor angiogenesis by p53: a new role for the guardian of the genome. *J Mol Med (Berl)*. 85:1175-1186.

Terman, A., and U.T. Brunk. 2004. Lipofuscin. *Int J Biochem Cell Biol*. 36:1400-1404.

Thiery, J.P., H. Acloque, R.Y. Huang, and M.A. Nieto. 2009. Epithelial-mesenchymal transitions in development and disease. *Cell*. 139:871-890.

Tolentino, M.J., S. Miller, A.R. Gaudio, and M.A. Sandberg. 1994. Visual field deficits in early age-related macular degeneration. *Vision Res*. 34:409-413.

Toska, E., and S.G. Roberts. 2014. Mechanisms of transcriptional regulation by WT1 (Wilms' tumour 1). *Biochem J*. 461:15-32.

Touhami, S., F. Beguier, S. Augustin, H. Charles-Messance, L. Vignaud, E.F. Nandrot, S. Reichman, V. Forster, T. Mathis, J.A. Sahel, B. Bodaghi, X. Guillonneau, and F. Sennlaub. 2018. Chronic exposure to tumor necrosis factor alpha induces retinal pigment epithelium cell dedifferentiation. *J Neuroinflammation*. 15:85.

Tremolada, G., C. Del Turco, R. Lattanzio, S. Maestroni, A. Maestroni, F. Bandello, and G. Zerbini. 2012. The role of angiogenesis in the development of proliferative diabetic retinopathy: impact of intravitreal anti-VEGF treatment. *Exp Diabetes Res*. 2012:728325.

Trepel, M. 2008. Neuroanatomie - Struktur und Funktion. Elsevier Urban&Fischer.

Ts'o, M.O., and E. Friedman. 1968. The retinal pigment epithelium. 3. Growth and development. *Arch Ophthalmol*. 80:214-216.

Ullah, I., N.D. Ritchie, and T.J. Evans. 2017. The interrelationship between phagocytosis, autophagy and formation of neutrophil extracellular traps following infection of human neutrophils by Streptococcus pneumoniae. *Innate Immun*. 23:413-423.

Unk. 2014. Cross section of the Human eye. Vol. 2019. Wikimedia commons.

Vafa, O., M. Wade, S. Kern, M. Beeche, T.K. Pandita, G.M. Hampton, and G.M. Wahl. 2002. c-Myc can induce DNA damage, increase reactive oxygen species, and mitigate p53 function: a mechanism for oncogene-induced genetic instability. *Mol Cell*. 9:1031-1044.

Vermes, I., C. Haanen, H. Steffens-Nakken, and C. Reutelingsperger. 1995. A novel assay for apoptosis. Flow cytometric detection of phosphatidylserine expression on early apoptotic cells using fluorescein labelled Annexin V. *J Immunol Methods*. 184:39-51.

Voss Kyhn, M., J.F. Kiilgaard, A.G. Lopez, E. Scherfig, J.U. Prause, and M. la Cour. 2007. The multifocal electroretinogram (mfERG) in the pig. *Acta Ophthalmol Scand*. 85:438-444.

Wagner, G.F., M. Hampong, C.M. Park, and D.H. Copp. 1986. Purification, characterization, and bioassay of teleocalcin, a glycoprotein from salmon corpuscles of Stannius. *Gen Comp Endocrinol*. 63:481-491.

Wakabayashi, K., K. Matsumoto, K. Takayama, M. Yoshimoto, and H. Takahashi. 1997. NACP, a presynaptic protein, immunoreactivity in Lewy bodies in Parkinson's disease. *Neurosci Lett*. 239:45-48.

Wang, L., Y. Chen, X. Li, Y. Zhang, E. Gulbins, and Y. Zhang. 2016. Enhancement of endothelial permeability by free fatty acid through lysosomal cathepsin B-mediated Nlrp3 inflammasome activation. *Oncotarget*. 7:73229-73241.

Wang, Y., L. Huang, M. Abdelrahim, Q. Cai, A. Truong, R. Bick, B. Poindexter, and D. Sheikh-Hamad. 2009a. Stanniocalcin-1 suppresses superoxide generation in macrophages through induction of mitochondrial UCP2. *J Leukoc Biol*. 86:981-988.

Wang, Y.E., A. Park, M. Lake, M. Pentecost, B. Torres, T.E. Yun, M.C. Wolf, M.R. Holbrook, A.N. Freiberg, and B. Lee. 2010. Ubiquitin-regulated nuclear-cytoplasmic trafficking of the Nipah virus matrix protein is important for viral budding. *PLoS Pathog*. 6:e1001186.

Wang, Z., M. Gerstein, and M. Snyder. 2009b. RNA-Seq: a revolutionary tool for transcriptomics. *Nat Rev Genet*. 10:57-63.

Watanabe, D., H. Takagi, K. Suzuma, H. Oh, H. Ohashi, and Y. Honda. 2005. Expression of connective tissue growth factor and its potential role in choroidal neovascularization. *Retina*. 25:911-918.

Watzke, R.C., J.D. Soldevilla, and D.R. Trune. 1993. Morphometric analysis of human retinal pigment epithelium: correlation with age and location. *Curr Eye Res*. 12:133-142.

Weale, R.A. 1975. Senile changes in visual acuity. *Trans Ophthalmol Soc U K*. 95:36-38.

Weigl, R. 2005. Longevity of mammals in captivity; from the Living Collections of the world: A list of mammalian longevity in captivity. Kleine Senckenberg-Reihe.

Weiter, J.J., F.C. Delori, G.L. Wing, and K.A. Fitch. 1986. Retinal pigment epithelial lipofuscin and melanin and choroidal melanin in human eyes. *Invest Ophthalmol Vis Sci*. 27:145-152.

Wellen, K.E., and G.S. Hotamisligil. 2005. Inflammation, stress, and diabetes. *J Clin Invest*. 115:1111-1119.

Whitfield, J.R., and L. Soucek. 2012. Tumor microenvironment: becoming sick of Myc. *Cell Mol Life Sci*. 69:931-934.

Witmer, A.N., G.F. Vrensen, C.J. Van Noorden, and R.O. Schlingemann. 2003. Vascular endothelial growth factors and angiogenesis in eye disease. *Prog Retin Eye Res*. 22:1-29.

Wong-Riley, M.T. 2010. Energy metabolism of the visual system. *Eye Brain*. 2:99-116.

Wu, Z., J. Ni, Y. Liu, J.L. Teeling, F. Takayama, A. Collcutt, P. Ibbett, and H. Nakanishi. 2017. Cathepsin B plays a critical role in inducing Alzheimer's disease-like phenotypes following chronic systemic exposure to lipopolysaccharide from Porphyromonas gingivalis in mice. *Brain Behav Immun*. 65:350-361.

Xiong, H., Z.G. Zhang, X.Q. Tian, D.F. Sun, Q.C. Liang, Y.J. Zhang, R. Lu, Y.X. Chen, and J.Y. Fang. 2008. Inhibition of JAK1, 2/STAT3 signaling induces apoptosis, cell cycle arrest, and reduces tumor cell invasion in colorectal cancer cells. *Neoplasia*. 10:287-297.

Xu, C., B. Bailly-Maitre, and J.C. Reed. 2005a. Endoplasmic reticulum stress: cell life and death decisions. *J Clin Invest*. 115:2656-2664.

Xu, H., M. Chen, and J.V. Forrester. 2009. Para-inflammation in the aging retina. *Prog Retin Eye Res*. 28:348-368.

Xu, M., T. Tchkonia, H. Ding, M. Ogrodnik, E.R. Lubbers, T. Pirtskhalava, T.A. White, K.O. Johnson, M.B. Stout, V. Mezera, N. Giorgadze, M.D. Jensen, N.K. LeBrasseur, and J.L. Kirkland. 2015. JAK inhibition alleviates the cellular senescence-associated secretory phenotype and frailty in old age. *Proc Natl Acad Sci U S A*. 112:E6301-6310.

Xu, Q., J. Briggs, S. Park, G. Niu, M. Kortylewski, S. Zhang, T. Gritsko, J. Turkson, H. Kay, G.L. Semenza, J.Q. Cheng, R. Jove, and H. Yu. 2005b. Targeting Stat3 blocks both HIF-1 and VEGF expression induced by multiple oncogenic growth signaling pathways. *Oncogene*. 24:5552-5560.

Yan, L.J. 2014. Positive oxidative stress in aging and aging-related disease tolerance. *Redox Biol*. 2:165-169.

You, L., Z. Wang, H. Li, J. Shou, Z. Jing, J. Xie, X. Sui, H. Pan, and W. Han. 2015. The role of STAT3 in autophagy. *Autophagy*. 11:729-739.

Young, R.W. 1967. The renewal of photoreceptor cell outer segments. *J Cell Biol*. 33:61-72.

Zahn, J.M., S. Poosala, A.B. Owen, D.K. Ingram, A. Lustig, A. Carter, A.T. Weeraratna, D.D. Taub, M. Gorospe, K. Mazan-Mamczarz, E.G. Lakatta, K.R. Boheler, X. Xu, M.P. Mattson, G. Falco, M.S. Ko, D. Schlessinger, J.

Firman, S.K. Kummerfeld, W.H. Wood, 3rd, A.B. Zonderman, S.K. Kim, and K.G. Becker. 2007. AGEMAP: a gene expression database for aging in mice. *PLoS Genet*. 3:e201.

Zarbin, M.A. 2004. Current concepts in the pathogenesis of age-related macular degeneration. *Arch Ophthalmol*. 122:598-614.

Zhang, S.S., J.Y. Wei, C. Li, C.J. Barnstable, and X.Y. Fu. 2003. Expression and activation of STAT proteins during mouse retina development. *Exp Eye Res*. 76:421-431.

Zhao, M., W. Xie, S.H. Tsai, T.W. Hein, B.A. Rocke, L. Kuo, and R.H. Rosa, Jr. 2018. Intravitreal Stanniocalcin-1 Enhances New Blood Vessel Growth in a Rat Model of Laser-Induced Choroidal Neovascularization. *Invest Ophthalmol Vis Sci*. 59:1125-1133.

Zhong, Y., J. Li, J.J. Wang, C. Chen, J.T. Tran, A. Saadi, Q. Yu, Y.Z. Le, M.N. Mandal, R.E. Anderson, and S.X. Zhang. 2012. X-box binding protein 1 is essential for the anti-oxidant defense and cell survival in the retinal pigment epithelium. *PLoS One*. 7:e38616.

Zuo, W., S. Jiang, Z. Guo, M.W. Feldman, and S. Tuljapurkar. 2018. Advancing front of old-age human survival. *Proc Natl Acad Sci U S A*. 115:11209-11214.

7 List of publications

7.1 Publications in peer-reviewed journals

1. K. Hadrian, H. Melkonyan, S. Schlatt, J. Wistuba, S. Wasmuth, A. Heiligenhaus, S. Thanos, M.R.R. Böhm (2019)
"Age-related distribution and potential role of SNCB in topographically different retinal areas of the common marmoset *Callithrix jacchus*, including the macula"
Experimental Eye Research, May 23;185:107676

2. S. König, K. Hadrian, S. Schlatt, J. Wistuba, S. Thanos, M.R.R. Böhm (2018)
"Topographic protein profiling of the age-related proteome in the retinal pigment epithelium of *Callithrix jacchus* with respect to macular degeneration"
Journal of Proteomics, Jan 16;191:1-15

3. M.R.R. Böhm, K. Hadrian, K. Brockhaus, H. Melkonyan, S. Thanos (2018)
"Age-Related Expression of Beta-Synuclein in the Ascending Visual Pathway and Comparative Analysis of its Function within the Neuroretina and Cerebral Cortex in-vitro",
Journal of Alzheimers Disease and Parkinsonism, Vol 8(1): 427

7.2 Oral presentations at scientific meetings

1. K. Hadrian, M. Lever, S. Schlatt, J. Wistuba, L. Klein-Hitpass, S. Rahmann, S. König, S. Thanos, N. Bornfeld, N.E. Bechrakis, M.R.R Böhm (2019)
"Expression und Charakterisierung von Cathepsin B im retinalen Pigmentepithel"
Jahrestagung des Vereins Rheinisch-Westfälischer Augenärzte

2. M. Lever, K. Hadrian, S. Thanos, S. Schlatt, J. Wistuba, S. König, N.E. Bechrakis, M.R.R. Böhm (2019)

"Vergleichende Analyse der Lebenszeitexpression von PARK7/DJ-1 in dem Choroidea-Pigmentepithel-Komplex von *Callithrix jacchus* in Bezug zur Topographie"

Jahrestagung des Vereins Rheinisch-Westfälischer Augenärzte

3. K. Hadrian, M. Lever, S. Schlatt, J. Wistuba, S. Thanos, S. Rahmann, L.Klein-Hitpass, M.R.R. Böhm (2018)

"The age-related transcriptome of the retinal pigment epithelium of the macular-bearing *Callithrix jacchus*"

Jahrestagung Deutsche Ophthalmologische Gesellschaft

4. M.R.R. Böhm, K. Hadrian, J. Wistuba, S. Schlatt, S. Thanos, S. König (2018)

"Topographische Differentialanalyse altersabhängig exprimierter Proteine im retinalen Pigmentepithel des *Callithrix jacchus*"

Jahrestagung des Vereins Rheinisch-Westfälischer Augenärzte

5. K. Hadrian, K. Brockhaus, T. Schockenhoff, H. Melkonyan, S. Thanos, M.R.R. Böhm (2017)

"Morphologische und molekularbiologische Veränderungen des alternden retinalen Pigmentepithels"

Jahrestagung des Vereins Rheinisch-Westfälischer Augenärzte

6. M.R.R. Böhm, K. Brockhaus, K. Hadrian, H. Melkonyan, S. Thanos (2017)

"Komparative Analyse der Rolle von altersreguliertem beta-Synculein in der Neuroretina und im visuellen Kortex"

Jahrestagung des Vereins Rheinisch-Westfälischer Augenärzte

7.3 Poster presentations at scientific meetings

1. K. Hadrian, M. Kasper, A. Heiligenhaus, S. Thanos, N.E. Bechrakis, M.R.R. Böhm (2019)

„Einfluss und Funktion von Cathepsin B auf ARPE-19 Zellen in einem Seneszenzmodell *in-vitro*“

Jahrestagung Deutsche Ophthalmologische Gesellschaft

2. K. Hadrian, M. Lever, S. Schlatt, J. Wistuba, S. Thanos, S. Rahmann, L. Klein-Hitpass, M.R.R. Böhm (2019)

“Expression and function of Cathepsin B in the retinal pigment epithelium”

Invest. Ophthalmol. Vis. Sci. 60

3. M.R.R. Böhm, K. Hadrian, S. Schlatt, J. Wistuba, S. Thanos, S. Rahmann, L. Klein-Hitpass (2019)

“The age-related transcriptome of the retinal pigment epithelium of the macular-bearing *Callithrix jacchus*”

Invest. Ophthalmol. Vis. Sci. 60

4. M.R.R. Böhm, K. Hadrian, M. Lever, S. Wasmuth, S. Schlatt, J. Wistuba, S. Thanos, S. König (2018)

“A protein atlas of the aging retinal pigment epithelium of *Callithrix jacchus*”

Jahrestagung Deutsche Ophthalmologische Gesellschaft

5. M. Lever, K. Hadrian, S. Schlatt, J. Wistuba, S. König, S. Thanos, M.R.R. Böhm (2018)

“Comparative analysis of the lifetime expression of PARK7/DJ-1 in the choroid-retinal pigment epithelial complex of *Callithrix jacchus* and Sprague Dawley rats”

Jahrestagung Deutsche Ophthalmologische Gesellschaft

6. K. Hadrian, H. Melkonyan, S. Schlatt, J. Wistuba, S. Wasmuth, A. Heiligenhaus, S. Thanos, M.R.R. Böhm (2018)

"Topological distribution and potential role of age-related β-synuclein in the retinal pigment epithelium"

Invest. Ophthalmol. Vis. Sci. 59

7. M.R.R. Böhm, K. Hadrian, S. Schlatt, J. Wistuba, S. Thanos, S. König (2018)

"Age-related topographic protein profiling of the retinal pigment epithelium of macular-bearing *Callithrix jacchus*"

Invest. Ophthalmol. Vis. Sci. 59

8. K. Hadrian, K. Brockhaus, T. Schockenhoff, H. Melkonyan, S. Thanos, M.R.R. Böhm (2017)

"Topological distribution and potential role of β-Synuclein in the aging RPE *in vitro*"

Jahrestagung Deutsche Ophthalmologische Gesellschaft

9. M.R.R. Böhm, K. Hadrian, S. Thanos, S. König (2017)

"Topographic differential analysis of the age-related proteome in the retinal pigment epithelium of *Callithrix jacchus*"

Jahrestagung Deutsche Ophthalmologische Gesellschaft

10. K. Hadrian, K. Brockhaus, H. Melkonyan, S. Thanos, M.R.R. Böhm (2017)

"Common age-related changes between visual cortex and neuroretina of rats"

12th Göttingen Meeting of the German Neuroscience Society

11. M. Breitkreuz, K. Hudek, T. Voelkel, L. Beckendorf, M. Krüger, N. Hamdani, W.A. Linke (2015)

"Phosphorylation of titin at the Z-disk/I-band junction as a potential mediator of sarcomere assembly"

J Muscle Res Cell Motil (2015)

8 Appendix

Danksagung

Zunächst möchte ich mich bei Herrn Dr. Böhm bedanken. Danke, dass Sie mir die Möglichkeit gaben, dieses spannende Thema zu bearbeiten. Ich bedanke mich für die Unterstützung, die Sie mir über die gemeinsameren Jahre gegeben haben und besonders für das entgegen gebrachten Vertrauens, unser Labor in Essen aufzubauen.
Ein besonderes Dankeschön geht an Prof. Solon Thanos. Solon, vielen Dank, dass du mich hast in deinem Labor arbeiten lassen und mir dort alle Freiräume und Möglichkeiten gabst, die ich brauchte. Ich danke dir für dein Vertrauen und für die vielen interessanten Gespräche, die nicht nur mein naturwissenschaftliches, sondern auch mein geschichtliches Wissen erweiterten. Ich wünsche dir einen tollen und bereichernden Ruhestand.
Mein Dank geht auch an das gesamte Team der experimentellen Ophthalmologie in Münster, insbesondere an Mechthild Wissing. Ihr habt mich beim Start meiner Promotion so gut unterstützt und mich direkt so liebevoll bei euch aufgenommen! Mecki, ich danke dir für die jahrelange Unterstützung lange über meine Zeit in Münster hinaus!
Ich danke dem Ophtha Lab des St. Franziskushospitals in Münster für die Unterstützung und die gemeinsamen Stunden in Labor. Besonders geht mein Dank hier an Dr. Susanne Wasmuth für unsere gemeinsame Arbeit mit den primären RPE Zellen, sowie an Dr. Maren Kasper für unsere Arbeit am FACS-Gerät.
Ich danke Prof. Simone König und PD Dr. Ludger Klein Hitpass für die Proteom- und Transkriptomdaten und dafür, dass ihre Türen bei schwierigen Fragen nach den Sequenzierungen für mich immer offenstanden.
Ich danke Prof. Stefan Schlatt und Dr. Joachim Wistuba vom Centrum für Reproduktionsmedizin und Andrologie für die Überlassung der *C. jacchus*-Augen.
Nach meinen Umzug nach Essen war zunächst alles anders. Doch dank meiner Kollegen im Histologielabor habe ich mich sehr schnell wieder zurechtfinden können. Vielen Dank! Mein besonderer Dank geht an Dr. Henning Thomassen. Danke für die

Mitbenutzung eurer Geräte und Chemikalien, für deine Expertise und für viele unterhaltsame Gespräche. Außerdem danke ich Mareike Horstmann, und der gesamten Arbeitsgruppe für Molekulare Ophthalmologie für eure Expertise und die Benutzung eurer Geräte, sowie Alexandra Brenzel vom IMCES. Ihr habt mich aufgebaut, wenn ich frustriert war und brachtet mich jederzeit zum Lachen.

Ein ganz lieber Dank geht auch an meine Endo-Mädels – Nina, Daniela, Irina und Eva – Danke für die Aufnahme in eurer kleinen Doktorandengruppe, für (leckere) Mittagessen und viele Gespräche!

Danke an meine Bochumer Buddys, besonders Karo, Tobi, Luke und Max, aber auch alle anderen von unserem verrückten Haufen. Obwohl wir uns nicht mehr täglich sehen, seid ihr immer für mich da, hört mir zu, auch wenn ich über Augen rede! Ich danke euch für 10 Jahre Freundschaft, Fachschaft, Erstifahrten, wo auch immer unsere Wege uns nach dem Studium hinführten!

Sabrina, danke für deine wissenschaftliche Expertise, deine Inspiration und deine Freundschaft und das Korrekturlesen dieser Arbeit.

Ich danke meinen Freunden, die mich bei allem, was ich bisher gemacht habe, unterstützt haben. Besonders Lea und Jill. Ihr beide holt mich aus jedem Tief und glaubt an mich, besonders wenn ich es nicht tue. Ihr begleitet mich einen Großteil meines Lebens und dafür danke ich euch!

Als letztes möchte ich meiner Familie danken. Meine Schwiegerfamile, die mich immer unterstützt, hinter mir steht und die meinen gesamten akademischen Weg mitverfolgt hat!

Mama und Papa, ohne euch wäre ich nicht da, wo ich jetzt bin. Ihr habt mich immer unterstützt, und ich kann mir zu jederzeit sicher sein, dass ihr an meiner Seite seid. Ich liebe euch!

Sven, du musstest so viel mit mir durchmachen! Danke für deine Unterstützung bei allem was ich mache! Du hast jede meiner Entscheidungen unterstützt, auch wenn sie bedeuteten, dass wir uns monatelang nicht gesehen haben. Danke, dass du losgefahren bist, um mir Nachos zu holen, wenn ich sie brauchte. Danke, dass du mir auch zuhörst, wenn ich über Augen spreche, trotzdem du sie gar nicht magst! Ich liebe dich!

Curriculum Vitae

Der Lebenslauf ist in der Online-Version aus Gründen des Datenschutzes nicht enthalten.

Eidesstaatliche Erklärung

Erklärung:

Hiermit erkläre ich, gem. § 6 Abs. (2) g) der Promotionsordnung der Fakultät für Biologie zur Erlangung der Dr. rer. nat., dass ich das Arbeitsgebiet, dem das Thema „Topographic differential analysis and function of age-related protein expression in the retinal pigment epithelium of *Callithrix jacchus*“ zuzuordnen ist, in Forschung und Lehre vertrete und den Antrag von Karina Hadrian befürworte und die Betreuung auch im Falle eines Weggangs, wenn nicht wichtige Gründe dem entgegenstehen, weiterführen werde.

Essen, den _____ _____

Unterschrift des Betreuers (Prof. oder PD) an der Universität Duisburg-Essen

Erklärung:

Hiermit erkläre ich, gem. § 7 Abs. (2) d) + f) der Promotionsordnung der Fakultät für Biologie zur Erlangung des Dr. rer. nat., dass ich die vorliegende Dissertation selbstständig verfasst und mich keiner anderen als der angegebenen Hilfsmittel bedient, bei der Abfassung der Dissertation nur die angegeben Hilfsmittel benutzt und alle wörtlich oder inhaltlich übernommenen Stellen als solche gekennzeichnet habe.

Essen, den _____ _____

Unterschrift des/r Doktoranden/in

Erklärung:

Hiermit erkläre ich, gem. § 7Abs. (2) e) + g) der Promotionsordnung der Fakultät für Biologie zur Erlangung des Dr. rer. nat., dass ich keine anderen Promotionen bzw. Promotionsversuche in der Vergangenheit durchgeführt habe und dass diese Arbeit von keiner anderen Fakultät / Fachbereich abgelehnt worden ist.

Essen, den _____ _____

Unterschrift des/r Doktoranden/in